ISSN 2542-1565

Vol. 17 2024 No. 02

GEOGRAPHY ENVIRONMENT SUSTAINABILITY

«The journal GEOGRAPHY, ENVIRONMENT, SUSTAINABILITY was founded in 2008 by Russian Geographical Society, the Lomonosov Moscow State University Geography Department, and the Russian Academy of Sciences Institute of Geography. Since that time the journal publishes **4 issues per year**, containing original research papers and reviews. The journal issues are open source and distributed through subscriptions, library exchanges of leading universities, and via the website through the world»

FOUNDERS OF THE JOURNAL: Russian Geographical Society, Faculty of Geography, Lomonosov Moscow State University and Institute of Geography of the Russian Academy of Sciences

The journal is published with financial support of the Russian Geographical Society.

The journal is registered in Federal service on supervision of observance of the legislation in sphere of mass communications and protection of a cultural heritage. The certificate of registration: ПИ № ФС77-67752, 2016, December 21.

PUBLISHER
Russian Geographical Society
Moscow, 109012 Russia
Novaya ploshchad, 10, korp. 2
Phone 8-800-700-18-45
E-mail: press@rgo.ru
www.rgo.ru/en

EDITORIAL OFFICE
Lomonosov Moscow State University
Moscow 119991 Russia
Leninskie Gory, 1,
Faculty of Geography, 1806a
Phone 7-495-9391552
Fax 7-495-9391552
E-mail: ges-journal@geogr.msu.ru
www.ges.rgo.ru

DESIGN
Layout designer: Tereshkin Anton
Moscow, 115088,
26 Simonovsky Val str., bldg. One
Phone: +7 (903) 108-04-44
E-mail: smile.tai@gmail.com

DOI prefix: 10.24057

Format A4 (210x297mm)

"GEOGRAPHY, ENVIRONMENT, SUSTAINABILITY" is the only original English-language journal in the field of geography and environmental sciences published in Russia. It is supposed to be an outlet from the Russian-speaking countries to Europe and an inlet from Europe to the Russian-speaking countries regarding environmental and Earth sciences, geography and sustainability. The main sections of the journal are the theory of geography and ecology, the theory of sustainable development, use of natural resources, natural resources assessment, global and regional changes of environment and climate, social-economical geography, ecological regional planning, sustainable regional development, applied aspects of geography and ecology, geoinformatics and ecological cartography, ecological problems of oil and gas sector, nature conservations, health and environment, and education for sustainable development.

OPEN ACCESS POLICY. "GEOGRAPHY, ENVIRONMENT, SUSTAINABILITY" is an open access journal. All articles are made freely available to readers immediately upon publication. Our open access policy is in accordance with the Budapest Open Access Initiative (BOAI) definition - it means that articles have free availability on the public internet, permitting any users to read, download, copy, distribute, print, search, or link to the full texts of these articles, crawl them for indexing, pass them as data to software, or use them for any other lawful purpose, without financial, legal, or technical barriers other than those inseparable from gaining access to the internet itself.

Date of publication: March 31st, 2024.

EDITORIAL BOARD

EDITORIAL OFFICE

CONTENTS

Disclaimer:

The information and opinions presented in the Journal reflect the views of the authors and not of the Journal or its Editorial Board or the Publisher. The GES Journal has used its best endeavors to ensure that the information is correct and current at the time of publication.

RESEARCH PAPER

URBAN TRANSFORMATION IN LAHORE: THREE DECADES OF LAND COVER CHANGES, GREEN SPACE DECLINE, AND SUSTAINABLE DEVELOPMENT CHALLENGES

Rimsha Azhar[1], Muhammad Asif Javed[2], Muhammad Nasar-u-Minallah[3]*, Silvia Machado[1], Muhammad Jabbar[4]
[1]Department of Environmental Sciences, FC College University, Lahore, 54000, Pakistan
[2]College of Earth and Environmental Sciences, University of Punjab, Lahore, 54000, Pakistan
[3]Institute of Geography, University of the Punjab, Lahore, 54000, Pakistan
[4]Department of Geography, University of Malaya, Kuala Lumpur, Malaysia
*Corresponding author: Nasarbhalli@gmail.com
Received: January 13th 2024 / Accepted: April 10th 2024 / Published: July 1st 2024
https://DOI-10.24057/2071-9388-2024-3204

ABSTRACT. Pakistan has experienced significant urbanization, characterized by rapid urban population growth and unplanned urban expansion, making it the most urbanized country in South Asia. This study focuses on Lahore, the second-largest megacity of Pakistan, and evaluates land cover changes over the last three decades (1990-2020). It also analyzes the relationship between urban green landscapes and unregulated urban expansion. The study reveals significant changes in the ecology of Lahore's urban landscape using Landsat imagery, including Landsat 5 TM, Landsat 8 OLI, and a 30m spatial resolution, along with population data from the Pakistan Bureau of Statistics. In particular, the study reveals a decline in urban green spaces and a significant expansion of urban built-up areas in Lahore. The annual urban area expansion rates were 24.2 km^2 (1990-2000), 12.1 km^2 (2000-2010), and 26.4 km^2 (2010-2020), while vegetation cover decreased 33.45 km^2 (1990-2000), 20 km^2 (2000-2010) in the first two decades but slightly increased from 2010 to 2020 at an annual rate of 14.17 km^2. As a result, there is a serious concern about the rapid decline of green space in Lahore. It is recommended that the administrative authorities follow the World Health Organization's guidelines regarding the need for green spaces. This study contributes to achieving the United Nations' Sustainable Development Goal 11th, indicator 11.3.1, and provides guidelines for conserving natural, social, and economic resources in the face of rapid urbanization.

KEYWORDS: land cover changes, green spaces, sustainable development, SDG 11, Lahore

CITATION: Azhar R., Javed M. A., Nasar-u-Minallah M., Machado S., Jabbar M. (2024). Urban Transformation in Lahore: Three Decades of Land Cover Changes, Green Space Decline, and Sustainable Development Challenges. Geography, Environment, Sustainability, 2(17), 6-17
https://DOI-10.24057/2071-9388-2024-3204

Conflict of interests: The authors reported no potential conflict of interest.

INTRODUCTION

The expansion of urban areas over time has led to the depletion of natural resources and environmental degradation, particularly green spaces, as shown by studies investigating land use and land cover changes (Puplampu and Boafo 2021). Ongoing urban growth in Pakistan's megacities, especially in Lahore, raises significant environmental and sustainability issues (Nasar-u-Minallah et al. 2021; Nasar-u-Minallah et al. 2023). The reduction of green spaces due to land overdevelopment, population growth, and industrial expansion has disrupted the delicate balance of ecosystems (Jabbar et al. 2024). Therefore, monitoring and preserving tree cover in urban areas is increasingly important for environmental conservation (Semeraro et al. 2021; Hanif et al. 2022; Fatima et al. 2023). Urban green spaces (UGS) are open areas in urban and semi-urban regions that are free to the public and characterized by substantial vegetation cover. These spaces include trees in parks, forests, roadways, farms, and environmental conservation areas. They are widely recognized for their ability to mitigate the adverse effects of urbanization on land use (Semeraro et al. 2021). Establishing and improving urban green spaces can serve as suitable infrastructure options to enhance the quality of life and promote the sustainability and security of biodiversity systems, energy, health, water, food, and flood mitigation (Zia et al. 2022). UGS play a crucial role in reducing the impact of urban heat islands and enhancing urban water management (Mukherjee et al. 2018; Nasar-u-Minallah 2018; Nasar-u-Minallah 2019; Nasar-u-Minallah and Ghaffar 2020). The development of urban green spaces is a fundamental goal in creating livable cities, as the quantity and distribution of UGS significantly influence a city's long-term sustainability (Jabbar et al. 2024). The overall number of green spaces in a particular area indicates a high-quality life and a healthy ecosystem (Alam et al. 2014). The development of UGS is crucial for creating livable cities, as their quantity and distribution are key to the sustainability of the city (Brown et al. 2010).

According to (United Nations 2018) projections, the global urban population will increase by 70% by 2050, leading to the expansion of metropolitan areas and an increase in natural resource consumption, which will negatively impact human health (Semeraro et al. 2021). As a large city, Lahore has been the subject of numerous studies examining urban and ecological issues (Bhalli and Ghaffar 2015; Nasar-u-Minallah 2023). Spatial and temporal analysis of land change in cities like Lahore can provide valuable insights for administrative authorities. The present research focuses on Lahore to better understand the distribution and provision of green spaces for a sustainable ecosystem. Consequently, it is essential to develop urbanization models, approaches, and programs that enhance the quality of life in urban areas while minimizing their local and global impacts (Semeraro et al. 2021). A comprehensive understanding of this phenomenon and its patterns can inform the effective utilization of urban green spaces. Despite the many studies on land use changes in Lahore, the evaluation of city agglomeration types and the relationship between green space and population growth using landscape metrics remain unexplored in the existing literature. An advanced platform, known as Google Earth Engine, enables the categorization and processing of multi-resolution and multi-temporal satellite images for specific sites, facilitating geospatial analysis (Lin et al. 2021). This web-based tool, freely accessible for academic research, has proven useful in examining urban landscape changes (Sidhu et al. 2018). Furthermore, the availability of Landsat satellite data since 1972, accessible online, allows for the analysis of surface patterns, contributing to outcomes with accuracy rates of at least 75% (Dwyer et al. 2018; Tsai et al. 2018; Zia et al. 2022; Sahar et al. 2023; Zia et al. 2023; Mazhar et al. 2024).

Urban green spaces play a crucial role in mitigating the adverse effects of rapid urban expansion by providing numerous environmental, social, and economic benefits (Jabbar et al. 2024). These spaces, including parks, gardens, and forests, act as vital lungs for cities, filtering air pollutants and mitigating the urban heat island effect (Alam et al. 2014; Garcia et al. 2019). They also enhance biodiversity, offering habitats for various species amidst urbanization. Moreover, urban green spaces contribute to the well-being of urban residents by providing opportunities for recreation, exercise, and social interaction, thus improving physical and mental health outcomes (Bratman et al. 2012). However, as cities expand, there is a growing concern over the loss of green spaces due to infrastructure development and urban sprawl, necessitating proactive planning strategies to preserve and expand these essential urban ecosystems (Fletcher et al. 2019).

Green spaces are increasingly recognized as vital components of urban areas, offering a multitude of benefits essential for city well-being and sustainability. Recent research emphasizes their crucial role in mitigating the impacts of climate change, particularly in reducing urban heat island effects and improving air quality (Schiopu & Teodosiu 2021; Nasar-u-Minallah 2019). These spaces also act as carbon sinks, sequestering carbon dioxide and other pollutants while simultaneously providing shade and cooling effects through evapotranspiration, enhancing urban resilience to rising temperatures (Shen et al. 2022). Furthermore, urban green spaces contribute significantly to public health by promoting physical activity, mental well-being, and social cohesion (Gascon et al. 2022). They offer opportunities for recreation, relaxation, and social interaction, which are increasingly valued in densely populated urban environments. Additionally, green spaces support urban biodiversity, provide habitats for diverse flora and fauna, and play a critical role in ecosystem services such as pollination and water filtration (Elmqvist et al. 2020). Therefore, the preservation and expansion of green spaces in urban areas are paramount for creating sustainable and livable cities that prioritize environmental quality and human health.

Urban expansion poses significant threats to green spaces, jeopardizing their ecological integrity and the numerous benefits they provide to urban communities. Recent studies highlight the escalating pressures on green spaces due to infrastructure development, population growth, and land-use changes (Bhalli and Ghaffar 2015; Minallah et al. 2016a; Minallah et al. 2016b; Bhalli et al. 2013) associated with urbanization (Soga et al. 2022; Bhalli et al. 2012a). These threats include habitat loss, fragmentation, and degradation, leading to declines in biodiversity and ecosystem services (Zhang et al. 2021). Additionally, urban expansion often results in the conversion of green spaces into impervious surfaces, exacerbating issues such as flooding and heat stress while reducing infiltration capacity and water quality (Chen et al. 2022; Zia et al. 2016b). Furthermore, the loss of green spaces diminishes opportunities for recreation, social interaction, and mental well-being among urban residents, exacerbating inequalities in access to nature (Grimm et al. 2021). Therefore, effective urban planning strategies that prioritize the conservation and sustainable management of green spaces are essential for mitigating the adverse impacts of urban expansion and ensuring the resilience and livability of cities.

The rapid expansion of urban areas poses a significant threat to green spaces, which provide ecological integrity and multilevel benefits to the environment and human well-being. As cities continue to grow at extraordinary rates, green spaces face increasing pressures from land-use changes. These threats result in habitat loss, fragmentation, and degradation, leading to declines in biodiversity and ecosystem services. Furthermore, the conversion of green spaces into impervious surfaces exacerbates issues such as urban heat island effects, flooding (Zia et al. 2021c), and water pollution, while also diminishing opportunities for recreation, social interaction, and mental health benefits among urban residents. Thus, understanding the complexities and impacts of rapid urban expansion on green spaces is essential for informing effective conservation strategies and urban planning initiatives aimed at preserving these vital urban ecosystems. The rapid growth of cities puts green spaces in danger. These areas, like parks and forests, are important for both nature and people. But as cities grow larger, more land is being utilized for buildings and roads, causing a reduction in green spaces. Animals and plants lose their homes, and communities lose the benefits such spaces bring, such as cleaner air and places to relax. When green spaces disappear, problems such as floods and pollution often become worse. Additionally, there are fewer places to enjoy nature or meet with friends outdoors. As such, it is crucial to understand how the rapid growth of cities can affect green spaces. By studying these patterns, green spaces can be protected sustainably. This study aims to deepen the understanding of Lahore's green space, distribution, and sustainability to provide useful knowledge for policymakers and urban planners.

MATERIAL AND METHODS

Study Area

Lahore, the second-largest megacity in the Punjab Province of Pakistan, is located on the left bank of the river Ravi (Shirazi et al. 2016), within latitudes 31.20°N to 31.71°N and longitudes 74.00°E to 74.65°E. Its exceptional connectivity with other urban and rural areas in the province, as well as its status as an industrial hub, have propelled its rapid urbanization and development over the past few decades. This rapid urbanization has markedly transformed the natural surface into the urban landscape (Zia et al. 2021a; Nasar-u-Minallah 2020). The population of the Lahore district has seen considerable growth, rising from 6.3 million (6,318,745 individuals) in 1998 to 11.13 million (11,126,285 individuals) in 2017 (GOP 2017). As a centre of culture, education, and business, Lahore plays a pivotal role in the region. The Lahore city district covers an area of 1772 km^2. For administrative purposes, the Lahore city district is divided into five tehsils: Lahore Cantt, Lahore City, Model Town, Raiwind, and Shalimar, further organized into nine zones/towns, as illustrated in Fig. 1.

Lahore is facing significant changes in its urban, social, and environmental landscape. Over recent years, the city has experienced rapid urbanization, with its built-up area nearly doubling between 1999 and 2011. This expansion has strained infrastructure and governance, leading to issues like uncontrolled urban growth and inefficiencies in managing construction (Bhalli et al. 2012b). To cope with this growth, Lahore requires well-organized institutions. Despite improvements in transportation and efforts to restore the walled city, effective population management remains crucial (Rana & Bhatti 2018). The population of the study area has steadily increased since the 1998 Census, resulting in urban sprawl, the loss of green spaces, and damage to natural habitats. This expansion, primarily occurring on agricultural land, poses significant socio-environmental challenges, including overpopulation and environmental degradation (Shirazi & Kazmi 2014).

Despite differences in infrastructure and socioeconomic growth among districts in Punjab province, Lahore remains the most developed. However, local administrations struggle to manage development challenges effectively despite national efforts to reduce these disparities (Rana & Arshad 2017). Environmental issues have significant socio-environmental impacts, particularly the loss of urban greenery and trees. Rapid urbanization in Lahore has led to a considerable decrease in green spaces, affecting the city's appearance and worsening environmental problems (Shirazi & Kazmi 2016). Public opinion polls indicate that population growth and urbanization are the primary drivers of vegetation loss, highlighting the importance of sustainable urban planning and preserving green areas.

Data Acquisition

This study utilized Landsat satellite imagery, with the specifics of the Landsat datasets presented in Table 1. The study used four Landsat images from different sensors, including three from Landsat 5 TM for 1990, 2000, and 2010 and one from Landsat 8 (OLI_TIRS) for 2020. These sensors vary in spectral, spatial, and temporal resolutions. Additionally, data from the Punjab Bureau of Statistics[1] played a crucial role in analyzing various city locations, enabling a comprehensive comparison of urbanization trends and changes in urban green spaces over the past

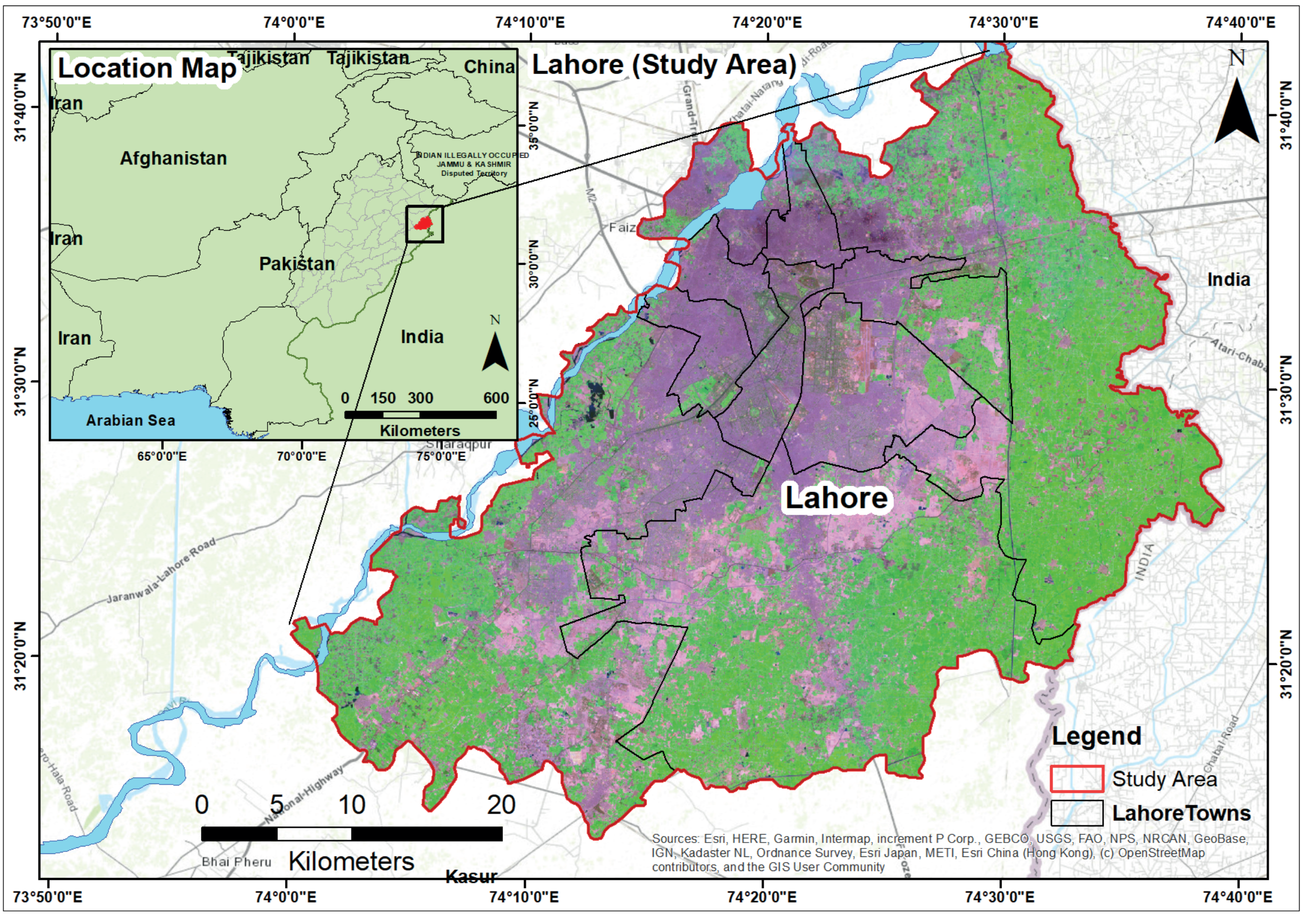

Fig. 1. Location map of the study area District Lahore

[1]Punjab Bureau of Statistics (2015). Punjab Development Statistics 2015. Lahore. Retrieved from http://www.bos.gop.pk/publicationreports

three decades. The Lahore district shape file, obtained from the Punjab Bureau of Statistics, was instrumental in this analysis. Population data were derived from the 1998 census, and projections for 2010 and 2020, based on the 2017 data, were sourced from the Punjab Bureau of Statistics website:

$$P(t) = P_0 ekt \tag{1}$$

where variable *t* represents time, *k* represents growth rate, and P_0 represents the initial population.

Data analysis

This study examines the spatial and temporal changes in land use and land cover in Lahore, Pakistan, and their relationship with the loss of Urban Green Spaces (UGS) and population growth. Landsat 5 TM and Landsat 8 OLI satellite imagery with a spatial resolution of 30 meters were employed for this analysis. The Google Earth Engine (GEE) was used to classify images of Lahore for the years 1990, 2000, 2010, and 2020. Additionally, the study applies a formula to evaluate indicator 11.3.1, as described by Nicolau et al. (2018):

$$LCRPGR = (Land\ consumption\ rate\ /\ Population\ growth\ rate) \tag{2}$$

where Land consumption rate= $ln\,(Urb_{t+n}/Urb_t)\,/\,n$ and Population growth $rate = ln\,(Pop_{t+n}\,/\,Pop_t)\,/\,n$

The analysis of spatiotemporal patterns of land use and land cover, along with its correlation with the decline of green spaces and population growth, was conducted in this study. The methodology was divided into three distinct categories, as illustrated in Fig. 2.

This study analyzed spatiotemporal patterns of land use and land cover, and its correlation with the decline of green spaces and population growth. Defined as publicly owned areas accessible without restriction (hereafter referred to as UGS), these spaces include parks, street roundabouts, and medians, which are all characterized by their lack of physical barriers to access. Data for the years 1990, 2000, 2010, and 2020 were acquired during February and March to select cloud-free images, as these months typically have minimal cloud cover. Landscape metrics were used to measure patterns and analyze changes in urban areas over specified periods. Each pixel in the satellite imagery grid represents a digital number corresponding to the captured data. A supervised image classification methodology was applied to categorize the data from the satellite imagery. Various tools for satellite image analysis provide a broad spectrum of capabilities for conducting different types of image classification. In this study, Landsat 5 TM and Landsat 8 OLI satellite images, with a spatial resolution of 30 meters, were processed and classified using Google Earth Engine. Machine learning classifiers, known for their superior accuracy over traditional methods, were used (Tsai et al. 2018).

Table 1. Landsat Datasets Specifications

Year	Satellite	Acquisition date	Accuracy (%)
1990	Landsat 5 TM	09-02-1990	88
2000	Landsat 5 TM	10-02-2000	82
2010	Landsat 5 TM	03-02-2010	92
2020	Landsat 8 (OLI_TIRS)	05-03-2020	86

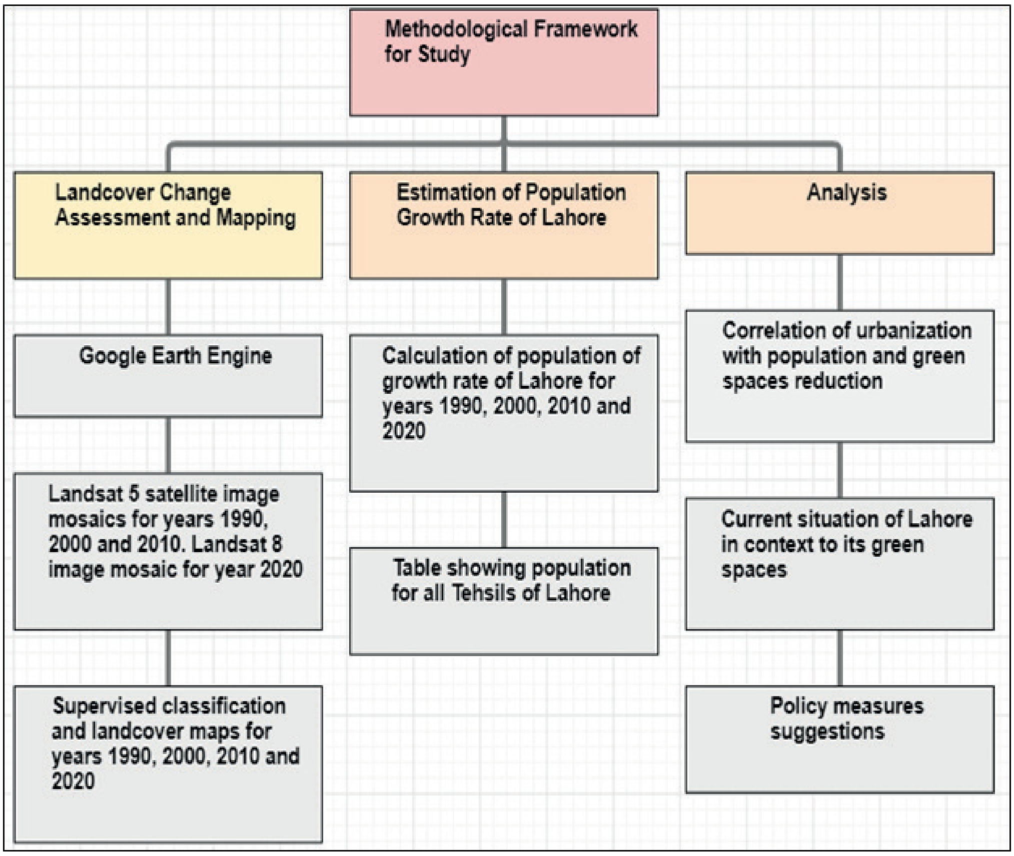

Fig. 2. Methodological framework of study

Table 1 details the satellite images used to classify land cover in the Lahore district for 1990, 2000, 2010, and 2020. Due to their high spatial resolution and advanced capabilities, the chosen satellite imagery and classification approach enhance the accuracy and reliability of the analysis. Machine learning algorithms for image classification require a substantial dataset, particularly more training data points for land cover representation. However, machine learning classifiers have consistently demonstrated greater accuracy than conventional image classification methods. This study utilized the CART algorithm, a binary decision tree method based on "if-then" questions at each node, for image classification. Applying the CART classifier to land cover mapping produced highly favourable outcomes, with accuracies typically exceeding 75%. The analysis identified four distinct land cover categories: vegetation, water bodies, urban areas, and barren areas. As noted by Megahed et al. (2015), the Kappa coefficient is a statistical measure for assessing the level of agreement in validating the obtained results. It ranges from +1, indicating perfect agreement, to -1, indicating complete disagreement, with 0 signifying an agreement level as expected by chance (Paudel & Yuan 2012). In this study, Kappa values were calculated for all classified images, showing promising results of 0.75 (for 1990), 0.71 (for 2000), 0.87 (for 2010), and 0.73 (for 2020). These Kappa coefficients confirm the reliability and robustness of the classification results across all analyzed images.

Estimation of the population of Lahore

The population estimates for the years 1990, 2000, 2010, and 2020 were obtained from available census data. Specifically, the population figures for 1990 and 2000 were calculated using the 1998 census data, while those for 2010 and 2020 were based on the 2017 data provided by the Pakistan Bureau of Statistics[2]. For Lahore Cantt Tehsil, the estimated population growth rate was 5.03% in 1990 and 3.07% in 2000, 2010, and 2020. In Lahore City Tehsil, the projected growth rate was 3.14% for 2000, 2010, and 2020, with a rate of 2.65% for 2000 in the same tehsil. The growth rate for Model Town Tehsil was estimated to be 3.14% for 2000, 2010, and 2020, and 3.48% for 2000. Raiwind Tehsil experienced a growth rate of 3.14% in 2000, 2010, and 2020 and 4.64% in 2000. Lastly, Shalimar Tehsil grew by 3.14% in 2000, 2010, and 2020, with a rate of 2.47% in 2000. Lastly, Shalimar Tehsil had a growth rate of 3.14 % in 2000, 2010, and 2020, with a rate of 2.47 % in 2000. The population growth estimation followed the formula $P(t) = P_0 ekt$, where $P(t)$ represents the population at a given time, P_0 is the initial population, t represents time, and k denotes the growth rate. This formula was used to project the population figures for different years, considering the estimated growth rates for each tehsil in Lahore.

RESULTS

Fig. 3(a) depicts the map of land use changes, providing a detailed overview of Lahore's land cover composition in 1990. This illustration visually represents urban land, water bodies, barren land, and vegetation cover, facilitating a clear understanding of Lahore's land dynamics during this specific period and highlighting the initial state of these critical land cover components. Fig. 3(b) delivers an in-depth view of the land cover changes within Lahore's tehsils in 2000, indicating a decrease in vegetation from 1205 km^2 to 870 km^2 and an increase in built-up area from 218 km^2 to 460 km^2. Fig. 3(c) presents a detailed

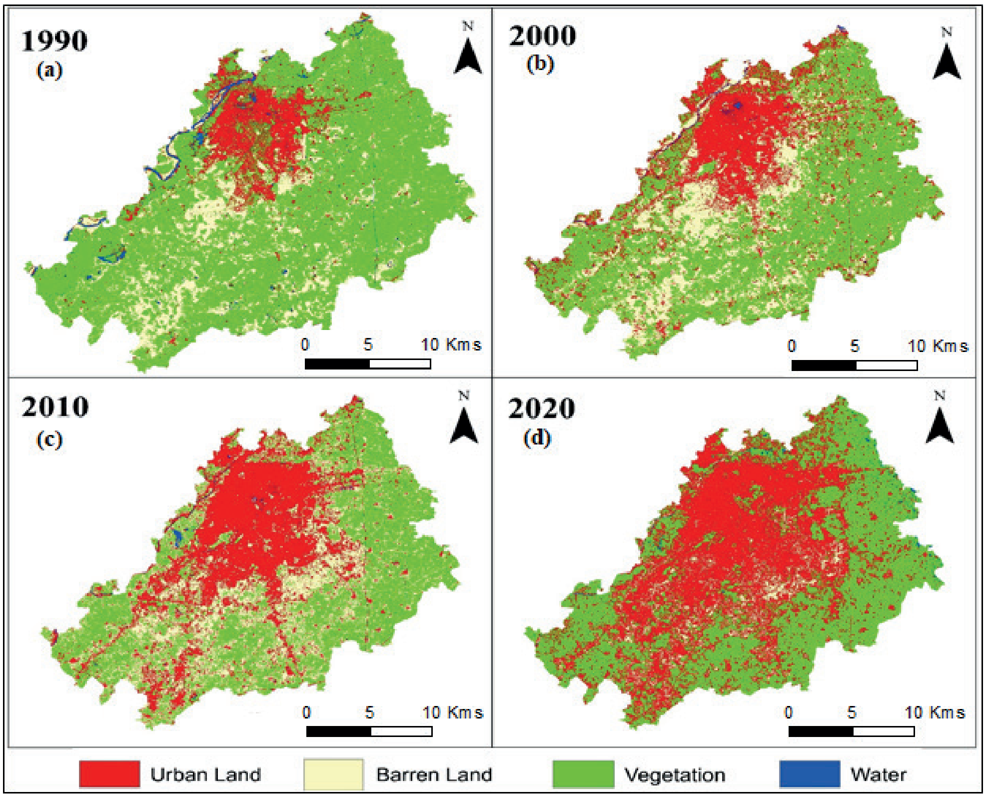

Fig. 3. Land Use/Land Covers of Lahore from 1990 to 2020

[2]Pakistan Bureau of Statistics (1998). Census report of Pakistan 1998. Islamabad. Retrieved from http://www.pbs.gov.pk/population-tables
Pakistan Bureau of Statistics (2017). Provisional summary results of 6th population and housing census 2017. Islamabad. Retrieved from http://www.pbscensus.gov.pk/
Pakistan Bureau of Statistics. Census 1998; 2005. http://www.pbs.gov.pk/
Pakistan Bureau of Statistics. Census 2017; 2018. http://www.pbs.gov.pk/

examination of the land cover of Lahore in 2010, revealing a decrease in vegetation from 870 km^2 to 671 km^2 and an increase in built-up area from 460 km^2 to 582 km^2. Lastly, Fig. 3(d) offers a comprehensive land cover assessment for Lahore's tehsils in 2020, showing an increase in vegetation from 671 km^2 to 812 km^2 and in the built-up area from 582 km^2 to 846 km^2.

Lahore's land use and land cover changes were calculated for all five tehsils (Lahore Cantt, Lahore City, Model Town, Raiwind, and Shalimar), as shown in the figures below. These images collectively provide a decade-by-decade overview of Lahore's land cover evolution from 1990 to 2020. For a specific year, each figure details the areas of urban land, water bodies, barren land, and vegetation cover within Lahore. This series of visuals facilitates a comparative analysis of how land use and environmental dynamics have shifted over time, offering valuable insights into land use trends and land cover change in the city. This study contributes new perspectives on land use and land cover change in Lahore and establishes a correlation between the reduction of green space and the increase in population and urbanization. The findings of this research align well with those of previously published studies, as illustrated in Fig. 4.

Fig. 5 illustrates the average changes in vegetation and urbanization. From 1990 to 2000, vegetation decreased by 33.45 km^2. Between 2000 and 2010, it further decreased by 20 km^2. However, from 2010 to 2020, vegetation increased by 14.17 km^2. This increase in vegetation is attributed to the expansion of housing societies, which typically include open spaces, parks, and areas of vegetation. Government initiatives, such as clean and green projects and the Billion Tree Tsunami project, have also contributed to this increase.

Fig. 6 depicts the land cover characteristics of Lahore's tehsils in 1990, detailing the areas in square kilometers for urban land, water bodies, barren land, and vegetation cover. Fig. 6 presents the land use/land covers of the study area for 2020 at the tehsil level, revealing a significant increase in built-up areas and a decrease in urban green spaces. These study area results indicate that the study area is facing rapid urbanization, which is removing green spaces from the study area. This figure is a valuable tool for understanding the land dynamics within Lahore at the beginning of the study period, providing exact measurements and proportions of these critical land categories in square kilometers.

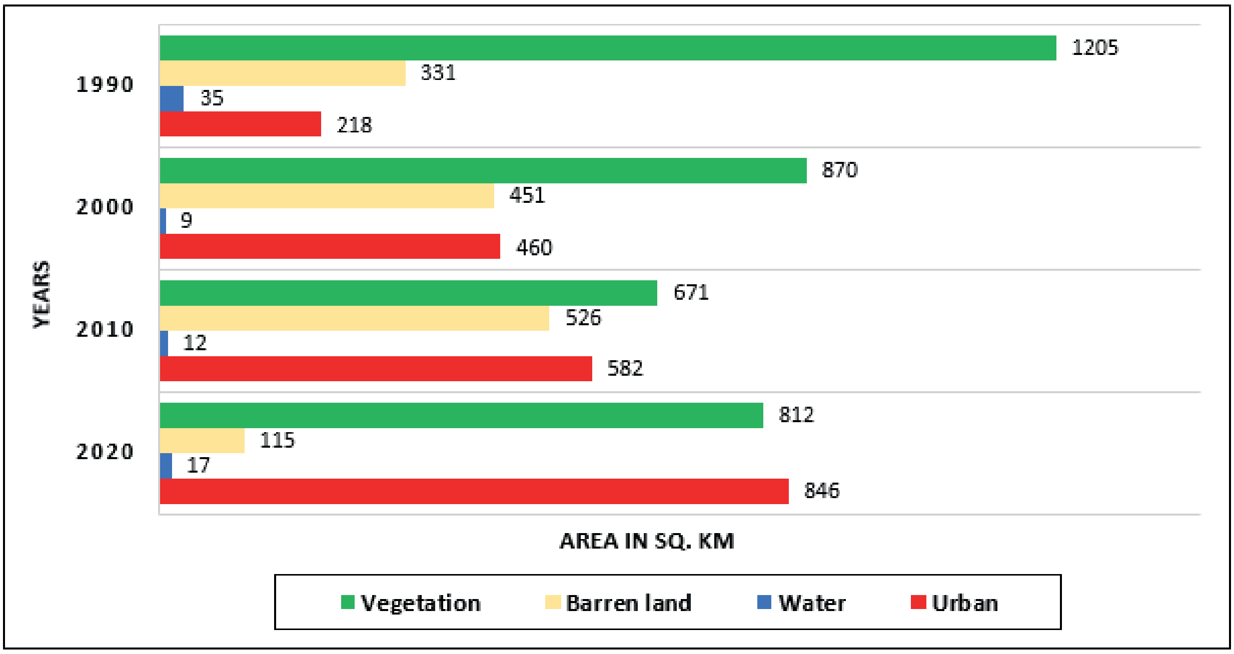

Fig. 4. Temporal statistics of Land cover changes in Lahore

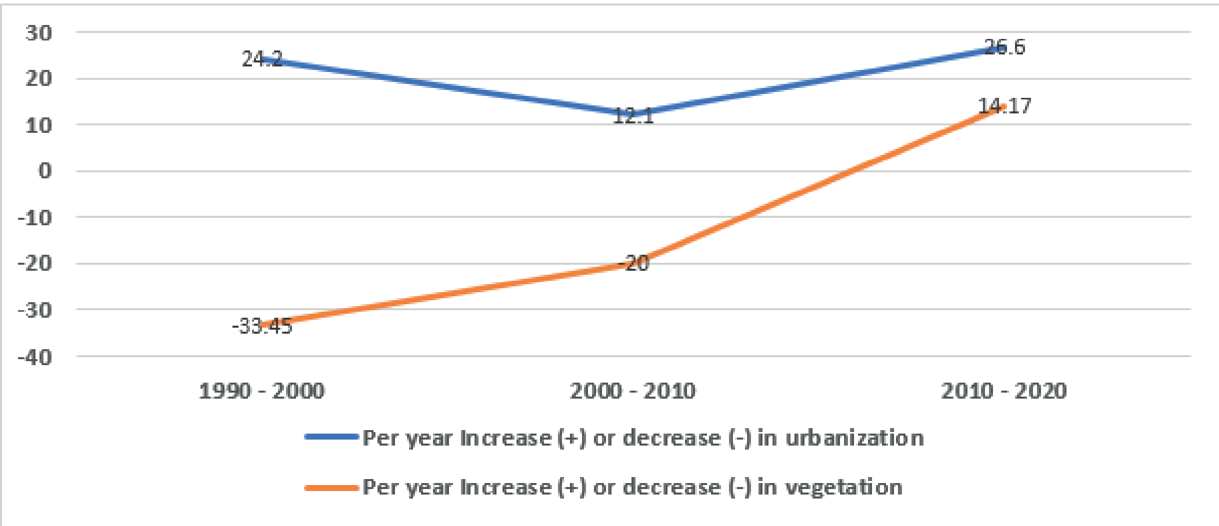

Fig. 5. Increase and decrease in vegetation and urbanization

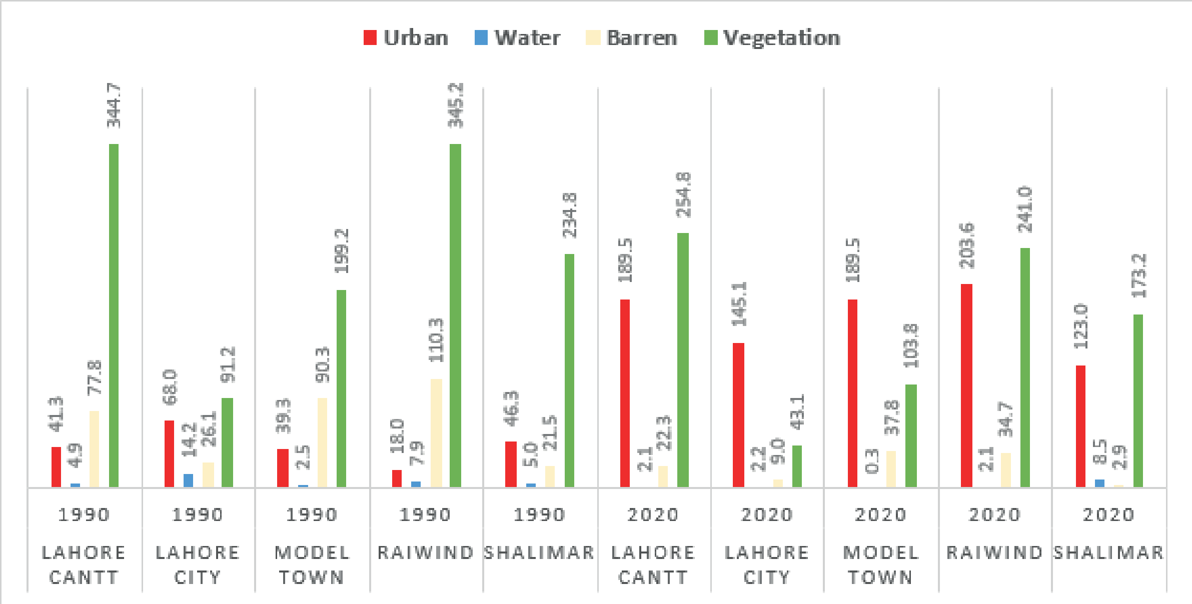

Fig. 6. Land Use/Land Cover changed in Lahore at Tehsil level in 1990 and 2020 in km²

The relationship between population density and Urban Green Spaces (UGS) in Lahore reveals a notable trend, which can be characterized as when population density increases, green spaces diminish. This study analyzed population data to calculate the number of individuals per square kilometer in Lahore, employing population growth rates from the Punjab Bureau of Statistics for various tehsils within the city. The study determined the population and green spaces per person by applying these growth rates for the years 1990, 2000, 2010, and 2020. The results indicate a significant decrease in vegetation across all tehsils of Lahore with increasing population density, illustrating an inverse relationship between population growth and green space availability, as depicted in Fig. 7.

The analysis of land use and land cover changes highlights that urbanization initially centred on the Walled City in 1990 and 2000. However, by 2010 and 2020, areas that were already populated saw further growth, leading to overpopulation, particularly in Shalimar, Cantonment, Gulberg, Samanabad, and Iqbal Town. The expansion of urban areas into these regions is clearly illustrated in the maps for 2010 (Fig. 3(c)) and 2020 (Fig. 3(d)). 1990 Lahore boasted 1205 km^2 of vegetation, with population density concentrated around the walled city. By 2000, urban land expansion led to a reduction in vegetation to 870.5 km^2, a trend that continued into 2010, with vegetation further decreasing to 670.8 km^2 amidst rapid population growth. By 2020, the urban area had expanded to 846.4 km^2, a significant increase from the 218 km^2 in 1990. The transformation of barren land into commercial areas and housing societies, often incorporating green spaces like parks and recreational facilities, led to a slight increase in vegetation by 14.17 km^2 between 2010 and 2020. These findings demonstrate the direct correlation between urbanization, increased population density, and the diminishing availability of green spaces. Fig. 7 provides a comprehensive analysis of the relationship between population density and UGS in Lahore from 1990 to 2020, visually highlighting the inverse correlation between population growth and the preservation of green spaces within the city over the three decades. Fig. 7 also offers a detailed examination of the relationship between population density and urbanization trends in Lahore over the years 1990, 2000, 2010, and 2020. This visual portrayal underscores a pronounced correlation, where population increases are closely linked to expansions in urban built-up areas. It demonstrates that as the population has risen, the extent of the urban built-up area within Lahore has also markedly increased, highlighting the direct connection between demographic changes and urban development in the city. This correlation is critical for understanding urban expansion dynamics and planning for sustainable urban growth, considering the impact on infrastructure, green spaces, and the overall urban ecosystem.

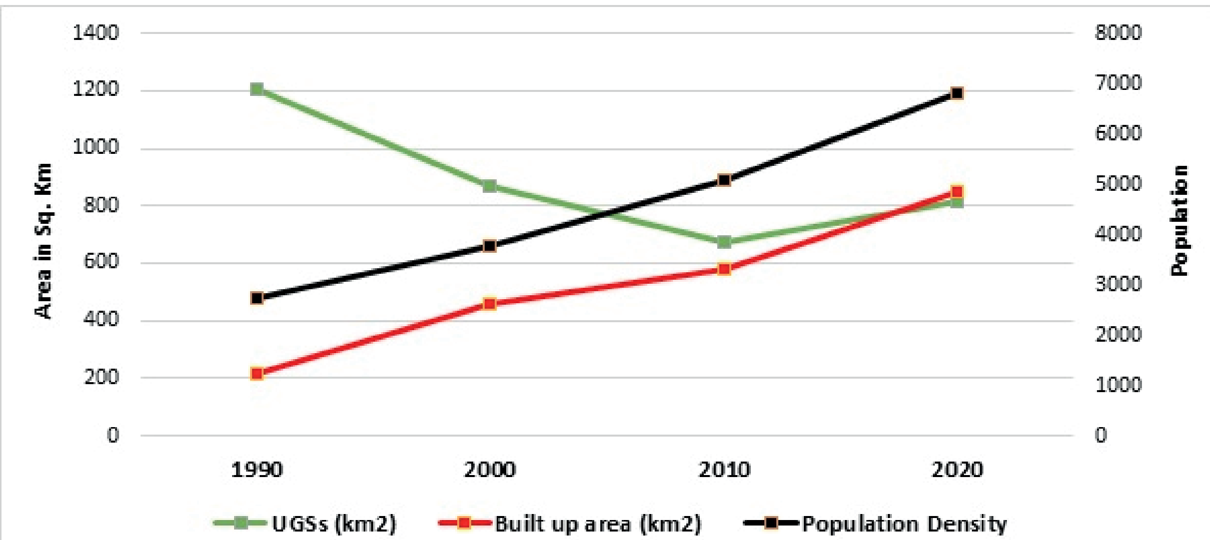

Fig. 7. Correlation between built-up area, UGSs and population density in Lahore

Green Spaces Access to Public

The World Health Organization (WHO) guidelines advocate for a minimum of 9 square meters of green space per person (Alam et al. 2014), serving as a crucial benchmark for designers and city administrators in their planning and remediation efforts (Alam et al. 2014). In Lahore, the 2016-2021 Master Plan proposes a land requirement ratio for open green spaces of 0.50 hectares per 1000 people, equating to 0.0005 hectares or 5 square meters per person. This ratio significantly undercuts the WHO's recommended guideline, highlighting a gap in the city's planning standards.

Furthermore, the Lahore Master Plan also fails to adequately categorize urban green spaces, primarily focusing on recreational spaces such as parks. However, a comprehensive review of the literature demonstrates the necessity of incorporating a variety of green spaces beyond mere recreational areas. Fig. 8 presents a comparative analysis of the urban green spaces available per person within the tehsils of Lahore for the years 1990, 2000, 2010, and 2020, measured in square meters. This analysis provides a detailed examination of the evolution of green space availability per capita over these decades. Most significantly, it displays the changes in urban green spaces concerning population growth, highlighting the effects of urbanization on access to green areas in Lahore.

The findings of this study indicate an abundance of green spaces distributed across all tehsils of Lahore, as shown in Fig. 8. Despite the urban expansion leading to decreased vegetation and a significant decline in green spaces over three decades, the results suggest that Lahore provides sufficient green spaces per person, aligning with the World Health Organization's (WHO) recommendation of a minimum of 9 square meters per person (Alam et al. 2014). However, it is critical to note the potential limitations of these findings due to inaccuracies in data measurement. Additionally, agricultural areas on the outskirts of Lahore were considered green spaces for this analysis, which may influence the overall assessment of urban green space availability.

In this study, overall environmental justice studies are integral to urban management discussions, highlighting the importance of equitable green space distribution among urban populations with important considerations such as ethnicity, culture, and socioeconomic status. These studies examine the spatial allocation of social benefits, including access to green spaces. The results have found that poor neighborhoods often have less access to these essential resources (Xiao et al. 2017; Wu et al. 2021). Since urban parks are a finite natural resource that cannot be provided indefinitely or uniformly across all areas, ensuring equitable access to green spaces is critical in urban planning and management.

Evaluation of SDG 11 Indicator 11.3.1

The evaluation of Sustainable Development Goal (SDG) 11th indicator 11.3.1 involved estimating the surface area occupied by urban areas and the population residing in these areas for each specified year, following the methodology proposed by Nicolau et al. (2018). This assessment aimed to examine the relationship between land consumption and population growth by calculating the land consumption rate (LCR) and population growth rate (PGR) and deriving the ratio of LCR to PGR (LCRPGR).

In Cantt Tehsil and Lahore City Tehsil, the LCRPGR ratio decreased across the periods between the years 1990-2000, 2000-2010, and 2010-2020. This indicates that population growth outpaced land consumption during these periods. Model Town Tehsil saw a decrease in the ratio between 1990-2000 and 2000-2010, suggesting a more substantial population increase than land consumption. However, the ratio increased from 2000-2010 to 2010-2020, reflecting land consumption and population growth. For Raiwind Tehsil, the LCRPGR ratio increased between 1990-2000 and 2000-2010, indicating a higher increase in land consumption relative to population growth. The ratio decreased from 2000-2010 to 2010-2020, indicating that population growth exceeded the land consumption rate during this latter period. In Shalimar Tehsil, a negative

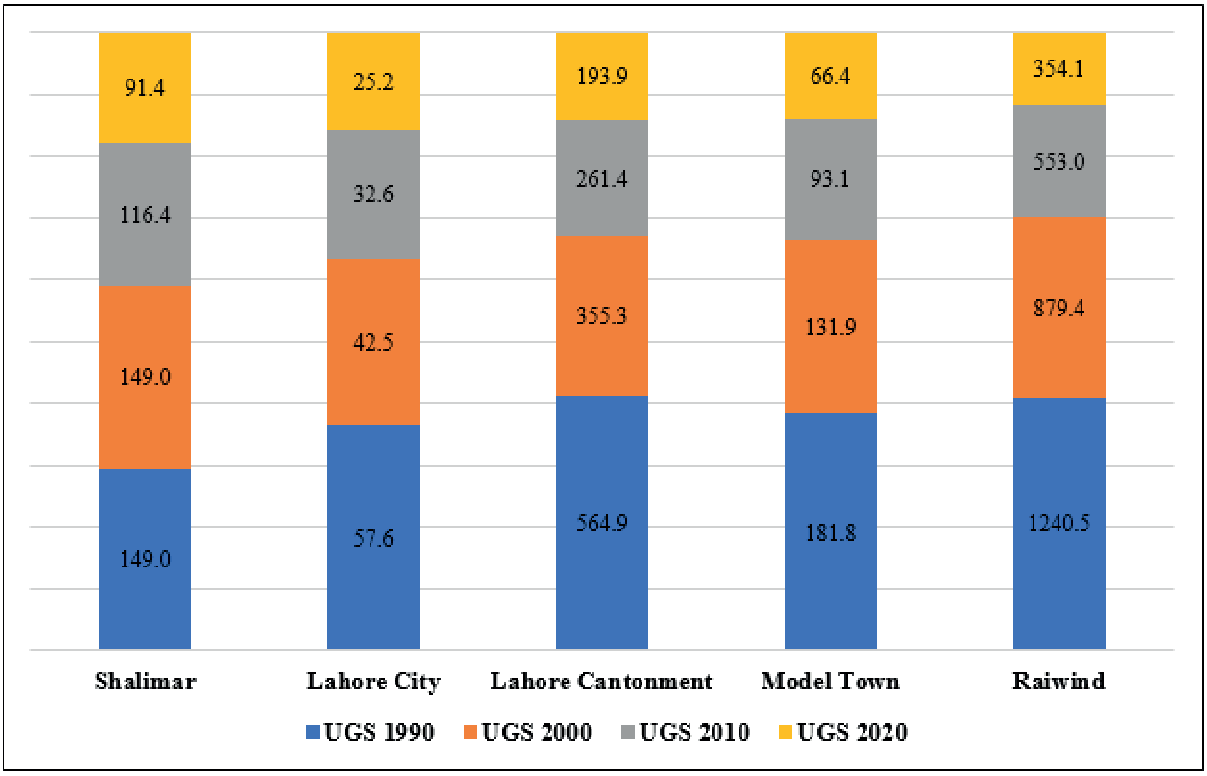

Fig. 8. Urban green spaces per person per meter (1990, 2000, 2010 and 2020)

LCRPGR value during 2000-2010 suggested a decrease in land consumption rate despite population increases, with both metrics showing increases from 2010-2020 (Table 2). These observations reveal intricate dynamics between land consumption and population growth across Lahore's tehsils, underscoring the variability of these trends over time and their implications for urban planning and sustainable development.

DISCUSSION

The detailed land use changes depicted in Fig. 3(a) provide an exhaustive snapshot of Lahore's land cover composition in 1990, shedding light on the initial conditions of urban land, water bodies, barren land, and vegetation cover. To place these findings within a broader context and establish connections with other research endeavors, it is critical to reference studies that examine urbanization patterns, land dynamics, and environmental shifts in rapidly growing cities. The study by Jabbar & Yusoff (2022) on urbanization patterns and their impact on vegetation cover in developing megacities offers valuable insights that may corroborate the observed decrease in vegetation cover in Lahore from 1990 to 2000, demonstrating commonalities in trends amid swift urban expansion.

Furthermore, the investigation conducted by Hanif et al. (2023) into the environmental repercussions of urban growth, particularly in terms of the expansion of built-up areas, can enhance our understanding of the increase in built-up areas in Lahore from 2000 to 2020, enriching the discourse on urbanization dynamics. Additionally, the study and discussion by Jabbar et al. (2021) on the role of green spaces in mitigating urban heat island effects dovetails with the observations in Fig. 3(d), where an uptick in vegetation cover in Lahore in 2020 is noted. This reference may highlight the importance of fostering green spaces within rapidly urbanizing contexts.

The observed diminution in green spaces in Lahore, combined with rising population density, necessitates an in-depth examination of the nexus between urbanization, population growth, and vegetation cover. This study dives into this complex relationship by utilizing population data from various tehsils in Lahore spanning between 1990, 2000, 2010, and 2020. The findings unveil a consistent inverse correlation between population density and vegetation across all tehsils, with the decline in green spaces paralleling increases in population density, as illustrated in Fig. 10. This pattern corroborates with literature such as Dadvand et al. (2019), which articulates the challenges urbanization poses to green spaces and the imperative for sustainable urban planning. The analysis of land use and land cover changes demonstrates the clustering of urbanization around the walled city in the earlier decades, transitioning to intensified population growth in already populated areas in subsequent years. Notably, regions such as Shalimar, Cantonment, Gulberg, Samanabad, and Iqbal Town experienced accelerated urbanization, as evidenced in Figs. 3(c) and 3(d). These trends align with Jabbar & Mohd Yusoff's (2022) findings, accentuating the spatial dynamics of urban growth and its ramifications on population patterns.

The progression from 1990 to 2020 reveals a considerable expansion of urban territories to the detriment of vegetation, revealing the intricate interrelation between urbanization, population density, and the contraction of green spaces over time. This narrative resonates with the research of Duan et al. (2018), which suggests that the sprawl of urbanization detrimentally affects natural landscapes. Furthermore, the observed proliferation of vegetation from 2010 to 2020, alongside a reduction in barren land, hints at initiatives to weave green spaces into the fabric of urban development, resonating with studies like Aboulnaga & Mostafa (2020), which highlight the beneficial impacts of strategic urban development on green area conservation. In summary, this investigation contributes to the expanding collection of research and data that sheds light on the complex intersection among urbanization, population growth, and the conservation of green spaces. By contrasting these findings with existing scholarly works, the overall shared discourse emphasizes the necessity for integrated urban planning approaches that balance the needs of populations with environmental stewardship.

LIMITATIONS

A key limitation of this research is the reliance on population census data from only 1998 and 2017, potentially leading to inaccuracies in calculating growth rates for the specific geographic units under study. The use of population data from disparate years introduces uncertainty in the calculations of population density and the associated rates of change. Furthermore, potential changes in geographic unit boundaries over time present an additional challenge. Such alterations can result in errors when estimating population densities and, by extension, impact the precision of change rate calculations.

CONCLUSION

The study highlights the changes in land cover from 1990 to 2020 and offers a thorough analysis of Lahore's rapid development and reduction in vegetation. It clarifies how and in what ways human activity and natural processes can affect the urban environment. It also highlights the challenges posed by the growth and expansion of housing societies. The research provides valuable insights for stakeholders like the Environment Protection Department and the Lahore Development Authority through an

Table 2. The ratio of land consumption rate to population growth rate

LCRPGR	1990 – 2000	2000 - 2010	2010 - 2020
Lahore Cantt	1.576	0.18	0.154
Lahore City	0.999	0.16	0.146
Model Town	0.343	0.013	0.121
Raiwind	0.685	1.01	0.107
Shalimar	0.409	-0.491	0.209

urban landscape matrix analysis, leading to well-informed decision-making to prevent the loss of green spaces. The study also emphasizes how vital green spaces are to urban well-being and how crucial it is to incorporate these areas into plans for urban growth. It further accentuates the requirement of resilience and sustainability in urban planning and pushes for a balanced approach to regulating land use and population density. The study's recommendations emphasize the importance of remote sensing methods and spatiotemporal analysis for efficient urban planning and management. The concept proposes a financially viable model for continuous urban study and monitoring that utilizes publicly available satellite images for periodic analysis. It is recommended that policymakers give precedence to sustainable urbanization initiatives, ensuring that green space planning is incorporated into development initiatives. This strategy improves the well-being of residents and urban biodiversity, and it synchronizes Lahore's urban development with environmental conservation objectives. By implementing the strategies above, Lahore may balance urban growth with ecological integrity and create a resilient and sustainable urban future.

REFERENCES

Aboulnaga M. and Mostafa M. (2020). Climate Change Adaptation: Prioritizing Districts for Urban Green Coverage to Mitigate High Temperatures and UHIE in Developing Countries. In: Sayigh, A. (eds) Renewable Energy and Sustainable Buildings. Innovative Renewable Energy. Springer, Cham., 825-837, DOI: 10.1007/978-3-030-18488-9_68 Alam R., Shirazi S.A., Bhalliand M.N. and Zia S. (2014). Spatial distribution of urban green spaces in Lahore, Pakistan: A case study of Gulberg Town. Pakistan Journal of Science, 66(3), 277-281

Bhalli M.N., Ghaffar A. and Shirazi S.A. (2012a). Spatio-temporal Patterns of Urban Growth in Faisalabad-Pakistan: A GIS Perspective. Journal of Research Society of Pakistan, 49(1), 115-134

Bhalli M.N., Ghaffar A. and Shirazi S.A. (2012b). Remote Sensing and GIS Applications for Monitoring and Assessment of the Urban Sprawl in Faisalabad-Pakistan. Pakistan Journal of Science, 64(3), 203-208

Bhalli M.N., Ghaffar A., and Shirazi S.A. and Parveen N. (2013). Use of Multi-Temporal Digital Data to Monitor LULC Changes in Faisalabad-Pakistan. Pakistan Journal of Science, 65(1), 58-62

Bhalli M.N. and Ghaffar A. (2015). Use of Geospatial Techniques in Monitoring Urban Expansion and Land Use Change Analysis: A Case of Lahore, Pakistan. Journal of Basic & Applied Sciences, 11, 265-273

Bratman G.N., Hamilton J.P., Hahn K.S., Daily G.C. and Gross J.J. (2012). Nature experience reduces rumination and subgenual prefrontal cortex activation. Proceedings of the National Academy of Sciences, 112(28), 8567-8572

Brown C., Bramley G. and Watkins D. (2010). Urban Green Nation: Building the evidence base. Commission for Architecture and the Built Environment

Chen W., Liu Y., Li F., Xiao R., and Tian Y. (2022). Impacts of urban expansion on hydrological processes: A review. Journal of Hydrology, 606, 127057

Dadvand P., Hariri S., Abbasi B., Heshmat R., Qorbani M., Motlagh M.E., Basagaña X., and Kelishadi R. (2019). Use of green spaces, self-satisfaction, and social contacts in adolescents: A population-based CASPIAN-V study. Environmental Research, 168, 171–177, DOI: 10.1016/j.envres.2018.09.033

Duan J., Wang Y., Fan C., Xia B., and de Groot R. (2018). Perception of urban environmental risks and the effects of urban green infrastructures (UGIs) on human well-being in four public green spaces of Guangzhou, China. Environmental Management, 62(3), 500–517, DOI: 10.1007/s00267-018-1068-8

Dwyer J.L., Roy D.P., Sauer B., Jenkerson C.B., Zhang H.K., and Lymburner L. (2018). Analysis ready data: enabling analysis of the Landsat archive. Remote Sensing, 10(9), 1363

Elmqvist T., Setälä H., Handel S.N., and Van Der Jagt A.P.N. (2020). Benefits of green spaces in urban environments. In: Handbook on Urban Development and Management in the Global South: Edward Elgar Publishing,209-228

Fatima M., Butt I., Nasar-u-Minallah M., Atta A., and Cheng G. (2023). Assessment of Air Pollution and Its Association with Population Health: Geo-Statistical Evidence from Pakistan. Geography, Environment, Sustainability, 16(2), 93-101, DOI: 10.24057/2071-9388-2022-155

Fletcher T.D., Shuster W., Hunt W.F., Ashley R., Butler D., Arthur S., and Semadeni-Davies A. (2019). SUDS, LID, BMPs, WSUD and more – The evolution and application of terminology surrounding urban drainage. Urban Water Journal, 16(7), 631-648

Garcia D., Zaragoza-Castells J., Cabeza M., and Oviedo J.L. (2019). Urban forests reduce ozone concentrations in the streets of Mediterranean cities. Environmental Pollution, 249, 869-877

Gascon M., Triguero-Mas M., Martinez D., Dadvand P., Rojas-Rueda D., Plasència A., and Nieuwenhuijsen M.J. (2022). Residential green spaces and mortality: A systematic review. Environment International, 161, 106959

GOP (2000) District Census Report of Lahore 1998. Population Census Organization, Statistics Division. Govt. of Pakistan, Islamabad

GOP (2013) Punjab Development Statistics 2011.Bureau of Statistics, Govt. of the Punjab, Lahore

Grimm N.B., Faeth S.H., Golubiewski N.E., Redman C.L., Wu J., Bai X., and Briggs J. M. (2021). Global change and the ecology of cities. Science, 319(5864), 756-760

Hanif A., Nasar-u-Minallah M., Zia S., Ashraf I. (2022) Mapping and Analysing the Park Cooling Intensity in Mitigation of Urban Heat Island Effect in Lahore, Pakistan. Korean Journal of Remote Sensing, 38(1), 127-137, DOI: 10.7780/kjrs.2022.38.1.10

Hanif A., Shirazi S.A., Jabbar M., Liaqat A., Zia S., and Yusoff M.M. (2023). Evaluating the Visitors' Perception and Available Ecosystem Services in Urban Parks Of Lahore (Pakistan) Research Paper. Geography, Environment, Sustainability, 15(4), 32–38

Jabbar M., and Mohd Yusoff M. (2022). Assessing and modelling the Role of Urban Green Spaces for Human Well-being in Lahore (Pakistan). Geocarto International, just-accepted, 1–21.

Jabbar M., and Yusoff M.M. (2022). Assessing The Spatiotemporal Urban Green Cover Changes and Their Impact on Land Surface Temperature and Urban Heat Island in Lahore (Pakistan). Geography, Environment, Sustainability, 15(1), 130–140.

Jabbar M., Nasar-u-Minallah M., and Yusoff M.M. (2024a). Measuring and modelling the association between human psychological well-being and urban green spaces of Lahore, Pakistan, Journal of Environmental Studies, and Sciences, DOI: 10.1007/s13412-024-00895-4

Jabbar M., Yusoff M.M., and Shafie A. (2021). Assessing the role of urban green spaces for human well-being: A systematic review. GeoJournal, DOI: 10.1007/s10708-021-10474-7

Lin Y. (2021). Mapping the Urban Impervious Surfaces at Different Scales Using Multisource Satellite Data (Doctoral dissertation, The Chinese University of Hong Kong (Hong Kong)).

Mazhar N., Nasar-u-Minallah M., Shirazi S.A. et al. (2024). Spatio-temporal patterns and dynamics of sensitivity to sandification, in the Drylands of South Punjab, Pakistan. GeoJournal, 89, (15), DOI: 10.1007/s10708-024-11014-9

Megahed Y, Cabral P, Silva J, and Caetano M. (2015). Land cover mapping analysis and urban growth modelling using remote sensing Techniques in greater Cairo region—Egypt. ISPRS Int J Geo-Inf, 4(3),1750–1769. DOI: 10.3390/ijgi4031750.53.

Minallah M.N., Ghaffar A., Rafique M., and Mohsin M. (2016a) Urban Growth and Socio-Economic Development in Gujranwala, Pakistan. Pakistan Journal of Science, 68(2), 176-183.

Minallah M.N., Rafique M., Anwar M.M., and Mohsin M. (2016b). Assessing the Urban Growth and Morphological Patterns of Gojra City, Pakistan. Sindh University Research Journal (Science Series), 48(2), 393-398.

Mukherjee M., and Takara K. (2018). Urban green space as a countermeasure to increasing urban risk and the UGS-3CC resilience framework. International Journal of Disaster Risk Reduction, 28, 854–861. https://doi.org/10.1016/j.ijdrr.2018.01.027

Mumtaz M. (2019). Climate change adaptation in the agriculture sector: an analysis of governance challenges in two Pakistani provinces (Doctoral dissertation).

Mundia C.N., and Aniya M. (2005). Analysis of land use/cover changes and urban expansion of Nairobi city using remote sensing and GIS. International Journal of Remote Sensing, 26(13), 2831-2849.

Mustafa D., and Sawas A. (2013). Urbanization and Political Change in Pakistan: exploring the known unknowns. Third World Quarterly, 34(7): 1293-1304.

Nadeem M., Aziz A., Al-Rashid M.A., Tesoriere G., Asim M., & Campisi T. (2021). Scaling the potential of compact city development: The case of Lahore, Pakistan. Sustainability, 13(9), 5257.

Nasar-u-Minallah M., (2018). Spatial and Temporal Change Assessment in Land Surface Temperature of Lahore using GIS and Remote Sensing Techniques. Proceedings of the Pakistan Academy of Sciences: A. Physical and Computational Sciences, 55 (3): 67–75.

Nasar-u-Minallah M. (2019). Retrieval of Land Surface Temperature of Lahore through Landsat-8 TIRS Data. International Journal of Economic and Environmental Geology, 10 (1), 70-77. https://doi.org/10.46660/ijeeg.Vol10.Iss1.2019.220

Nasar-u-Minallah M. (2020). Exploring the Relationship between Land Surface Temperature and Land use change in Lahore using Landsat Data. Pakistan Journal of Scientific & Industrial Research Series A: Physical Sciences. 63A (3), 188-200.

Nasar-u-Minallah M., and Ghaffar A. (2020). Temporal Variations in Minimum, Maximum and Mean Temperature Trends of Lahore-Pakistan during 1950-2018. Proceedings of the Pakistan Academy of Sciences: A. Physical and Computational Sciences: 57 (2): 21-33.

Nasar-u-Minallah M., Zia S., Rahman A., and Riaz O. (2021). Spatio-Temporal Analysis of Urban Expansion and Future Growth Patterns of Lahore, Pakistan. Geography, Environment, Sustainability. 14(3):41-53. https://doi.org/10.24057/2071-9388-2020-215

Nasar-u-Minallah M., Haase D., Qureshi S., Zia S. Munnaza, F. (2023). Ecological monitoring of urban thermal field variance index and determining the surface urban heat island effects in Lahore, Pakistan. Environ Monit Assess 195, 1212. https://doi.org/10.1007/s10661-023-11799-1

Nicolau R., David J., Caetano M., and Pereira J. (2018). The Ratio of Land Consumption Rate to Population Growth Rate—Analysis of Different Formulations Applied to Mainland Portugal. ISPRS International Journal of Geo-Information, 8(1), 10. https://doi.org/10.3390/ijgi8010010

Nicolau R., David J., Caetano M., and Pereira J.M. (2018). The ratio of land consumption rate to population growth rate—Analysis of different formulations applied to mainland Portugal. ISPRS International Journal of Geo-Information, 8(1), 10.

Onder S., and Kocbeker Z. (2012). Importance of the green belts to reduce noise pollution and determination of roadside noise reduction effectiveness of bushes in Konya, Turkey. International Journal of Agricultural and Biosystems Engineering, 6(6), 373-376.

Paudel S. and Yuan F. (2012). Assessing landscape changes and dynamics using patch analysis and GIS modelling. Int J Appl Earth Obs Geoinf., 16(1), 66–76. https://doi.org/10.1016/j.jag.2011.12.003.

Pervaiz S., Javid K., Khan F.Z. Talib B., Siddiqui R., Ranjha M. M., and Akram M.A.N. (2019). Spatial analysis of vegetation cover in urban green space under new government agenda of clean and green Pakistan to tackle climate change. Journal of Ecological Engineering, 20(4).

Puplampu D. A., and Boafo Y.A. (2021). Exploring the impacts of urban expansion on green spaces availability and delivery of ecosystem services in the Accra metropolis. Environmental Challenges, 5, 100283.

Rana I.A. and Bhatti S.S. (2018). Lahore, Pakistan–Urbanization challenges and opportunities. Cities, 72, 348-355.

Rana I., and Bhatti S. (2018). Lahore, Pakistan – Urbanization challenges and opportunities. Cities, 72, 348-355. https://doi.org/10.1016/J.CITIES.2017.09.014

Rana I., Bhatti S., and Arshad H.S. (2017). Assessing the socioeconomic and infrastructure development disparity – a case study of city districts of Punjab, Pakistan. International Journal of Urban Sustainable Development, 9, 346-358. https://doi.org/10.1080/19463138.2017.1320286

Rigolon A., Browning M.H., Lee K., and Shin, S. (2018). Access to urban green space in cities of the Global South: A systematic literature review. Urban Science, 2(3), 67.

Riaz O. (2013). Urban change detection of Lahore (Pakistan) using a time series of satellite images since 1972. Asian journal of natural and applied sciences, 2(4), 101-104.

Sahar J., Nasar-u-Minallah M., Parveen N., and Zia S. (2023). Desertification vulnerability assessment through geospatial techniques in Bahawalpur division of Punjab, Pakistan. GeoJournal. 88(6), 6035-6052. https://doi.org/10.1007/s10708-023-10955-x

Saleem S., and Saleem, S. (2016). Spatial and temporal evolution of vegetation cover in Lahore, Pakistan. Bulletin of Environmental Studies, 1(3), 82.

Saleemi M.U. (2015). Urban change detection of Lahore (Pakistan) using the Thematic Mapper Images of Landsat since 1992–2010. In Proceedings of the Fourth International Conference on Aerospace Science and Engineering (ICASE 2015), Islamabad, Pakistan (Vol. 2).

Schiopu N. and Teodosiu C. (2021). The role of urban green spaces in mitigating the effects of climate change in the context of urbanization. Sustainability, 13(15), 8399.

Schlosberg D. 2007. Defining environmental justice: theories, movements, and nature. Oxford: Oxford University Press.

Semeraro T., Scarano A., Buccolieri R., Santino A., and Aarrevaara E. (2021). Planning of urban green spaces: An ecological perspective on human benefits. Land, 10(2), 105.

Shakrullah K. (2019). An assessment of land use and land cover changes in Lahore (Pakistan) and New Delhi (India) using geospatial techniques. Pakistan Journal of Science, 71(4).

Shen Z., Liu S., Cao J., Chen Q., Liu M., Wang S., and Wu J. (2022). Effects of urban green space on urban heat island effects: A review. Journal of Cleaner Production, 341, 130757.

Shirazi S. A., and Kazmi J.H. (2016). Analysis of socio-environmental impacts of the loss of urban trees and vegetation in Lahore, Pakistan: a review of public perception. Ecological Processes, 5(1), 1-12.

Shirazi S.A., and Kazmi S. (2014). Analysis of Population Growth and Urban Development in Lahore-Pakistan Using Geospatial Techniques: Suggesting Some Future Options. South Asian Studies, 29, 269.

Shirazi S.A., and Kazmi S.J.H. (2014). Analysis of population growth and urban development in Lahore-Pakistan using geospatial techniques: Suggesting some future options. South Asian Studies, 29(01), 269-280.

Sidhu N., Pebesma E., and Câmara, G. (2018). Using Google Earth Engine to detect land cover change: Singapore as a use case. European Journal of Remote Sensing, 51(1), 486-500.

Soga M., Yamano H. and Koike S. (2022). Impacts of urban expansion on biodiversity: A global synthesis. Landscape and Urban Planning, 227, 105026.

Tsai Y. H. Stow D., Chen H. L., Lewison R., An L., and Shi L. (2018). Mapping vegetation and land use types in Fanjingshan National Nature Reserve using Google Earth engine. Remote Sensing, 10(6). https://doi.org/10.3390/rs10060927

UNDP, U. (2019). Population Growth: Implications for Human Development.

UN-Habitat. (2021). SDG11.3.1Metadata.

Wu L., and Kim S. K. (2021). Exploring the equality of accessing urban green spaces: A comparative study of 341 Chinese cities. Ecological Indicators, 121, 107080.

Xiao Y., Lu Y., Guo Y., and Yuan Y. (2017). Estimating the willingness to pay for green space services in Shanghai: Implications for social equity in urban China. Urban Forestry & Urban Greening, 26, 95-103.

Zia S., Yaqoob S., Nasar-u-Minallah M., Hanif A., Aslam A., (2021a) Relationship Analysis between Vegetation and Traffic Noise Pollution: A Case Study of Lahore, Pakistan. International Journal of Economic and Environmental Geology, 12 (3) 65-69. https://doi.org/10.46660/ijeeg.Vol12.Iss3.2021.624

Zia S., Shirazi S. A. Nasar-u-Minallah M., (2021b) Vulnerability Assessment of Urban Floods in Lahore, Pakistan using GIS-based integrated Analytical Hierarchy Approach. Proceedings of the Pakistan Academy of Sciences: A. Physical and Computational Sciences: 58(1), 85-96.

Zia S., Shirazi S. A., Nasar-u-Minallah M., Batool, M., (2021c) Urban Floods and Suitability Analysis of Rainwater Harvesting Potential Areas in Lahore City, Pakistan. International Journal of Economic and Environmental Geology, 12 (2), 13-20. https://doi.org/10.46660/ijeeg.Vol12.Iss2.2021.581

Zia S., Mohsin M., Nasar-u-Minallah M., and Hanif A. (2022). Site Suitability Analysis for Urban Settlements along River Jhelum, Pakistan using GIS and Remote Sensing Techniques. Indonesian Journal of Geography, 54(2), 223 – 239. https://doi.org/10.22146/ijg.72354

Zia S., Nasar-u-Minallah M., Zahra N., Hanif A. (2022). The Effect of Urban Green Spaces in Reducing Urban Flooding in Lahore, Pakistan, Using Geospatial Techniques, Geography, Environment, Sustainability, 3(15), 47-55. https://DOI-10.24057/2071-9388-2021-135

Zia S., Ashraf A., Nasar-u-Minallah M., Hanif A., and Parveen N. (2023). Parametric Study of Urban Morphology on Buildings Solar Energy Potential: A Case Study of Model Town Lahore, Pakistan. Pakistan Journal of Science, 75 (3), 586-597

Zhang Y., Feng Q., Wang R., Zhou D., Cai J., Chen Y., and Wu J. (2021). Impacts of urbanization on biodiversity and ecosystem services in China: A synthesis of current knowledge and research gaps. Landscape Ecology, 36(5), 1297-1317.

RESEARCH PAPER

IMPACT OF TOURISM ON PRISTINE HABITATS AT THE AVACHINSKY PASS (KAMCHATKA), A WORLD HERITAGE SITE

I. Popov[1*], A. Moiseev[2], A. Iurmanov[3], A. Romanov[2], E. Karpov[4], K. Orlova[5], N. Tereshchenko[6], E. Emets[7], Y. Lebedev[8], A. Gnedenko[9]

[1]Department of Applied Ecology, Faculty of Biology, St. Petersburg State University, 7/9 Universitetskaya nab., St. Petersburg, 199034, Russia

[2]Moscow State University, Faculty of Geography, Leninskie Gory, 1, Moscow, Russia

[3]K.A. Timiryazev Institute of Plant Physiology Russian Academy of Sciences, st. Botanicheskaya, 35, Moscow, 127276, Russia

[4]Nature park «Vulcani Kamchatki» (684000, 33 Zavoyko st., Elizovo, Kamchatskiy krai, Russia

[5]V.V. Dokuchaev Soil Science Institute, Department of soil genesis, geography and classification, 7 building 2, Pyzhyovskiy lane, Moscow, 119017, Russia

[6]University of Göttingen. Wilhelmsplatz 1, 37073 Göttingen, Germany

[7]Vitus Bering Kamchatka State University, st. Pogranichnaya, 4, Petropavlovsk-Kamchatsky, 683032, Kamchatka Krai, Russia

[8]Peoples' Friendship University of Russia, st. Miklukho-Maklaya, 6, Moscow, 117198, Russia

[9]Institute of Geography Russian Academy of Sciences, st. Staromonetniy, 29, Moscow, 119017, Russia

*Corresponding author: i.y.popov@spbu.ru

Received: November 5th 2023 / Accepted: April 10th 2024 / Published: July 1st 2024

https://DOI-10.24057/2071-9388-2024-3111

ABSTRACT. The volcanoes of Kamchatka are a World Heritage Site. They are of aesthetic, conservation, and scientific value; therefore, they must be protected from negative anthropogenic influences. However, according to the recent assessment by the International Union for Conservation of Nature, this site inspires significant concern. A similar viewpoint was also expressed in the local press. A part of the site, Avachinsky Pass, inspires a particular concern. This is a place between the volcanoes Koryaksky and Avachinsky. An excessive number of visitors was considered the main threat because it resulted in the trampling of soil and the extirpation of threatened animals. We performed a survey of the Avachinsky Pass aiming to estimate its state. Based on aerial pictures and observation we composed a scheme of habitats over the area around Avachinsky Pass revealing the disturbed plots of land. Moreover, we registered vertebrates considering them as biological indicators. It became clear that tourism has a significant impact on the state of the Avachinsky Pass, but the affected area is relatively small. Despite a large number of visitors, the survey revealed high biodiversity. We registered 19 species of birds and 9 species of mammals. Among them, black-capped marmots are especially informative as they have a settled way of life; they do occur on the Pass. The absence of grazing and logging contributes to the conservation of elfin forests and other plant communities on the slopes making the object resistant to anthropogenic impacts. Off-road vehicles pose the biggest threat to bare-ground revegetation.

KEYWORDS: biodiversity, habitats, Kamchatka, mammals, mountains, tourists

CITATION: Popov I., Moiseev A., Iurmanov A., Romanov A., Karpov E., Orlova K., Tereshchenko N., Emets E., Lebedev Y., Gnedenko A. (2024). Impact Of Tourism On Pristine Habitats At The Avachinsky Pass (Kamchatka), A World Heritage Site. Geography, Environment, Sustainability, 2(17), 18-25

https://DOI-10.24057/2071-9388-2024-3111

ACKNOWLEDGEMENTS: The authors are grateful to the administration of Nature Park «Vulkany Kamchatki» and Sports and Training Center for Winter Sports «Avachinsky» for the assistance in field work, and Veronika Ildarovna Mikhl for the correction of the English language. Igor Popov acknowledges the support from the Russian Science Foundation, project No 23-24-00031. Anton Iurmanov thanks the Ministry of Science and Higher Education of the Russian Federation for the assistance.

Conflict of interests: The authors reported no potential conflict of interest.

INTRODUCTION

World Heritage Sites work as an effective measure of environmental conservation as they cover particularly picturesque landscapes, habitats of threatened species, and areas of high biodiversity (Osipova et al. 2017). Several sites are tourist attractions and their role in this respect is continuously increasing (Bak et al. 2019; Job et al. 2017; Li et al. 2008; Yang et al. 2019). However, tourism can have a significant negative impact on the environment (Cherkasova et al. 2022; Newsome et al. 2002; Pickering and Hill 2007; Sun and Walsh 1998; Zhong et al. 2011). One of the heritage sites negatively affected by tourism is «Volcanoes of Kamchatka». According to the assessment of the International Union for the Conservation of Nature, it is of significant concern (Osipova et al. 2017), which is also shared by the local press. Recently it was claimed that a part of the site is in a "crisis" (Nenasheva et al. 2020). This means that off-road movements by vehicles, development, trampling soil and plants, and the extirpation of animals are progressing in Avachinsky Pass, an area on the slopes of two volcanoes. Therefore, the necessity to conduct a survey aimed at assessing of the Avachinsky Pass state became evident. We completed this work in 2021. We focused primarily on biodiversity, we found out what animals and plants occur there, and analyzed them as biological indicators. These data represent interest not only in respect of the "local crisis", but in the context of discussing the normal state of mountain ecosystems, the anthropogenic impact on them, and the organization of tourism in protected wildlife areas.

Study area, methods

Avachinsky Pass is a strip of land between Avachinsky and Koryaksky volcanoes. The first one is 2741 m high, the second - 3456 m. Both volcanoes are active. Avachinsky is one of the most active volcanoes in Kamchatka: fifteen eruptions have been recorded since 1737, the last one happened in 1991. The eruptions of Koryaksky have been less frequent; only three eruptions have been registered so far, the last one occurred in 2008. On the upper point of the Pass, a picturesque mountain with rocks on the top is located. It is called Verbliud, which means "camel" because of the hump-looking two peaks. It is assumed that the mountain is either a result of the Koryaksky volcano's extrusive activity (when the protruding viscous lava piled on the surface and subsequently solidified) or the result of a strong eruption of Avachinsky volcano[1].

Avachinsky and Koryaksky volcanoes are called "home volcanoes" for Petropavlovsk-Kamchatsky, the main city of Kamchatka. They are an important attraction for the locals and numerous tourists. Several thousand of them visit the Pass and volcanoes every year, and this number continuously increases. This site is popular all year round. In summer, hikers and volcano-climbers visit the Pass for its picturesque views. In winter, it attracts skiers and snowboarders[2]. The Pass is a part of the protected area Nalychevo Nature Park. The access to the Pass used to be restricted, but since 2020 it has been declared a free-access area. This decision raised concerns among scientists (Nenasheva et al. 2020). The way to the volcanoes passes through the Sukhaya River valley (its name means "dry"). During the season of intense snowmelt, the mud slurry runs through it, but afterwards the river dries out and its bottom is used as a road. The source of the river is located at the Verbliud mountain; therefore, it is accessible by car (Chernomorets et al. 2010). The use of vehicles in the Pass is forbidden, but this ban is often violated.

Most studies conducted in this area are devoted to the monitoring of the activity of Avachinsky and Koryaksky volcanoes because of the high motivation of local authorities to predict possible volcanic catastrophes that may affect Petropavlovsk-Kamchatsky (Girina et al. 2019). However, biodiversity also attracts attention: several botanical researches have been performed at these volcanoes over the past decades. A list of local flora was their main result; it includes 235 species of vascular plants (Yakubov et al. 2001). No similar species count has been made for animals, but three animal species were studied at the Pass: black-capped marmot (*Marmota camtschatica*), North American ground squirrel (*Spermophilus parryii*), and red fox (*Vulpes vulpes*). The first was seldom encountered; their disturbance by visitors was pointed out (Zykov 2017; Nenasheva et al. 2020). The other two species, on the contrary, tend to become synanthropic at the Pass; they often occur near houses and roads.

For our survey of the Pass, we used a method of direct investigation. The walk routes were arranged in such a way that they crossed various biotopes and gave a comprehensive vision of the territory. We described the vegetation, recorded birds, mammals or their traces (since there were numerous plots covered by snow, the footprints were well visible) and the signs of human activities. Special attention was paid to black-capped marmots as their settlements are relatively stationary and therefore, they serve as a tourism impact indicator. Combining the results of the survey with the aerial photos (Google and Sentinel-2) and cartographic materials we composed a map of habitats. Identification of habitats was carried out in accordance with the guidelines summarized by V.K. Zhuchkova and E.M. Rakovskaya (2004). The observations were carried out from June 23 to June 27, and then from September 11 to 22, 2021.

Results

The routes covered an area of 816 hectares. We surveyed a part of the Sukhaya river valley, the slopes around, the Pass itself, the Verbliud mountain, a part of the slopes of Avachinsky and Koriaksky volcanoes. Eight kinds of habitats have been identified: open ground areas without vegetation, plots with sparse pioneer vegetation (plants cover 3-5% of the surface), plots with pioneer vegetation (about 20%), stony tundra, grassy tundra, disturbed meadow tundra, sparse elfin woodland, disturbed communities dominated by ruderal species. These plots form a "mosaic" in which small plots with different patterns of vegetation alternate, the performed routes covered all of them (Fig. 1, Fig. 2, Table 1).

There are several buildings at the Pass – tourist bases and control posts. A part of surrounding plots of land were either trampled or covered by ruderal vegetation; littered plots also occurred there. Total area of such plots was 31.7 hectares. Moreover, traces of vehicles, trails and other evidence of touristic activity were found on the open ground areas, plots with pioneer vegetation located on the bottom of the Sukhaya River, around Verbliud mountain and at the narrowest section of the Pass (Fig. 1). Such traces are almost absent at the slopes of the Sukhaya River valley. Verbliud mountain was the center of attraction of visitors; it was covered by a network of trails. The top of the mountain

[1]Special protected natural areas of Russia [Online]. (2005). Available from: http://oopt.aari.ru/ref/597 (Accessed: 17th of February 2022)
[2]Kamchatka Volcanoes Nature Park [Online]. (2011). Available from: http://vulcanikamchatki.ru/ (Accessed: 15th of February 2022)

was trampled, vegetation was absent at the area of 700 m^2. There are also trails to the tops of volcanoes, but they are not numerous and do not cover a significant area.

We recorded the traces of hare (*Lepus timidus*), bear (*Ursus arctos*), fox (*Vulpes vulpes*), wolf (*Canis lupus*), snow sheep (*Ovis nivicola*), wolverine (*Gulo gulo*), lynx (*Lynx lynx*); observed and photographed marmot, fox, bear, and ground squirrels. We failed in our attempts to record small rodents and insectivores, finding neither holes nor traces, and only observing domestic mouse (*Mus musculus*) near the buildings. Mammals occurred mostly on the slopes of the river valley. Ground squirrels were numerous; they concentrated at the dry bottom of the river next to the road and houses; they were hardly afraid of humans and eagerly took the food offered by visitors. The other mammals did not approach the houses, but some of them were registered at the frequently visited plots located at the center of the Pass. It turned out that a settlement of marmots exists on the top of Verbliud mountain and nearby. Snow sheep were also registered on the mountain; their traces were found on the highest point, which is the main attraction for tourists.

As for the birds, 19 species have been recorded: Lesser Sand Plover (*Charadrius mongolus*), Common Cuckoo (*Cuculus canorus*), Rock Ptarmigan (*Lagopus muta*), Common Raven (*Corvus corax*), Kamchatka Leaf Warbler (*Phylloscopus examinandus*), Siberian Rubythroat (*Luscinia calliope*), Northern Red-flanked Bluetail (*Tarsiger cyanurus*), Brown-headed Thrush (*Turdus chrysolaus*), Olive-backed Pipit (*Anthus hodgsoni*), Buff-bellied Pipit (*Anthus rubescens*), Grey Wagtail (*Motacilla cinerea*), Oriental Greenfinch (*Chloris sinica*), Brambling (*Fringilla montifringilla*), Common Redpoll (*Acanthis flammea*), Common Rosefinch (*Carpodacus erythrinus*), Pine Grosbeak (*Pinicolae nucleator*), Asian Rosy-finch (*Leucosticte arctoa*), Grey Bunting (*Ocyris variabilis*), Snow Bunting (*Plectrophenax nivalis*). The birds occurred over the whole surveyed area including the central part with scarce vegetation. One bird species, Lesser Sand Plover, prefers this very habitat. Although near the Verbliud mountain the plant cover is so poor, that even this bird is absent.

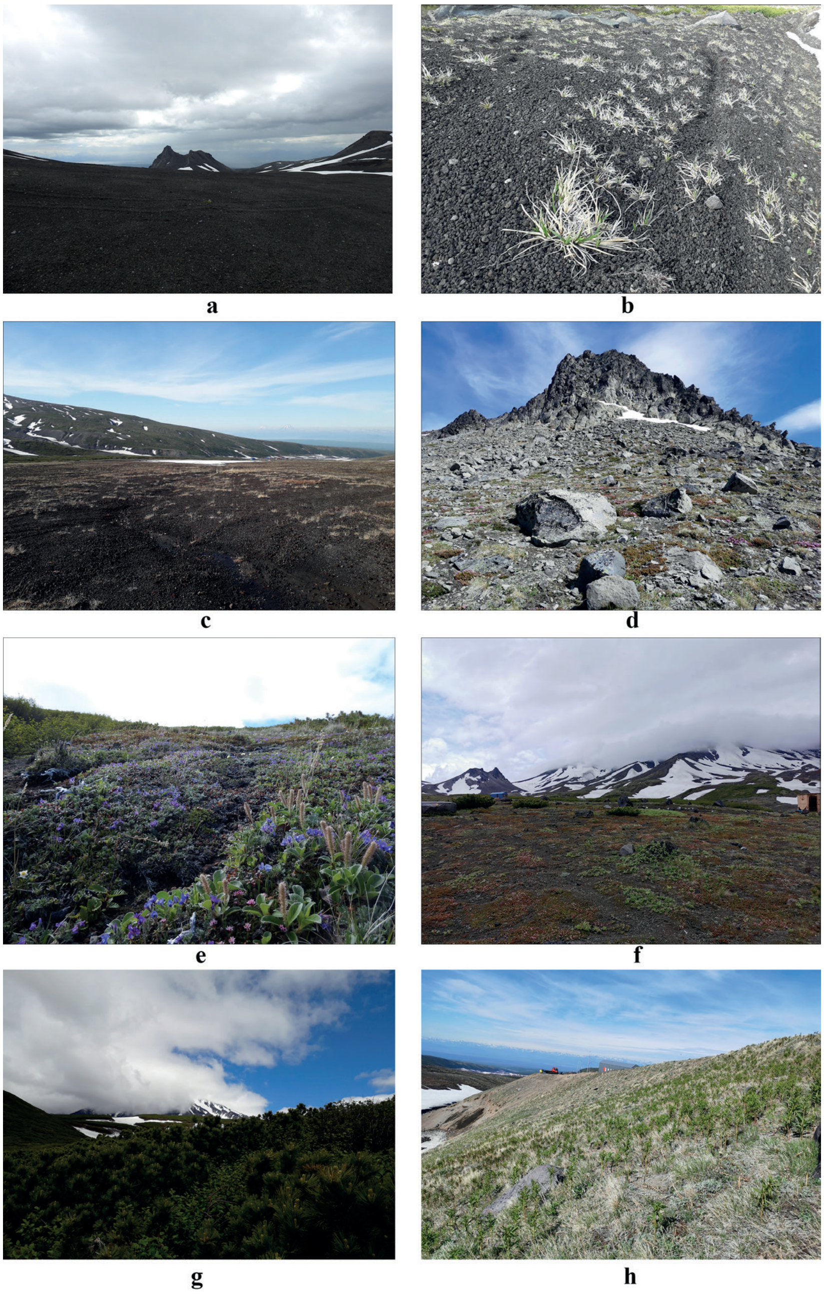

Fig. 1. Habitats of the Avachinsky Pass: a) open ground areas without vegetation (with Verbliud mountain in the background); b) plots with sparse pioneer vegetation (with traces of vehicles); c) plots with pioneer vegetation; d) stony tundra; e) grassy tundra; f) disturbed meadow tundra; g) sparse elfin woodland; h) disturbed communities dominated by ruderal species

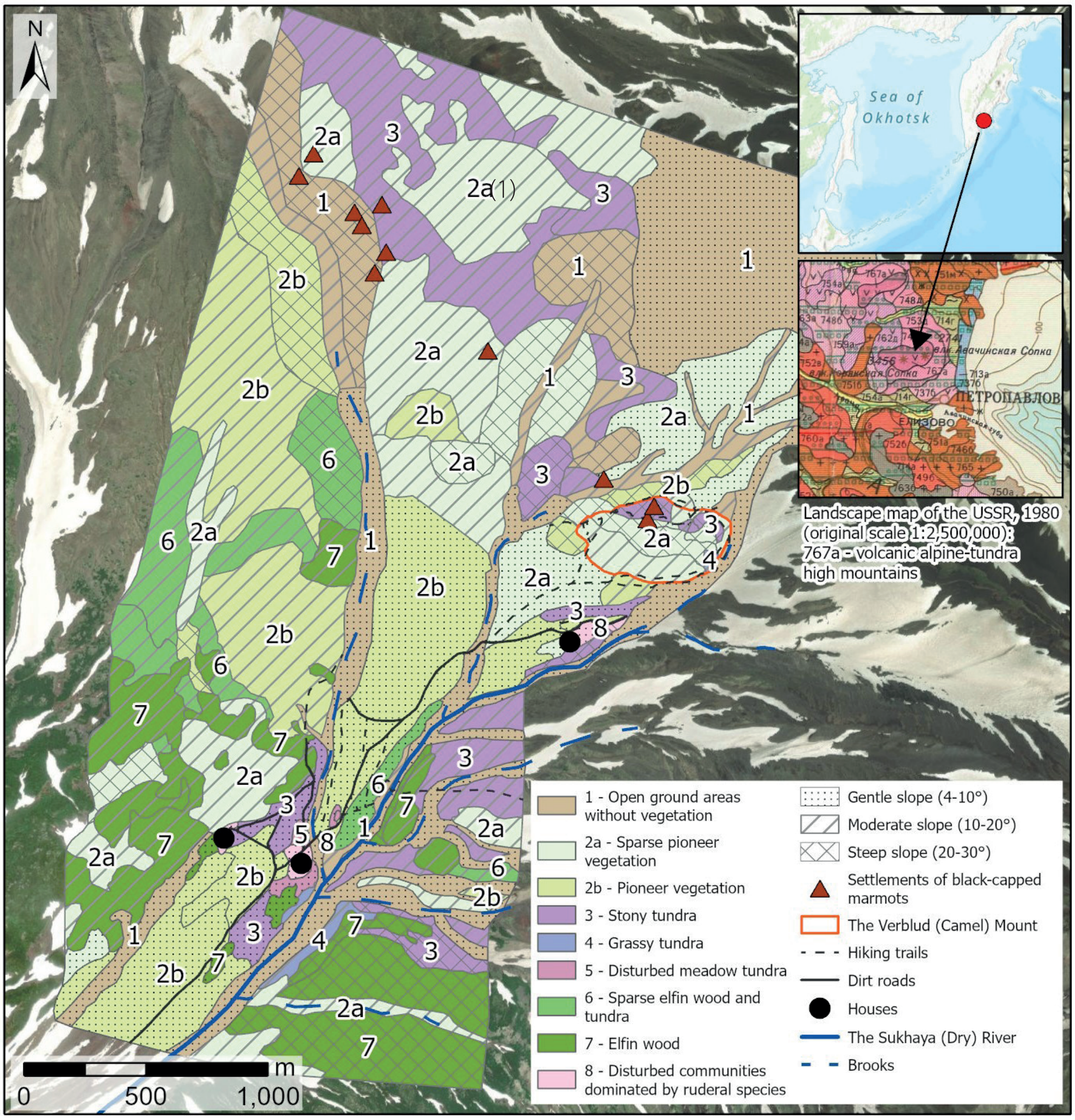

Fig. 2. Habitats of the Avachinsky Pass

Table 1. Composition of habitats on the Avachinsky Pass and length of performed routes by habitats

Habitat	Area, ha	Area, %	Route length, km	Habitat	Area, ha	Area, %	Route length, km
1 - Open ground areas without vegetation	144.3	17.3	11.5	5 - Disturbed meadow tundra	2.2	0.3	1.4
2a – Plots with sparse pioneer vegetation	229.1	27.5	12.1	6 - Sparse elfin wood and tundra	47.8	5.7	6.9
2b – Plots with pioneer vegetation	192.8	23.2	12.3	7 - Elfin wood	100.0	12.0	8.5
3 - Stony tundra	109.3	13.1	13.3	8 - Disturbed communities dominated by ruderal species	3.4	0.4	1.5
4 - Grassy tundra	3.4	0.4	1.5	Total	816.5	100	69.0

Discussion

The survey showed that the "crisis" can be attributed only to a part of the Pass. Most of the visitors try to use the available trails wishing to climb as high as possible, and they are hardly interested in anything else. Therefore, the actively visited zone turned out to be small. Animal presence also indicates this fact. In spite of the short period of the survey, we registered almost all species of birds and mammals that could be expected (Lobkov 1986; Smetanin 2011). The presence of Lesser Sand Plover deserves special attention as it is an endangered species. It nests only in the Russian Far East. According to the IUCN assessment, it suffers from "myriad of threats at all stages of its migration cycle" (disturbance of mudflat loss, increase of human population at the coastline of Asia, direct extermination, windfarms, etc.). Negative impacts on nesting sites are also mentioned, although they are understudied (BirdLife International 2023). The other recorded bird species are not considered threatened, but half of them have negative population trends because of the anthropogenic transformation of habitats (Table 2). The presence of such species is evidence of the rather good state of the environment on the Pass and its high conservation value. Such a diversity is rare for other Russian mountainous tourism destinations (like, for example, in Elbrus area or other peaks of Caucasus).

As for the mammals, even two relatively new species for the area under study have been noted, which are wolf and lynx. The wolves were uncommon in southern Kamchatka in the past (Valentsev and Snegur 2019). They invaded the peninsula from the north, and their existence is dependent from the reindeer (*Rangifer tarandus*) population. However, now they are spreading southwards even irrespective of reindeer. A similar situation concerns the lynx. This species appeared in Kamchatka only in the beginning of XX century, afterward it populated the peninsula more or less successfully (Valentsov and Mosolov 2004). Probably, several small unrecorded rodents or insectivores also occur on the Pass, although had they do, they are very small in numbers. They were not mentioned in the previous studies on the mammals of the Pass (Zykov 2017; Nenasheva et al. 2020). Mammals are rather numerous at the Pass as it is a crossroad of their migration routes: bears, foxes, lynxes, and hares pass it when moving from one valley to another, while snow sheep and marmots cross it moving across highlands. The latter species is relatively sedentary, but it still needs movements out of its settlements during periods of reproduction and dispersion of juveniles. Moreover, some marmots have a wandering lifestyle (Lebedko and Valentsev 2003). Although all recorded mammal species are not considered threatened in a global scale, at least two of them, snow sheep and marmot, still inspire concerns. A part of their populations is already included in the Red Data Book of Russia (marmot of Transbaikalia and Chukotka, snow sheep of Putorana, Chukotka and Kodar mountains) (Brandler et al. 2021; Sipko and Poiarkov 2021) the others approach such status. They are declining in Kamchatka. It happens mostly because of continuous hunting. They are not numerous because of natural causes, but they are still considered game animals in Kamchatka (Fil and Mosolov 2010; Lebedko and Valentsev 2003). Moreover, in the northern part of Kamchatka, a deer-raising takes place, this also negatively influences them. Not only the deer but rather herders and their dogs either kill or disturb wild mammals. About 20 years ago, this factor weakened because the number of domestic reindeer decreased (Lebedko and Valentsev 2003). However, recently the local authorities encouraged the deer herding. For example, in 2021 more than 300 mln rubles (around 4,1 mln $) were donated to the deer farmers[4]. Evidently, this increases the significance of the southern refuges for highland species. Although sometimes the marmots are disturbed at the Avachinsky Pass (Nenasheva et al. 2020; Zykov 2017), they still occur there, as well as the snow sheep. It gives rise to cautious optimism as it turns out that conservation of biodiversity is possible even in spite of the touristic attraction.

Regardless of the encouraging conclusion concerning the "crisis", the negative impacts on the Pass are still significant. Amateur off-road motorcycle or jeep racing remains a critical concern. They try to move as far as possible considering such actions as "heroism". It is not

Table 2. Recorded bird species and their conservation assessment according to the IUCN Red list of threatened species (2024)[3]

No	Species	Assessment in the IUCN red list of threatened species		No	Species	Assessment in the IUCN red list of threatened species	
		category	current population trend			category	current population trend
1	Lesser Sand Plover *Charadrius mongolus*	EN	decreasing	11	Grey Wagtail *Motacilla cinerea*	LC	stable
2	Common Cuckoo *Cuculus canorus*	LC	decreasing	12	Oriental Greenfinch *Chloris sinica*	LC	stable
3	Rock Ptarmigan *Lagopus muta*	LC	decreasing	13	Brambling *(Fringilla montifringilla)*	LC	decreasing
4	Common Raven *Corvus corax*	LC	increasing	14	Common Redpoll *Acanthis flammea*	LC	decreasing
5	Kamchatka Leaf Warbler *Phylloscopus examinandus*	LC	stable	15	Common Rosefinch *Carpodacus erythrinus*	LC	decreasing
6	Siberian Rubythroat *Luscinia calliope*	LC	stable	16	Pine Grosbeak *Pinicola enucleator*	LC	decreasing
7	Northern Red-flanked Bluetail *Tarsiger cyanurus*	LC	stable	17	Asian Rosy-finch *Leucosticte arctoa*	LC	decreasing
8	Brown-headed Thrush *Turdus chrysolaus*	LC	unknown	18	Grey Bunting *Emberiza variabilis*	LC	stable
9	Olive-backed Pipit *Anthus hodgsoni*	LC	stable	19	Snow Bunting *Plectrophenax nivalis*	LC	decreasing
10	Buff-bellied Pipit *Anthus rubescens*	LC	decreasing		-		-

[3]IUCN Red list of threatened species [Online] Available from: (https://www.iucnredlist.org) (Accessed: 8th of March 2024)
[4]Government of Kamchatka Krai [Online]. (2001). Available from: https://www.kamgov.ru/ (Accessed: 15th of February 2022)

clear, which measures would be helpful to manage these activities, because they can overcome any fences or other barriers that could potentially be installed on the way to the Pass. Uncontrolled intensive off-road racing causes degradation of vegetation and therefore intensification of erosion processes. Intensive erosion causes landslips, shallowing of the rivers, habitat loss, etc. Such a perspective is evidently highly undesirable. Meanwhile, vegetation cover at the Pass is sometimes completely destroyed by volcanic activity and revegetation evolves slowly even without human disturbance. Under such circumstances, off-road racing must be prevented (during hot season). Otherwise, it will intensify because of the general increase in the number of visitors. Recently, tourism has been encouraged by the local administration. According to the "Social and economic development strategy of Kamchatka up to 2025", Avachinsky's tourist attraction group is one of the recreation centers. The government plans to develop a "recreation tourism cluster" there (Government of Kamchatka Region 2001). Probably, the status of the World Heritage Site will contribute to these initiatives. It is known that such particularity can be used as an additional point of tourist attraction (Canale et al. 2019; Mariani and Guizzardi 2020). However, in this case, there are factors that are more important: proximity to Petropavlovsk-Kamchatsky and a good accessibility. Halaktyrsky Beach is an example of the nearest territory with similar problems of sustainable development. And just like with the Avachinsky Pass, the issue of the development of the territory as a tourist cluster is based on the creation of a sustainable infrastructure (Iurmanov et al. 2023). Further development of the studied territory should be carried out on the basis of the parity of interests of both nature conservation and tourism activities, which will preserve unique natural objects and tourist attractiveness.

It is interesting to point out that the Pass represents the natural or "normal" state of mountainous vegetation outside of the central disturbed zone. Usually, mountainous areas are affected by logging, grazing and overgrazing; therefore, open areas are being formed in the highlands. Wild ungulates also support them. Total deforestation and overgrazing are negative processes as they intensify soil erosion and landslips (Bitukov and Shagarov 2017). However, the encroachment of bushes to the open areas (pastures) is often considered a negative process because it destroys the habitats of some species and decreases the ecosystem services (Brandt et al. 2013). In our case neither logging, nor grazing takes place, and the wild ungulates are almost absent. Snow sheep inhabit only the highest parts of the slopes, and their number is limited. In the lower zone, the ungulates are not present at all. Probably, they will appear in the near future, because the moose (Alces alces) have been recently introduced to south Kamchatka (Smetanin 2011), but no traces of them have been recorded at the Pass so far. As a result, the plants grow undisturbed. In a situation like this, usually the trees and shrubs form very dense thickets, open areas disappear, and the conservation value of such areas becomes doubtful (Popov et al. 2023). However, in the case under consideration, it does not happen, because the volcanoes reset to zero the vegetation from time to time. Below a highland zone with scarce vegetation, most of the slopes are covered by elfin trees, but they contain numerous gaps filled by small meadows, talus, and rocks. The revealed "mosaic" of various habitats can be considered a desirable optimum, which keeps the ground on the slopes and creates a suitable environment for various animals.

Conclusion

Tourism has affected Avachinsky Pass negatively, but presently its influence is spatially limited. Unlike most mountainous areas, grazing and tree cutting are not typical for the area; therefore, the Pass is relatively resistant to negative anthropogenic influence. Elfin forests and the other vegetation occupy large areas on the slopes; providing a natural protection from landslips and providing habitat for numerous animal species. In spite of the small size of the area affected by visitors, their impact still inspires concern. Within the most visited section of the pass, the plots covered by very scarce vegetation or without vegetation occupy 58%. Since tourists travel through these areas using a variety of vehicles (despite the ban), their overgrowth of vegetation occurs slowly. Meanwhile, the Pass is located at the source of a river. The vegetation loss increases the risk of landslides, which can be catastrophic.

REFERENCES

Bak S., Min C. K. and Roh T. S. (2019). Impacts of UNESCO-listed tangible and intangible heritages on tourism. Journal of Travel and Tourism Marketing, 36, 917-927, DOI:10.1080/10548408.2019.1658034

BirdLife International. [online]. (2023). Charadrius mongolus. The IUCN Red List of Threatened Species. e.T230027154A234712764. Available at: https://dx.doi.org/10.2305/IUCN.UK.2023-1.RLTS.T230027154A234712764.en. [Accessed 29 Febr. 2024].

Bitukov N. A. and Shagarov L. M. (2017). Degradation of water protection of the Western Caucasus mountain oakeries as a result of felling. Nature Conservation Research, 2(3), DOI: 10.24189/ncr.2017.006

Brandler O. V., Badmaev B.B. and Zheleznov N. K. (2021). Marmot Marmota camtschatica Pallas, 1811. In: Red data book of Russia. Moscow: FGBU VNII Ecologia, 960 – 962 [in Russian]

Brandt J.S., Haynes M.A., Kuemmerle T., Waller D.M. and Radeloff V.C. (2013). Regime shift on the roof of the world: Alpine meadows converting to shrublands in the southern Himalayas. Biological Conservation, 158, 116-127, DOI:10.1016/j.biocon.2012.07.026

Canale R. R., De Simone E., Di Maio A., Parenti B. (2019). UNESCO World Heritage sites and tourism attractiveness: The case of Italian provinces. Land Use Policy, 85, 114-120, DOI: 10.1016/j.landusepol.2019.03.037

Cherkasova A.A., Iurmanov A.A., Kokane P., Maslakov A.A., Petkovich M., Petrushina M.N., Tabelinova A., Tolipov A., Yakubov G. and Yushina Y. (2022). Prielbrusye national park environmental changes due to increasing tourism activity. Geography, Environment, Sustainability 15, 4 115–123. DOI: 10.24057/2071-9388-2022-108

Chernomorets S.S. and Seynova I.B. (2010). Debris Flows on Volcanoes. A Tutorial. Moscow: Faculty of Geography, M.V. Lomonosov Moscow State University. ESC PHSE. 72 p. [In Russian]

Fil V. I. and Mosolov V. I. (2010). Snow sheep of Kamchatka. Petropavlovsk-Kamchatsky: Kamchatpress. [In Russian]

Girina O.A., Ozerov A.Yu., Melnikov D.V. and Manevich A.G. (2019). Avachinsky volcano: monitoring and basic characteristics of eruptions. In: Volcanism and related processes. Proceedings of the XXII All-Russian Scientific Conference dedicated to the Day of the Volcanologist, March 28-29, 11-14. [In Russian]

Iurmanov A., Sazonau A., Alenova A., Basalai K., Kozizoda A., Sinchuk N., Tigranyan M., Bassiouny M., Khaled A., Tawfik J. (2023). Hlaktyrsky beach: problems and prospects of sustainable development. In: P. Ya. Baklanov. K. S. Ganzei. A. V. Mashkov, ed., Geosystems of North-East Asia: natural, natural resource and socio-economic structures. Collection of scientific articles. Vladivostok: Pacific Geographical Institute of the Far Eastern Branch of the RAS, 201-205, DOI: 10.35735/9785604844175_201. [In Russian]

Job H., Becken S. and Lane B. (2017). Protected Areas in a neoliberal world and the role of tourism in supporting conservation and sustainable development: An assessment of strategic planning, zoning, impact monitoring, and tourism management at natural World Heritage Sites. Journal of Sustainable Tourism, 25 (12), 1697–1718, DOI: 10.1080/09669582.2017.1377432

Lebedko A.V. and Valentsev A.S. (2003). Monitoring materials for the black-capped marmot in the southern part of the Sredinny Range in Kamchatka. Proceedings of KF TIG FEB RAS, 4, 44-60. [In Russian]

Li M., Wu B., and Cai L. (2008). Tourism development of World Heritage Sites in China: A geographic perspective. Tourism Management, 29(2), 308–319, DOI: 10.1016/j.tourman.2007.03.013

Lobkov E. G. (1986). Nesting birds of Kamchatka. Vladivostok: Far Eastern Scientific Center of the Academy of Sciences of the USSR. [In Russian]

Mariani M. and Guizzardi A. (2019). Does Designation as a UNESCO World Heritage Site Influence Tourist Evaluation of a Local Destination? Journal of Travel Research, 59, 22-36, DOI: 10.1177/0047287518821737

Nenasheva E. M., Karpov E. A. and Danilov S. K. (2020). Avacha pass as part of a specially protected natural area in a state of ecological crisis. In: A. M. Tokranov, ed., Conservation of biodiversity of Kamchatka and surrounding seas, Petropavlovsk Kamchatsky; Kamchatpress, 180-184. [In Russian]

Newsome D., Moore S.A. and Dowling R.K. (2002). Natural Area Tourism: Ecology, Impacts and Management. Bristol, United Kingdom: Channel View.

Osipov E., Shadie P., Zwahlen C., Osti M., Shi Y., Kormos C., Bertzky B., Murai M., Van Merm R. and Badman T. (2017). IUCN World Heritage Outlook 2: A conservation Assessment of All Natural World Heritage Sites. Gland: IUCN.

Pickering C. and Hill W. (2007). Impacts of recreation and tourism on plantbiodiversity and vegetation in protected areas in Australia. Journal of Environmental Management, 85(4), 791–800, DOI: 10.1016/j.jenvman.2006.11.02

Popov I., Iurmanov A. and Abakumov E. (2023). Assessment of the Conservation Value of Abandoned Land on Gogland Island, Baltic Sea. Land, 12, 10, 1946, DOI: 10.3390/land12101946

Sipko T. V. and Poiarkov A. D. (2021). Marmot Marmota camtschatica Pallas, 1811. In; Red data book of Russia. Moscow: FGBU VNII Ecologia, 1041 – 1045 [in Russian]

Smetanin A. N. (2011). Mammalian fauna of Kamchatka and its commercial and hunting species. Bulletin of hunting, 8 (1), 35-47. [In Russian]

Special protected natural areas of Russia [online]. (2005). Available at: http://oopt.aari.ru/ref/597 [Accessed 17 Febr. 2022]

Sun D. and Walsh D. (1998). Review of studies on environmental impacts ofrecreation and tourism in Australia. Journal of Environmental Management, 53(4), 323–338, DOI: 10.1006/jema.1998.0200

Valentsov, A.S. and Mosolov V.I. (2004). Lynx on the Kamchatka Peninsula. Proceedings of KF TIG FEB RAS, 5, 10-28. [In Russian]

Valentsev, A. S. and Snegur P. P. (2019). Number and systematic status of the Kamchatka wolf. Bulletin of hunting, 16 (3), 211-218. [In Russian]

Yakubov, V. V., Chernyagina O. A. and Berkutenko A. N. (2001). Flora of the Avachinsky volcano (south-east Kamchatka peninsula). In: A. N. Polezhaev, ed., Flora and climatic conditions of the North Pacific (a collection of scientific papers). Magadan: IBPS DVO RAN, 3-30.

Yang Y., Xue L. and Jones T. (2019). Tourism-enhancing effect of World Heritage Sites: Panacea or placebo? A meta-analysis. Annals of Tourism Research, 75, 29-41. DOI: 10.1016/j.annals.2018.12.007

Zhong L., Deng J., Song Z. and Ding P. (2011). Research on environmental impacts of tourism in China: Progress and prospect. Journal of Environmental Management, 92 (11), 2972–2983, DOI: 10.1016/j.jenvman.2011.07.011

Zhuchkova V. K. and Rakovskaya E. M. (2004). Methods of complex physiographic research. Moscow: Akademiya. [In Russian]

Zykov V.V. (2017). Mapping the settlements and calculation the number of Marmota Camchatica (Pallas, 1811) in the area of the Avacha volcano (Nalychevo nature park). In: Kumarkov A. A., ed., Protected natural areas of the Kamchatka Territory: work experience, management problems and development prospects: reports of the Second Regional Scientific and Practical Conference (a collection of scientific papers). Petropavlovsk Kamchatsky, Kamchatpress: 99-102. [In Russian]

RESEARCH PAPER

INACCURACY OF RELATIVE ELEVATIONS ON UAV-BASED DIGITAL ELEVATION MODELS WITHOUT PRECISE REFERENCE INFORMATION

Victoria V. Zorina[1*], Andrey L. Entin[1]

[1]Department of Cartography and Geoinformatics, Faculty of Geography, Lomonosov Moscow State University, Leninskie Gory 1, Moscow 119991, Russia

***Corresponding author:** zorinavv@my.msu.ru

Received: November 17th 2023 / Accepted: April 10th 2024 / Published: July 1st 2024

https://DOI-10.24057/2071-9388-2024-3123

ABSTRACT. Imagery obtained from unmanned aerial vehicle (UAV) is widely used for land surface modelling. Recent research prove that digital elevation models (DEMs) created from UAV imagery are characterized by a high rate of accuracy and reliability. Most of these studies are focused on assessing absolute elevation accuracy of the UAV DEMs, but the accuracy of relative elevations (i.e., accuracy of reproducing of local elevation differences within DEM) also should be considered. In this paper, we focus on the precision of replicating relative elevations in DEMs derived from imagery captured via UAVs without precise coordinate reference. To evaluate this accuracy, we use datasets of aerial images processed in two different methods: one with on-board coordinates obtained from a GNSS receiver, and the other based on precise coordinates calculated with the Post-Processing Kinematic (PPK) method. The sites selected for assessment are not look like each other in terms of terrain and forest cover characteristics to track the difference of modelling in the divergent areas. Constructed DEMs were compared with reference fragments of global DEMs by the statistical indices for the difference fields. The findings indicate that the absence of an accurate coordinate reference does not have a substantial impact on the precision of reproducing relative elevations in the DEM. This makes it possible to use UAV materials without precise coordinate reference for modelling in most geographical studies, where the error of terrain steepness values of 0.9° can be considered acceptable.

KEYWORDS: unmanned aerial vehicles (UAV); unmanned aerial imagery; digital elevation model (DEM); digital surface model (DSM); GNSS; post-processing kinematic; accuracy; relative elevations

CITATION: Zorina V. V., Entin A. L. (2024). Inaccuracy Of Relative Elevations On UAV-Based Digital Elevation Models without Precise Reference Information. Geography, Environment, Sustainability, 2(17), 26-35
https://DOI-10.24057/2071-9388-2024-3123

ACKNOWLEDGEMENTS: Geoscan Gemini UAV, hardware and Agisoft Metashape software were provided by the Centre of Collective Usage "Geoportal MSU". Aerial photography of Site 1 was supported by RSF project 21-17-00058. Aerial photography of the Site 2, processing and analysis of the results were carried out under the state assignment (project number 121051400061-9).

Conflict of interests: The authors reported no potential conflict of interest.

INTRODUCTION

Digital elevation models (DEMs) and digital surface models (DSMs) are a valuable source of information for geographical research in various fields. UAV photography is one of the leading methods for construction high spatial resolution DEMs. UAVs provide spatial data of a very high resolution, which allows for large-scale geographic research, i.e., creation of thematic and topographic maps, surveying, and other engineering applications (Guan et al. 2022; Mohamad et al. 2022; Uysal et al. 2015). Many researchers conducted in geography to investigate large-scale geographic phenomena, use unmanned aerial imagery materials (Biljecki et al. 2016; Deev et al. 2023; Suchilin et al. 2021; Svistunov et al. 2022).

UAV-derived digital elevation models are used to obtain accurate quantitative elevation characteristics, modelling and forecasting of external land forming phenomena. To leverage the outcomes of UAV imagery in scientific research, it is crucial to verify the precision of the generated DEMs. In this context, accuracy pertains to the congruence of relative DEM elevations and elevations of real Earth surface, as well as the correct representation of landforms. Many research tasks require assessment of DEM accuracy, especially in terms of corresponding between absolute elevations of DEM and actual terrain. This is accomplished by ensuring that survey materials are provided with precise coordinate reference (Benassi et al. 2017; Eisenbeiss 2009). The primary techniques for precise georeferencing of aerial surveys involve the measurement of ground control points' coordinates or equipping the UAV with a geodetic-class GNSS receiver, enabling it to operate in PPK (Post Processing Kinematic) or RTK (Real Time Kinematic) mode with satellite systems (Famiglietti et al. 2021; Padró et al. 2019; Tomaštík et al. 2019). However, the use of UAVs with a high-precision GNSS receiver is more expensive (including in case of loss or damage of the device) and may also require higher operator skills level, so low-cost UAVs weighing up to 2 kg are widely used in geographical surveys.

Low-cost UAVs are usually small-size quadcopters which are available for users with different pilot experience level and for different types of demands. The most popular of them are drones made by DJI, Xiaomi, Autel, etc (DJI - Official Website 2023). However, these devices cannot provide aerial imagery materials with accurate georeferencing without ground control points: the coordinates measured by the onboard GNSS receiver are accurate to a few meters, depending on the DEM and survey conditions. Therefore, surveys are often carried out without precise georeferencing, which can lead to errors and inaccuracies in the results when the survey results are used in the future research (Neitzel and Klonowski 2012; Szypuła 2023).

In recent years, several studies have assessed the precision and accuracy of DEMs and DEMs derived from UAV imagery. These studies have focused on assessing the accuracy of absolute elevations of the DEMs (Barba et al. 2019; Benassi et al. 2017; Liu et al. 2022). The papers conduct a statistical analysis of georeferencing accuracy, examining its correlation with the chosen coordinate referencing technique, the quantity of ground control points employed, and various other contributing factors. Horizontal accuracy (X and Y model shifts) and elevation accuracy (absolute errors) is calculated. Simultaneously, it is important to highlight that the aspects of DEM reliability, such as the accuracy of relative elevations representations and DEM orientation in relation to the terrain, have not received adequate research attention.

This research aims to evaluate the precision of relative elevation replication in DEMs generated from UAV imagery without precise coordinate reference. To achieve this objective, we conduct a comparative analysis between DEMs obtained from UAV imagery and reference sections extracted from available global DEMs. The choice of reference global DEMs of much lower detail is determined by the inaccessibility of higher resolution materials. As we analyse the general trend of distortions and geometric deformations of DEMs from unmanned aerial imagery data, the use of detailed materials is not necessary. Two sets of DEMs derived from the same aerial imagery data are used for comparison, but one group was processed without precise georeferencing and the other using data from a high-precision on-board GNSS receiver. The height difference between the created and reference models is calculated and investigated. In addition to the absolute values of the difference, we are interested in the presence of noticeable trends in the difference fields. Expressed spatial trends of the difference may indicate the inclination of the created DEM relative to the reference one and, consequently, the mismatch of elevations, which, in our opinion, reduces the reliability of the DEM.

MATERIALS AND METHODS

We estimate DEM relative elevation accuracy using unmanned aerial imagery data on two sites with distinct topographical features. The first site, with an area of 0.6 km^2, is located on the slope of the Kurai Ridge, Chuya River basin, Altai Republic, near the village of Chagan-Uzun. It is characterised by steep slopes (up to 12°), and there are also landforms with much steeper slopes. Elevations of the site vary from 1500 to 2500 m a.s.l. The site lacks dense forestation, with limited herbaceous cover and occasional shrubs, making the area open and facilitating easy access to terrain information. There is also a landslide body captured on relatively recent UAV's data. Global elevation models do not capture this landslide because the data for these models were acquired much earlier. An overview of the site is shown on Fig. 1. The second site, with an area of 0.3 km^2, is located on the Karelian shore of the Kandalaksha Bay of the White Sea, Kindo Peninsula. It is characterised by gentle topography (slope steepness up to 5°) with little roughness. Due to the point cloud class export and subsequent lack of overlap, the majority of the second site, characterized by a significant forest cover, is excluded from the image creation process. Thus, only the marine littoral along the coast is considered as a surface without vegetation. An overview of the site 2 is shown on Fig. 2.

UAV materials. The materials of two large-scale unmanned aerial surveys obtained from the Geoscan Gemini geodetic aerial survey complex (Geoscan Group of

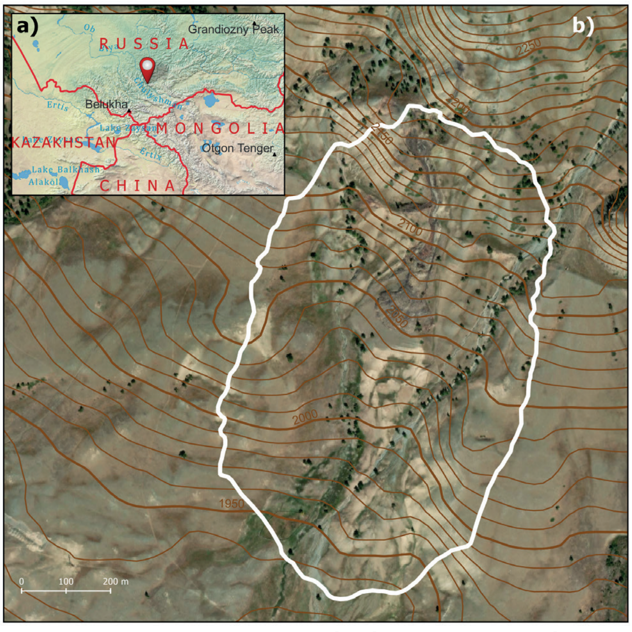

Fig. 1. Site 1: (a) location map; (b) the test area on the Kurai Ridge, Eastern Altai

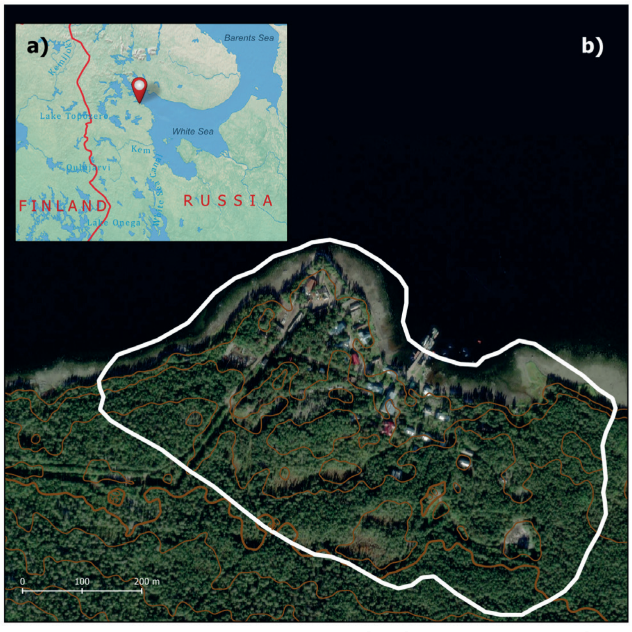

Fig. 2. Site 2: (a) location map; (b) the test area on the Karelian shore of the Kandalaksha Bay

Companies 2023) were used in the study. The complex is designed to perform aerial survey works with obtaining high-precision spatial data. The UAV is a quadcopter with 1.9 kg weight, maximum altitude 500 m and flight time up to 40 minutes. It carries a Sony UMC-R10C Camera, an optical camera mounted on a gimbal. The maximum resolution of the camera is 20.1 megapixels; the sensor size is 23.2 x 15.4 mm; the focal length is 20 mm. The direction of nadir shooting is provided by tilting the vehicle when moving forward. The UAV is equipped with a high-precision GNSS receiver U-blox ZED-F9. The receiver tracks GPS, GLONASS, Galileo and BeiDou signals; position accuracy in differential mode is about 10 mm (Geoscan Gemini Manual 2023). It should be noted that in autonomous mode (without the use of a base station), the position accuracy is reduced. Topcon HiPer V satellite receiver is used as a base station for aerial surveying Topcon HiPer V (Topcon HiPer V 2012).

Geoscan Gemini is classified as a professional unmanned aerial photography device. The GNSS receiver installed on it allows making observations in phase mode. This distinguishes Gemini from low-cost UAVs, such as DJI Phantom or DJI Mavic, equipped with a coded GNSS receiver. In our opinion, the accuracy of the "raw" coordinates measured by the phase receiver in autonomous mode is comparable to the accuracy of the coordinates determined by the code receiver (Kaplan and Hegarty 2017). Therefore, the evaluation of unmanned aerial imagery materials with Geoscan based on coordinates without post-processing allows us to approximate the accuracy characteristics of materials from a low-cost UAV without plan-altitude justification.

The aerial survey materials for each site include an array of aerial images, an observation file from the base station and a GNSS observation file from the on-board receiver. For the first site, 402 images were acquired from an altitude of 100 m, front overlap of 80% and side overlap of 60%. For the second site, 447 images were acquired from an altitude of 120 m, front overlap 80% and side overlap 60%. It's also worth noting that the Geoscan planner used during the survey allows us to plan the fly-task with the terrain in mind - this keeps roughly the same height above the surface over the entire survey area.

Selection of reference DEMs providing comparative analysis of unmanned aerial imagery results. Global digital elevation DEMs, which are publicly available for users, were used as reference DEMs (Table 1).

SRTM is an elevation model obtained by radar topographic survey, the resolution of the DEM is 1´´ (about 30 m). SRTM data were submitted in 2000: the survey was carried out in February 2000 for 11 days. Elevation is measured from the EGM96 geoid. The vertical accuracy of the DEM published in the official documentation, is 16 m. The use of the DEM is limited by the geographical location of the study areas: coverage is limited to the area between 60°N and 54°S (Farr et al. 2007).

ASTER GDEM. The model is a result of processing of stereoscopic imagery by a satellite thermal emission and reflection radiometer. The ASTER GDEM creation methodology consisted of automated processing of the entire ASTER archive, stereo correlation, cloud masking to remove cloud pixels, data summarisation followed by averaging of pixel values and extraction of artefacts The spatial resolution of the DEM is 1´´ (about 30 m), Elevation is measured from the EGM 96 geoid. The mean vertical error of the DEM is 20 m. Available to users since 2009, with an improved DEM released in 2019 (Fujisada et al. 2012).

ALOS PALSAR DEM is an elevation model with a spatial resolution of 12.5 m, obtained by resampling existing elevation models, mostly SRTM. It is available since 2015. The DEM undergoes elevation correction: elevations are measured from an ellipsoid (as opposed to SRTM, which uses the EGM96 geoid model), then resampled. The Alaska Satellite Facility, which provides the data, warns users that the materials are intended to interpret the results of radiometric terrain correction, and its using instead of DEM is not recommended (ALOS PALSAR - Radiometric Terrain Correction 2023). Thus, vertical height errors are not given in the official DEM documentation. However, research studies have evaluated the possibility of using ALOS PALSAR DEM as a digital elevation model. The results of these studies conclude that it is acceptable to use ALOS in geographical research, based on the scale of the results obtained (Ferreira and Cabral 2021; Ihsan 2021; Ngula Niipele and Chen 2019). The use of the DEM is limited by the geographical location of the study sites: coverage is restricted to 60°N and 54°S, as the coverage of the ALOS PALSAR DEM is directly dependent on the coverage of the product used for oversampling (SRTMGL1). The vertical accuracy of the DEM is 16 m.

ALOS WORLD 3D-30 (AW3D30) is a global digital surface model dataset with a spatial resolution of 1´´ (about 30 m), released in 2015 by Japan Aerospace Exploration Agency (JAXA). Based on panchromatic stereo images from the ALOS satellite acquired between 2006 and 2011. Available to users since 2016 and the dataset is currently being updated and improved. The vertical accuracy of these models is on the order of 5 m, with elevations measured from geoid EGM96 (Takaku et al. 2014).

ArcticDEM is an elevation model constructed for the entire Arctic from stereo pairs of very high resolution Maxar satellite imagery, includes data from WorldView-1, WorldView-2, WorldView-3 and GeoEye-1 acquired between 2007 and 2022 during March and April months. Individual DEM strips are compiled from DigitalGlobe images. It has a 2-metre spatial resolution. Elevations are measured from an ellipsoid. Average vertical DEM error is up to 4 meters. Available to users since 2017 (Noh and Howat 2017; Porter 2018).

FABDEM is an elevation model with a spatial resolution of 1´´ (about 30 m). It is available to users from 2021 and is currently being updated. The model is obtained by removing the elevation values of non-relief objects (buildings, forests) from the Copernicus GLO-30 DEM. The elevation is measured from the EGM2008 geoid. Machine learning techniques are used to derive the DEM, where the systematic error of the heights of buildings and trees is removed from the COPDEM30 model. Once non-relief heights are removed, the DEM is post-processed, where a median pixel value filter is applied (Hawker et al. 2022). According to the cited study, 90% of errors of elevation values for open areas are up to 8 m, for slightly sloping open areas are up to 5 m, for densely built-up and heavily forested areas of terrain, where significant removal of "non-relief" elevation values was carried out, the value of vertical error is about 10 m.

For the first site, 4 reference DEMs were selected: SRTM DEM 1 arc-second; ALOS PALSAR DEM; AW3D30 DEM; FABDEM. For the second site, 4 reference DEMs were selected: ASTER GDEM V3; AW3D30 DEM; Arctic DEM; FABDEM. DEMs have acceptable values of absolute elevation accuracy indicators, which can guarantee a reliable result of relative elevation estimation, i.e. the difference fields between UAV DEM and reference DEM (Uuemaa et al. 2020; Karlson et al. 2021; Saberi et al. 2023; Meadows et al. 2024). An estimate of the accuracy of the relative elevation of the reference DEM has not been reported previously in the literature. Most studies are focused on estimation of absolute elevation

Table 1. Comparative characteristics of reference DEMs

Reference DEM	Horizontal datum	Vertical datum	Resolution	Vertical accuracy	Source
SRTM DEM (1 arc-second)	EPSG:4326 WGS84	Geoid EGM96	1 arc -second ~ 30 m	± 16 m	(Siemonsma 2015)
ASTER GDEM	EPSG:4326 WGS84	Geoid EGM96	1 arc -second ~ 30 m	± 20m	(ASTER Global DEM Validation Summary Report 2009)
ALOS PALSAR DEM	EPSG:32645 WGS 84 / UTM zone 45N	Ellipsoid	12.5 m	± 16 m	(ASF engineering 2015)
ALOS WORLD 3D-30 (AW3D30)	EPSG:4326 WGS84	Geoid EGM96	1 arc -second ~ 30 m	± 5 m	(ALOS Global Digital Surface Model (DSM) Product Description 2019)
ArcticDEM	EPSG:3413 WGS 84 / NSIDC Sea Ice Polar Stereographic North	Ellipsoid	2 m	± 4 m	(ArcticDEM - Polar Geospatial Centre 2023)
FABDEM	EPSG:4326 WGS84	Geoid EGM2008	1 arc -second ~ 30 m	± 10 m	(Hawker et al. 2022)

and comparison is made with GNSS and LiDAR data. But we can compare the differences between the elevations of reference and UAV DEMs, leaving out possible inaccuracies of global DEMs. When comparing global DEM in pairs with UAV DEM, one of the models is known to be reliable (UAV DEM with PPK coordinates).

Research methods. For the study it is necessary to carry out photogrammetric processing of aerial imagery arrays for each site in two ways: based on "raw" onboard coordinates of GNSS receiver and with coordinates refined by PPK method. For this purpose, the kinematics track obtained from the GNSS receiver is post-processed first. Then the photogrammetric processing is performed directly, the purpose of which is to obtain dense point clouds. For each reference DEM, two-point clouds (based on "raw" and PPK coordinates, respectively) were obtained, and the processing was carried out in the coordinate and elevation system of the target DEM. The point clouds were classified to identify points belonging to the ground surface, after which DEMs geometrically aligned with the reference DEMs were constructed based on these points. Then, for each pair of DEMs (constructed and reference DEMs), the difference of elevation at each point was calculated. The obtained differences were analysed: characteristics such as standard deviation and mean of the difference surfaces were calculated and compared, the linear trend of the surface and the slope angle of the resulting plane were calculated. If the DEM obtained without precise coordinate referencing exhibits characteristics comparable to the DEM obtained from precise coordinates, this indicates the validity of the first DEM. More detailed description of each of the steps is given below.

Processing of GNSS receiver coordinates and UAV onboard coordinates was performed in CREDO GNSS software. The processing consisted in calculating the coordinates of external event points of the onboard GNSS receiver track. For this purpose, observations at the base station, the coordinates of which were determined in advance, were used. As a result of processing, the refined coordinates of the image projection centers were obtained.

UAV imagery data processing was performed in Agisoft Metashape Professional software. For DEM sets using raw coordinates, the following operations were performed: setting the target coordinate and elevation system, mutual orientation of the images, building a dense point cloud, and finally classification to determine the points of the bare earth class. For DEM sets using exact coordinates, the difference was that before mutual orientation, the import of exact coordinates of the centers of the image projections obtained in the previous step was performed. The processing resulted in point clouds of class "Ground", which were exported in LAS format. The point density of cloud was 26.6 points/m^2 for the first site and 14.7 points/m^2 for the second site.

Construction of DEM for comparison with benchmarks. Creation of raster (gridded) DEMs was performed in SAGA GIS using the Shapes to Grid tool. Point clouds in LAS format exported at the previous step were used as source data. The cell size and coverage of the target rasters were set according to the reference DEM fragments. Cell elevations of the target rasters were calculated as mean values of elevation of points falling within a cell.

Calculation and analysis of height differences between constructed and reference DEMs. We calculate algebraic difference between UAV DEM and reference DEM. Since point clouds are characterised by much higher spatial resolution than fragments of reference DEMs, we can neglect possible planned displacement of these materials relative to each other.

Due to the forested nature of Site 2, the forested area is completely excluded from the analysis. Non-forested fragments include the littoral, adjacent shoreline areas and isolated glades in the forest.

The nature of elevation displacement of the constructed DEM relative to the reference DEM determines other more complex deformations of DEM: tilt and geometric deformation. The range of values of *algebraic raster difference* is from below to above zero numbers. Values below zero indicate that elevations of the constructed DEM are less than elevations of the reference DEM (underestimated relative to the reference DEM); values above zero for the constructed DEM is overestimated relative to the reference DEM; zero values indicate coincidence of elevations of both DEMs.

For each difference field, mean and standard deviation (STD) were determined. *Mean* determines the measure of mixing of the distribution density of relative elevation values to a certain value; this value will be an indicator of the difference between two surfaces (constructed and reference). The closer the value is to zero, the greater the coincidence of the compared DEMs. The *standard deviation* determines the nature of this bias: the closer the value is to zero, the higher the density of distribution of values close to the mean, and, accordingly, the values of the difference fields in most cases are equal to the mean. In addition, linear trend surfaces were constructed for each difference field. The trend was constructed using the Trend tool from the ArcGIS Pro Spatial Analyst module. The steepness of the trend surface was calculated to estimate the slope of the constructed DEM surface relative to the reference DEM. The purpose of trend in this study is to show a pattern of the difference in elevation values of the constructed and reference DEMs to higher or lower values. The trend thus determines whether the slope of the interpolated surface is observed or not. *The Slope* calculation function is then applied to the trend to obtain a certain number which is a measure of the slope of the trend surface and, consequently, of the DEM surface from unmanned aerial imagery data.

RESULTS

Site 1: slope of the Kurai Ridge, Chuya River basin, Altai Republic (near Chagan-Uzun village). For Site 1, 8 difference rasters were calculated from the data of unmanned aerial imagery and reference DEMs: 4 differences for DEMs based on "raw" coordinates and 4 differences for DEMs based on PPK coordinates. Images of the difference images are shown in Fig. 3. Comparative analyses were performed on three characteristics for each algebraic difference image. The listed characteristics for site 1 are summarised in Table 2.

SRTM DEM. When calculating the characteristics for the first two pairs of comparisons with the reference DEM, the mean difference values were obtained: –1.4 m for the "Raw" DEM and 1.1 m for the PPK DEM. The values of the constructed DEMs differ from the reference DEM by one order of magnitude (underestimation of the "Raw" DEM, overestimation of the PPK DEM), it is assumed that the use of accurate coordinate referencing does not improve the modelling result. This is also evidenced by the value of the STD, which is similar for both differences (3.41 and 3.22 respectively). However, the value of the slope of the trend surface slightly improved after PPK coordinate processing: 0.19° for the DEM using raw coordinates, 0.04° for the DEM using processed coordinates. Both differences are characterised by an overestimation of positive landform

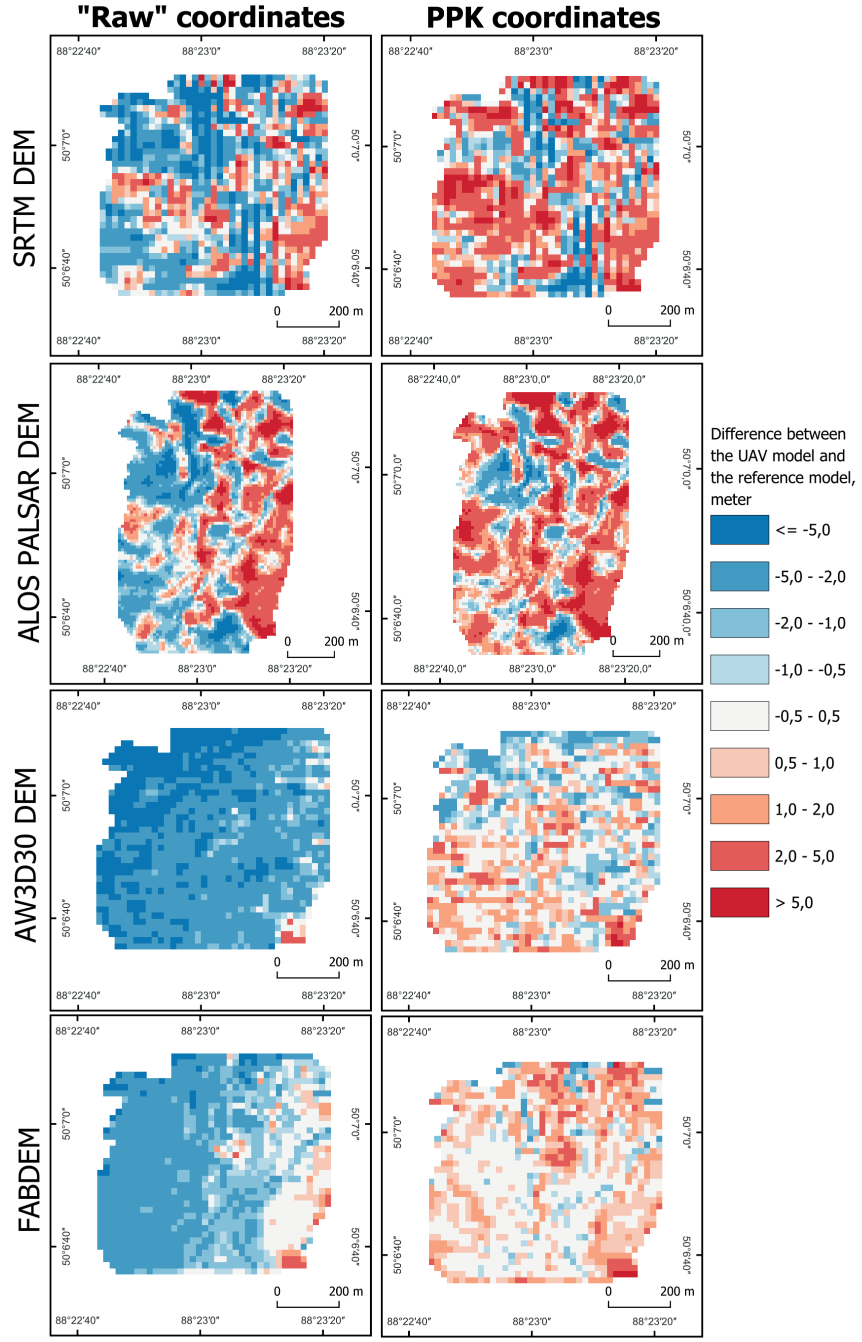

Fig. 3. Result of algebraic elevation difference of site 1 DEMs

Table 2. Statistical analysis of site 1

	"Raw" coordinates		PPK coordinates	
SRTM DEM	MEAN, m	-1.4	MEAN, m	1.1
	STD	3.41	STD	3.22
	SLOPE, °	0.19	SLOPE, °	0.04
ALOS PALSAR DEM	"Raw" coordinates		PPK coordinates	
	MEAN, m	-0.04	MEAN, m	1.47
	STD	3.1	STD	2.91
	SLOPE, °	0.4	SLOPE, °	0.08
AW3D30 DEM	"Raw" coordinates		PPK coordinates	
	MEAN, m	-4.06	MEAN, m	0.08
	STD	1.97	STD	1.44
	SLOPE, °	0.26	SLOPE, °	0.09
FABDEM	"Raw" coordinates		PPK coordinates	
	MEAN, m	-1.95	MEAN, m	0.53
	STD	1.67	STD	1.11
	SLOPE, °	0.25	SLOPE, °	0.02

areas and an underestimation of negative landforms: thus, the DEMs from unmanned aerial photography data appear more dissected relief, compared to the reference DEM (Fig. 3). When evaluating the results from the "Raw" data and PPK data, it is noted that the difference between the "Raw" data has lower values for the western part of the DEM, some areas are 5 meters or lower. The slope angle of the elevation difference trend plane (Table 2) for the DEM with "Raw" coordinates is 0.19° and for the DEM with accurate coordinates is 0.04°. This indicates that the DEM built based on "Raw" coordinates of image projection centers is insignificantly tilted relative to the terrain. The change of values by an order of magnitude confirms the theory of DEM inclination in the western, north-western direction. Mean is significantly more distant from zero values at one order of SRTM. Compared to SRTM, the DEM for the original coordinates is generally lower than expected and is tilted in the west, northwest direction. When PPK coordinates are processed, the elevation DEM is levelled, but the overall DEM becomes higher than the reference DEM, on average, by a meter, but for individual positive and negative landforms the difference is between 2 and 5 m with positive (about 32% of the area) and negative (less than 10% of the area) character, respectively.

ALOS PALSAR DEM. The performance calculation for the second two pairs of comparisons with the reference DEM yielded mean difference values of –0.04 m for the "Raw" coordinates DEM and 1.47 m for the PPK coordinates DEM. The mean difference value for the DEM by "Raw" coordinates is better than that of the DEM with accurate coordinate referencing and the STD value is similar for both differences (3.1 and 2.91 respectively). When comparing the values of the slope of the trend surface, there is also a noticeable improvement after PPK coordinate processing: 0.4° for the DEM using raw coordinates versus 0.08° for the DEM using processed coordinates. ALOS is constructed by resampling SRTM, so the results of comparison with these two DEMs are visually similar. The difference values for the underestimation sites are predominantly between –2 and –5 m; overestimations, similarly, between 2 and 5 m, which is systematic (Table 2). The slope trend of the DEM from the original data is preserved. For the DEM from PPK data there is a shift of the mean value to the area of positive values, the DEM is generally higher than expected (about 70% of the territory).

AW3D30 DEM. When calculating the characteristics for the third two pairs of comparisons with the reference DEM, the mean difference values were obtained: –4.06 m for the DEM by "Raw" coordinates and 0.08 m for the DEM by PPK coordinates. From this comparison, it can be concluded that the result of the DEM construction with accurate coordinate referencing is comparatively better. However, the value of STD, which is similar for both differences (1.97 and 1.44 respectively) also indicate the heterogeneity of the distribution of the mean difference index. The value of the slope of the trend surface improved slightly after PPK coordinate processing, 0.26° versus 0.09°. The trend of the slope of the DEM on the original data is maintained. When the coordinates are processed, the DEM is levelled, the values of the steepness index of the trend surface decrease by an order of magnitude, leading to values negligibly small (Table 2). Before coordinate recalculation, the DEM has a mean significantly far from zero, indicating an underestimation of height values relative to the reference DEM. Post-processing of coordinates of image projection centers allows to bring expectation values almost to zero, thus, most difference values are (more than 50% of the territory) in the range from –1 to 1 meter, which for DEM resolution of 30 m/pix can be considered acceptable and the relief DEM is generally correct.

FABDEM. When calculating the characteristics for the last two pairs of comparisons with the reference DEM for the first site, the mean difference values were obtained: –1.95 m for the DEM using "Raw" coordinates and 0.53 m for the DEM using PPK coordinates. The use of accurate coordinate referencing slightly improves the modelling result. However, the value of STD, which is 1.67 and 1.11 for both differences, respectively, also indicates the heterogeneity of the distribution of the mean difference index. The value of the slope of the trend surface slightly improved after PPK coordinate processing, 0.25° versus 0.02°. Similar to the previous three comparisons, there is a slope of the UAV DEM over the initial elevation values and an underestimation relative to the reference DEM by a value of about 2 m. The recalculation of the coordinates brings the expectation value closer to zero (Table 2), but indicates an average excess of values of 0.5 m. These values are concentrated mainly on positive landforms and the landslide body, which represents an abrupt change in topography: the body is absent on the reference DEMs, the landslide is fresh and recorded only on the UAV DEMs (Fig. 3). The majority of elevation difference values for the PPK DEM are in the range of 0.5 to 1 meters (more than 45% of the area), which can also be considered acceptable for the DEM resolution of 30 m/pix, the constructed relief DEM is generally correct.

Site 2: Karelian coast of the Kandalaksha Bay of the White Sea, Kindo Peninsula (area of Primorsky settlement). Similarly, the assessment methodology was tested at Site 2: calculations were carried out using 4 references DEMs in two versions, for the original georeferenced data and post-processed data (Fig. 4). Comparative analyses were performed on three characteristics for each algebraic difference image. The listed characteristics for site 2 are prepared separate sets of characteristics are for the whole territory (Table 3) and for non-forested areas (Table 4).

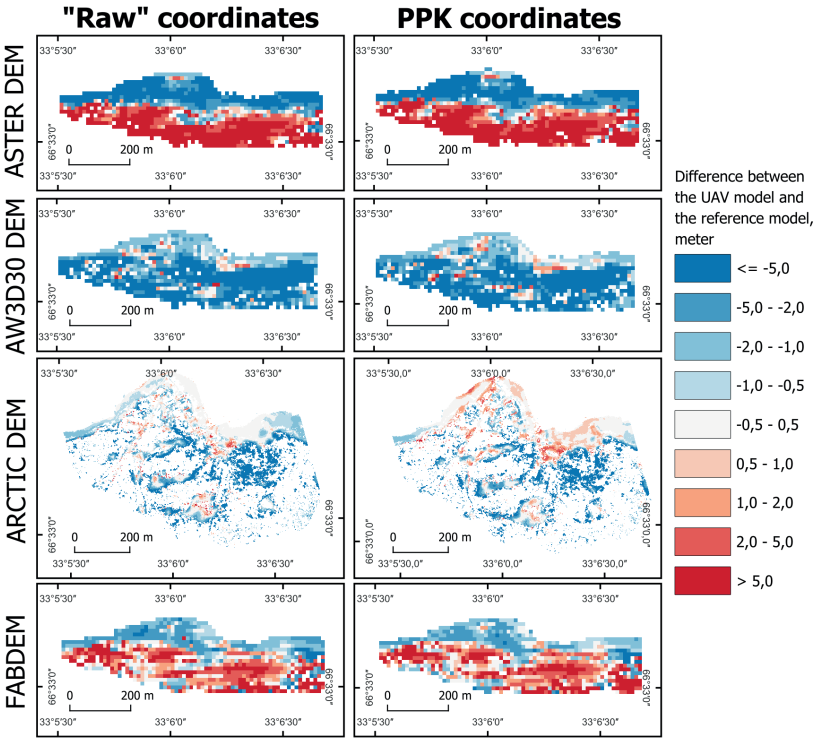

Fig. 4. Result of algebraic elevation difference of site 2 DEMs

Table 3. Statistical analysis of site 2

	"Raw" coordinates		PPK coordinates	
ASTER DEM	MEAN, m	1.59	MEAN, m	1.97
	STD	7.63	STD	7.53
	SLOPE, °	2.51	SLOPE, °	2.43
AW3D30 DEM	"Raw" coordinates		PPK coordinates	
	MEAN, m	-5.64	MEAN, m	-5.25
	STD	5.05	STD	5.03
	SLOPE, °	0.74	SLOPE, °	0.89
ARCTIC DEM	"Raw" coordinates		PPK coordinates	
	MEAN, m	-3.44	MEAN, m	–2.91
	STD	4.89	STD	4.93
	SLOPE, °	0.71	SLOPE, °	0.9
FABDEM	"Raw" coordinates		PPK coordinates	
	MEAN, m	1.13	MEAN, m	1.35
	STD	4.31	STD	4.31
	SLOPE, °	0.82	SLOPE, °	0.76

Table 4. Statistical analysis of site 2 (littoral)

ASTER DEM	"Raw" coordinates		PPK coordinates	
	MEAN, m	-6.65	MEAN, m	-6.32
	STD	2.44	STD	2.45
	SLOPE, °	0.87	SLOPE, °	0.86
AW3D30 DEM	"Raw" coordinates		PPK coordinates	
	MEAN, m	-1.45	MEAN, m	-1.08
	STD	0.78	STD	0.64
	SLOPE, °	0.06	SLOPE, °	0.03
ARCTIC DEM	"Raw" coordinates		PPK coordinates	
	MEAN, m	-0.36	MEAN, m	0.14
	STD	0.55	STD	0.71
	SLOPE, °	0.17	SLOPE, °	0.32
FABDEM	"Raw" coordinates		PPK coordinates	
	MEAN, m	-1.82	MEAN, m	-1.41
	STD	1.06	STD	1.1
	SLOPE, °	0.06	SLOPE, °	0.06

ASTER GDEM V3. For the second group of comparisons for site 2, the first pair of difference fields for the non-forested part of the territory, the mean difference values were obtained: -6.65 m for the DEM using "Raw" coordinates and –6.32 m for the DEM using PPK coordinates. The use of precise coordinate reference has no qualitative effect on the modelling result. This is also evidenced by the value of STD, which is similar for both differences (2.44 and 2.45 respectively), the value of the slope of the trend surface (0.87° and 0.86° respectively). When compared with ASTER, both DEMs show a similar result (Fig. 4): The littoral is underestimated relative to the reference DEM, with elevation difference values exceeding –5 m, more than 85% of the littoral plot for the original coordinates and more than 78% of the littoral plot for the equated coordinates. The difference values for the littoral section (Table 4) also demonstrate systematic underestimation of the DEM.

AW3D30 DEM. Similarly, for the second comparison, the use of precise coordinate referencing has no qualitative effect on the modelling result: the mean difference values are –1.45 m and –1.08 m for the "Raw" coordinates DEM and the PPK coordinates DEM, respectively; the STD values are 0.78 and 0.64; the slope angles of the trend surface are 0.06° and 0.03°. The values of elevation differences in the littoral area for both DEMs range from –2 to –1 meters (69% of the area for the PPK DEM, 45% of the area for equated coordinates), in some places slightly exceeding the value of –0.5 meters (13% of the area vs. 27% of the area). The UAV DEMs are underestimated relative to the reference DEM but are within the 30 m/pix resolution of the original DEM (Fig. 4). The overall slope of the DEM, captured by the steepness value of the interpolated trend surface, is not corrected through coordinate post-processing (Table 3), but the parameter value is negligible for the littoral section (Table 4). AW3D is a surface DEM that contains information not only on topography but also on vegetation. For the vegetation plot, the UAV DEM is underestimated by values of about 10 m, which is acceptable. When exporting the point cloud, only terrain elevation points were used, the reference DEM in these plots is represented by vegetation heights. Thus, we can conclude that the classification of the point cloud and the subsequent filtering of UAV survey data into "relief" and "non-relief" is correct.

Arctic DEM. This comparison is the most reliable, as the initial resolution of the reference DEM of 2m/pix is close to the resolution of the DEMs obtained by unmanned aerial imagery, compared to the rest of the global elevation DEMs (Fig. 4). The comparison with the Arctic DEM shows a slightly different result: while the mean difference improves by 0.14 m for the PPK DEM (–0.36 m for the "Raw" DEM), the STD and slope values of the trend surface deteriorate when using precise coordinate referencing. Thus, these values are 0.55 and 0.17° for the "Raw" DEM, respectively, and 0.71 and 0.32° for the DEM with accurate coordinate referencing. The littoral at this site for both DEMs, with GNSS initial values and equated through PPK, is within the range of values from -0.5 to 0.5 m (about 58% of the littoral area for the initial and equated DEMs), only in some areas from -1 to 1 meters (27% vs. 32% of the littoral area). The values of mean and STD are as close to zero values as possible (Table 4). Thus, the highest density of distribution is observed at values of –0.36 m of height difference for the original coordinates and 0.14 m for the equated coordinates. The use of accurate coordinate reference does not significantly but improves the vertical accuracy of the digital elevation DEM. It can be concluded that the values of DEM heights from unmanned aerial imagery data are correct, with the post-processing coordinates not significantly affecting the result. However, the overall slope of the DEM, fixed by the steepness value of the interpolated trend surface, is not corrected by coordinates post-processing (Table 3).

FABDEM. When calculating the characteristics for the last two pairs of comparisons with the reference DEM for the second site, the mean difference values were obtained: –1.82 m for the DEM using "Raw" coordinates and –1.41 m for the DEM using PPK coordinates. The use of accurate coordinate referencing slightly improves the modelling result. However, the value of STD deteriorates slightly after PPK coordinates processing: 1.06 and 1.1, respectively. The value of the slope of the trend surface remains unchanged, the exact coordinate reference does not affect the overall slope of the DEM is 0.06°. The values of elevation differences in the littoral area for both DEMs also range from –2 to –1 m (44% of the littoral area for the DEM based on the original coordinate values, 35% of the littoral area for the DEM based on the equated coordinate values), in places reducing this value to –0.5 m (13% vs. 25% of the littoral area, respectively). The UAV DEMs are underestimated relative to the reference DEM over the littoral area but are within the 30 m/pix resolution of the original DEM for this area (Fig. 4). The general slope of the DEM, fixed by the steepness value of the interpolated trend surface, is not corrected by post-processing of the coordinates (Table 3); for the littoral section the value of the parameter is negligibly small (Table 4). It is also worth noting the excess of elevation values for the forested section of the DEM up to 10 m. Since FABDEM assumes the absence of vegetation and buildings on the DEM, and the UAV DEMs were filtered for "non-relief" values, it is probably possible to judge possible errors in removing vegetation heights from FABDEM for a particular site. The statistics collected on vegetation and building values for the subsequent filtering of the reference DEM are collected in a highly discrete manner and interpolated for areas where these values are insufficient.

DISCUSSION

Evaluation of terrain modelling results using unmanned aerial imagery data was carried out on two sites differing in the character of relief and vegetation: one site is devoid of vegetation and has a complex terrain; the second site, with a relatively simple terrain, is 80% forested and partially built up. The change of elevations during DEM creation by the initial data received from the onboard GNSS receiver and by the equated PPK coordinates is considered. For the area with gentle relief the use of equated coordinates does not significantly affect the DEM height accuracy. However, we cannot rule out that this result was the result of a random coincidence of mathematical calculations, but it allows to use the materials constructed from the original data of unmanned aerial imagery. Geometrical features of the relief are considered, the DEM can be considered reliable. It is acceptable to use DEM for relief classifications, calculations of morphometric and morphological characteristics of terrain. The limitation will be a few tasks in which the calculation of multi-temporal dynamics of terrain is carried out. Thus, when analysing multi-temporal relief DEMs, the use of initial data requires accurate agreement not only of elevation values, but also the plan accuracy of all the DEMs used.

The situation is different for the territory with more complex relief. When building elevation DEMs for slopes using the original data, geometric deformations may occur, due to which the correctness of the results obtained based on these DEMs may not be achieved. In such cases it is recommended to use high-precision survey complexes or plan-altitude substantiation of the surveyed area. The study has shown that the altitude accuracy after coordinates post-processing increases, and minor geometric deformation of DEM in the form of inclination of the whole surface is corrected.

The point clouds obtained from photogrammetric processing of UAV imagery arrays are characterised by very high spatial resolution of about 10 points/m^2, which corresponds to large mapping scales. The reference DEMs taken for comparison in this study have incomparably lower spatial resolution. Consequently, comparison of these materials does not allow us to characterise the accuracy of representation of individual landforms (and especially micro- and nano-forms, which are not reflected in the fragments of global DEMs), but the presence of systematic trends in height differences may indicate distortions of detailed DEMs in general. In our case, the slope of the difference trend surface is noteworthy: for area 2, the difference of this characteristic between the DEMs obtained from the "raw" and accurate coordinates of the image projection centers is insignificant, while for area 1, a systematic slope of the "Raw" DEM of the order of 0.2° (an order of magnitude larger than for the PPK DEM) is observed. As far as we can judge, such deviation is insignificant for the most research tasks of local coverage, but we should keep in mind the influence of this deviation when carrying out diagnostic or monitoring works using low-cost UAVs.

It should be noted that the study did not cover areas with more complex and dissected relief with different degrees of forest cover, as well as with flat and slightly sloping relief with different degrees of forest cover and built-up areas. Therefore, we cannot unequivocally judge the applicability of the study conclusions for absolutely all surveyed areas. In order to obtain a reliable modelling result from unmanned aerial photography data for heavily forested or built-up areas, additional data on the height of buildings or vegetation cover may be required, which, in turn, should be coordinated with the corrected DEM. Tasks that require precise referencing of several types of cartographic and thematic materials, multi-temporal spatial data, are performed under the condition of minimum error of relative heights of analysed DEMs, as well as reliability of topography generation. Absolute georeferencing accuracy of unmanned aerial survey materials contributes to the reduction of this error. These tasks may include: assessment of the landform dynamics, landform detection, modelling of hazardous geological processes. However, it is worth noting the importance of understanding the peculiarities of tectonic processes on the studied sites. Also, the conclusions of the study may not be applicable to the tasks where unmanned aerial imagery are used as part of topographic and geodetic works.

Summing up the comparative and statistical analysis of the DEM results for both sites, we can conclude that post-processing of the coordinates of the image projection centers during unmanned aerial imagery does not significantly affect the elevation accuracy of the elevation modelling results, provided that the methodology is followed, and the parameters of UAV imagery correspond to the parameters of aerial imagery used for photogrammetric terrain modelling.

CONCLUSIONS

The paper studies possible distortions of relative heights on DEMs created from UAV photography without precise coordinate reference. For this purpose, a comparative analysis of DEMs constructed from unmanned aerial imagery data using two variants of projection center coordinates was carried out: based on "Raw" coordinates obtained from the onboard GNSS receiver and based on coordinates processed relative to the ground base station. As reference DEMs for comparison, we used fragments of global DEMs and DSMs: SRTM DEM, ASTER GDEM, ALOS PALSAR DEM, ArcticDEM, FABDEM. Such characteristics as algebraic raster difference, linear trend of the raster surface, slope angle of the trend surface, standard deviation, mean was considered when comparing the reference DEMs and the constructed ones. The study allowed to establish that relative elevations on DEMs obtained from UAV imagery data without precise coordinate reference are reproduced reliably. At the same time, the vertical accuracy of the obtained DEMs is acceptable for the most geographical studies, where the error of steepness values up to 0.9° can be considered acceptable. Nevertheless, for orographically complex and highly dissected terrain, additional research is required to absolutely exclude the influence of terrain character on the results of modelling based on unmanned aerial imagery data without accurate georeferencing.

REFERENCES

ALOS Global Digital Surface Model (DSM) Product Description. (2019) Earth Observation Research Center, Japan Aerospace Exploration Agency

ASF engineering. (2015). ASF Radiometrically Terrain Corrected ALOS PALSAR products. Product guide

ASTER Global DEM Validation Summary Report. (2009). ASTER GDEM Validation Team: METI/ERSDAC, NASA/LPDAAC, USGS/EROS. In cooperation with NGA and Other Collaborators

Barba S., Barbarella M., Di Benedetto A., Fiani M., Gujski L. and Limongiello M. (2019). Accuracy Assessment of 3D Photogrammetric Models from an Unmanned Aerial Vehicle. Drones, 3(4), 79. DOI: 10.3390/drones3040079

Benassi F., Dall'Asta E., Diotri F., Forlani G., Morra di Cella U., Roncella R. and Santise M. (2017). Testing Accuracy and Repeatability of UAV Blocks Oriented with GNSS-Supported Aerial Triangulation. Remote Sensing, 9(2), 172. DOI: 10.3390/rs9020172

Biljecki F., Ledoux H. and Stoter J. (2016). Generation of multi-LOD 3D city models in CityGML with the procedural modelling engine Random3Dcity. ISPRS Annals of the Photogrammetry, Remote Sensing and Spatial Information Sciences, IV-4/W1, 51–59. DOI: 10.5194/isprs-annals-IV-4-W1-51-2016

Deev E., Borodovskiy A. and Entin A. (2023). Earthquake-induced deformation at archaeological sites in southeastern Gorny Altai (Siberia, Russia). Archaeological Research in Asia, 34, 100431. DOI: 10.1016/j.ara.2023.100431

Eisenbeiss H. (2009). UAV photogrammetry, 1 Band [ETH Zurich; Application/pdf]. DOI: 10.3929/ETHZ-A-005939264

Famiglietti N.A., Cecere G., Grasso C., Memmolo A. and Vicari A. (2021). A Test on the Potential of a Low Cost Unmanned Aerial Vehicle RTK/PPK Solution for Precision Positioning. Sensors, 21(11), 3882. DOI: 10.3390/s21113882

Farr T.G., Rosen P.A., Caro E., Crippen R., Duren R., Hensley S., Kobrick M., Paller M., Rodriguez E., Roth L., Seal D., Shaffer S., Shimada J., Umland J., Werner M., Oskin M., Burbank D. and Alsdorf D. (2007). The Shuttle Radar Topography Mission. Reviews of Geophysics, 45(2), RG2004. DOI: 10.1029/2005RG000183

Ferreira Z. and Cabral P. (2021). Vertical Accuracy Assessment of ALOS PALSAR, GMTED2010, SRTM and Topodata Digital Elevation Models: Proceedings of the 7th International Conference on Geographical Information Systems Theory, Applications and Management, 116–124. DOI: 10.5220/0010404001160124

Fujisada H., Urai M. and Iwasaki A. (2012). Technical Methodology for ASTER Global DEM. IEEE Transactions on Geoscience and Remote Sensing, 50(10), 3725–3736. DOI: 10.1109/TGRS.2012.2187300

Geoscan Gemini Manual. (2023).

Guan S., Zhu Z. and Wang G. (2022). A Review on UAV-Based Remote Sensing Technologies for Construction and Civil Applications. Drones, 6(5), 117. DOI: 10.3390/drones6050117

Hawker L., Uhe P., Paulo L., Sosa J., Savage J., Sampson C. and Neal J. (2022). A 30 m global map of elevation with forests and buildings removed. Environmental Research Letters, 17(2), 024016. DOI: 10.1088/1748-9326/ac4d4f

Ihsan H.M. (2021). Vertical accuracy assessment on Sentinel-1, ALOS PALSAR, and DEMNAS in the Ciater Basin. Jurnal Geografi Gea, 21 (1), 16-25.

Kaplan E.D., Hegarty J. (2017) Understanding GPS: principles and applications, 2nd edn. Artech House, London

Karlson M., Bastviken D., Reese H. (2021) Error Characteristics of Pan-Arctic Digital Elevation Models and Elevation Derivatives in Northern Sweden. Remote Sens, 13, 4653. DOI: 10.3390/rs13224653

Liu X., Lian X., Yang W., Wang F., Han Y. and Zhang Y. (2022). Accuracy Assessment of a UAV Direct Georeferencing Method and Impact of the Configuration of Ground Control Points. Drones, 6(2), 30. DOI: 10.3390/drones6020030

Meadows M., Jones S., Reinke K. (2024) Vertical accuracy assessment of freely available global DEMs (FABDEM, Copernicus DEM, NASADEM, AW3D30 and SRTM) in flood-prone environments, International Journal of Digital Earth, 17(1), DOI: 10.1080/17538947.2024.2308734

Mohamad N., Ahmad A. and Md Din A.H. (2022). A review of UAV photogrammetry application in assessing surface elevation changes. Journal of Information System and Technology Management, 7(25), 195–204. DOI: 10.35631/JISTM.725016

Neitzel F. and Klonowski J. (2012). Mobile 3D mapping with a low-cost UAV system. The International Archives of the Photogrammetry, Remote Sensing and Spatial Information Sciences, XXXVIII-1/C22, 39–44. DOI: 10.5194/isprsarchives-XXXVIII-1-C22-39-2011

Ngula Niipele J. and Chen J. (2019). The usefulness of alos-palsar dem data for drainage extraction in semi-arid environments in The Iishana sub-basin. Journal of Hydrology: Regional Studies, 21, 57–67. DOI: 10.1016/j.ejrh.2018.11.003

Noh M.-J. and Howat I.M. (2017). The Surface Extraction from TIN based Search-space Minimization (SETSM) algorithm. ISPRS Journal of Photogrammetry and Remote Sensing, 129, 55–76. DOI: 10.1016/j.isprsjprs.2017.04.019

Padró J.-C., Muñoz F.-J., Planas J. and Pons X. (2019). Comparison of four UAV georeferencing methods for environmental monitoring purposes focusing on the combined use with airborne and satellite remote sensing platforms. International Journal of Applied Earth Observation and Geoinformation, 75, 130–140. DOI: 10.1016/j.jag.2018.10.018

Porter C. (2018). 2m Topography and Surface Change Detection over the Arctic. Blue waters symposium

Saberi, A., Kabolizadeh, M., Rangzan, K. & Abrehdary, M. (2023). Accuracy assessment and improvement of SRTM, ASTER, FABDEM, and MERIT DEMs by polynomial and optimization algorithm: A case study (Khuzestan Province, Iran). Open Geosciences, 15(1), 20220455. DOI: 10.1515/geo-2022-0455

Siemonsma D. (2015). The Shuttle Radar Topography Mission (SRTM) Collection User Guide.

Suchilin A., Belaya N., Voskresensky I., Mikheeva S., Zorina V., Ushakova L., Shaforostov V. and Sokratov S. (2021). Methods for studying the morphology of abrasion-accumulative coast of the West coast of the Crimea using UAV and GNSS (on the example of a land of the territory of Great Sevastopol). InterCarto. InterGIS, 27(1), 351–363. DOI: 10.35595/2414-9179-2021-1-27-351-363

Svistunov M.I., Kurbanov R.N., Murray A.S., Taratunina N.A., Semikolennykh D.V., Entin A.L., Deev Ye.V., Zolnikov I.D. and Panin A.V. (2022). Constraining the age of Quaternary megafloods in the Altai Mountains (Russia) using luminescence. Quaternary Geochronology, 73, 101399. DOI: 10.1016/j.quageo.2022.101399

Szypuła B. (2023). Accuracy of UAV-based DEMs without ground control points. GeoInformatica. DOI: 10.1007/s10707-023-00498-1

Takaku J., Tadono T. and Tsutsui K. (2014). Generation of High-Resolution Global DSM from ALOS PRISM. The International Archives of the Photogrammetry, Remote Sensing and Spatial Information Sciences, XL–4, 243–248. DOI: 10.5194/isprsarchives-XL-4-243-2014

Tomaštík J., Mokroš M., Surový P., Grznárová A. and Merganič J. (2019). UAV RTK/PPK Method—An Optimal Solution for Mapping Inaccessible Forested Areas? Remote Sensing, 11(6), 721. DOI: 10.3390/rs11060721

Topcon HiPer V – user manual. (2012Copyright Topcon Positioning Systems, Inc

Uuemaa E., Ahi S., Montibeller B., Muru M., Kmoch A. (2020) Vertical Accuracy of Freely Available Global Digital Elevation Models (ASTER, AW3D30, MERIT, TanDEM-X, SRTM, and NASADEM). Remote Sens., 12, 3482. DOI: 10.3390/rs12213482

Uysal M., Toprak A.S. and Polat N. (2015). DEM generation with UAV Photogrammetry and accuracy analysis in Sahitler hill. Measurement, 73, 539–543. DOI: 10.1016/j.measurement.2015.06.010

RESEARCH PAPER

BURNED AREA DETECTION USING CONVOLUTIONAL NEURAL NETWORK BASED ON SPATIAL INFORMATION OF SYNTHETIC APERTURE RADAR DATA IN INDONESIA

Anugrah Indah Lestari[1*], Dony Kushardono[1], Athar Abdurrahman Bayanuddin[2]
[1]National Research and Innovation Agency, Cibinong, West Java, Indonesia 16911
[2]Directorate of Laboratory Management, Research Facilities, and Science and Technology Park, National Research and Innovation Agency, Parepare, South Sulawesi, Indonesia 91131
***Corresponding author:** anugrah.indah.lestari@brin.go.id
Received: November 2nd 2023 / Accepted: April 10th 2024 / Published: July 1st 2024
https://DOI-10.24057/2071-9388-2024-3109

ABSTRACT. Forest and land fires are disasters that often occur in Indonesia which affects neighbouring countries. The burned area can be observed using remote sensing. Synthetic aperture radar (SAR) sensor data is advantageous since it can penetrate clouds and smoke. However, image analysis of SAR data differs from optical data, which is based on properties such as intensity, texture, and polarimetric feature. This research aims to propose a method to detect burned areas from the extracted feature of Sentinel-1 data. The features were classified using the Convolutional Neural Network (CNN) classifier. To find the best input features, several classification schemes were tested, including intensity and polarimetric features by applying the Boxcar speckle filter and the Gray Level Co-occurrence Matrix (GLCM) texture feature without using the Boxcar speckle filter. Additionally, this research investigates the significance of a window size parameter for each scheme. The results show the highest overall accuracy achieved 84% using CNN classification utilizing the GLCM texture features and without conducting the Boxcar speckle filter on the window size of 17×17 pixels when tested on the part region of Pulang Pisau Regency and Kapuas Regency, Central Kalimantan in 2019. The total burned area was 76,098.6 ha. The use of GLCM texture features without conducting the Boxcar speckle filter as input classification performs better than using intensity and polarimetric features that undergo the Boxcar speckle filter. Combining intensity and polarimetric features with performing the Boxcar speckle filter improves better classification performance over utilizing them separately. Furthermore, the selection of window size also contributes to improve the model performance.

KEYWORDS: burned area, convolutional neural network, gray level co-occurrence matrix texture feature, synthetic aperture radar

CITATION: Lestari A. I., Kushardono D., Bayanuddin A. A. (2024). Burned Area Detection Using Convolutional Neural Network Based On Spatial Information Of Synthetic Aperture Radar Data In Indonesia. Geography, Environment, Sustainability, 2(17), 36-48
https://DOI-10.24057/2071-9388-2024-3109

ACKNOWLEDGEMENTS: The authors sincerely thank the Research Center for Remote Sensing, Research Organization for Aeronautics and Space, National Research and Innovation Agency for providing very-high resolution images. Also, the authors would like to acknowledge the Ministry of Environment and Forestry Republic of Indonesia for providing Burned Area and Land Cover Maps.

Conflict of interests: The authors reported no potential conflict of interest.

INTRODUCTION

The land and forest fires that occurred in Indonesia become an international issue since they affect bordering countries. Land and forest fire incidents cause several environmental and health issues due to air pollution from the fog, bad haze, and carbon in the air (Ho et al. 2019). In 2019, Malaysia and Singapore endured the suffocating presence of a thick haze for an entire week, causing severe air pollution and discomfort in both countries, due to transboundary haze from Indonesia (Nguyen et al. 2022; Sakti et al. 2023; Yeung 2019[1]). According to the report of the Ministry of Environment and Forestry (MoEF) Republic of Indonesia[2], the most severe burned occurrence in Indonesia happened in 2015 up to 2.6 million hectares, followed by 1.64 million hectares in 2019, primarily in Kalimantan and Sumatera Islands (Ministry of Environment and Forestry 2019).

[1]Yeung, J. (2019) Indonesian forests are burning, and Malaysia and Singapore are choking on the fumes. [online] Available at: https://www.huahintoday.com/sports/indonesian-forests-still-burning-and-malaysia-and-singapore-are-choking-on-the-fumes/#:~:text=More%20than%20930%2C000%20hectares%20%28about%202.3%20million%20acres%29,all%20week%2C%20with%20air%20quality%20reaching%20unhealthy%20levels [Accessed 20 June 2023]
[2]Ministry of Environment and Forestry (MoEF) Republic of Indonesia. (2019). Recapitulation of Forest and Land Fire Area (Ha) per Province in Indonesia. (in Indonesian). [online] Available at: https://sipongi.menlhk.go.id/ [Accessed 21 Apr 2023]

The Indonesian government has been implementing some strategies for land and forest fire management since 2015. One of the strategies is a method development for calculating the burned areas. Monitoring the fire event requires the use of remote sensing data for burned area mapping as part of a system from detection to post-fire management (Efransjah et al. 2020). Some optical imageries such as Landsat and Sentinel-2 have been utilized as the primary data for mapping the burned area as the main data. Recently, the automatic mapping approach has been developed by the Indonesian government, but it is still in the early stages of development (Efransjah et al. 2022). However, the presence of clouds or smoke above the burned areas limits the observation utilizing the optical remote sensing data. The use of multi-sensor satellite imageries is a solution to generate a better-burned area map by combining optical and SAR satellite imageries (Abdikan et al. 2022; Arjasakusuma et al. 2022; Sudiana et al. 2023). Single satellite data input can lead to underestimating burned area calculations due to fewer revisit times. Gaveau et al report that using Setinel-2 data resulted in the burned area in 2019 reaching 3.11 Mha across Indonesia (Gaveau et al. 2021). It was twice as estimated by the Indonesian government's MOEF by using manual delineation on Landsat-8 images. On the other hand, stand-alone SAR data has the ability to generate high accuracy in burned area mapping.

Synthetic aperture radar (SAR) is a non-optical sensor of remote sensing that has been investigated for use in burned area mapping (Ban et al. 2020; Hosseini and Lim 2023;Tanase et al. 2010), mainly because it can penetrate the cloud and the smoke over the burned areas, non-weather depends as well. Some studies have been investigating Sentinel-1's capability to map the burned areas, using interferometric coherence and backscatter time series (Tanase et al. 2020), unsupervised classification using radar properties (De Luca et al. 2021), random forest (Hosseini and Lim 2023), deep learning CNN (Luft et al. 2022), and near real-time monitoring using a deep learning approach (Ban et al. 2020), as well as the automatic framework using Deep Convolutional Neural Network (DCNN) (Radman et al. 2023).

Texture features and polarimetric features are important extracted features that need to be selected in classification using SAR images (Singh and Kaur 2011). An urban land cover classification was studied using an SAR image. It results in selected texture features such as mean intensity, semivariograms, variance, and weighted-rank fill ratio improving the classification result (Dekker 2003). SAR image classification using the Sandia National Laboratories dataset was performed using texture features such as gray level co-occurrence matrix (GLCM) and Gabor filters (GFs) and reduced using canonical correlation analysis (CCA). It results in good performance and high efficiency (Ismail et al. 2014). The Sentinel-1 image's texture features were used to identify lead using a random forest algorithm, which resulted in high precision (Murashkin et al. 2018). Furthermore, window size is an important parameter in texture features as a larger window size tends to give stable results (Wen et al. 2009).

Besides the texture features and polarimetric features, speckle is a type of noise that may influence the results of the application obtained from the SAR data. A comparison among several despeckling methods was performed such as Frost, Gamma maximum a posteriori (MAP), Lee, Median, and Boxcar filter using Sentinel-1 images, resulting in the Boxcar filter outperforming them in identifying mangrove forests (Ansari et al. 2020). Also, the boxcar filter proved easy and effective for homogenous regions (Mullissa et al. 2022).

In the matter of Indonesia's burned area mapping, the research regarding the optimum feature of Sentinel-1 C-band SAR is still insufficient. Moreover, adequate radar input features are needed since Indonesia consists of various landscapes to obtain high accuracy in burned area detection. Therefore, this research proposed a method to detect burned areas based on our investigation from the extracted feature of Sentinel-1 data. The extracted feature is then classified using the 1-D CNN classifier since CNN can be treated as state-of-the-art in image classification. We investigate several classification schemes from the extracted features of σ^0 and γ^0 in VH and VV polarization of mosaic images in pre-fire events as well as post-fire events such as intensity and polarimetric features with performing Boxcar speckle filtering as well as GLCM texture feature without performing Boxcar speckle filter to look for the optimum parameter.

MATERIALS AND METHODS

Research Location and Data

This research examined a subset of Pulang Pisau Regency and Kapuas Regency, Central Kalimantan, Indonesia (see Fig. 1) since this province is one of the most affected regions in 2019 (MoEF 2019). Generally, the Muller and Swachner and hilly areas dominate the northern part of this province, while the lowland zone, swamp, and brackish lie in the southern part (Central Kalimantan Province Environmental Agency 2020). The ecosystems found in Central Kalimantan are rain forest, peat forest, heath forest, swamp forest, lowland forest, upland forest, mangrove forests, and plantation forest (Center for Kalimantan Ecoregion Development Control Ministry of Environment and Forestry 2016; Central Kalimantan Province Environmental Agency 2020). According to Statistics Indonesia, Pulang Pisau Regency and Kapuas Regency have various land cover types including hilly areas in the north region and swamps as well as coastal areas in the south area (Statistics Indonesia 2010, 2023). According to the Land Cover Map from the MoEF, the research area's land cover types include swamp, shrub swamp, shrub, bare land, plantation, built-up land, mangrove, secondary swamp forest, paddy field, and agriculture area, as illustrated in Fig. 1.

This research used Sentinel-1 GRD data derived from Google Earth Engine. Table 1 provides detailed information about the Sentinel-1 data used in this research. The date description in Table 1 indicates that pre-fire events occurred from 6-23 July 2019, while post-fire events occurred from 10-27 October 2019. As the classification was a supervised approach, Fig. 2 shows the Satellite pour de l'Observation de la Terre (SPOT) images dated 2 September and 8 October 2019, as well as 10 October 2018 with a resolution of 1.5 meters that were used in this research as the reference data. The Land Cover Map from the MoEF in 2019, was utilized to determine the land cover type at the research site. The active fire data from MODIS and the Visible Infrared Imaging Radiometer Suite (VIIRS) sensor in July – October 2019, collected from the National Aeronautics and Space Administration (NASA), were used in this research as a consideration of the occurrence of burned areas. Furthermore, MODIS's burned area monthly global 500 m, MCD64A1, derived from Google Earth Engine, was employed in this research. The burned area information from the MoEF in 2019 was also used to find out the burned area location and month of fire.

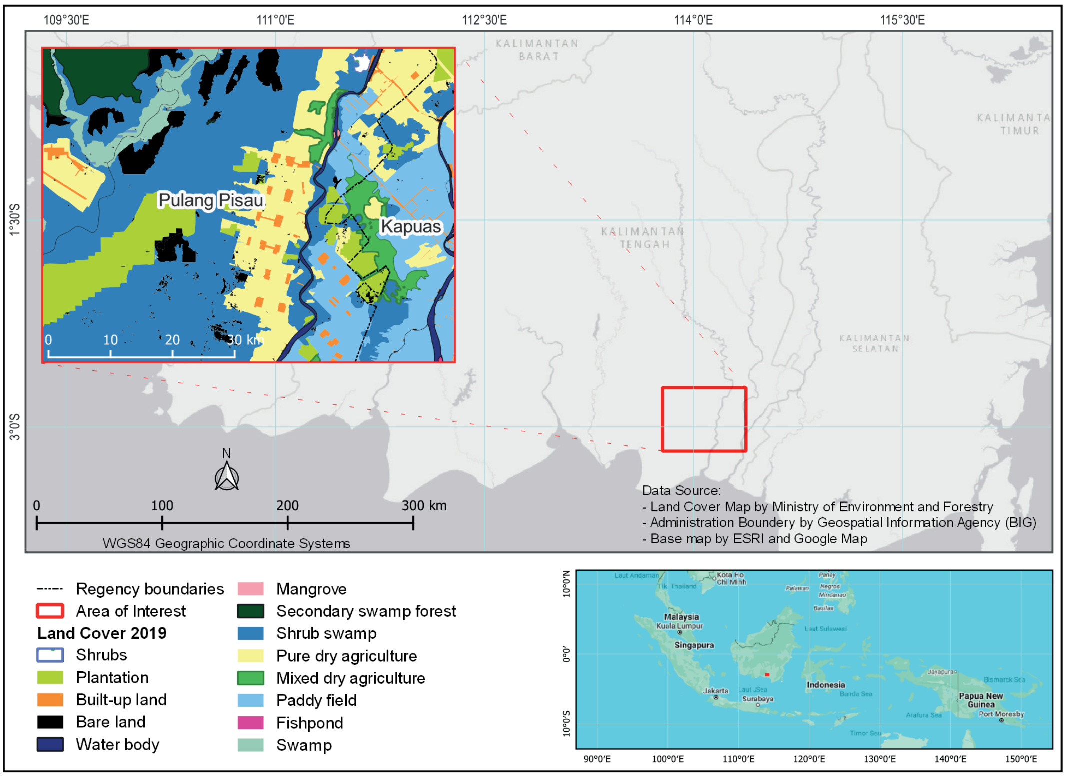

Fig. 1. The area of interest (red rectangle) investigated in the research

Table 1. Sentinel-1 data details for the research

Parameters	Descriptions	
Date	Pre-fire: July 2019	Post-fire: October 2019
Frequency	5.405 GHz	
Pixel Spacing	10 meters	
Orbit	Descending	
Product Type	Ground range detected (GRD)	
Acquisition Mode	Interferometric wide swath	
Polarization Mode	VV and VH	

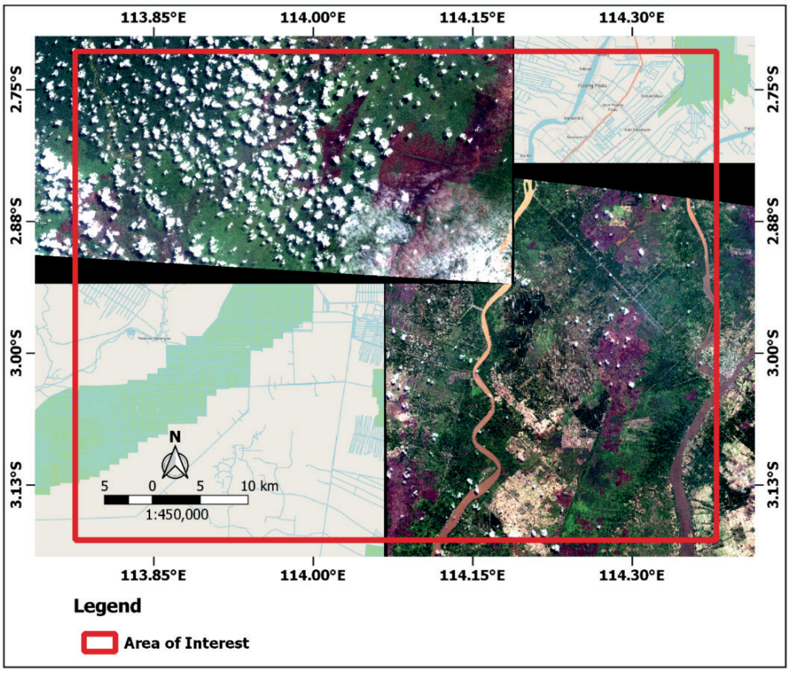

Fig. 2. SPOT data coverage in an area of interest

Methodology

Fig. 3 depicts the flowchart used in this study. It comprises image pre-processing, training and validation data construction, classification, performance evaluation, and burned area information generation.

The SAR data pre-processing was performed using Google Earth Engine (GEE) which includes producing gamma nought (γ^0) from sigma nought (σ^0). This research utilized two types of two backscatter coefficients namely σ^0 and γ^0 on VH and VV polarizations. σ^0 is described as an average of radar reflectivity per unit area in the ground plane (Hossain and Easson 2009; Small 2011), while γ^0 is the reflected radar signal per unit area perpendicular to the slant plane (Small 2011). As σ^0 relies on a variance of the incidence angle, γ0 can assist in minimizing incidence angle dependence (Emery and Camps 2017). These backscatter coefficients can be expressed in mathematical expression as follows (Srivastava et al. 2022):

$$\sigma^0 = 10\log_{10}(DN^2) + K \tag{1}$$

$$\gamma^0 = \frac{\sigma^0}{\cos\theta} \tag{2}$$

where DN is digital number from SAR amplitude image, K is a calibration factor, and θ is incidence angle.

After the pre-processing step, feature extraction and Gray Level Co-occurrence Matrix (GLCM) texture feature extraction were performed. Before feature extraction, the investigation was performed by implementing the Boxcar speckle. The Boxcar filter is basically an averaging filter that changes the centre pixel by a mean value of a moving window N × N (Yahia et al. 2020). Meanwhile, the GLCM texture feature was extracted without speckle filtering, as shown in Fig. 3. The variation of window size was conducted in speckle filtering and GLCM texture feature extraction, with the following pixel sizes 5×5, 7×7, 9×9, 11×11, 13×13, 15×15, and 17×17. This disparate experiment was done to understand the effectiveness of feature extraction after the Boxcar speckle filter, compared with the performance of GLCM texture feature extraction with differing window sizes.

The selection of training and validation data was performed by interpreting SPOT data as a reference, which is shown in Fig. 2. The model was developed using Convolutional Neural Network 1D (CNN-1D). Following that, classification was performed to obtain the burned area information.

Polarimetric and Texture Features

This research used several features such as radar burn ratio (RBR), radar burn difference (RBD), Δ radar vegetation index (ΔRVI), and Δ dual-polarization SAR vegetation index (ΔDPSVI). RBR and RBD on VH polarization perform well in differentiating between burned and unburned areas (Lasaponara and Tucci 2019). In addition, RVI and DPSVI are good indicators of backscatter changes mainly for vegetation (De Luca et al. 2021; Mandal et al. 2020; Periasamy 2018). These features can be expressed as follows:

$$RBR_{xy} = \log_{10}\frac{Post-fire\ average\ backscatter_{xy}}{Pre-fire\ average\ backscatter_{xy}} \tag{3}$$

$$RBD_{xy} = Post\text{-}fire\ average\ backscatter_{xy} - Pre\text{-}fire\ average\ backscatter_{xy} \tag{4}$$

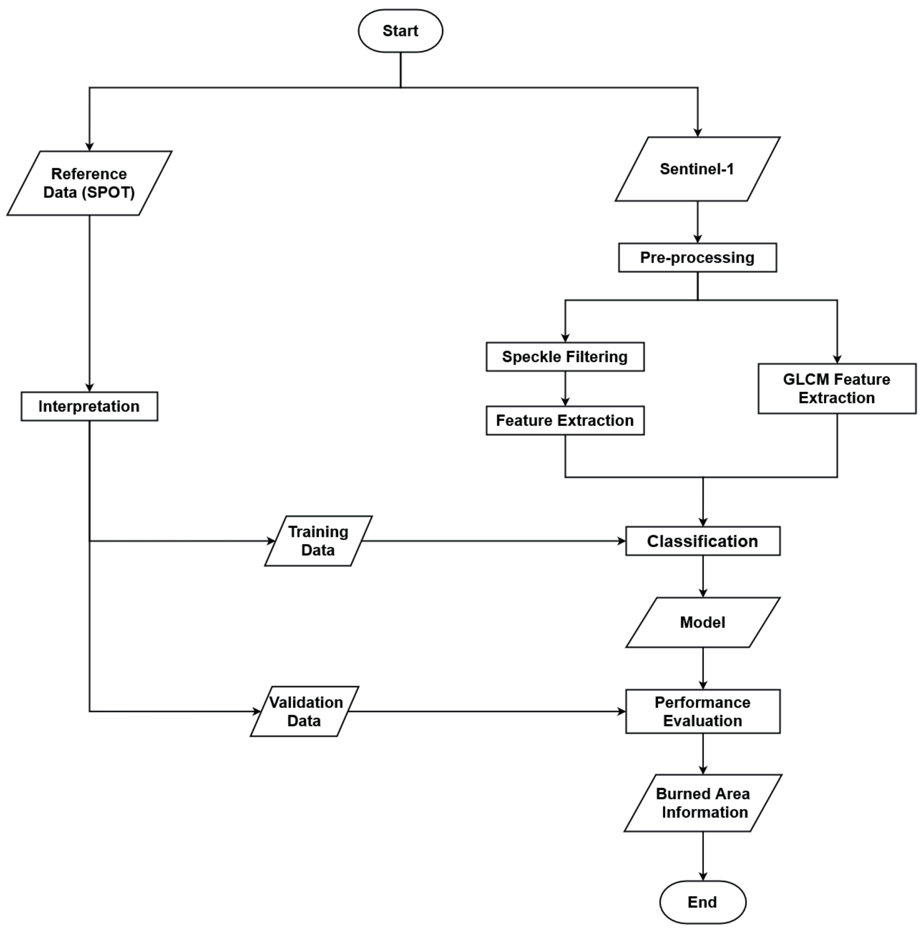

Fig. 3. Research flowchart

$$RVI = \frac{4VH_{time\ average}}{VV_{time\ average} + VH_{time\ average}} \tag{5}$$

$$DPSVI = \frac{VV_{time\ average} + VH_{time\ average}}{VV_{time\ average}} \tag{6}$$

GLCM is an important texture feature that has been used in SAR image processing for several applications (Champion et al. 2014; James et al. 2021; Lestari et al. 2021; Soh and Tsatsoulis 1999). This research used several GLCM texture features such as contrast, entropy, homogeneity, and mean since the features are adequate to discriminate between burned and unburned areas (Mutai 2019). Table 2 shows the mathematical expression of the used GLCM texture features (Anand et al. 2023).

Training and Validation Dataset Generation

In constructing the dataset, high-resolution SPOT images were utilized to label burned and unburned areas. Besides, the occurrence of burned areas was also checked using high-level confidence in burned area information from the MoEF, which means the area had been checked by field investigation. The dataset was divided into training and validation data, which comprised burned and unburned classes. The distribution between the training and validation datasets was 70:30. This research collected 176,100 pixels, which contained 88,460 pixels of burned and 87,640 of unburned classes for training, and 76,032 pixels comprising 38,632 of burned and 37,400 of unburned classes for validation.

Classification Schematic

To examine the optimum classification parameter for burned area detection, there are four schemes that were investigated in this research as shown in Table 3. In the first scheme, σ^0 and γ^0 of mosaic images in pre-fire events and post-fire events were used as inputs, resulting in 8 bands. Then, indices logRBR, RBD, ΔRVI, ΔDPSVI on σ^0 and γ^0 were utilized for Scheme -2, so the inputs become 12 bands. Next, the inputs on Scheme -1 and Scheme -2 were combined and were investigated in Scheme -3. Last, GLCM texture features were used as inputs for Schemes -4.

Classification Design

A convolutional neural network (CNN) is a deep learning type that has the advantage of being able to extract features automatically (LeCun et al. 2015). This research focuses on 1-D CNN where the architecture is built and trained using one-dimensional data. 1-D CNN has the advantage of having relatively low computational complexity and computational requirements so that it can be used for real-time applications (Kiranyaz et al. 2021). In addition, for the utilization of remote sensing data, the use of multi-temporal remote sensing data and the CNN 1-D method is effective in increasing the accuracy of up to 1.9% (Guidici and Clark 2017) and 4% (Song et al. 2019) in classifying land cover. Generally, CNN is a network consisting of several layers where the previous layer's output is connected in sequential order to the next input involving trained weights and biases. CNN comprises three main operations: convolution, nonlinearity, and pooling/subsampling (Zhang et al. 2018). An architecture of one-dimensional CNN consists of an input layer, a convolutional layer, a pooling layer, and a fully connected layer. This research used two convolutional layers, one pooling layer, one dropout layer, and two hidden layers. In this research, the convolutional layers used a kernel size of 2 × 2. The hidden layer used a Rectified Linear Unit as an activation function. A sigmoid function was utilized in the output layer. In addition, the Adam optimizer and binary cross-entropy were utilized as they classify two classes. The learning rate was set to 0.001 with an epoch of 500.

Table 2. Mathematical expression of the GLCM texture features used in the research

GLCM Texture Feature	Mathematical Expression
Contrast	$\sum_{n=1}^{L} n^2 \sum_{x=1}^{L} \sum_{X=1}^{L} P(x,y)$
Entropy	$-\sum_{x=1}^{L} \sum_{X=1}^{L} P(x,y)\, lgP(x,y)$
Homogeneity	$\sum_{x=1}^{L} \sum_{X=1}^{L} \lvert i-j \rvert P(x,y)$
Mean	$\sum_{x=1}^{L} \sum_{X=1}^{L} x.P(x,y)$

Table 3. Classification schemes

Scheme	Bands/Features
1	8 bands VH and VV polarization of σ^0 and γ^0 of pre-fire and post-fire events
2	12 bands of logRBR, RBD, ΔRVI, ΔDPSVI on σ^0 and γ^0
3	20 bands with features consist of Scheme -1 and Scheme -2
4	32 texture feature bands VH and VV polarization of σ^0 and $\gamma^0$of homogeneity, entropy, contrast, and mean in pre-fire and post-fire events

The classification model development was conducted using a workstation with the specifications of an Intel Xeon Gold 6130 CPU @2.10 GHz, and 32 GB RAM. In addition, the Python programming language was used for a deep learning model development using the "TensorFlow" and "Keras" libraries. Geospatial Data Abstraction Library (GDAL) was employed for supervising geospatial image processing, such as data type conversion.

Performance Metrics

Several metrics were used to evaluate the classification model's performance, i.e., overall accuracy (OA), precision, recall, F1-Score, and Cohen's Kappa (K) as stated in Eq. (7) – (11). Overall accuracy is the ratio between our model correctly classified and all the tested data namely true positive (TP), true negative (TN), false positive (FP), and false negative (FN). Precision shows a portion of the predicted burned class that is correct. The recall implies the proportion of a class that is classified correctly based on reference data information (ground truth). Precision and recall become the optimum parameters for class imbalance problems. Meanwhile, the F1-Score is the metric that combines precision and recall and utilizes their harmonic mean. Cohen's Kappa is used to measure the degree of agreement between the predicted results and the reference data. The pe value in Equation (11) shows the probability of change between the predicted results and the reference data (Molin and Jee 2021).

$$Overall\ accuracy\ (OA) = \frac{TP+TN}{TP+TN+FP+FN} \tag{7}$$

$$Precision = \frac{TP}{TP+FP} \tag{8}$$

$$Recall = \frac{TP}{TP+FP} \tag{9}$$

$$F1-Score = 2\times\frac{(Precision \times Recall)}{(Precision \times Recall)} \tag{10}$$

$$Cohen's\ Kappa\ (K) = \frac{Overall\ accuracy - \rho_e}{1-\rho_e} \tag{11}$$

RESULTS

Burned Area Detection Classification Result for Every Scheme

In Scheme -1, where the 8 bands SAR data undergo Boxcar filter, the highest OA, F1-Score, and K values were found in the window size of 13×13 are 0.8060; 0.8050; and 0.6121 respectively as shown in Table 4. For precision and recall values, window sizes of 15×15 and 11×11 were found to be the best settings for precision and recall scores in both performance evaluations. As stated in (Landis and Koff, 1977), this finding demonstrates that the K value using window sizes of 13×13 and 17×17 was categorized as a substantial agreement for Scheme -1, while the other window sizes were categorized as moderate agreement.

Scheme -2 used 12 bands of SAR features that undergo Boxcar filtering as inputs. The window size of 15×15 yielded the highest OA and K values of 0.7822 and 0.5648, respectively. For precision, recall, and F1-score values, the highest value was achieved at a window size of 13×13, 9×9, and 11×11 respectively. The model in Scheme -2 with various window sizes shows an agreement between predicted results and reference data that was categorized as moderate agreement (ranging from 0.4570-0.5648) as shown in Table 4.

In Scheme -3, in which the inputs were a combination of Scheme -1 and Scheme -2 SAR features, the highest OA, recall, F1-Score, and K values were found at a window size of 17×17 with the following value namely 0.8342; 0.8204; 0.8341; and 0.6685 respectively. For precision value, window sizes of 13×13 was the most effective parameter for obtaining the highest value. In Scheme -3, the model showed substantial agreement, except when using a window size of 5×5 based on K value.

In Scheme -4, in which the inputs were the selected GLCM texture features, a window size of 17×17 resulted in the highest OA, recall, precision, F1-Score, and K with the following value of 0.8461; 0.8035; 0.8831; 0.8414; and 0.6926 respectively. In this scheme, a substantial agreement was found in the model with a window size of 13×13, 15×15, and 17×17, while the others were moderate agreement as seen in Table 3.

These results also indicate that an increase in the number of features for classification will result in a longer processing time during training, as demonstrated by Scheme -4, which utilizes the most features. However, increasing the window size does not necessarily increase the training time as depicted in Schemes -1- 4 in Table 4.

Performance Comparison of Different Schemes in Detecting Burned Areas

Fig. 4 depicts the comparison of burned area classification performance indicated by OA, recall, precision, F1-score, and K in each scheme. Comparing Scheme -1 to -4, the highest OA, precision, F1-Score, and K values were achieved in the model Scheme -4 with a window size of 17×17, as shown in Fig. 4. It means that this model has a potency to minimize a mistake in determining the burned area which should be an unburned area. Fig. 5 shows the burned area classification result using Scheme -4 with a window size of 17×17. The highest recall value was in Scheme -3 with a window size of 17×17. This finding also indicates that the burned areas in the area of interest are primarily found in shrub swamps, pure dry agriculture, and paddy fields. It reveals that the burned areas occurred caused by anthropogenic activities.

Compared to Scheme -1 and Scheme -2, combined SAR features such as intensity and polarimetric features in Scheme -3 help to boost the performance in each window size. Additionally, the findings emphasize the importance of selecting SAR features with different window sizes to improve the model's classification performance This research also demonstrates the feasibility of using combined SAR features in Schemes -1 and -2, along with Boxcar's speckle filter in Scheme -3, and Scheme -4, which employs the GLCM texture feature without speckle filtering, for burned area detection.

Fig. 6 displays the results of burned area detection on a selected area in Scheme-1 which has window size of 5×5, and Scheme-4 which has window size of 17×17, representing the worst and the best models, respectively. The blue polygon in Fig. 6 represents a burned area reference derived from SPOT images. When comparing the two figures visually, misclassification of the burned area is mostly on a window size of 5×5 which shows the inability to show burned area patterns as indicated by the yellow and

Table 4. The performance results of burned area classification using the CNN methods for Schemes -1 to -4

Window Size	Scheme -1					
	OA	Recall	Precision	F1 -Score	K	Training Time (min)
5×5	0.7194	0.6903	0.7400	0.7142	0.4392	208.48
7×7	0.7474	0.7429	0.7558	0.7493	0.4949	204.51
9×9	0.7768	0.7772	0.7821	0.7796	0.5535	202.77
11×11	0.7941	0.8116	0.7892	0.8003	0.5880	195.45
13×13	0.8060	0.7882	0.8225	0.8050	0.6121	199.44
15×15	0.7987	0.7553	0.8330	0.7923	0.5980	201.06
17×17	0.8029	0.7950	0.8130	0.8039	0.6059	199.67
Window Size	Scheme -2					
5×5	0.7285	0.7308	0.7338	0.7323	0.4570	234.38
7×7	0.7513	0.7714	0.7473	0.7592	0.5023	229.19
9×9	0.7747	0.7903	0.7718	0.7809	0.5492	229.12
11×11	0.7799	0.7727	0.7897	0.7811	0.5599	227.51
13×13	0.7777	0.7307	0.8128	0.7696	0.5559	221.47
15×15	0.7822	0.7491	0.8082	0.7775	0.5648	225.03
17×17	0.7752	0.7402	0.8020	0.7699	0.5508	231.16
Window Size	Scheme -3					
5×5	0.7635	0.7834	0.7588	0.7709	0.5265	264.69
7×7	0.8024	0.7943	0.8126	0.8033	0.6048	271.84
9×9	0.8026	0.7909	0.8151	0.8028	0.6052	274.34
11×11	0.8130	0.7709	0.8473	0.8073	0.6265	263.05
13×13	0.8183	0.7810	0.8493	0.8137	0.6370	263.91
15×15	0.8226	0.8176	0.8307	0.8241	0.6453	273.81
17×17	0.8342	0.8204	0.8483	0.8341	0.6685	270.40
Window Size	Scheme -4					
5×5	0.7043	0.7686	0.6868	0.7254	0.4074	323.22
7×7	0.7410	0.7125	0.7622	0.7365	0.4824	326.04
9×9	0.7760	0.7997	0.7687	0.7839	0.5515	317.50
11×11	0.7931	0.7480	0.8282	0.7861	0.5868	330.08
13×13	0.8204	0.7869	0.8486	0.8166	0.6411	319.72
15×15	0.8252	0.7944	0.8516	0.8220	0.6507	326.07
17×17	0.8461	0.8035	0.8831	0.8414	0.6926	330.66

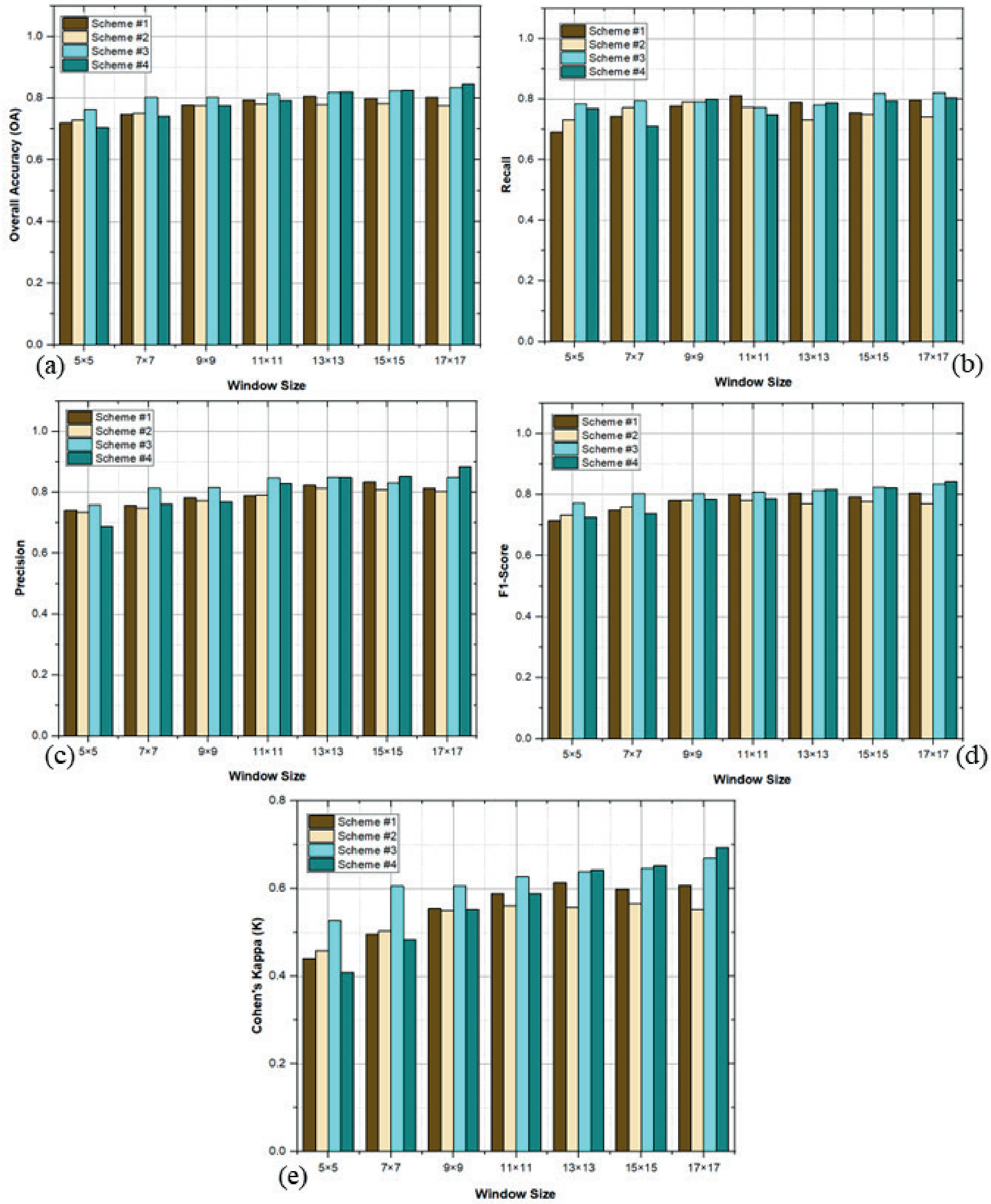

Fig. 4. Performance of burned area classification model using CNN method for Scheme -1 to -4 with performance metrics (a) OA; (b) recall; (c) precision; (d) F1-score; (e) Cohen's Kappa

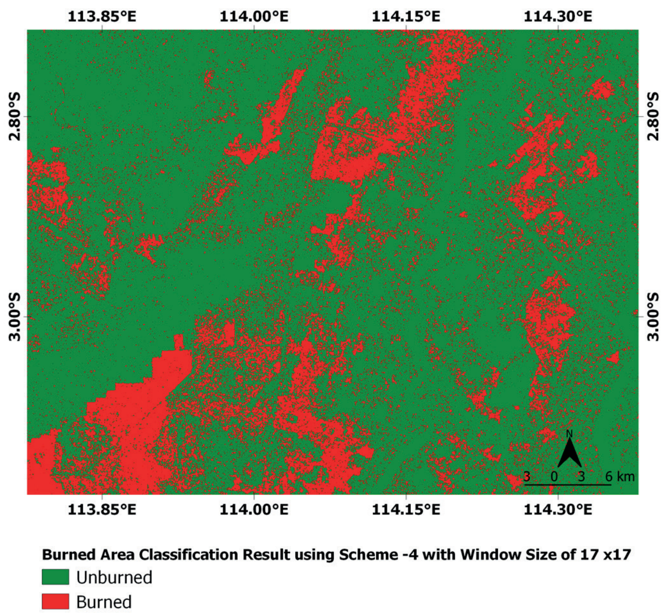

Fig. 5. Burned area classification result for Scheme -4 with a window size of 17×17

orange colours from the Sentinel-1 in Fig 6a. Furthermore, several pixels on the outside of the blue polygon, which are shrub and agricultural area, are incorrectly identified as burned areas. This may occur because the speckle filter's window size is insufficient for extracting surface roughness information between objects. Consequently, finding the optimal window size is essential in acquiring object information, and increasing the window size may reduce misclassification.

Burned Area Estimation

The total burned area in our area of interest based on the best performance is 76,098.6 ha. It includes the total of burned area that is not covered by the SPOT imageries as shown in Fig. 2. It also demonstrates that the Sentinel-1 is successful in identifying the burned area even it is covered by the cloud. Fig. 7 depicts the comparison of the selected subset of burned area classification results between the Scheme -1 with the lowest performance (window size of 5×5) and the Scheme -4 with the highest performance (window size of 17×17), as well as SPOT image is used as reference visually. It shows a misclassification mainly occurred in Scheme -1 with the window size of 5×5 (see Fig 7b). It fails to accentuate the pattern of burned areas and there is no clear boundary between burned and unburned classes. It is proven by the low value of recall. There are a lot of small pixels identified as burn areas which spread almost all the subset, except for the water body that was almost completely identified as unburned areas.

As shown in Fig. 7c, compared to the Figs. 7a and 7b, the burned areas were shaped in a better pattern and were more compact (see white circle on the right). The little pixels identified as unburned areas inside the burned land area had been minimized and aggregated into bigger polygons for the misclassification of unburned areas outside the burned land. However, it still left several areas spread outside the burned land that were misclassified as burned areas. The misclassification of the burned area from Figs. 7b and 7c is shown by the bare land area for plantations that is indicated as devegetation (see yellow circle on the left).

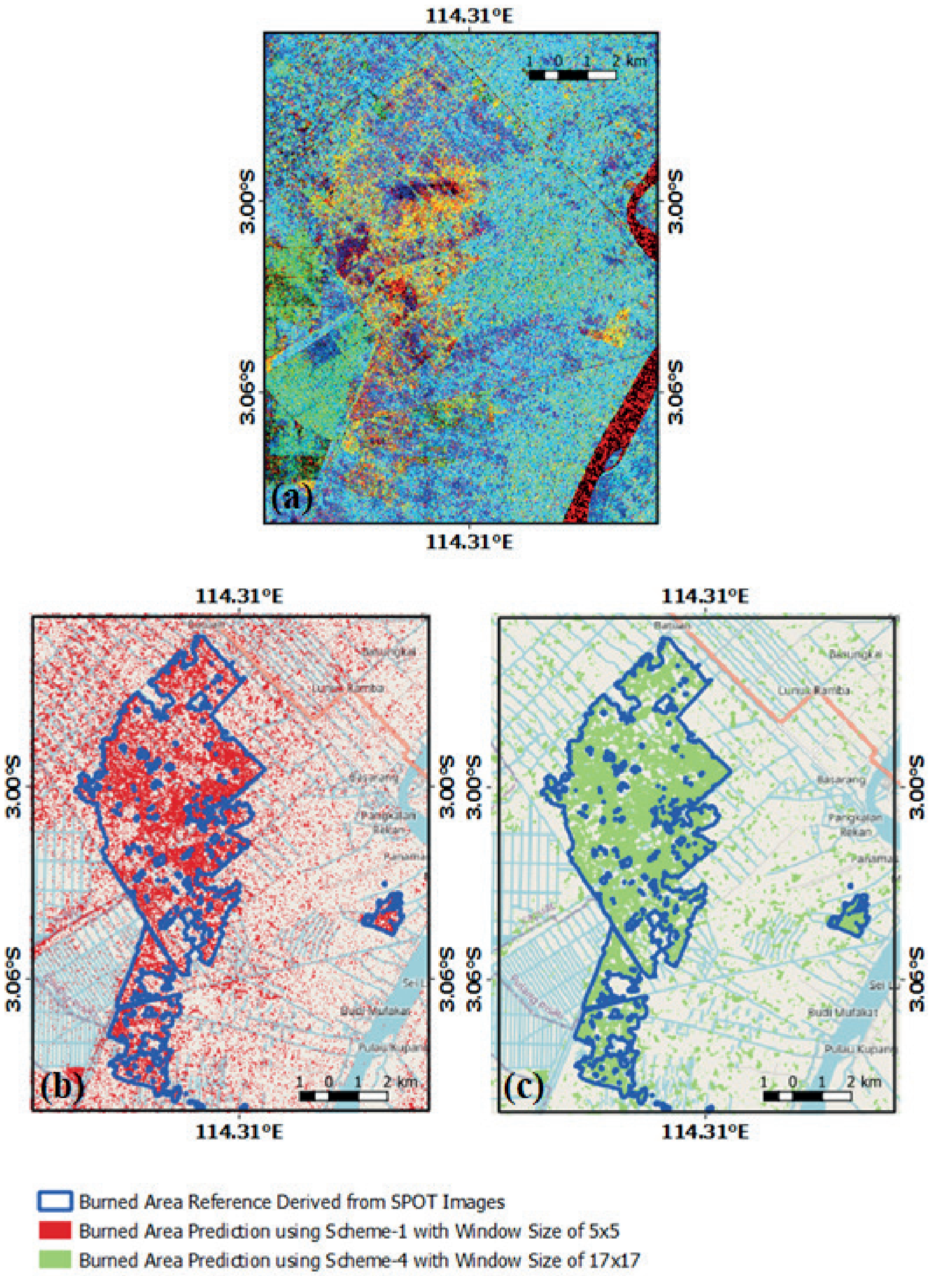

Fig. 6. (a) Sentinel-1 images of post-fire events (R= $VH_{pre\text{-}fire\ event} - VH_{post\text{-}fire\ event}$, G = $VV_{pre\text{-}fire\ event}$, B = $VH_{post\text{-}fire\ event}$); (b) The burned area detection result using scheme -1 with window size of 5×5; (c) The burned area detection result using Scheme -4 with window size of 17×17

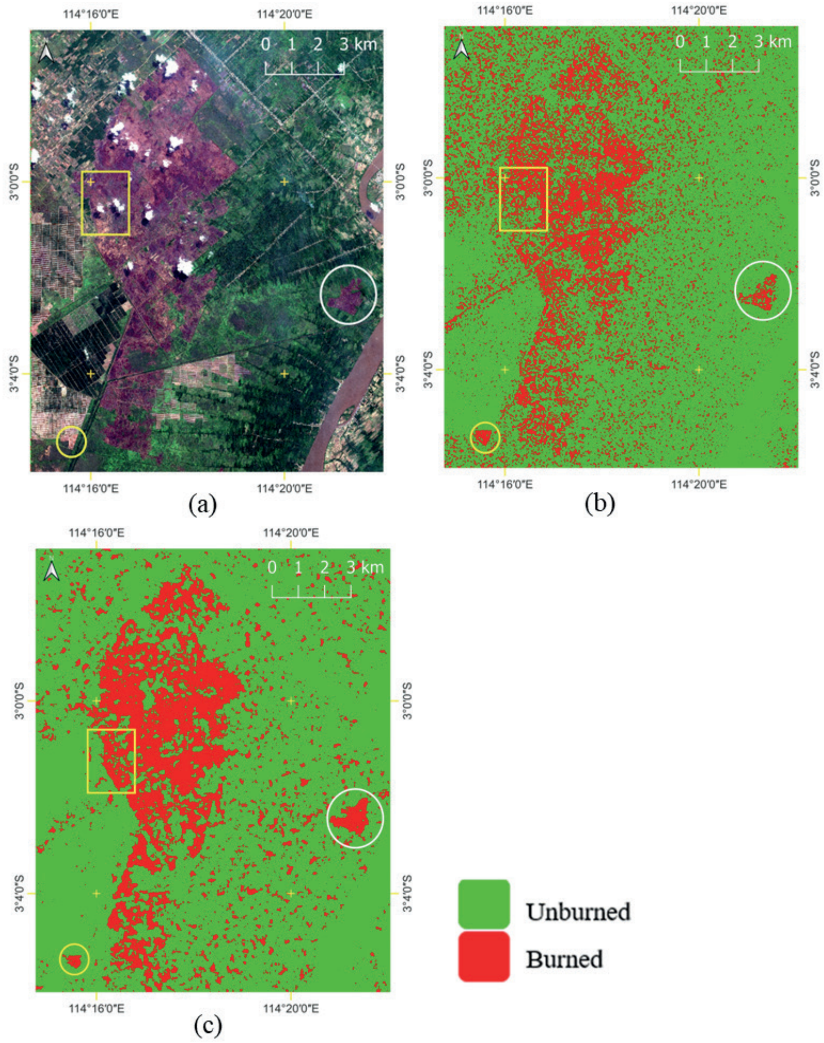

Fig. 7. A subset of burned area; (a) SPOT image as reference; (b) classification result Scheme -1 with window size of 5×5; (c) classification result Scheme -4 with window size of 17×17

The subset of burned area for the best performance scheme and SPOT images were then calculated with the WGS 1984 PDC Mercator as a reference projection system to compare both burned areas. For the model with the highest OA, precision, F1-Score, and K values which is in Scheme -4 with a window size of 17×17, the burned area prediction is up to 4,974.72 ha, whereas the burned area from SPOT images is 4,521.51 ha. It exhibits that the selected subset of burned area estimation using Scheme -4 had approximately 90% agreement with the reference data, SPOT images.

The model in Scheme -4 was also tested in the same area in a different year, 2018. Fig. 8 depicts the burned area classification result. The OA, precision, recall, F1-Score, and K values are 0.7850; 0.8775; 0.6755; 0.7633; and 0.5722 respectively. According to these performance metrics, the model has a good capability to detect the burned area.

DISCUSSION

This research demonstrates the importance of feature and texture selection to increase the model's performance classification. In comparison to the result of (Sudiana et al. 2023), optimum features and window size could increase the evaluation parameter values while using the same classification method. The increase in OA value ranged from 0.58-13.25% with the highest in Scheme -4 which uses GLCM texture features with a window size of 17×17 and without conducting Boxcar's speckle filter. This is also consistent with Gibson et. al's findings (Gibson et al. 2023) that the mean and variance texture indices of larger window sizes (both 11 and 7) are the most important variables for fire severity and fire extent models using Sentinel-1 data. It occurs as GLCM texture features apply a probability of a pixel with a certain gray-level value meeting with a neighbour pixel with a defined gray-level value (James et al. 2021).

The high accuracy of our finding in larger window sizes also depends on the size and pattern of burned areas, which are relatively large with only a few small patches of burned area. Similar to De Luca et al. (De Luca et al. 2021) the research used a large window size (11x11) because small fires were not considered (i.e. less than 0.5 km2). A smaller window size should be considered for small and scattered burned areas. The effectiveness of using a large window size also depends on the spatial resolution of the SAR image, as the finer the spatial resolution of the SAR images, the more heterogeneous the backscatter value for each land cover (Chen et al. 2004; Dorigo et al. 2012). Moreover, Boxcar's speckle filter implements an average filter which leads to increased entropy since different scattering mechanisms can be involved along with the increase in window size (Xie et al. 2018). Furthermore, Boxcar's speckle filter tends to reduce resolution as the window size increases.

According to our research, CNN-1D is feasible to implement because its method is not too complex and does not require much training time. Therefore, this method

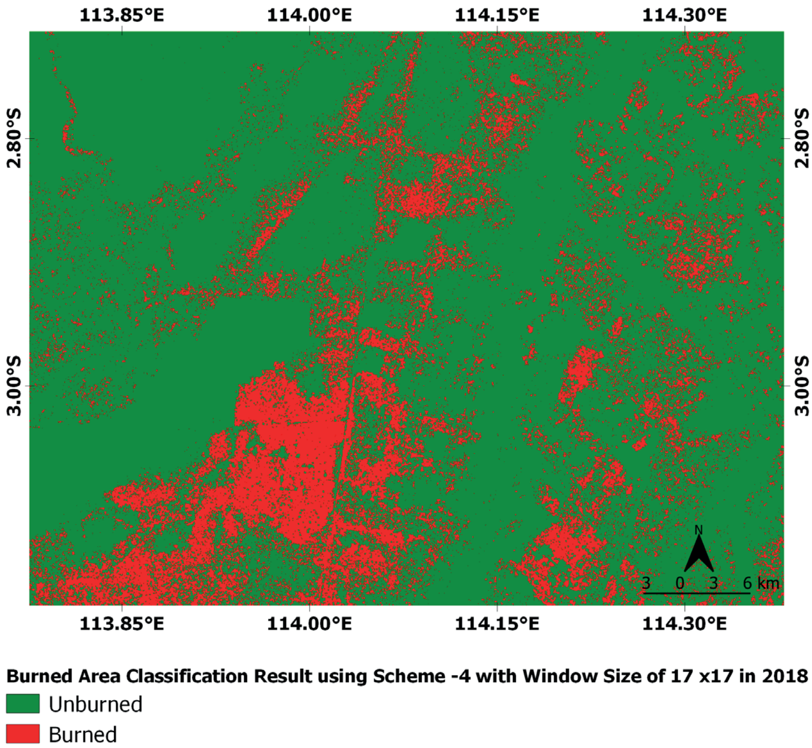

Fig. 8. Burned area classification results for 2018

is suitable for large-scale implementation. There are still numerous pixels that were misclassified since this method considers the pixel value, particularly in the agriculture area which varies seasonally and results in a change in backscatter. Therefore, the object-based approach should be considered to distinguish between the burned area and the misclassified pixels in the agriculture sector.

This research demonstrates the potential of SAR data as a complementary data for detecting burned areas, especially in situations where the observed area is cloudy, hazy, or located in a remote area. Then, by defining the optimum parameters, it may help to decrease misclassification of burned areas. In terms of time savings, window size selection does not significantly affect training time. However, the more polarimetric features and textures used, the longer the processing time.

CONCLUSIONS

This research indicated that the selection of texture features and polarimetric features is essential to optimize the performance of classification. The results obtained show that the highest overall accuracy using CNN classification was achieved at 84.61% in Scheme -4 which uses GLCM texture features and without conducting the Boxcar speckle filter on the window size of 17×17. The total burned area in the area of interest reaches 76,098.6 ha. This research shows that the burned areas in the area of interest are mainly located in shrub swamps, pure dry agriculture, and paddy fields land cover types, implying that they were caused by anthropogenic activities.

This research also shows that the performance of classification by using GLCM texture features without applying the Boxcar speckle filter is better than using intensity and polarimetric features with the Boxcar speckle filter. Furthermore, combining intensity and polarimetric features with a Boxcar speckle filter results in better classification performance than utilizing them separately. In addition, the selection of window size also helps to increase the model's performance. Compared to SPOT images as a reference, the agreement of the burned area estimation on the selected subset reaches approximately 90%.

Furthermore, based on our proposed method of using Sentinel-1 SAR data, this information can help to estimate the carbon loss of burned areas based on the fuel type (land cover) in the research area over time, even if the area is highly covered by the cloud. In future works, this model should be investigated in areas with different landscape characteristics or steep terrain areas since it is crucial. In addition, additional approaches such as decision-level-fusion need to be explored for detecting burned areas in different landscapes or steep areas.

REFERENCES

Abdikan S., Bayik C., Sekertekin A., Balcik F.B., Karimzadeh S., Matsuoka M., and Sanli F.B. (2022). Burned Area Detection Using Multi-Sensor SAR, Optical, and Thermal Data in Mediterranean Pine Forest. Forests, 13(2), 347, DOI: 10.3390/f13020347.

Anand R., Shanthi T., Sabeenian R.S., and Veni S. (2023). GLCM Feature-Based Texture Image Classification Using Machine Learning Algorithms. In: B.V. Kumar., P. Sivakumar., B. Surendiran., and J. Ding, eds., Smart Computer Vision EAI/Springer Innovations in Communication and Computing, Cham: Springer Nature, 103-125, DOI: 10.1007/978-3-031-20541-5_5.

Ansari J., Ghosh S.M., Dev Behera M., and Gupta K. S. (2020). A Study on Speckle Removal Techniques for Sentinel-1A SAR Data Over Sundarbans, Mangrove Forest, India. 2020 IEEE India Geoscience and Remote Sensing Symposium (InGARSS), 90-93, DOI: 10.1109/InGARSS48198.2020.9358929.

Arjasakusuma S., Kusuma S.S., Vetrita Y., Prasasti I., and Arief R. (2022). Monthly Burned-Area Mapping Using Multi-Sensor Integration of Sentinel-1 and Sentinel-2 and Machine Learning: Case Study of 2019's Fire Events in South Sumatra Province, Indonesia. Remote Sensing Applications: Society and Environment, 27, 100790, DOI: 10.1016/j.rsase.2022.100790.

Ban Y., Zhang P., Nascetti A., Bevington A.R., and Wulder M.A. (2020). Near Real-Time Wildfire Progression Monitoring with Sentinel-1 SAR Time Series and Deep Learning. Scientific Reports, 10(1), 1–15, DOI: 10.1038/s41598-019-56967-x.

Center for Kalimantan Ecoregion Development Control Ministry of Environment and Forestry Republic of Indonesia. (2016). Capacity of Natural Resources and The Environment of The Kalimantan Ecoregion Based on Ecosystem Services. (in Indonesian). Palangkaraya: Central Kalimantan Province Environmental Agency.

Central Kalimantan Province Environmental Agency. (2020). Environmental Performance Information Document in 2019 for Central Kalimantan Province. (in Indonesian). Palangkaraya: Central Kalimantan Province Environmental Agency.

Champion I., Germain C., Da Costa J.P., Alborini A., and Dubois-Fernandez P. (2014). Retrieval of Forest Stand Age from SAR Image Texture for Varying Distance and Orientation Values of The Gray Level Co-Occurrence Matrix. IEEE Geosci. Remote Sensing Lett., 11(1), 5–9, DOI: 10.1109/LGRS.2013.2244060.

Chen D., Stow D.A., and Gong P. (2004). Examining The Effect of Spatial Resolution and Texture Window Size on Classification Accuracy: An Urban Environment Case. International Journal of Remote Sensing, 25, 2177–2192, DOI: 10.1080/01431160310001618464.

De Luca G., Silva J.M.N., and Modica G. (2021). A Workflow Based on Sentinel-1 SAR Data and Open-Source Algorithms for Unsupervised Burned Area Detection in Mediterranean Ecosystems. GIScience & Remote Sensing, 58(4), 516-541, DOI: 10.1080/15481603.2021.1907896.

Dekker R.J. (2003). Texture Analysis and Classification of ERS SAR Images for Map Updating of Urban Areas in The Netherlands. IEEE Trans. Geosci. Remote Sensing, 41(9), 1950–1958, DOI: 10.1109/TGRS.2003.814628.

Dorigo W., Lucieer A., Podobnikar T., and Čarni A. (2012). Mapping Invasive Fallopia Japonica by Combined Spectral, Spatial, and Temporal Analysis of Digital Orthophotos. International Journal of Applied Earth Observation and Geoinformation, 19, 185–195, DOI: 10.1016/j.jag.2012.05.004.

Efransjah., Murniningtyas S., Muttaqin M.Z., eds., (2022). The state of Indonesia's Forests 2022. Jakarta: Ministry of Environtment and Forestry.

Efransjah., Murniningtyas S., Erwinsyah., and Damayanti, E.K., eds., (2020). The state of Indonesia's Forests 2020. Jakarta: Ministry of Environtment and Forestry.

Emery W.J. and Camps A. (2017). Introduction to Satellite Remote Sensing: Atmosphere, Ocean, Land and Cryosphere Applications. Amsterdam, Netherlands: Elsevier, DOI: 10.1016/C2015-0-04517-8.

Gaveau D.L.A., Descals A., Salim M.A., Sheil D., and Sloan S. (2021). Refined Burned-Area Mapping Protocol Using Sentinel-2 Data Increases Estimate of 2019 Indonesian Burning. Earth System Science Data, 13(11), 5353–5368, DOI: 10.5194/essd-13-5353-2021.

Gibson R. K., Mitchell A., and Chang H.C. (2023). Image texture analysis enhances classification of fire extent and severity using Sentinel 1 and 2 satellite imagery. Remote Sensing, 15(14), 3512, DOI: 10.3390/rs15143512.

Guidic, D. and Clark M. (2017). One-Dimensional Convolutional Neural Network Land-Cover Classification of Multi-Seasonal Hyperspectral Imagery in The San Francisco Bay Area, California. Remote Sensing, 9(6), 629, DOI: 10.3390/rs9060629.

Ho A.F.W., Zheng H., Earnest A., Cheong K.H., Pek P.P., Seok J.Y., Liu N., Kwan Y.H., Tan J.W.C., Wong T.H., Hausenloy D.J., Foo L.L., Tan B.Y.Q., and Ong M.E.H. (2019). Time-Stratified Case Crossover Study of The Association of Outdoor Ambient Air Pollution with The Risk of Acute Myocardial Infarction in The Context of Seasonal Exposure to The Southeast Asian Haze Problem. Journal of the American Heart Association, 8(6), e011272, DOI: 10.1161/JAHA.118.011272.

Hossain A.K.M.A. and Easson G. (2009). Microwave remote sensing of soil moisture in semi-arid environment. InTech, DOI: 10.5772/8301.

Hosseini M. and Lim S. (2023). Burned Area Detection Using Sentinel-1 SAR Data: A Case Study of Kangaroo Island, South Australia. Applied Geography, 151, 102854, DOI: 10.1016/j.apgeog.2022.102854.

Ismail A.S., Gao X., and Deng C. (2014). SAR Image Classification Based on Texture Feature Fusion. 2014 IEEE China Summit & International Conference on Signal and Information Processing (ChinaSIP), 153-156, DOI: 10.1109/ChinaSIP.2014.6889221.

James J., Heddallikar A., Choudhari P., and Chopde S. (2021). Analysis of Features in SAR Imagery Using GLCM Segmentation Algorithm. In: G.K.Verma, B. Soni, S. Bourennane, and A.C.B. Ramos, eds., Transactions on Computer Systems and Networks Data Science: Theory, Algorithms, And Applications. Singapore: Springer Singapore, 253-266, DOI: 10.1007/978-981-16-1681-5.

Kiranyaz S., Avci O., Abdeljaber O., Ince T., Gabbouj M., and Inman D.J. (2021). 1D Convolutional Neural Networks and Applications: A Survey. Mechanical Systems and Signal Processing, 151, 107398, DOI: 10.1016/j.ymssp.2020.107398.

Landis J.R. and Koch G.G. (1977). The Measurement of Observer Agreement for Categorical Data. Biometrics, 33(1), 159-174.

Lasaponara R. and Tucci B. (2019). Identification of Burned Areas and Severity Using SAR Sentinel-1. IEEE Geosci. Remote Sensing Lett., 16(6), 917–921, DOI: 10.1109/LGRS.2018.2888641.

LeCun Y., Bengio Y., and Hinton G. (2015). Deep Learning. Nature, 521(7553), 436–444, DOI: 10.1038/nature14539.

Lestari A.I., Rizkinia M., and Sudiana D. (2021). Evaluation of Combining Optical and SAR Imagery for Burned Area Mapping Using Machine Learning. 2021 IEEE 11th Annual Computing and Communication Workshop and Conference (CCWC), 52-59, DOI: 10.1109/CCWC51732.2021.9376117.

Luft H., Schillaci C., Ceccherini G., Vieira D., and Lipani A. (2022). Deep Learning Based Burnt Area Mapping Using Sentinel 1 for The Santa Cruz Mountains Lightning Complex (CZU) and Creek Fires 2020. Fire, 5(5), 163, DOI: 10.3390/fire5050163.

Mandal D., Kumar V., Ratha D., Dey S., Bhattacharya A., Lopez-Sanchez J.M., McNairn H., and Rao Y.S. (2020). Dual Polarimetric Radar Vegetation Index for Crop Growth Monitoring Using Sentinel-1 SAR Data. Remote Sensing of Environment, 247,111954, DOI: 10.1016/j.rse.2020.111954.

Ministry of Environment and Forestry (MoEF) Republic of Indonesia. (2019). Recapitulation of Forest and Land Fire Area (Ha) per Province in Indonesia. (in Indonesian). [online] Available at: https://sipongi.menlhk.go.id/ [Accessed 21 Apr 2023].

Molin S. and Jee K. (2021). Hands-On Data Analysis with Pandas: A Python Data Science Handbook for Data Collection, Wrangling, Analysis, and Visualization. Birmingham: Packt Publishing.

Mullissa A.G., Marcos D., Tuia D., Herold M., and Reiche J. (2022). deSpeckNet: Generalizing Deep Learning-Based SAR Image Despeckling. IEEE Trans. Geosci. Remote Sensing, 60, 1–15, DOI: 10.1109/TGRS.2020.3042694.

Murashkin D., Spreen G., Huntemann M., and Dierking W. (2018). Method for Detection of Leads from Sentinel-1 SAR Images. Ann. Glaciol., 59,124–136, DOI: 10.1017/aog.2018.6.

Mutai, S.C. (2019). Analysis of Burnt Scar Using Optical and Radar Satellite Data. Master thesis. Enschede: University of Twente.

Nguyen L.S.P., Chang J.H.W., Griffith S.M., Hien T.T., Kong S.S.K., Le H.N., Huang, H.Y., Sheu, G.R., and Lin, N.H. (2022). Trans-Boundary Air Pollution in A Southeast Asian Megacity: Case Studies of The Synoptic Meteorological Mechanisms and Impacts on Air Quality. Atmospheric Pollution Research, 13, 101366, DOI: 10.1016/j.apr.2022.101366.

Periasamy, S. (2018). Significance of Dual Polarimetric Synthetic Aperture Radar in Biomass Retrieval: An Attempt on Sentinel-1. Remote Sensing of Environment, 217, 537–549, DOI: https://doi.org/10.1016/j.rse.2018.09.003.

Radman A., Shah-Hosseini R., and Homayouni S. (2023). An Unsupervised Saliency-Guided Deep Convolutional Neural Network for Accurate Burn Mapping from Sentinel-1 SAR Data. Remote Sensing, 15(5), 1184, DOI: 10.3390/rs15051184.

Sakti A.D., Anggraini T.S., Ihsan K.T.N., Misra P., Trang N.T.Q., Pradhan B., Wenten I.G., Hadi P.O., and Wikantika K. (2023). Multi-Air Pollution Risk Assessment in Southeast Asia Region Using Integrated Remote Sensing and Socio-Economic Data Products. Science of The Total Environment. 854, 158825, DOI: 10.1016/j.scitotenv.2022.158825.

Singh M. and Kaur G. (2011). SAR Image Classification Using PCA and Texture Analysis. In: Das, V.V., Thomas, G., Lumban Gaol, F., eds., Information Technology and Mobile Communication, Communications in Computer and Information Science. Heidelberg: Springer Berlin., 435-439, DOI: 10.1007/978-3-642-20573-6_78.

Small D. (2011). Flattening Gamma: Radiometric Terrain Correction for SAR Imagery. IEEE Trans. Geosci. Remote Sensing, 49(8), 3081–3093, DOI: 10.1109/TGRS.2011.2120616.

Soh L.K. and Tsatsoulis C. (1999). Texture Analysis of SAR Sea Ice Imagery Using Gray Level Co-Occurrence Matrices. IEEE Trans. Geosci. Remote Sensing, 37(2),780–795.

Song Y., Zhang Z., Baghbaderani R.K., Wang F., Qu Y., Stuttsy, C., and Qi H. (2019). Land Cover Classification for Satellite Images Through 1D CNN, 10th Workshop on Hyperspectral Imaging and Signal Processing: Evolution in Remote Sensing (WHISPERS), 1-5, DOI: 10.1109/WHISPERS.2019.8921180.

Gupta D. K., Prashar S., Singh S., Srivastava, P.K., and Prasad, R. (2022). Introduction to Radar Remote Sensing. In: P.K. Srivastava, D.K. Gupta, T. Islam, D. Han, and R. Prasad, eds., Radar Remote Sensing: Applications and Challenges, Earth Observation Series. Amsterdam: Elsevier, 3-27, DOI: 10.1016/B978-0-12-823457-0.00018-5

Statistics Indonesia. (2010). Kapuas in Figures 2010. Kuala Kapuas, Kapuas: Statistic of Kapuas Regency.

Statistics Indonesia. (2023). Pulang Pisau Regency in Figures 2023. Kahayan Hilir, Pulang Pisau: Statistics of Pulang Pisau Regency.

Sudiana D., Lestari A.I., Riyanto I., Rizkinia M., Arief R., Prabuwono A.S., and Sumantyo J.T.S. (2023) A Hybrid Convolutional Neural Network and Random Forest for Burned Area Identification with Optical and Synthetic Aperture Radar (SAR) Data. Remote Sensing, 15(3), 728, DOI: 10.3390/rs15030728.

Tanase M.A., Belenguer-Plomer M.A., Roteta E., Bastarrika A., Wheeler J., Fernández-Carrillo Á., Tansey K., Wiedemann W., Navratil P., Lohberger S., Siegert F., and Chuvieco E. (2020). Burned Area Detection and Mapping: Intercomparison of Sentinel-1 and Sentinel-2 Based Algorithms Over Tropical Africa. Remote Sensing, 12(2), 334, DOI: 10.3390/rs12020334.

Tanase M.A., Santoro M., Riva J.D.L., Pérez-Cabello F., and Toan T.L. (2010). Sensitivity of X-, C-, And L-Band SAR Backscatter to Burn Severity in Mediterranean Pine Forests. IEEE Transactions on Geoscience and Remote Sensing, 48(10), 3663-3675, DOI: 10.1109/TGRS.2010.2049653.

Wen C., ZhangY., and Deng K. (2009). Urban Area Classification in High Resolution SAR Based on Texture Features. The International Conference on Geo-spatial Solutions for Emergency Management and the 50th Anniversary of the Chinese Academy of Surveying and Mapping, Beijing, China, 281-285.

Xie J., Li Z., Zhou C., Fang Y., and Zhang Q. (2018). Speckle Filtering of GF-3 Polarimetric SAR Data with Joint Restriction Principle. Sensors, 18(5), 1533, DOI: 10.3390/s18051533.

Yahia M., Ali T., Mortula M.M., Abdelfattah R., Mahdy S.E., and Arampola N.S. (2020). Enhancement of SAR Speckle Denoising Using The Improved Iterative Filter. IEEE J. Sel. Top. Appl. Earth Observations Remote Sensing, 13, 859–871, DOI: 10.1109/JSTARS.2020.2973920.

Yeung J. (2019) Indonesian forests are burning, and Malaysia and Singapore are choking on the fumes. [online] Available at: https://www.huahintoday.com/sports/indonesian-forests-still-burning-and-malaysia-and-singapore-are-choking-on-the-fumes/#:~:text=More%20than%20930%2C000%20hectares%20%28about%202.3%20million%20acres%29,all%20week%2C%20with%20air%20quality%20reaching%20unhealthy%20levels [Accessed 20 June 2023].

Zhang C., PanX., Li H., Gardiner A., Sargent I., Hare J., and Atkinson P.M. (2018). A Hybrid MLP-CNN Classifier for Very Fine Resolution Remotely Sensed Image Classification. ISPRS Journal of Photogrammetry and Remote Sensing, 140,133–144, DOI: 10.1016/j.isprsjprs.2017.07.014.

RESEARCH PAPER

LAND SUITABILITY OF COFFEE CULTIVATION UNDER CLIMATE CHANGE INFLUENCE IN THE ECUADORIAN AMAZON

Marco Omar Vizuete Montero[1*], Aurora A. Ariza[2], Nancy M. Barreno[2], Hilter Farley Figueroa-Saavedra[2], Andrea F. Porras[3], Yul Aguilar[3], Wladimir Moya[4]
[1]Universidad de Antioquia – Facultad de Ciencias Agrarias, No 50E-31, 0601060 Medellín – Colombia.
[2]Escuela Superior Politécnica de Chimborazo (ESPOCH), Facultad de Agronomía, Fray Gaspar de Carvajal, Orellana and Riobamba campus, EC060155 – Orellana, Ecuador.
[3]Instituto Superior Tecnológico Martha Bucarám de Roldós, vía Aeropuerto, 170707, Nueva Loja, Lago Agrio, Ecuador
[4]Universidad de Los Lagos, Departamento de Ciencias Biológicas, Laboratorio de Ecología, 5290000 Osorno, Chile
*Corresponding author: movizuetem@libertadores.edu.co
Received: July 8th 2023 / Accepted: April 10th 2024 / Published: July 1st 2024
https://DOI-10.24057/2071-9388-2024-2969

ABSTRACT. In this study, the influence of climate change on land suitability for coffee cultivation in the Ecuadorian Amazon (EA) was investigated using five global circulation models (GCMs) in two different socioeconomic pathways (SSP126 and SSP585). Eleven physioedaphological factors were selected for the analysis and were combined with the most influential bioclimatic variables to model past, present and future suitable areas in five provinces of the EA. In assessing past suitability areas, key determinants varied based on land suitability levels. High suitability areas were primarily influenced by factors such as texture, organic matter content, soil fertility, soil depth, slope, and aspect, while pH, salinity, toxicity, drainage, and stoniness were more associated with moderate suitability areas. The present high suitability areas were influenced by texture, organic matter content, soil fertility, soil depth, and slope, whereas aspect, pH, salinity, toxicity, drainage, and stoniness were more prominent in modeling moderate areas. The ensemble estimation model projected distinct future scenarios for coffee cultivation; under the worst climate scenario (SSP585), Zamora Chinchipe and Morona Santiago, particularly in the east, face considerable unsuitability. Conversely, the more favorable scenario (SSP126) indicates high suitability across Pastaza, Orellana, and Sucumbios, with limited suitability in border areas adjacent to the Highland region. This study highlights the importance of implementing timely adaptation strategies to improve resilience to climate change impacts in the coffee sector.

KEYWORDS: climate-adaptation strategies, coffee, Ecuadorian Amazon, GIS-based modeling, global circulation models

CITATION: Vizuete Montero M. O., Ariza A. A., Barreno N. M., Figueroa-Saavedra H. F., Porras A. F., Aguilar Y., Moya W. (2024). Land Suitability Of Coffee Cultivation Under Climate Change Influence In The Ecuadorian Amazon. Geography, Environment, Sustainability, 2(17), 49-62
https://DOI-10.24057/2071-9388-2024-2969

ACKNOWLEDGEMENTS: The authors thank colleagues from various disciplines who cooperated and provided suggestions for the final version of the paper.

Conflict of interests: The authors reported no potential conflict of interest.

INTRODUCTION

Within the realms of international trade, coffee holds significant prominence both as a pivotal agricultural commodity and a globally consumed beverage. Ecuador, exhibiting notable prowess as a coffee producer, distinguishes itself by exporting a comprehensive array of coffee types, encompassing washed Arabica, natural Arabica, and Robusta (dos Santos and Boffo 2021). Robusta coffee (*Coffea canephora* Pierre) and Arabica coffee (*Coffea arabica* Linnaeus) stand out as economically consequential coffee varieties in Ecuador. Notably, Arabica coffee enjoys heightened demand owing to its superior quality as a beverage (Zambrano-Flores et al. 2018), however, the heightened sensitivity of Arabica coffee to climatic variables renders it susceptible to the impacts of climate change (Pham et al. 2019). This vulnerability is attributed to Arabica coffee's cultivation within specific temperature and precipitation ranges, delineated as 17-23°C and 800-2000 mm year-1, respectively (Tavares et al. 2018). Existing studies corroborate the deleterious effects of climate change on the suitability of areas for coffee cultivation across diverse regions (Gomes et al. 2020; Chavez et al. 2021; Chemura et al. 2021; Jawo et al. 2022).

Fourteen pivotal agroecological factors exert influence over coffee cultivation and production, encompassing physiographic factors such as slope and aspect, as well as edaphological elements like soil texture, fertility, salinity, and toxicity, among others (Hameed et al. 2020). The combination of these factors results in a unique profile for each soil type, whether local or regional. Consequently, even within identical geographical zones where the same coffee variety is cultivated, discernible variations in soil characteristics persist (Chemura et al. 2021). Despite the dependence of coffee production on specific climatic and physio-edaphological determinants, there is a noticeable dearth of comprehensive studies regarding the impact of climate change on both Robusta and Arabica coffee types in the Ecuadorian Amazon (EA), particularly when examined at the province scale.

The study employs five distinct Global Circulation Models (GCMs) under the best-case (SSP126) and worst-case (SSP585) scenarios, and integrates eleven physio-edaphological factors with the most influential bioclimatic variables to model land suitability maps for coffee cultivation. The resulting models delineate the optimal regions for historical (1970-2000), actual (2023), and future (2040) periods across the five provinces constituting the EA as the study area.

MATERIALS AND METHODS

Study area

The five provinces (Fig. 1), constituting the Amazon region, are situated in the southwestern region of Ecuador. These provinces, namely Sucumbios, Orellana, Napo, Pastaza, Morona Santiago, and Zamora Chinchipe, collectively constitute 43% of the Ecuadorian territory. This region, hereafter referred to as the EA, embodies a critical component of the larger Amazon biome (Cabrera-Barona et al. 2020).

The EA encompasses an expansive area of approximately 120,000 km^2, exhibiting an altitudinal range from 100 to 800 meters above sea level (masl). Recognized for its luxuriant vegetation emblematic of humid-tropical forests, as noted by Espinoza et al. (2018), this region stands as a distinctive ecological entity. Notably, coffee plantations occupy an estimated 60,000 hectares within the EA, with the provinces of Sucumbios, Orellana, and Zamora Chinchipe accounting for approximately 34% of Ecuador's total coffee production.

Bioclimatic data

The WorldClim database version 2.1 was the main source for collecting climate data for the past period (1970-2000) and future period (2021-2040) in the region studied[1]. This database provides comprehensive information on 19 bioclimatic variables (Appendix A), encompassing annual temperature and precipitation trends (Fick and Hijmans 2017).

Four variables (minimum and maximum temperature (°C), average temperature (°C), precipitation (mm)) of past climate data were downloaded at spatial resolution of 30 seconds. By the other hand, future climate data were derived from five distinct Global Circulation Models (GCMs) sourced from the Coupled Model Intercomparison Project Phase 6 (CMIP6)[2]. The selected GCMs included CanESM5, CNRM-CM6-1, HadGEM3-GC31-LL, IPSL-CM6A-LR, and MIROC6. These projections were conducted under the two contrasting climate change scenarios, namely the worst-case scenario (SSP585) and the best-case scenario (SSP126) at 30 seconds of spatial resolution. These models were selected because have demonstrated good performance in simulating historical climate conditions, capturing observed patterns, and showing skill in reproducing key climate features relevant for the study region (Olmo et al. 2022; Reboita et al. 2022). In addition the selected models are known for their ability to simulate the bioclimatic variables relevant to coffee cultivation (Bunn et al. 2015; de Sousa et al. 2019; Gomes et al. 2020).

Studies such as those conducted by Wu et al. (2021) and Monteverde et al. (2022) have substantiated the apt representation of anticipated alterations in global mean temperature and precipitation within tropical and Amazon regions of the chosen GCMs. Employing the

Fig. 1. Geographical location of the study areas

[1]worldclim.org/data/worldclim21.html
[2]https://wcrp-cmip.org/cmip-phase-6-cmip6/

Table 1. Selected GCMs for climate change projections in the Ecuadorian Amazon

Model Name	Institution	Spatial Resolution	Scenario
CanESM5	Canadian Centre for Climate Modelling and Analysis	Global	SSP585 SSP126
CNRM-CM6-1	National Centre for Meteorological Research	Global	SSP585 SSP126
HadGEM3-GC31-LL	Met Office Hadley	Global	SSP585 SSP126
IPSL-CM6A-LR	Institut Pierre-Simon LaPlace	Global	SSP585 SSP126
MIROC6	Research Institute for Global Change	Global	SSP585 SSP126

delta method, the GCM outputs underwent downscaling, enabling the computation of variances between model outputs pertaining to historical conditions (1970-2000), actual (2023), and future projections (2040) concerning changes in land suitability. The outcome comprises a high-resolution surface, duly corrected for bias, characterizing the prevailing climate conditions and the 2060 time-slice across the 19 bioclimatic variables.

Physio-edaphological data

Eleven physio-edaphological factors covered crucial attributes for coffee production such as soil pH, soil texture, salinity, organic matter content, soil fertility, toxicity, drainage, stoniness, soil depth, slope, and soil aspect. This data set was obtained from the agroecological criteria for coffee cultivation established by the Ministry of Agriculture and Livestock (MAGAP) and the National Institute for Agricultural Research (INIAP) within continental Ecuador.

Data collecting

In order to analyze the changes in the spatial distribution of areas suitable for Arabica and Robusta coffee during the past and present periods, only the bioclimatic variables that most contributed to determining the suitability of the land for coffee production were selected. This information was compiled from the available literature for the last 15 years (Appendix B).

The search targeted articles that explicitly provided information on the percentage contribution of bioclimatic variables, as modeled through MaxEnt, concerning both the augmentation and diminution of land suitability for coffee production. The MaxEnt model, widely employed in modeling species distribution, environmental conditions, and the repercussions of climate change on crop suitability, operating at local, regional, and global scales (Akpoti et al. 2019; Khalil et al. 2021; Moya et al. 2017; Sarvina et al. 2022; Zhang et al. 2021).

Starting with an initial search that included 209 global studies, , strict selection criteria were meticulously applied. These criteria comprised the necessity for studies to furnish: (a) percentage contribution values of bioclimatic variables; (b) a focus on neotropical or Amazonian ecosystems; (c) engagement in historical and projected bioclimatic simulation studies; and (d) contextualization within the domain of climate change. Following the application of these criteria, a refined selection yielded a total of 10 studies deemed pertinent for the subsequent analysis and formulation of assessments concerning past, present, and future land suitability within the five provinces of the EA.

Evaluation of the land's suitability for coffee cultivation in the past period

Once the 10 studies were selected, the contribution percentages of each climatic variable reported in the results section or annexes of each article were ranked from highest to lowest based on expert's knowledge. Once ranked, an overall average of the relative contribution of each climate variable was calculated. Finally, only the first five bioclimatic variables that together represented 100% (Table 2) were selected in order to build the maps.
Using the weighted overlay tool in ArcGIS version 10.3 software, each selected bioclimatic variable and eleven physio-edaphological factors were assigned weights based on expert's knowledge. The relative weight of all selected bioclimatic variables was accounted for 50%, and the remaining 50% was accounted for by eleven physioedaphological factors (Table 2).

The weights were normalized in order for all of them to sum up to 1. For the weighted overlay tool, the following formula of normalization was used (Ayehu & Atnafu 2015).

$$Normalized\ weight = \frac{Weight\ of\ Factor}{Sum\ of\ all\ weights}$$

For the weighted climate factor the following formula was used (Ferretti & Pomarico 2013).

$$Weighted\ climate\ factor = \frac{Normalized\ weight}{Climate\ variable\ value}$$

Finally, the weighted overlay tool combined these factors to generate a suitability index.

Evaluation of the land suitability for coffee-growing area in the present period

Each physio-edaphological variable underwent classification based on the agro-ecological criteria outlined by MAGAP and INIAP within continental Ecuador and experts' knowledge. These criteria establish land suitability thresholds, ranging from optimal, moderate, marginal, low, and no suitability, in alignment with the agro-ecological requirements stipulated for both Arabica and Robusta coffee varieties.

In the initial phase of the analysis, each layer was procured and imported into ArcGIS in shapefile (shp) format. Following this, all physio-edaphological factors were extracted based on the study area's defined geographical boundaries. Using the reclassification tool, these factors were then classified into four distinct suitability thresholds. The values assigned ranged from 1 to 4, where "1" denoted high land suitability for coffee cultivation, and "4" indicated low owing to inherent soil

Table 2. Selected bioclimatic variables and physioedaphological factors with their weights used to model land suitability maps

	Relative average contribution (%) from the studies	Climatic variable value reported in the specific regions of the studies	Relative weight of factors based on expert consultation
Bioclimatic variable			
Bio 10	32,60	25 °C	12%
Bio 1	17,75	22 °C	10%
Bio 6	17,47	18 °C	8%
Bio 19	17,03	800 -2000 mm	10%
Bio 13	15,81	2500 - 3000 mm	10%
Physioedaphological factors			
Soil texture			10%
Organic matter content	-	-	8%
Soil depth	-	-	8%
Soil fertility	-	-	7%
pH	-	-	6%
Slope	-	-	5%
Drainage	-	-	5%
Aspect	-	-	4%
Stoniness	-	-	3%
Salinity	-	-	2%
Toxicity	-	-	2%

characteristics. Following this reclassification, a homogenization process was undertaken to standardize the geospatial data. The rescaling operation, achieved through the implementation of the resampling tool, resulted in the representation of data in a uniform manner with a 30-meter pixel resolution.

Assessment of the land's suitability for coffee cultivation in the future

Utilizing the five GCMs within specified climate change scenarios (SSP585, SSP126), the climate projections undergo downscaling employing the delta method that corrected the average bias in the monthly GCM projections by first calculating the change (or delta difference between the transient future and historical climate in the GCM simulation), then interpolating this change, and finally adding it to historical observations (e.g., WorldClim). A model ensemble approach by combining the downscaled outputs from the five GCMs was utilized by averaging the results of each model and integrating them with the eleven physio-edaphological variables relevant to coffee cultivation. Finally, the model ensemble estimation by combining the classified outputs of physio-edaphological variables with the ensemble bioclimatic data was executed. Fig. 2 provides a flow chart that summarizes the entire research methodology.

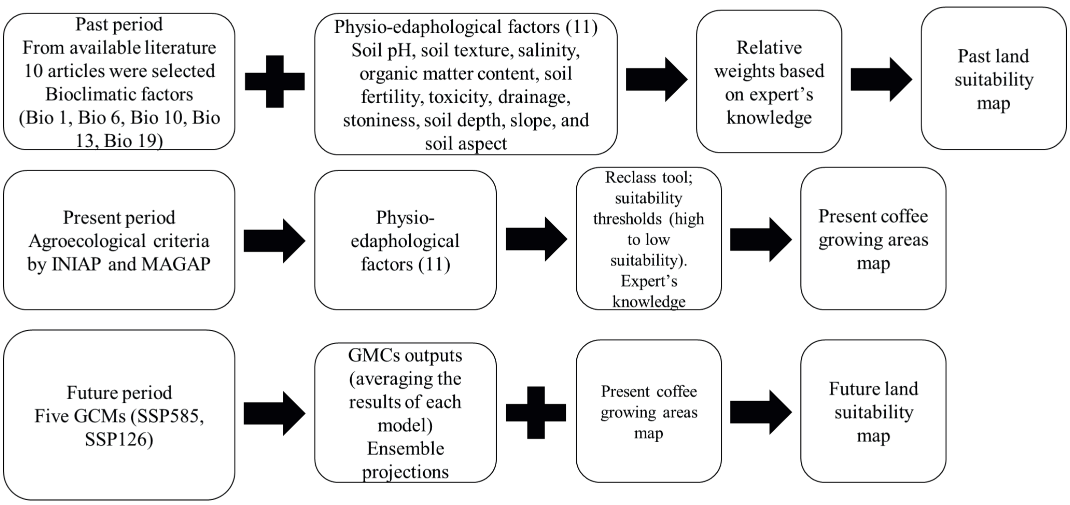

Fig. 2. Methodological framework employed in the research study

RESULTS

In Fig. 3a, the past reclassified map, which amalgamates ten physio-edaphological factors incorporating climatic parameters, is presented based on the suitability thresholds outlined in the guidelines of MAGAP and INIAP. The outcomes reveal that a total land area of 56,103 km^2, constituting 54% of the EA territory, exhibits high suitability for coffee production. Conversely, the remaining 47,736 km^2, representing 46%, is characterized by areas of moderate suitability. Morona Santiago and Orellana provinces emerge as having the largest extents of high suitability, encompassing 27,347 km^2 (26%) and 26,350 km^2 (25%), respectively. Additionally, the provinces displaying the most substantial areas of moderate suitability are the southeastern region of Pastaza and the southwestern region of Morona Santiago, spanning 29,231 km^2 (34%) and 23,930 km^2 (28%), respectively.

In Fig. 3b, the presentation of the same ten physio-edaphological factors, prescribed by the guidelines of the same institutions (MAGAP and INIAP), provides insights into the alterations within these areas from historical records to the current year. Presently, an aggregate of 86,290 km^2 encompasses regions of high suitability for coffee cultivation, particularly bordering the highlands region of Ecuador along the EA. Conversely, the residual area of 358,151.65 km^2 characterizes areas displaying moderate suitability for both coffee varieties. Notably, there are no projections indicating areas that are medium, low, or unsuitability for the current year. The extents of high land suitability range from 5,701 km^2 to 12,047 km^2 across all provinces, with the province of Pastaza emerging as the most substantial, encompassing 29,231 km^2, followed by the province of Morona Santiago with 23,930 km^2.

The regions characterized by moderate suitability for coffee cultivation, when devoid of the impact of climatic variables, exhibited uniformity across all provinces, encompassing an approximate aggregate of 88,000 km^2. The sole exception pertains to Zamora Chinchipe, where the extent of such areas measured 5,437 km^2 (Table 3).

In the ensemble estimation model (Fig. 4), under the worst-case scenario, the findings reveal that the provinces with the most

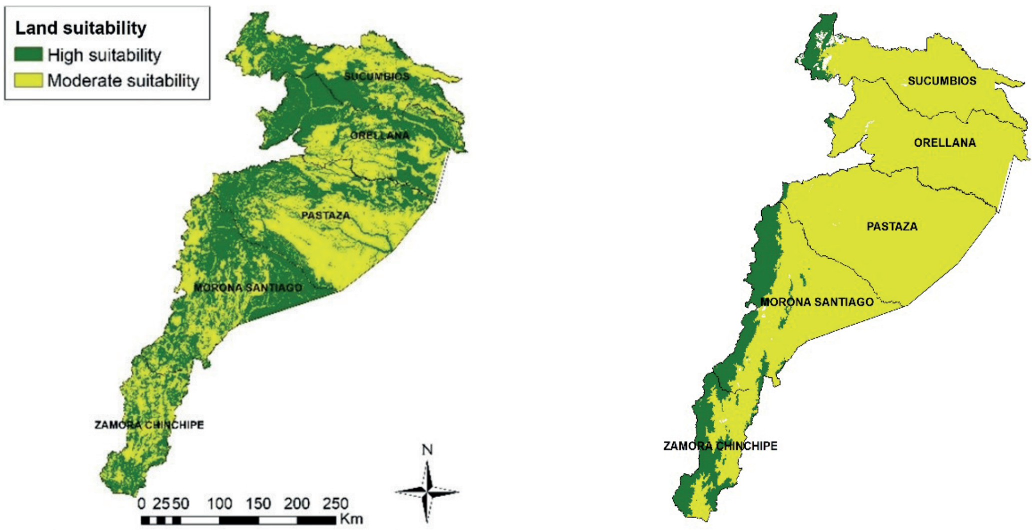

(a) (b)

Fig. 3. (a) Delineates a model incorporating climatic parameters and physio-edaphological factors derived from literature. (b) represents a model founded upon physio-edaphological factors prescribed by guidelines of the MAGAP and the INIAP as well as experts' knowledge

Table 3. Temporal dynamics of soil suitability for coffee cultivation across provinces: Comparative analysis of historical and current scenarios. ZC: Zamora Chinchipe; MS: Morona Santiago; PZ: Pastaza; OR: Orellana; SC: Sucumbíos

Provinces	Temporal variations in land suitability areas considering the impact of climate change over time (1970-2000) (km^2)		Land suitability areas without considering bioclimatic factors (km^2)	
	High	Moderate	High	Moderate
ZC	5.018	7.931	5.701	5.437
MS	11.087	27.347	23.930	88.182
PZ	142.19	21.854	29.231	88.164
OR	111.82	26.350	15.380	88.166
SC	1.843	20.501	12.047	88.201
EA	18.203	103.986	86.290	358.151

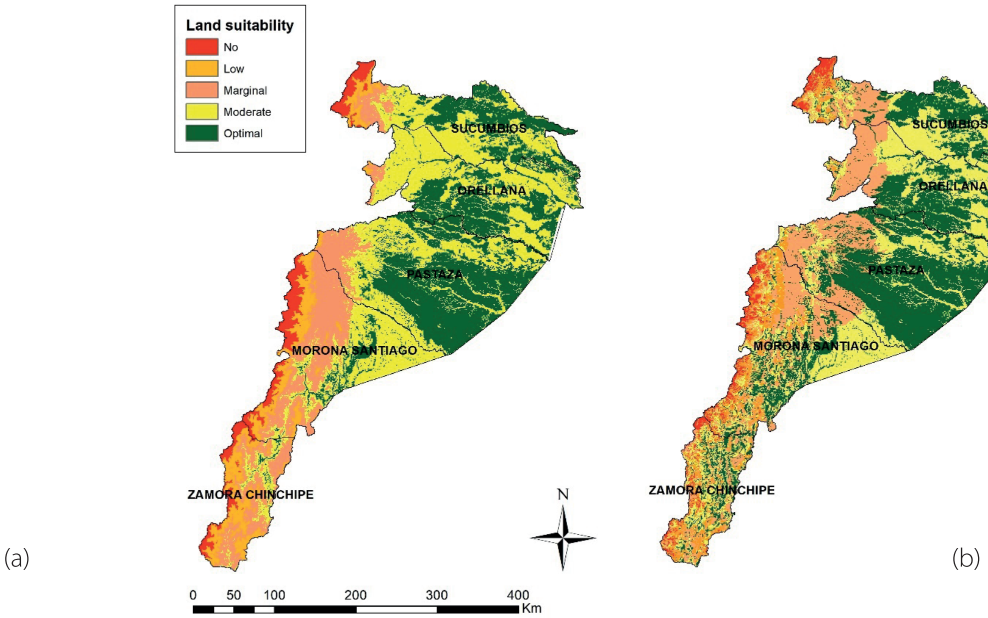

Fig. 4. Ensemble projections for GCMs in its (a) best scenario (SSP126) and worst scenario (SSP585) within the study area

extensive areas unsuitable for coffee cultivation, attributable to the influence of climate change, were Zamora Chinchipe and Morona Santiago, particularly in their eastern sectors. Conversely, in the SSP126 scenario, high land suitability was observed for the provinces of Pastaza, Orellana, and Sucumbios, encompassing their entire territorial expanse. Notably, only the border areas with the Highland region in these provinces were limited to unsuitable areas for coffee cultivation.

Table 4 delineates the percentage variations in high land suitability areas for coffee cultivation across the five GCMs under the best and worst-case scenarios in comparison to existing areas. Broadly, relative to the currently suitable coffee cultivation areas, substantial and predominantly adverse changes in land suitability are evident for both scenarios during the 2021-2040 period. This translates to an approximately 80% reduction in suitable areas, with instances of complete loss noted, particularly pronounced in provinces such as Pastaza and Orellana. In specific instances, the reduction in suitable areas is comparatively modest, as illustrated by the best-case scenario exhibiting an 11% loss for Zamora Chinchipe employing the CNRM-CM6-1 model, and a 30% reduction for Sucumbios with the CanESM5 model.

Table 4. Comparative analysis of changes in land suitability areas for coffee cultivation: Best-case (SSP126) and worst-case (SSP585) scenarios in comparison to current coffee areas. ZC: Zamora Chinchipe; MS: Morona Santiago; PZ: Pastaza; OR: Orellana; SC: Sucumbíos

Provinces	Current coffee growing areas	CanESM5				CNRM-CM6-1				HadGEM3-GC31-LL			
		SSP126		SSP585		SSP126		SSP585		SSP126		SSP585	
	km²	km²	%	km²	%	km²	%	km²	%	km²	%	km²	%
ZC	7.931	455	94	10.047	27	7.029	11	4.990	37	538	93	1.225	85
MS	27.347	8.159	70	6.896	75	7.852	71	6.161	78	6.304	77	2.547	91
PZ	21.854	25.698	18	52	100	421	98	134	99	9.482	57	7	100
OR	26.350	20.632	22	-	100	198	99	99	100	12.664	52	5.7	100
SC	20.501	13.992	32	1.870	91	2.120	90	2.225	89	7.833	62	1.127	95
EA	103.986	68.938	34	18.867	82	17.621	83	13.611	87	36.823	64	4.913	95

Provinces	Current coffee growing areas	IPSL-CM6A-LR				MIROC6			
		SSP126		SSP585		SSP126		SSP585	
	km²	km²	%	km²	%	km²	%	km²	%
ZC	7.931	447	94	1.214	85	490	94	656.5	92
MS	27.347	6.352	77	2.549	91	6.317	77	1.019	96
PZ	21.854	9.407	57	7.4	100	9.488	57	-	100
OR	26.350	12.645	52	5.7	100	12.662	52	-	100
SC	20.501	7.770	62	1.134	94	7.837	62	710.2	97
EA	103.986	36.621	65	4.911	95	36.796	65	2.386	98

The provinces with the most pronounced potential reduction in suitable areas for coffee cultivation were identified as Zamora Chinchipe and Morona Santiago, with respective reductions of 77% and 74% in the best-case scenario. Conversely, all provinces, excluding Zamora Chinchipe, displayed substantial reductions of 85%, 99%, and 93%, respectively, in the worst-case climate change scenario. At the broader scale of the EA, these projections signify an anticipated greater reduction in suitable areas for coffee cultivation, particularly evident with the CNRM-CM6-1 model under the best scenario (83%), and the MIROC6 model under the worst scenario (98%).

Moreover, discernible in the provinces of Zamora Chinchipe and Pastaza is a notable expansion in areas deemed suitable for coffee cultivation, exhibiting increases of 27% and 18% in the worst and best scenarios, respectively. It is noteworthy that the magnitude of change in suitable areas for coffee cultivation is more pronounced in the worst scenario, averaging an 87% reduction in surface area across all GCMs, with MIROC6 presenting the highest magnitude. Conversely, in the best scenario, the reduction in suitable areas averages around 64% across all GCMs, with the CNRM-CM6-1 model registering the most substantial reduction.

Fig. 5a, highlights areas sensitive to climate change using the worst-case scenario and zonal changes in specific areas within the EA. It can be noted that compare to current period (Fig. 3b), central areas of all the provinces are sensitive to climate change in the future period, specially Orellana, Morona Santiago, Pastaza and Zamora Chinchipe due to the presence of marginal, moderate and high areas. In the worst case scenario (Fig. 5b) reveal that all provinces show areas with moderate changes in land use. These changes are mainly manifested in the transformation of forests, shrub and herbaceous vegetation, as well as agricultural land to anthropogenic zones, (areas affected by human activity). This could suggest the presence of significant transformations in these areas, either due to the expansion of human activities, changes in forest cover, or evolution in land use for agricultural or livestock purposes. In general, the results indicate that the areas identified in the south and north of Zamora Chinchipe, as well as in the eastern part of the provinces of Morona Santiago, Pastaza, Orellana and Sucumbíos, are experiencing moderate changes in land use, with a tendency towards anthropogenic transformation.

DISCUSSION

This study conducted an assessment of land suitability areas for coffee cultivation, encompassing both Arabica and Robusta varieties, through the integration of climatic and soil physio-edaphological factors. Employing five GCMs, the investigation considered scenarios representing both the best and worst climatic conditions.

The results of our study highlight that the mean temperature of the warmest quarter (Bio10) and annual mean temperature (Bio1) emerge as pivotal climatic factors significantly influencing the modulation of past period land suitability maps. These temperature variables, along with the temperature of the coldest and warmest month, as well as precipitation during the wettest and driest month, have been substantiated as limiting factors in historical projections of bioclimatic variables, as demonstrated by Hijmans et al. (2005).

Vast areas in the EA exhibit significant suitability for coffee production, with approximately 54% of the territory demonstrating high suitability in the recent past. This finding aligns with the growing economic and agricultural importance of coffee cultivation in the region. Morona Santiago and Orellana, in particular, emerge as the most prominent provinces in terms of land area with high suitability, covering an impressive 26% and 25% of the territory respectively. This information supports the potential viability of these provinces as important coffee producers in the future. Comparing these results with previous studies on suitability for coffee cultivation, a coherence in certain patterns can be observed, which highlighted the high suitability of specific regions for coffee production (Chemura et al. 2021; Läderach et al. 2017; Ranjitkar et al. 2016). The coincidence between the present findings and those of previous studies strengthens the validity of the suitability identified in Morona Santiago and Orellana, consolidating the importance of these areas as strategic points for coffee cultivation.

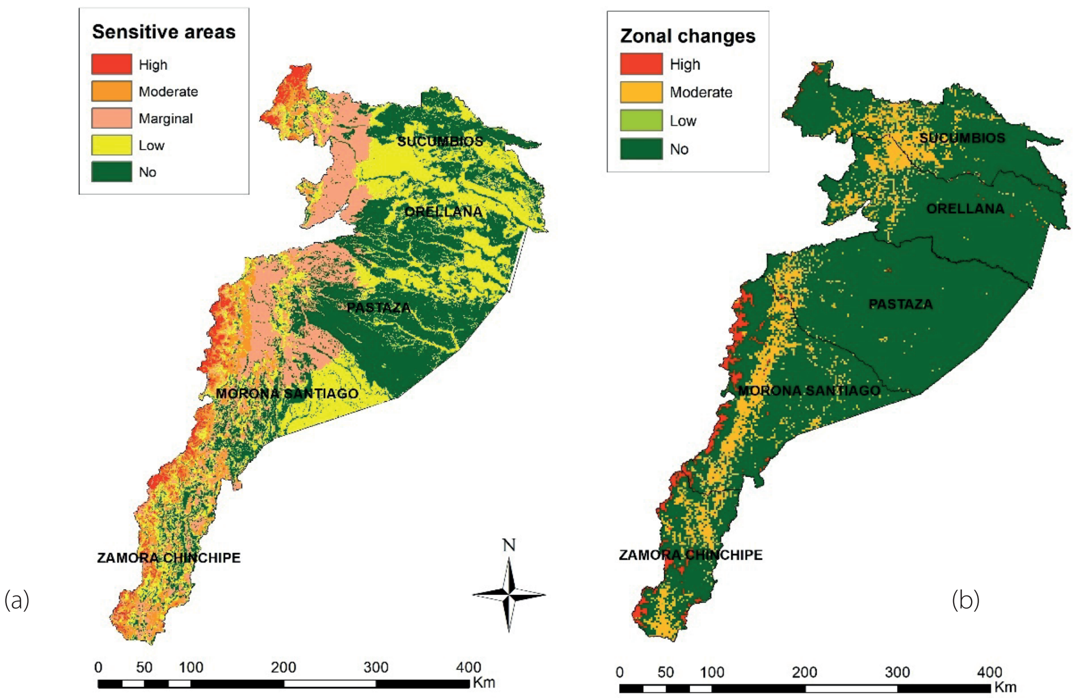

Fig. 5. (a) Sensitive areas to climate change using the worst-case scenario, whereas (b) shows zonal changes in specific areas

Although high suitability for coffee production is an encouraging indicator of agricultural development, it is crucial to consider the sustainability and environmental aspects associated of this activity. Additional studies, have examined the interaction between the expansion of agricultural crops, including coffee, and its impact on biodiversity and ecosystem services (Barrios et al. 2018; De Beenhouwer et al. 2013). In addition, it is essential to address the variability in suitability identified in the present study, especially in the provinces of Pastaza and Morona Santiago, where areas with moderate suitability are observed. Previous studies, have explored agricultural management strategies and sustainable practices to optimize production in areas with moderate suitability (Castro-Tanzi et al. 2012; D'haeze et al. 2005), highlighting the importance of adopting adaptive approaches to ensure the long-term resilience of the coffee sector in these regions.

It is interesting to note that the results do not identify areas of medium, low or unsuitable suitability for coffee cultivation in the present period. This absence of less favorable projections can be interpreted as a positive sign for coffee activity in the study region. Previous studies (Benti et al. 2022; Chemura et al. 2021; Salas et al. 2020), have addressed the influence of climatic and geographic factors on the suitability for coffee cultivation, corroborating the idea that the topography and climatic conditions specific to the highlands of Ecuador contribute significantly to the high suitability that the present study has identified.

In terms of specific extensions of high suitability, variations between 5,701 km^2 and 12,047 km^2 in all provinces were observed, with Pastaza being the province with the largest extension, followed closely by Morona Santiago. This specific distribution highlights intra-provincial variability and underscores the importance of considering local factors in the design of agricultural development strategies.

The results obtained through the ensemble estimation model under different climate change scenarios (SSP585 and SSP126) provide an enlightening view on the susceptibility of Ecuadorian provinces to future conditions. The identification of the provinces of Zamora Chinchipe and Morona Santiago as the most affected in the worst case scenario (SSP585) reflects a worrying trend towards a decrease in areas suitable for coffee cultivation in these regions, especially in their eastern sectors. This finding is consistent with previous research, which also highlighted the vulnerability of other similar regions to the impacts of climate change due to the increase in temperatures and the alteration of climatic conditions traditionally favorable for coffee cultivation (Beltrán-Tolosa et al. 2022; Koh et al. 2020; Rahn et al. 2014).

However, the variability in results between scenarios highlights the need to consider diverse future trajectories in agricultural planning. has explored the utility of ensemble models to address uncertainty associated with climate projections (Parker 2013; Shortridge & Zaitchik 2018; Zumwald et al. 2020). These findings highlight the importance of considering multiple scenarios to inform strategic agricultural decisions and policies, recognizing the complexity of climatic factors and their influence on suitability for coffee cultivation.

On the other hand, the results highlighting the sensitivity to climate change in the central areas of several Ecuadorian provinces, especially Orellana, Morona Santiago, Pastaza and Zamora Chinchipe, shed light on the complex interaction between climate change and land use in the region. This pattern of sensitivity in central areas could have significant implications for agriculture, particularly for coffee cultivation, which is highly dependent on specific climatic conditions. Previous research has also highlighted the vulnerability of these regions to the impacts of climate change, such as changes in precipitation patterns and temperatures, which could potentially impact the suitability of the land for coffee cultivation (Gomes et al. 2020; Jawo et al. 2022; Lemma & Megersa 2021).

The identification of areas with moderate land use changes in all provinces, especially under the worst climate scenario (SSP585), suggests significant landscape transformations. The transition from forests, shrubs, and herbaceous vegetation, as well as agricultural land, to anthropogenic zones, points to changes induced by human activities. This finding is in line with previous studies, which have explored the relationship between the expansion of human activities and changes in land use, highlighting the need for sustainable management strategies to mitigate negative impacts on biodiversity and ecosystem health (Haggar et al. 2013; Navidad et al. 2023; Verbist et al. 2005). The projected changes in temperature associated with the worst-case scenario towards the culmination of the 2040 period appear to contribute to a discernible decrease in high suitability areas. This corroborates findings in the study by Gomes et al. (2020), wherein the anticipated alterations in temperature and precipitation are postulated to result in a substantial reduction in suitability for coffee production. The critical role of these variables (Bio1 and Bio10) lies in the simultaneous increase in temperature and reduction in precipitation, potentially inducing elevated evapotranspiration rates and a subsequent decline in water availability, thereby prolonging dry seasons.

The anticipated change in land suitability by 2040 suggests an average decrease of 63% in the best-case scenario and 87% in the worst-case scenario for coffee cultivation across the EA; this reduction is likely influenced significantly by the extent of each province and the GCMs utilized. Comparable shifts have been documented in global and regional studies, projecting a potential 90% decrease in suitable areas for coffee production by 2050 (Bunn et al. 2015; Läderach et al. 2017).

In the present study, the projected 87% reduction in suitable areas, particularly in the SSP585 scenario, is anticipated to predominantly impact the Amazon forest within the five provinces, potentially impacting the livelihoods of local communities for whom coffee cultivation is a primary activity. Nevertheless, recent research suggests that the expected adverse effects of rising temperatures and altered rainfall patterns on coffee production may be partially offset by a fertilizing effect of CO_2 associated with greenhouse gas emissions, offering a potential offset of 13-21% (Rahn et al. 2018; DaMatta et al. 2019). The analysis by Cassamo et al. (2023) indicates that future scenarios (SSP126, SSP585) could have detrimental effects on the Mozambican Arabica industry, particularly under Agroforestry Systems (AFS) and full sun systems, with the latter experiencing more pronounced adverse effects. By the period 2041-2060, suitable areas are projected to diminish by approximately one-half to two-thirds under AFS, contingent on the specific scenarios considered.

In response to the challenges posed by climate change, particularly the rise in temperatures and precipitation deficits, the adoption of AFS has been proposed as a viable adaptation strategy to preserve the current expanse of high land suitability for coffee production (de Sousa et al. 2019; Sebatta et al. 2019). To mitigate the impact of climate change on coffee production, farmers have the potential to enhance adaptation strategies by increasing the shade cover in AFS beyond the 50% threshold; this necessitates tailored shade management throughout the year, involving reduced shade cover post-harvest when coffee plants require heightened solar energy for node development (Gomes et al. 2020).

The imperative significance of implementing and applying AFS has been underscored in various studies, with notable applications observed, particularly in the Coast region of Ecuador (Jarrett et al. 2017; Vaca et al. 2018). This strategy emerges as a viable option to effectively mitigate the impact of climate change on coffee cultivation. It is crucial that local coffee farmers in the EA region comprehend the nuanced effects of climate change, and this understanding can be fostered through ongoing training sessions facilitated by specialists and scientists within the coffee sector. Furthermore, this study advocates for future research endeavors that integrate climatic, physio-edaphological, and socio-economic factors in modeling predictions, thereby enhancing their informativeness, particularly at the regional or national scale. Such an integrated approach has the potential to generate context-specific recommendations for the successful implementation of coffee agroforestry systems.

CONCLUSIONS

In conclusion, this research highlights the critical importance of climatic variables, specifically the mean temperature of the warmest quarter (Bio10) and the mean annual temperature (Bio1), in the modulation of soil suitability maps in past periods. These climatic variables are revealed as fundamental factors that significantly influence environmental conditions, delineating soil suitability for both varieties of coffee cultivation.

The study also highlighted the high suitability of extensive areas within the study area (EA) for coffee production during the past period, covering approximately 54% of the territory. This finding not only reflects the region's historical relevance in coffee production, but also aligns with the growing economic and agricultural importance of coffee cultivation nationally and internationally.

The provinces of Morona Santiago and Orellana stand out as the most promising in terms of land areas with high aptitude, covering a remarkable 26% and 25% of the territory, respectively. This distribution highlights the significant contribution that these provinces can make to the coffee sector, positioning them as key players in the future coffee production landscape. The identification of these provinces as strategic areas supports effective planning for the region's sustainable coffee growing development .

The detailed analysis of the projections of suitability for coffee cultivation in all the provinces of the study area reveals key aspects that have an impact on the viability and planning of the coffee sector. A particularly significant finding is the absence of areas identified as medium, low or unsuitable for coffee cultivation in the current period in all provinces. This fact, which highlights the homogeneity of favorable conditions in the region, can be interpreted as a positive indicator for coffee activity, suggesting a favorable scenario for the expansion and sustainability of coffee production in the study area.

The ensemble estimation model employed elucidates distinctive scenarios for the future of coffee cultivation in the EA. Under the SSP585 climate change scenario, Zamora Chinchipe and Morona Santiago, particularly their eastern sectors, emerge as provinces facing significant unsuitability for coffee cultivation. Contrastingly, the SSP126 scenario presents a more optimistic outlook, revealing high land suitability across the entire territorial expanse of Pastaza, Orellana, and Sucumbios provinces. It is noteworthy that areas bordering the Highland region within these provinces exhibit only unsuitable conditions for coffee cultivation.

In addition, this study highlights the inescapable interconnection between climate change and land use dynamics in several Ecuadorian provinces, with a special focus on Orellana, Morona Santiago, Pastaza and Zamora Chinchipe. The identification of these core areas as particularly sensitive to climate change sheds light on a complex interaction that could have substantial implications for regional agriculture, especially with regard to coffee cultivation, a sector highly dependent on specific climatic conditions.

This pattern of sensitivity highlights the vulnerability of the core areas of these provinces, pointing to the pressing need for adaptive strategies in agricultural planning and land use management. Coffee cultivation, which is an activity that takes place in a specific climatic environment, is particularly affected by variations in climatic conditions. Understanding this sensitivity provides a solid basis for developing mitigation and adaptation measures to safeguard the resilience of regional agriculture to the challenges of climate change.

REFERENCES

Akpoti K. Kabo-bah A.T. and Zwart S.J. (2019). Review - Agricultural land suitability analysis: State-of-the-art and outlooks for integration of climate change analysis. Agricultural Systems, 173, 172-208, DOI: 10.1016/j.agsy.2019.02.013

Ayehu G. and Atnafu S. (2015). Land Suitability Analysis for Rice Production: A GIS Based Multi-Criteria Decision Approach. American Journal of Geographic Information System, 4(3), 95-104, DOI: 10.5923/j.ajgis.20150403.02

Barrios E. Valencia V. Jonsson M. Brauman A. Hairiah K. Mortimer P.E. and Okubo S. (2018). Contribution of trees to the conservation of biodiversity and ecosystem services in agricultural landscapes. International Journal of Biodiversity Science, Ecosystem Services & Management, 14(1), 1-16, DOI: 10.1080/21513732.2017.1399167

Beltrán-Tolosa L.M. Cruz-Garcia G.S. Ocampo J. Pradhan P. and Quintero M. (2022). Rural livelihood diversification is associated with lower vulnerability to climate change in the Andean-Amazon foothills. PLOS Climate, 1(11), e0000051. DOI: 10.1371/journal.pclm.0000051

Benti F. Diga G.M. Feyisa G.L. and Tolesa A.R. (2022). Modeling coffee (Coffea arabica L.) climate suitability under current and future scenario in Jimma zone, Ethiopia. Environmental Monitoring and Assessment, 194(4), 271. DOI: 10.1007/s10661-022-09895-9

Bunn C. Läderach P. Rivera O.O. and Kirschke D. (2015). A bitter cup: Climate change profile of global production of Arabica and Robusta coffee. Climatic Change, 129(1), 89-101. DOI: 10.1007/s10584-014-1306-x

Cabrera-Barona P.F. Bayón M. Durán G. Bonilla A. and Mejía V. (2020). Generating and Mapping Amazonian Urban Regions Using a Geospatial Approach. ISPRS International Journal of Geographic Information, 9(7), 453. DOI: 10.3390/ijgi9070453

Cassamo C.T. Draper D. Romeiras M.M. Marques I. Chiulele R. Rodrigues M. Stalmans M. Partelli F.L. Ribeiro-Barros A. and Ramalho J.C. (2023). Impact of climate changes in the suitable areas for Coffea arabica L. production in Mozambique: Agroforestry as an alternative management system to strengthen crop sustainability. Agriculture, Ecosystems & Environment, 346, 108341. DOI: 10.1016/j.agee.2022.108341

Castro-Tanzi S. Dietsch T. Urena N. Vindas L. and Chandler M. (2012). Analysis of management and site factors to improve the sustainability of smallholder coffee production in Tarrazú, Costa Rica. Agriculture, Ecosystems & Environment, 155, 172-181. DOI: 10.1016/j.agee.2012.04.013

Chavez E. Wade J. Miernicki E.A. Torres M. Stanek E.C. Subía C. Caicedo C. Tinoco L. and Margenot A.J. (2021). Apparent nitrogen limitation of Robusta coffee yields in young agroforestry systems. Agronomy Journal, 113(6), 5398-5411. DOI: 10.1002/agj2.20725

Chemura A. Mudereri B.T. Yalew A.W. and Gornott C. (2021). Climate change and specialty coffee potential in Ethiopia. Scientific Reports, 11(1), 8097. DOI: 10.1038/s41598-021-87647-4

DaMatta F.M. Rahn E. Läderach P. Ghini R. and Ramalho J.C. (2019). Why could the coffee crop endure climate change and global warming to a greater extent than previously estimated? Climatic Change, 152(1), 167-178. DOI: 10.1007/s10584-018-2346-4

De Beenhouwer M. Aerts R. and Honnay O. (2013). A global meta-analysis of the biodiversity and ecosystem service benefits of coffee and cacao agroforestry. Agriculture, Ecosystems & Environment, 175, 1-7. DOI: 10.1016/j.agee.2013.05.003

D'haeze D. Deckers J. Raes D. Phong T.A. and Loi H.V. (2005). Environmental and socio-economic impacts of institutional reforms on the agricultural sector of Vietnam: Land suitability assessment for Robusta coffee in the Dak Gan region. Agriculture, Ecosystems & Environment, 105(1), 59-76. DOI: 10.1016/j.agee.2004.05.009

de Sousa K. van Zonneveld M. Holmgren M. Kindt R. and Ordoñez J.C. (2019). The future of coffee and cocoa agroforestry in a warmer Mesoamerica. Scientific Report, 9(1), 8828. DOI: 10.1038/s41598-019-45491-7

dos Santos H.D. and Boffo E.F. 2021. Coffee beyond the cup: Analytical techniques used in chemical composition research—a review. European Food Research and Technology, 247(4), 749-775. DOI: 10.1007/s00217-020-03679-6

Espinoza J.L. Jara-Alvear J. and Urdiales L. (2018). Sustainability of Renewable Energy Projects in the Amazonian Region. In: M.E. Tyler, ed., Sustainable Energy Mix in Fragile Environments: Frameworks and Perspectives, 1st ed. Springer International Publishing., 107-139, DOI: 10.1007/978-3-319-69399-6_7

Ferretti V. and Pomarico S. (2013). Ecological land suitability analysis through spatial indicators: An application of the Analytic Network Process technique and Ordered Weighted Average approach. Ecological Indicators, 34, 507-519. DOI: 10.1016/j.ecolind.2013.06.005

Fick S.E. and Hijmans R.J. (2017). Worldclim 2: New 1-km spatial resolution climate surfaces for global land areas. International Journal of Climatology, 37(12), 4302-4315. DOI:10.1002/joc.5086

Gomes L.C. Bianchi F. Cardoso I.M. Fernandes R.B. Filho E.I. and Schulte R.P. (2020). Agroforestry systems can mitigate the impacts of climate change on coffee production: A spatially explicit assessment in Brazil. Agriculture Ecosystem and Environment, 294, 106858. DOI: 10.1016/j.agee.2020.106858

Haggar J. Medina B. Aguilar R.M. and Munoz C. (2013). Land Use Change on Coffee Farms in Southern Guatemala and its Environmental Consequences. Environmental Management, 51(4), 811-823. DOI: 10.1007/s00267-013-0019-7

Hameed A. Hussain S.A. and Suleria H.A. (2020). «Coffee Bean-Related» Agroecological Factors Affecting the Coffee. In: J. Mérillon and K. Ramawat, eds., Co-Evolution of Secondary Metabolites, 1st ed. Springer International Publishing., 641-705, DOI: 10.1007/978-3-319-96397-6_21

Hijmans R.J. Cameron S.E. Parra J.L. Jones P.G. and Jarvis A. (2005). Very high-resolution interpolated climate surfaces for global land areas. International Journal of Climatology, 25(15), 1965-1978. DOI: 10.1002/joc.1276

Jarrett C. Cummins I. and Logan-Hines E. (2017). Adapting Indigenous Agroforestry Systems for Integrative Landscape Management and Sustainable Supply Chain Development in Napo, Ecuador. In: F. Montagnini, ed., Integrating Landscapes: Agroforestry for Biodiversity Conservation and Food Sovereignty, 2nd ed. Springer International Publishing., 283-309, DOI: 10.1007/978-3-319-69371-2_12

Jawo T.O. Kyereh D. and Lojka B. (2022). The impact of climate change on coffee production of small farmers and their adaptation strategies: A review. Climate and Development, 0(0), 1-17. DOI: 10.1080/17565529.2022.2057906

Khalil T. Asad S.A. Khubaib N. Baig A. Atif S. Umar, M. et al. (2021). Climate change and potential distribution of potato (Solanum tuberosum) crop cultivation in Pakistan using Maxent. AIMS Agriculture and Food. 6(2), 663-676. DOI: 10.3934/agrfood.2021039

Koh I. Garrett R. Janetos A. and Mueller N.D. (2020). Climate risks to Brazilian coffee production. Environmental Research Letters, 15(10), 104015. DOI: 10.1088/1748-9326/aba471

Läderach P. Ramirez–Villegas J. Navarro-Racines C. Zelaya C. Martinez–Valle A. Jarvis A. (2017). Climate change adaptation of coffee production in space and time. Climatic Change, 141(1), 47-62. DOI: 10.1007/s10584-016-1788-9

Lemma D. and Megersa H. (2021). Impact of Climate Change on East African Coffee Production and Its Mitigation Strategies. World Journal of Agricultural Sciences, 17(2), 81-89. DOI: 10.5829/idosi.wjas.2021.81.89

Monteverde C. De Sales F. and Jones C. (2022). Evaluation of the CMIP6 Performance in Simulating Precipitation in the Amazon River Basin. Climate, 10(8), 122. DOI: 10.3390/cli10080122

Moya W. Jacome G. and Yoo C. (2017). Past, current, and future trends of red spiny lobster based on PCA with MaxEnt model in Galapagos Islands, Ecuador. Ecology and Evolution, 7(13), 4881-4890. DOI: 10.1002/ece3.3054

Navidad D.L. Marceleño S.M.L. Nájera A. Nájera O. and Ramírez J.P. (2023). Effects of Land Cover and Land Use Change on Nature's Contributions to People of the Shade-Grown Coffee Agroecosystem: An Analysis of Cumbres de Huicicila, Nayarit, Mexico. Conservation, 3(3), 426-443. DOI: 10.3390/conservation3030029

Olmo M.E. Espinoza J.C. Bettolli M.L. Sierra J.P. Junquas C. Arias P.A. Moron V. and Balmaceda-Huarte R. (2022). Circulation Patterns and Associated Rainfall Over South Tropical South America: GCMs Evaluation During the Dry-To-Wet Transition Season. Journal of Geophysical Research: Atmospheres, 127(12), e2022JD036468. DOI: 10.1029/2022JD036468

Parker, W.S. (2013). Ensemble modeling, uncertainty and robust predictions. WIREs Climate Change, 4(3), 213-223. DOI: 10.1002/wcc.220

Pham Y. Reardon-Smith K. Mushtaq S. and Cockfield G. (2019). The impact of climate change and variability on coffee production: A systematic review. Climatic Change, 156(4), 609-630. DOI: 10.1007/s10584-019-02538-y

Rahn E. Läderach P. Baca M. Cressy C. Schroth G. Malin D. van Rikxoort H. and Shriver J. (2014). Climate change adaptation, mitigation and livelihood benefits in coffee production: Where are the synergies? Mitigation and Adaptation Strategies for Global Change, 19(8), 1119-1137. DOI: 10.1007/s11027-013-9467-x

Rahn E. Vaast P. Läderach P. van Asten P. Jassogne L. and Ghazoul J. (2018). Exploring adaptation strategies of coffee production to climate change using a process-based model. Ecological Modelling, 371, 76-89. DOI: 10.1016/j.ecolmodel.2018.01.009

Ranjitkar S. Sujakhu N.M. Merz J. Kindt R. Xu J. Matin M.A. Ali M. and Zomer R.J. (2016). Suitability Analysis and Projected Climate Change Impact on Banana and Coffee Production Zones in Nepal. PLOS ONE, 11(9), e0163916. DOI: 10.1371/journal.pone.0163916

Reboita M.S. Kuki C.A.C. Marrafon V.H. de Souza C.A. Ferreira G.W.S. Teodoro T. and Lima J.W.M. (2022). South America climate change revealed through climate indices projected by GCMs and Eta-RCM ensembles. Climate Dynamics, 58(1), 459-485. DOI: 10.1007/s00382-021-05918-2

Salas R. Gómez D. Silva J.O. Rojas N.B. Oliva M. Terrones R.E. Iliquín D. Barboza E. and Barrena M.Á. (2020). Land Suitability for Coffee (Coffea arabica) Growing in Amazonas, Peru: Integrated Use of AHP, GIS and RS. ISPRS International Journal of Geo-Information, 9(11), 673. DOI: 10.3390/ijgi9110673

Sarvina Y. June T. Sutjahjo S.H. Nurmalina R. and Surmaini E. (2022). Climatic Suitability for Robusta Coffee in West Lampung Under Climate Change. IOP Conference Series: Earth and Environmental Science, 950(1), 012019. DOI: 10.1088/1755-1315/950/1/012019

Sebatta C. Mugisha J. Bagamba F. Nuppenau E.A. Domptail S.E. Kowalski B. et al. (2019). Pathways to sustainable intensification of the coffee-banana agroecosystems in the Mt. Elgon region. Cogent Food & Agriculture, 5(1), 1611051. DOI: 10.1080/23311932.2019.1611051

Shortridge J.E. and Zaitchik B.F. (2018). Characterizing climate change risks by linking robust decision frameworks and uncertain probabilistic projections. Climatic Change, 151(3), 525-539. DOI:10.1007/s10584-018-2324-x

Tavares P. da S. Giarolla A. Chou S.C. Silva A.J. de P. and Lyra A. de A. (2018). Climate change impact on the potential yield of Arabica coffee in southeast Brazil. Regional Environmental Change, 18(3), 873-883. DOI: 10.1007/s10113-017-1236-z

Verbist B. Dinata A.E. and Budidarsono S. (2005). Factors driving land use change: Effects on watershed functions in a coffee agroforestry system in Lampung, Sumatra. Agricultural Systems, 85(3), 254-270. DOI: 10.1016/j.agsy.2005.06.010

Wu Y. Miao C. Sun Y. AghaKouchak A. Shen C. and Fan X. (2021). Global Observations and CMIP6 Simulations of Compound Extremes of Monthly Temperature and Precipitation. GeoHealth. 5(5), e2021GH000390. DOI: 10.1029/2021GH000390

Zambrano-Flores F.G. Loor-Solorzano R.G. Plaza-Avellán L.F. Jaimez-Arellano R. E. Guerrero-Castillo H.E. Casanova-Mendoza T.D. et al. (2018). Relationship between productivity and integral bean quality in advanced selections of Robusta coffee (Coffea canephora) in Ecuador. Agrociencia, 52(4), 593-607.

Zhang S. Liu X. Wang X. Gao Y. and Yang Q. (2021). Evaluation of coffee ecological adaptability using Fuzzy, AHP, and GIS in Yunnan Province, China. Arabian Journal of Geosciences, 14(14), 1366. DOI: 10.1007/s12517-021-07795-9

Zumwald M. Knüsel B. Baumberger C. Hirsch G. Bresch D.N. and Knutti R. (2020). Understanding and assessing uncertainty of observational climate datasets for model evaluation using ensembles. WIREs Climate Change, 11(5), e654. DOI:10.1002/wcc.654

APPENDICES

Appendix A. List of the 19 bioclimatic variables

BIO 1	Annual Mean Temperature
BIO 2	Mean Diurnal Range (Mean of monthly (max temperature - min temperature))
BIO 3	Isothermality (BIO2/BIO7) (* 100)
BIO 4	Temperature Seasonality (standard deviation *100)
BIO 5	Max Temperature of Warmest Month
BIO 6	Min Temperature of Coldest Month
BIO 7	Temperature Annual Range (BIO5-BIO6)
BIO 8	Mean Temperature of Wettest Quarter
BIO 9	Mean Temperature of Driest Quarter
BIO 10	Mean Temperature of Warmest Quarter
BIO 11	Mean Temperature of Coldest Quarter
BIO 12	Annual Precipitation
BIO 13	Precipitation of Wettest Month
BIO 14	Precipitation of Driest Month
BIO 15	Precipitation Seasonality (Coefficient of Variation)
BIO 16	Precipitation of Wettest Quarter
BIO 17	Precipitation of Driest Quarter
BIO 18	Precipitation of Warmest Quarter
BIO 19	Precipitation of Coldest Quarter

Appendix B. Contribution percentajes of bioclimatic variables from avaliableliterature

Reference	Topic	Year	Region	Bioclimatic factors	% Contribution
Purba et al	Modeling the plantation area of geographical indication product under climate change: Gayo Arabica coffee (coffea arabica)	2019	Indonesia	Bio 12 Bio 13 Bio 4 Bio 16 Bio 14 Bio 9 Bio 8 Bio 2 Bio 17 Bio 15 Bio 1	40 26,1 9,6 7 4,6 3 2,9 2,4 2,3 2,1 0,1
Schroth et al	Towards a climate change adaptation strategy for coffee communities and ecosystems in the Sierra Madre de Chiapas, Mexico	2009	México	Bio 16 Bio 5 Bio 19 Bio 13 Bio 17 Bio 3 Bio 9 Bio 4 Bio 8	44,7 21 17,8 10,7 10,7 8,5 8,5 6,6 6,5

Fekadu et al	GIS-based assessment of climate change impacts on forest habitable Aframomum corrorima (Braun) in Southwest Ethiopia coffee forest	2020	Ethiopia	Bio 1 Bio 11 Bio 13 Bio 12 Bio 3 Bio 16 Bio 7 Bio 6 Bio 2 Bio 5 Bio 9	49,7 21,4 7,5 5,2 4,3 3,6 2,8 2,3 1,3 1,2 0,4
Gomes et al	Agroforestry systems can mitigate the impacts of climate change on coffee production: A spatially explicit assessment in Brazil	2020	Brazil	Bio 10 Bio 19 Bio 3 Bio 4 Bio 13 Bio 12	63,2 21,4 6,76 5,9 2,59 0,08
Chemura et al	Bioclimatic modelling of current and projected climatic suitability of coffee (Coffea arabica) production in Zimbabwe	2021	Indonesia	Bio 19 Bio 15 Bio 3 Bio 9 Bio 18 Bio 11 Bio 16 Bio 7	43,8 26,3 12,9 5,4 4,7 4,5 2,4 0
Bunn et al	A bitter cup: climate change profile of global production of Arabica and Robusta coffee	2015	Global	Bio 5 Bio 10 Bio 8 Bio 2 Bio 1 Bio 7 Bio 4 Bio 6 Bio 9 Bio 18 Bio 11 Bio 13 Bio 15 Bio 12 Bio 16 Bio 3 Bio 17 Bio 14 Bio 19	11 11 9,5 8 7,5 6,5 5 4,5 4,5 4,5 4 4 4 3,5 3,5 3 2,5 2 2
Zhang et al	AHP-GIS and MaxEnt for delineation of potential distribution of Arabica coffee plantation under future climate in Yunnan, China	2021	China	Bio 6 Bio 5 Bio 12 Bio 7 Bio 4 Bio 15 Bio 14	24,6 20,6 10,7 4 1,3 1,3 0,5
Laderach et al	Predicted impact of climate change on coffee supply chains	2011	Nicaragua	Bio 13 Bio 10 Bio 19 Bio 18 Bio 12 Bio 16 Bio 7 Bio 8 Bio 9 Bio 4 Bio 5 Bio 17	44 23,6 6,5 6,3 6 5,2 3,5 1,2 1,2 0,8 0,6 0,4

Abrha	Climate change impact on coffee and the pollinator bee suitable area interaction in Raya Azebo, Ethiopia	2018	Ethiopia	Bio 15 Bio 18 Bio 19 Bio 7 Bio 14 Bio 3 Bio 16 Bio 17 Bio 8 Bio 5 Bio 4	23,3 21,3 10,7 9,3 7,3 6 5,9 4,3 4,1 3,5 2,8
De Oliveira et al	Influence of temperature and altitude on the expansion of coffee crops in Matas de minas, Brazil	2020	Brazil	Bio 15 Bio 1 Bio 4 Bio 12	17,4 13,7 9,2 5,1

Appendix C. Agroecological requirements for coffee crop in Ecuador proposed by INIAP. (A) Arabica; (R) Robusta

Factor	Variable	Agroecological suitability			
		Optimal	Moderate	Marginal	No suitable
Soil	Slope	0 -25%	25-50%	50-70%	>70%
	Texture	Loam, silt loam, clay loam, sandy clay loam, silty clay loam, clay loam, sandy clay loam, silty clay loam, silty clay loam, sandy clay loam silt loam	Sandy loam, silty loam, sandy loam, sandy loam	Sandy (fine, medium, coarse)	Clay (>60%)
	Depth	Deep	Moderately deep	Shallow	Shallow superficial
	Stoniness	No	Few	Frequent	Abundant
	Drainage	Good	moderate	Poorly drained	Excessive
	pH	Slightly acidic, Neutral	Acidic	Moderately alkaline	Very acidic, Alkaline
	Toxicity	Without	Slight	Half	High
	Organic matter content	Very High, High	Medium	Low	Very low
	Salinity	Without	Medium	High	Very high
	Fertility	Very High, High	Medium	Low	Very low
Climate	Precipitation (mm year^{-1})	800-2000 (A) 2000 – 3000 (R)	500-800; 2000-2500 (A) 3000-3500 (R)		>500; >3000 (A) >4000 (R)
	Temperature (°C)	17-23 (A) 20-26 (R)	16-17; 23-24 (A) 18-20 (R)	17-18 (R)	<16 >24 (A) <17 (R)
	Altitude (asml)	400-1800 (A) 600 (R)	1. 400; 1800-2000 (A)		>2000 (A) >600 (R)

RESEARCH PAPER

UNRAVELING THE SPATIAL DYNAMICS: EXPLORING THE URBAN FORM CHARACTERISTICS AND COVID-19 CASES IN YOGYAKARTA CITY, INDONESIA

Nugroho Purwono[1*], Irsyad Adhi Waskita Hutama[2,3], Bambang Hari Wibisono[2]
[1]Research Center for Population, National Research and Innovation Agency (BRIN), Jl. Gatot Subroto No.10, Jakarta, Indonesia
[2]Department of Architectural and Planning, Faculty of Engineering, Universitas Gadjah Mada, Yogyakarta, Indonesia
[3]Department of Planning, Architecture and Environmental System, Shibaura Institute of Technology, Japan
***Corresponding author:** inugpurwono@gmail.com
Received: May 30th, 2023 / Accepted: April 10th 2024 / Published: July 1st 2024
https://DOI-10.24057/2071-9388-2024-2917

ABSTRACT. The urban area is a spatial system that significantly impacts residents' health risks. Despite the fact that urban areas house only 55% of the global population, they account for 95% of COVID-19 cases, highlighting the urgent need to understand the role of the urban environment in disease spread. This research explores the critical impact of urban form characteristics on public health risks, focusing primarily on the dynamics of COVID-19 transmission. The aim of the study study is to elucidate the spatial association between urban form elements such as connectivity, density, and heterogeneity and the incidence of COVID-19 cases, with a specific focus on Yogyakarta. Using global (OLS) and local (GWR) spatial regression models, we analyzed the relationship between these elements and COVID-19 prevalence at the neighborhood level rigorously. Our findings reveal a pronounced spatial correlation, particularly highlighting the significance of connectivity and heterogeneity. These factors explain over 95% of the variance in case numbers, while density shows no substantial link. This study's originality lies in its hypothesis-driven examination of urban form impact on COVID-19 transmission, providing new insights into the spatial determinants of health risks in urban settings. Practical implications of our research are profound, providing evidence-based guidance for urban planning and disaster preparedness strategies to mitigate future health crises better. The study contributes valuable insights into designing healthier and more sustainable urban environments by providing a nuanced understanding of how the urban form influences the spread of disease.

KEYWORDS: urban form, COVID-19 case, neighborhood unit, spatial relationship

CITATION: Nugroho Purwono, Irsyad A.W. Hutama, Bambang H. Wibisono (2024). Unraveling The Spatial Dynamics: Exploring The Urban Form Characteristics And Covid-19 Cases In Yogyakarta City, Indonesia. Geography, Environment, Sustainability, 2(17), 63-77
https://DOI-10.24057/2071-9388-2024-2917

ACKNOWLEDGEMENTS: This study received funding from the Pusbindiklatren - Ministry of National Development Planning of the Republic of Indonesia (Bappenas). We would like to express our gratitude to Dr. Isti Hidayati, Dr. Yori Herwangi, and our colleagues at UGM for their valuable comments that considerably improved the study.

Conflict of interests: The authors reported no potential conflict of interest.

INTRODUCTION

Recent findings published by UN-Habitat highlight that urban areas are at the forefront of the COVID-19 pandemic (UN-Habitat 2021). Urban areas have accounted for 95% of reported cases worldwide since the onset of the pandemic, and the United Nations (UN) recommends that cities implement effective strategies for urban management to address this situation. The COVID-19 situation in many urban areas exhibits diverse dynamics, including in the Special Region of Yogyakarta. The local government has reported escalating issues throughout the months during the situation, with the Sleman and Bantul districts exhibiting the highest distribution of confirmed cases compared to the Yogyakarta City area. The city's case ratio is surpassing the provincial average, with an average of 4.86 cases per 100 people, and the highest incidence rate at 0.07%, signifying seven active cases for every 100 residents in each neighborhood unit. Data from the Yogyakarta City Health Service highlights a notable escalation in case rates during mid-2021, particularly in June and July. This increase is predominantly seen in areas with very high population densities, reaching up to 100 people per hectare. The discrepancy can be attributed to the higher-risk population in these two communities, which are concentrated in urban areas, while the city of Yogyakarta itself serves as the central hub and epicenter of urban activity, spreading its influence throughout the surrounding regional area (Subkhi & Mardiansjah, 2019).

Regarding research substance, spatial morphology should consider the physical aspect of urban form as a crucial contextual element. The concept of spatial configuration plays a critical role in shaping urban forms and their characteristics of interaction (Whitehand et al., 1996; Seungkoo Jo, 1998; Clifton et al., 2008; Cortes, 2005; Berghauser Pont, 2018;). This issue is significant because urban forms reflect the impact and historical patterns of human activities and external factors, which shape the image and character of living spaces in tangible and measurable dimensions (Wheeler, 1971; Hillier & Iida, 2005; Batty, 2008). Various perspectives highlight the significant influence of urban forms on mobility patterns and human activities (Marshall et al., 2018). Another study highlights the detrimental impact of socio-economic inequalities on pandemic resilience, emphasizing the urgent need to address these inequalities through the pursuit of Sustainable Development Goals (Bhattacharjee & Sattar, 2021). By bridging these gaps, cities can increase their resilience and improve living standards for all residents.

Additionally, the research examines into the intricate socio-geographical dynamics of COVID-19, illustrating how natural and socio-economic factors interact to shape the pandemic spread and societal norms (Kolosov et al., 2021). The analysis of urban concepts suggests that human interactions within an area are closely linked to the spatial configuration of that area. Furthermore, existing literature indicates that outbreaks of infectious diseases like COVID-19 tend to spread according to specific pathways (Hamidi et al., 2020; Kim et al., 2020; Liu, 2020). The spread of these diseases is intricately linked to the physical environment where the outbreak occurs (Fathi et al., 2020; Gross et al., 2020). Urban forms, therefore, encompass physical features and spatial configurations that can act as catalysts for disease spread (Sharifi & Khavarian-Garmsir, 2020).

In the context of COVID-19, urban areas play a crucial role in the spread of the disease and the level of outbreak risk. This is influenced by factors such as infrastructure, design, land use patterns, and population size (Hamidi et al., 2020; Silalahi et al., 2020). Furthermore, the literature underscores the transformative potential of deliberate urban design in equipping global neighborhoods to effectively confront pandemics (Ghishan et al., 2023). By prioritizing health-conscious and navigable living environments while simultaneously mitigating disease transmission risks, cities can bolster community resilience worldwide. The significance of population density and proximity to pandemic epicenters as key determinants suggests that sustainable development goals (SDGs) could markedly enhance pandemic preparedness and urban health outcomes (da Silva et al., 2021). Therefore, it is important to consider the environmental aspects of urban areas and the typologies of spaces and their interactions (Brizuela et al., 2019; Yao et al., 2021). However, the discussion regarding the association between urban space characteristics and disease outbreaks still raises numerous questions, particularly regarding the risk factors involved (Aritenang, 2022; Wahid & Setyono, 2022). Consequently, the relationship between urban forms and infectious diseases has reached a definite consensus, requiring a more cases study research with a comprehensive multi-factorial approach to urban spatial elements.

This study hypothesizes that the spatial characteristics of urban form, including connectivity, density, and heterogeneity, influence the distribution and spread of COVID-19 cases in urban areas. To address existing gaps in the literature, we investigate these relationships through a mixed-method approach using GIS spatial statistics and Space Syntax analysis in the context of Yogyakarta, Indonesia. This research question focuses on exploring the correlation between urban form elements and COVID-19 cases, identifying spatial patterns, and understanding the impact of urban spatial configurations on disease transmission risk. By utilizing a specific case study and integrating quantitative analysis with spatial data exploration techniques, our study aims to provide unique insights into the spatial dynamics of COVID-19 transmission in Indonesian urban contexts, contributing valuable knowledge for urban planning and public health interventions.

MATERIALS AND METHODS

Study Area

This study focuses on quantitative measurements to examine the relationship between health dimensions, specifically the level of COVID-19 cases, and various elements of urban form, including spatial connectivity and accessibility, density aspects, and heterogeneity of spatial functions. The study was conducted in Yogyakarta City, which consists of 14 sub-districts (Kemantren) and 45 neighborhoods (Kelurahan) as the spatial units for analysis. These units represent the smallest spatial scale for data processing and analysis. Fig. 1 provides a visual representation of the unit of observation and a description of the research location.

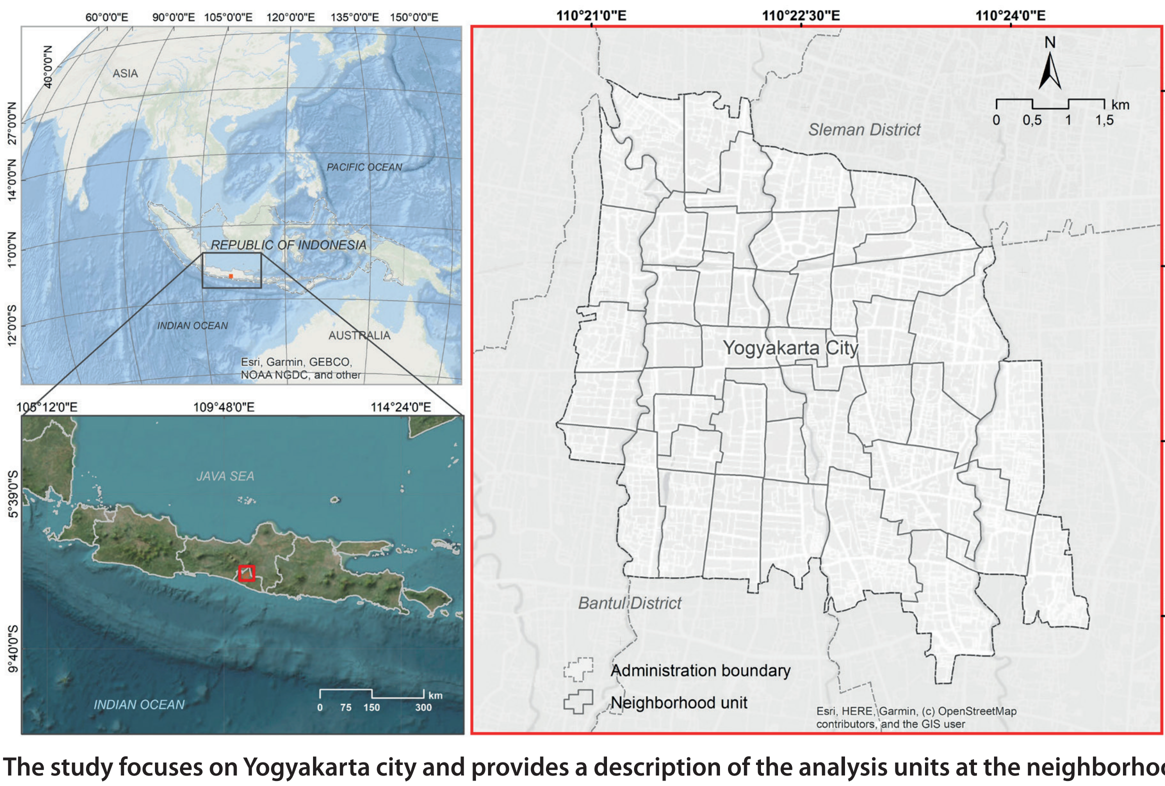

Fig. 1. The study focuses on Yogyakarta city and provides a description of the analysis units at the neighborhood scale

The observation period spans one and a half years, from March 2020 to August 2021. All data were aggregated on a monthly cumulative basis for each neighborhood unit. The measured parameters of urban form are categorized into three elements: spatial connectivity, spatial density, and heterogeneity of spatial functions. Each of these elements is calculated using methods from relevant literature. Geospatial data (shapefiles of street networks, building footprints, and building functions) were collected from the municipal spatial planning authority, ensuring the reliability of the input data.

Methodology and Data Analysis

Urban form refers to the physical characteristics and spatial layout of urban areas (Batty, 2008; Berghauser Pont, 2018). It encompasses the arrangement, design, and configuration of various elements within the built environment, such as land use, streets, buildings, public spaces, and other physical infrastructure. In this research context, we use three parameters as critical components of spatial configuration: connectivity and accessibility, density, and spatial heterogeneity.

Spatial connectivity and accessibility are assessed using the space syntax approach (Hillier, 1988; Hillier et al., 2007;

Table 1. Description of urban morphological aspect and each parameter methods

Aspect	Methods/ analysis	Parameters	Variable notation	Data source
COVID-19 Cases	Spatial Autocorrelation (Global Moran's I)	Spatial pattern of case prevalence	Y	Local public health authorities (*Dinkes Kota Yogyakarta*)
Connectivity-Accessibility	Space Syntax (integration)	Global spatial integration	X_1	Topographic maps: *Rupa Bumi Indonesia* (BIG)
		Local spatial integration	X_2	
	Space Syntax (choice/ centrality)	Global betweenness centralities	X_3	
		Local betweenness centralities	X_4	
Urban Density	Spatial (weighted) density	Built up area density	X_5	Open Street Map (OSM)
		Settlement density	X_6	
		Population density	X_7	Population and civil registration authorities (*Disdukcapil Kota Yogyakarta*)
Heterogeneity	Spatial (Shannon's) entropy	Public facilities dispersion	X_8	Open Street Map (OSM);
		Land use mix concentration	X_9	Department of land and spatial planning (*DPTR Kota Yogyakarta*)

* The data are grouped according to the variables in a spatial relationship model, i.e., the aspect of case occurrence and urban form characteristics.

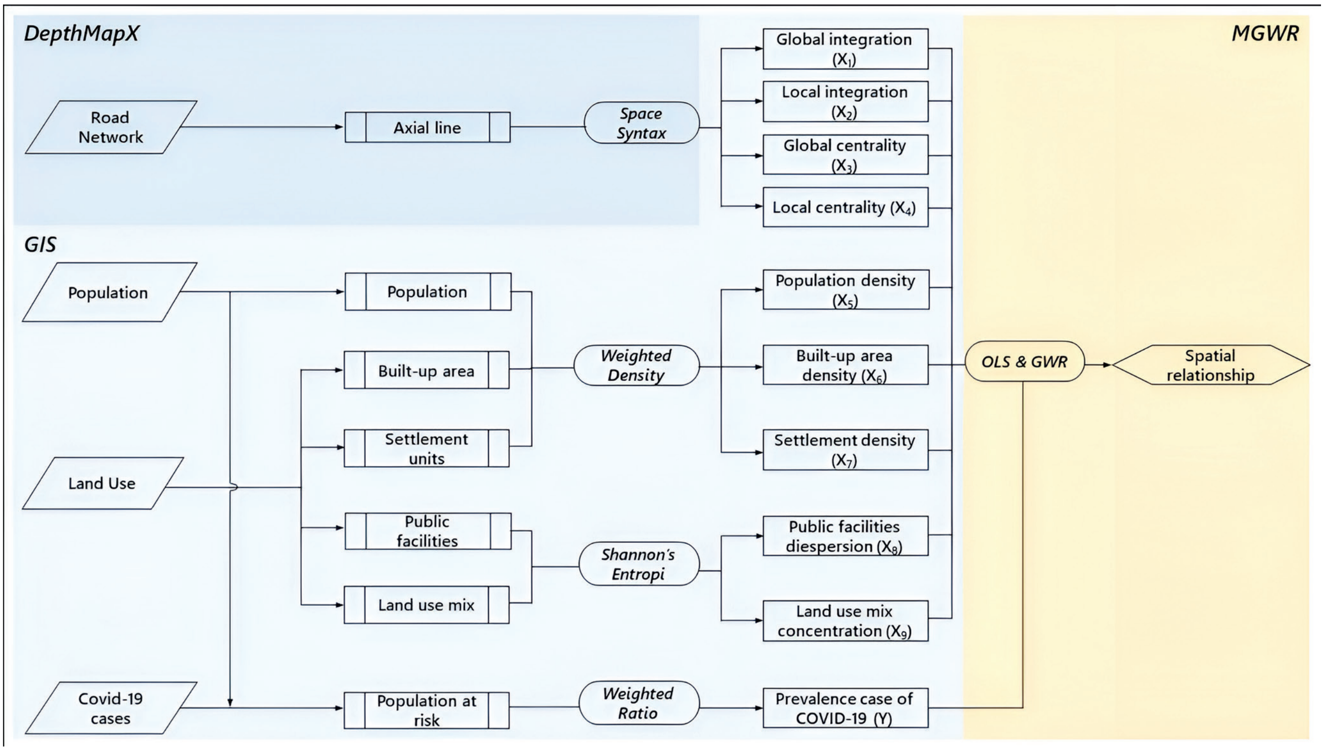

Fig. 2. The stages of data processing and analysis

Varoudis et al., 2013), which analyzes spatial arrangements from building scales to urban areas (Berghauser Pont, 2018). By examining the topology of road networks, space syntax models potential movements, interactions, and patterns of people (Van Nes & Yamu, 2018). In this study, the road network coverage is adjusted to the observation area boundary, with a 500-meter buffer radius from the outer boundary to minimize edge effects of the road network geometry (Gil, 2016). Parameters used in space syntax analysis include mean depth, integration, and betweenness centrality, which are crucial for estimating spatial accessibility within each observation area. Density aspect incorporates population size, built-up area, and settlement density. Density calculation in this study uses a statistically weighted measure, modifying the conventional approach to improve accuracy (Ottensmann, 2018). The aspect of spatial heterogeneity is assessed by quantitatively characterizing landscape pattern differences using the entropy matrix calculations, which have been demonstrated to be relevant in describing urban landscapes (Wang & Zhao, 2018). Variables used in the entropy calculation include the distribution of public facilities and spaces, as well as the land use mix within each observation unit (Jackson, 2003; Lu et al., 2020).

To explore the relationship between urban form elements and COVID-19 cases, a spatial statistical analysis using modeling techniques was conducted. The conceptualization of the models consists of a global relationship model utilizing Ordinary Least Squares (OLS) regression (Páez & Scott, 2004; Mollalo et al., 2020) and a local relationship model employing Geographically Weighted Regression (Brunsdon et al., 1996; Nakaya et al., 2005; Oshan et al., 2019). Both models utilize spatial statistical techniques to investigate the relationship between variables in a location-based context. These models differ from traditional regression in that they consider the geographic attributes of each measured variable in their calculations (Berliner, 2015).

The OLS model is used to examine the relationship between a dependent variable and a set of explanatory variables in a global context, where the spatial variability of each variable is generally equated (Getis & Ord, 2010). The OLS model is represented by the following Eq. 1:

$$y_i = \beta_0 + \sum_{i=i\ldots3} \beta ixi + \varepsilon \quad (1)$$

where in area *i*, y_i is the dependent variable, which represents the degree of incidence; *β0* is the intercept; *xi* is the selected explanatory variable; β is the regression coefficient; and ε is the random error or residual generated by the model.

On the other hand, the Geographically Weighted Regression (GWR) model examines the local relationship between the dependent variable and the explanatory variable, incorporating location weights in the form of a bandwidth or kernel (Brunsdon et al., 1996). In this study, the GWR technique is adjusted to the Poisson distribution, due to the discrete nature of the dependent variable that represents disease cases (Nakaya et al., 2005). The Poisson distribution includes an offset value that is determined by the population size at risk to increase the model's sensitivity in capturing local effects on various factors that influence the dependent variable, in this case, the prevalence of COVID-19 cases. The Eq. 2 for the GWR model is as follows:

$$y_i = poisson\left[N_i exp\left(\beta_0\left(u_i, v_i\right) + \Sigma_k \beta_k\left(u_i, v_i\right) x_{k,i}\right)\right] \quad (2)$$

where β_0 (u_i, v_i) is the intercept coefficient at location *i*; β_k (u_i, v_i) is the coefficient of the explanatory variable $X_{k,i}$ for location *i*; *N* is the offset value at location *i*; and (u_i, v_i) is the coordinate matrix at location *i*.

The data analysis process begins by converting each parameter into geospatial format. Each parameter is then processed based on its respective variable category, which is defined as a dependent variable (response) or independent variable (explanatory). In this study, the response variable refers to the number of COVID-19 cases, whereas the explanatory variables derive from the calculation of parameters associated with urban form elements.

Once all the data has been formatted in the same way, each data point can be processed according to the criteria and categories of variables to be analyzed. The analysis process involves several applications and methods, including space syntax using DepthmapX, Geographic Information System (GIS), and Multiscale Geographic Weighted Regression (MGWR). The spatial relationship analysis is conducted by integrating all the data into a modeling application to obtain statistical test results. The data flow in this study is illustrated in Fig. 2 and involves grouping variables according to the unit of analysis for both the dependent and independent variables. The case prevalence variable is aggregated periodically based on observation time, while the urban form is analyzed at the neighborhood unit level. This ensures that the output of each parameter can be analyzed on a uniform scale.

RESULTS

Spatial Pattern of Covid-19 Cases

The prevalence of COVID-19 cases in the study area provides an understanding of the extent to which the disease has affected the population over a specific time period. This prevalence is represented by cumulative proportions, which offer a measure of the likelihood that individuals will be affected by the disease at any given time. Analysis results reveal variations in prevalence among different neighborhood units. Throughout the entire observation period, the average prevalence across all observation areas was 5.19 cases. The Notoprajan area has the lowest prevalence, averaging only 3.10 cases, whereas the Kotabaru area has the highest prevalence, with an average of 7.24 cases. Other areas with high prevalence include Semaki, Mantrijeron, Rejowinangun, Purwokinanti, Terban, Purbayan, Muja Muju, Prenggan, and Bausasran, with prevalence values ranging from 6.18 to 6.77 per respective population. These areas exhibit an above-average case prevalence, indicating a higher risk of COVID-19 transmission compared to other observation areas. The prevalence of COVID-19 in each neighborhood unit across the study area is presented in Table 2.

Furthermore, the spatial analysis conducted on these parameters provides a detailed description of the pattern and distribution of values, offering explicit insights. The analysis of prevalence values in each neighborhood unit reveals a spatial clustering pattern. This is supported by the results of the spatial autocorrelation test that indicates a significant relationship among the prevalence values. The prevalence values in the study area exhibit an expected index value of -0.023, with a variance of 0.009. The Global Moran's I index yields a value of 0.329, with a *p-value* of 0.000 and a *z-score* of 3.822. In a statistical context, the index value interpretation suggests that the spatial patterns observed are unlikely to occur randomly across the observation units. The significant Moran's index value indicates that the prevalence rate of COVID-19 cases in both high and low classes demonstrates a spatial distribution that corresponds to

Table 2. The results of the prevalence case in each neighborhood unit

Neighborhood	Population	Case	Prevalence		Neighborhood	Population	Case	Prevalence
Baciro	12347	683	5.53		Pandeyan	12213	566	4.63
Bausasran	7505	464	6.18		Panembahan	9062	545	6.01
Bener	4958	260	5.24		Patangpuluhan	7721	354	4.58
Brontokusuman	10853	495	4.56		Patehan	5901	329	5.58
Bumijo	10313	506	4.91		Prawirodirjan	9358	492	5.26
Cokrodiningratan	8870	356	4.01		Prenggan	11501	717	6.23
Demangan	8708	472	5.42		Pringgokusuman	12284	506	4.12
Gedongkiwo	14044	680	4.84		Purbayan	10286	657	6.39
Giwangan	8028	378	4.71		Purwokinanti	6186	398	6.43
Gowongan	7947	300	3.78		Rejowinangun	12807	844	6.59
Gunungketur	4536	270	5.95		Semaki	5185	351	6.77
Kadipaten	6816	387	5.68		Sorosutan	15623	667	4.27
Karangwaru	9712	458	4.72		Sosromenduran	7417	294	3.96
Keparakan	9822	407	4.14		Suryatmajan	4616	230	4.98
Klitren	9672	531	5.49		Suryodiningratan	11270	572	5.08
Kotabaru	2929	212	7.24		Tahunan	9194	478	5.20
Kricak	13336	557	4.18		Tegalpanggung	9204	550	5.98
Mantrijeron	10148	669	6.59		Tegalrejo	9250	423	4.57
Muja Muju	10946	692	6.32		Terban	9269	595	6.42
Ngampilan	10224	418	4.09		Warungboto	9253	467	5.05
Ngupasan	5603	323	5.76		Wirobrajan	9346	438	4.69
Notoprajan	8215	255	3.10		Wirogunan	11285	474	4.20
Pakuncen	10941	449	4.10					

*Prevalence values are calculated for every 100 people in each neighborhood; the highlighted columns show values above the average in each class

their respective class values. This implies the presence of spatial autocorrelation, where areas with similar prevalence values tend to cluster together. A summary of the statistical test (Global Moran's I) for this parameter is depicted in Fig. 3.

The Connectivity and Accessibility Aspect

The analysis of connectivity and accessibility of the observation units is based on the concept of space syntax, which examines the connectedness of the road networks and their spatial configuration. This aspect is considered crucial for understanding the potential movement by identifying more frequently accessed routes. The results include the integration (INT) and centrality (CH) indexes of the road networks, assessed at local and global radii (see Table 3). The local radius measures spatial integration within an 800-meter range, while the global radius represents patterns on a larger spatial scale, taking into account movement from outside the study area.

The integration analysis results indicate that there are varying levels of inter-spatial accessibility across all observation areas. Figs. 4 (a) and (b) illustrate the pattern of the integration index, which indicates inter-spatial accessibility throughout the observation areas. Higher integration values indicate greater spatial accessibility, reflecting the potential for movement within the urban system. The concentration is observed in the Warungboto, Rejowinangun, Gunungketur, Semaki, and Giwangan areas, indicating the potential for movement within the local and global radius. The highest level is concentrated in the middle-to-southeast area (represented by the area with red lines). Meanwhile, the lowest index reveals that the distribution pattern spreads to the northwest, or the area of the city bordered with other districts (represented by the area with blue lines).

The results of the centrality analysis show that areas such as Gunungketur and Semaki display a relatively high centrality pattern, indicating their significance in terms of through-movement at the local radius. Similarly, global centrality is concentrated in the areas traversed by primary and secondary collector paths, as shown by the red lines in Figs. 4 (c) and (d). This centrality suggests a consolidated road network in these regions, where effective connections can be established between any pair of spatial elements within each unit. Overall, the analysis of betweenness centrality provides insights into the potential for efficient movement and the effectiveness of road networks in the study area, both at the local and global coverage.

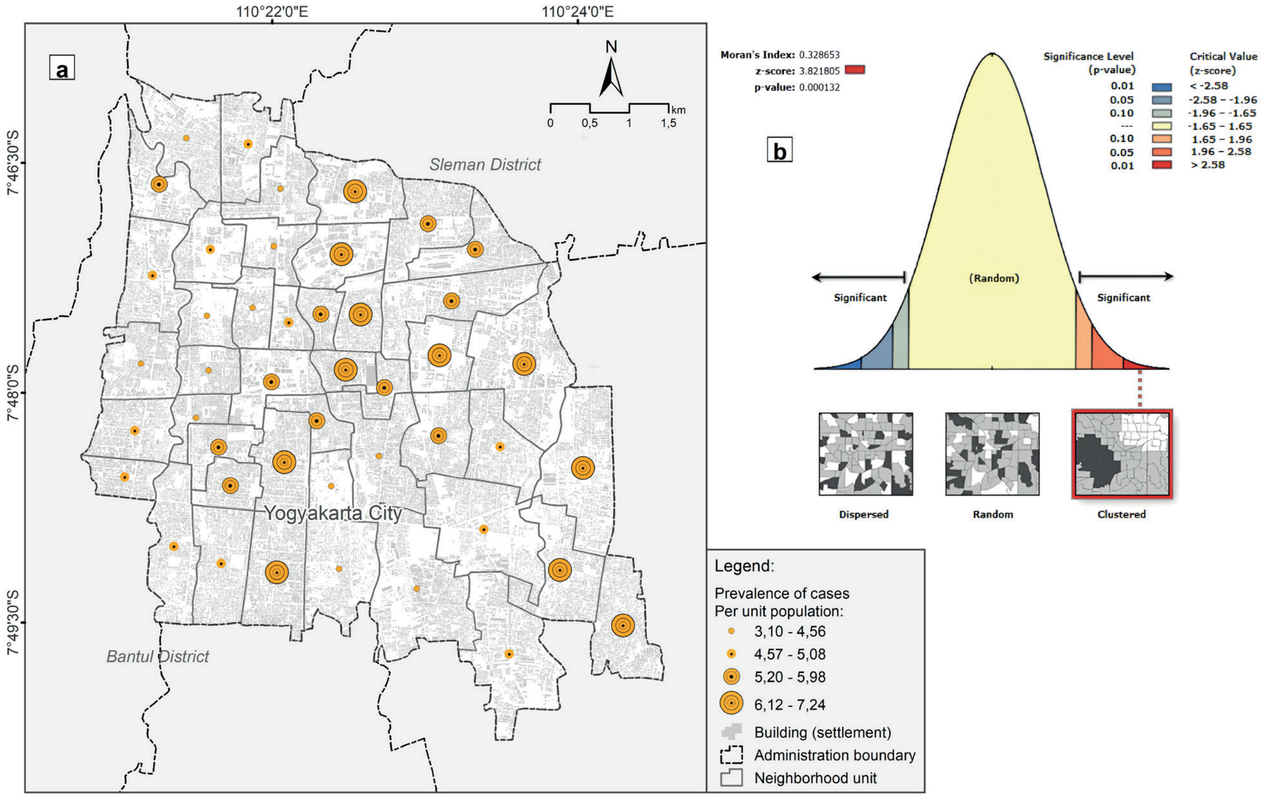

Fig. 3. (a) The illustration shows the prevalence of cases in each neighborhood unit; (b) The results of the spatial statistical test showed a clustered pattern in the observation area

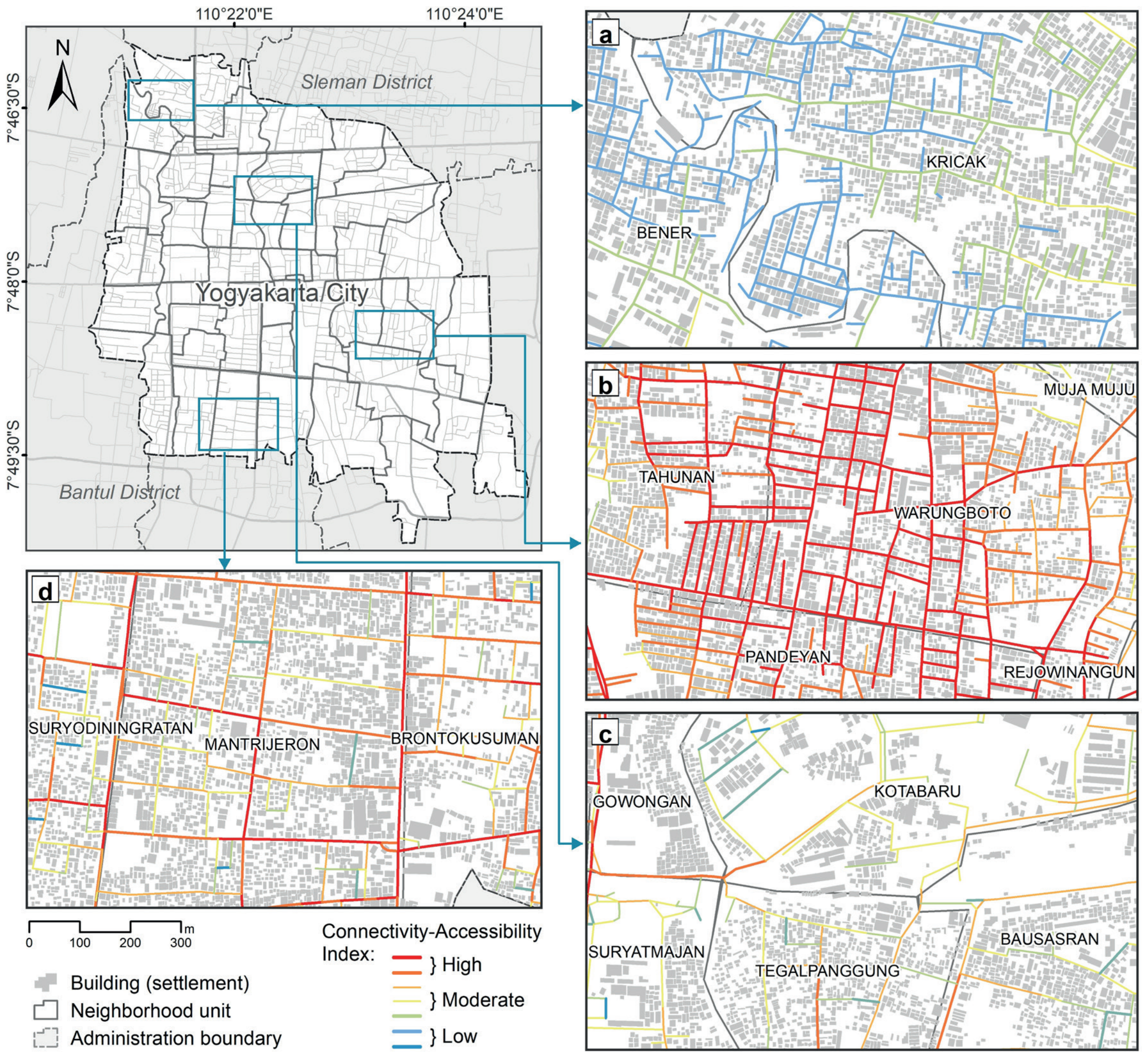

Fig. 4. The results of the connectivity-accessibility analysis using the space syntax are as follows: (a) low-level global integration; (b) high-level local integration; (c) moderate global centrality; and (d) high-level local centrality

Table 3. Average index of integration and centrality of road networks in each neighborhood unit

Neighborhood	INT (local)	INT (global)	CH (local)	CH (global)		Neighborhood	INT (local)	INT (global)	CH (local)	CH (global)
Baciro	2.593	4.708	0.896	0.176		Pandeyan	2.962	5.035	0.873	0.379
Bausasran	2.189	4.666	0.696	0.187		Panembahan	1.917	4.825	0.550	0.405
Bener	1.422	3.188	0.652	0.070		Patangpuluhan	1.594	5.287	0.201	0.405
Brontokusuman	2.071	4.474	0.733	0.110		Patehan	1.390	4.108	0.489	0.039
Bumijo	2.311	4.435	0.846	0.283		Prawirodirjan	2.467	5.543	0.647	1.013
Cokrodiningratan	2.257	3.961	0.795	0.375		Prenggan	2.825	4.514	1.275	0.176
Demangan	1.715	4.106	0.485	0.047		Pringgokusuman	2.772	4.955	1.068	0.261
Gedongkiwo	1.691	4.482	0.529	0.233		Purbayan	1.870	3.677	0.986	0.142
Giwangan	2.189	4.178	0.854	0.129		Purwokinanti	2.423	5.404	0.709	0.518
Gowongan	2.474	4.905	0.707	0.897		Rejowinangun	2.932	5.058	1.040	0.335
Gunungketur	3.031	5.760	0.990	1.276		Semaki	3.194	5.423	1.121	0.772
Kadipaten	1.736	4.751	0.605	0.102		Sorosutan	2.322	4.603	0.750	0.149
Karangwaru	1.696	3.326	0.594	0.112		Sosromenduran	2.525	5.054	0.722	0.119
Keparakan	2.258	5.071	0.715	0.554		Suryatmajan	2.665	5.201	0.841	0.568
Klitren	1.832	4.043	0.606	0.174		Suryodiningratan	2.296	4.531	0.709	0.199
Kotabaru	1.482	3.764	0.397	0.028		Tahunan	2.914	4.871	1.087	0.139
Kricak	1.837	3.357	0.891	0.072		Tegalpanggung	1.683	4.348	0.693	0.193
Mantrijeron	2.472	4.778	0.762	0.310		Tegalrejo	2.334	4.488	0.789	0.200
Muja Muju	2.197	4.952	0.609	0.291		Terban	1.766	3.950	0.532	0.179
Ngampilan	2.179	4.822	0.707	0.197		Warungboto	3.457	5.123	1.412	0.281
Ngupasan	2.127	5.317	0.390	0.180		Wirobrajan	2.059	5.079	0.440	0.168
Notoprajan	1.647	5.424	0.405	0.749		Wirogunan	2.568	5.299	0.794	0.503
Pakuncen	2.466	4.802	0.887	0.357						

The average index is used to determine the values of integration and centrality for each neighborhood unit. The results are presented in Table 3. Certain areas exhibit high values for all parameters, as exemplified by Gunungketur and Semaki, with values of 5.76 and 5.42 respectively. Other areas, such as Preggan and Warungboto, have values of 1.28 and 1.41 respectively, which demonstrate high centrality within the local radius. These areas should be considered as they indicate significant potential for spatial accessibility. Overall, the average index provides valuable insights into the levels of integration and centrality in each neighborhood unit, highlighting areas with high connectivity and accessibility.

The Urban Density Aspect

The aspect of urban spatial density encompasses three variables: built-up area density, settlement density, and population density. Built-up area density indicates the intensity of space utilization by non-residential structures, expressed as the ratio of non-residential built-up areas to the total area of a neighborhood. Similarly, settlement density reflects the ratio of land area occupied by residential buildings in the neighborhood. Population density, on the other hand, measures the number of residents per unit area in each neighborhood.

The spatial analysis of urban spatial density is presented in Fig. 5. Built-up area density is derived from the land use blocks within each observation unit, excluding non-residential areas, parks, and riverbanks (Fig. 5a). The results reveal Bumijo, Cokrodiningratan, and Gowongan as examples of high-level built-up area density ratios exceeding 90%. On the other hand, Pakuncen exhibits the lowest density ratio at 70.9%. Despite being the lowest, this value still indicates a relatively high occupancy of built-up land, representing disproportionate land use. Across the entire study area, Yogyakarta falls under the category of cities with very high levels of built-up area density, with an average ratio exceeding 87%. This implies that space utilization and intensity are primarily dominated by built-up areas, leaving less than one-fifth of the total area as open space.

Settlement density captures the level of dwelling intensity within each neighborhood, quantified by the number of buildings (Figs. 5b and 5d). The data for dwelling units is obtained from building footprint records, encompassing various types of residential structures such as houses, flats, apartments, dormitories, and boarding houses, as well as accommodation facilities like inns, hotels, motels, and villas. The results demonstrate that Tegalpanggung and Ngupasan exhibit the highest settlement density, with an average value of 38 units per hectare. This finding aligns with the actual conditions on the field, where Tegalpanggung is characterized by slum areas, particularly along the western side of the Kali Code riverbank. In Ngupasan, the spatial proximity between residential buildings is notably close, resulting in the highest settlement density within the study area.

The analysis of population density reveals that the Yogyakarta city experiences a generally high level of density. Approximately 60% of all neighborhood units are in the very high-density category, for example, Tegalpanggung area (Fig. 5c). Meanwhile, only one neighborhood unit is categorized as moderate density is observed solely in Kotabaru. This result is consistent with the actual conditions on the field, where the number of residents in that particular area is relatively lower compared to other neighborhoods, reflecting the city's population dynamics and distribution.

The analysis of urban spatial heterogeneity yields an index that serves as a measure of concentration for public facilities and land use mix in the entire study area, as depicted in Fig. 6(a). The entropy index calculations generate relative values, providing a spatially quantitative measure of the concentration of these variables. The results show a variety of values for the entropy index of public facilities across each neighborhood area, indicating variations in the distribution of urban space function. On the other hand, the analysis of land use mix reveals a low level of diversity or heterogeneity in all observation areas, suggesting a concentration of specific service functions in certain areas.

The relationship between the entropy index for facilities and the land use mix demonstrates a positive correlation. The graph in Fig. 6(b) illustrates a linear trend between these two variables, with an R^2 value of 0.3107. Although this correlation value may not be considered high, it suggests that the distribution and variability of public facilities tend to align with the pattern of land use mix. In other words, the location of urban service facilities generally corresponds to the heterogeneity of spatial functions within the observation area.

Spatial Relationship Testing

Global Model Estimation using OLS:

The OLS method was used to estimate the global relationship between the response variable and a set of explanatory variables. The OLS results provide predictions on a global scale and include statistical information such as coefficient estimates for the explanatory variables and residual values for each observed variable. The model's performance was evaluated through diagnostic tests to assess its adequacy. Estimated variable coefficients and test results are presented in Table 4.

The AICc (Akaike's Information Criterion-Corrected)

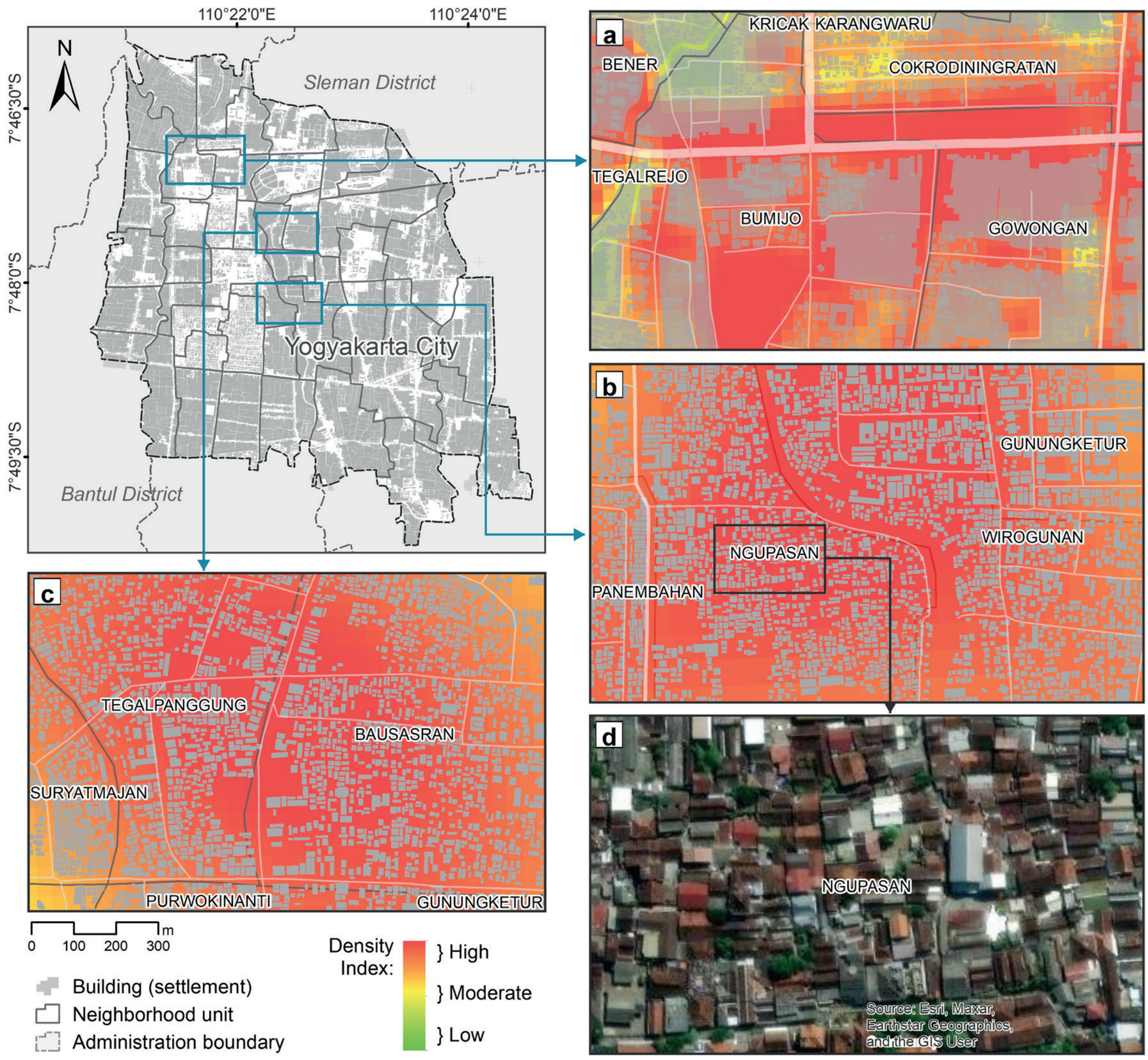

Fig. 5. Urban spatial density of every neighborhood unit includes: (a) high-level built-up density with a ratio of >90% per-unit area, (b) high-level settlement density with >30 units per hectare, (c) high-level population density with >400 people per hectare, and (d) visualization of settlements from high-resolution satellite imagery

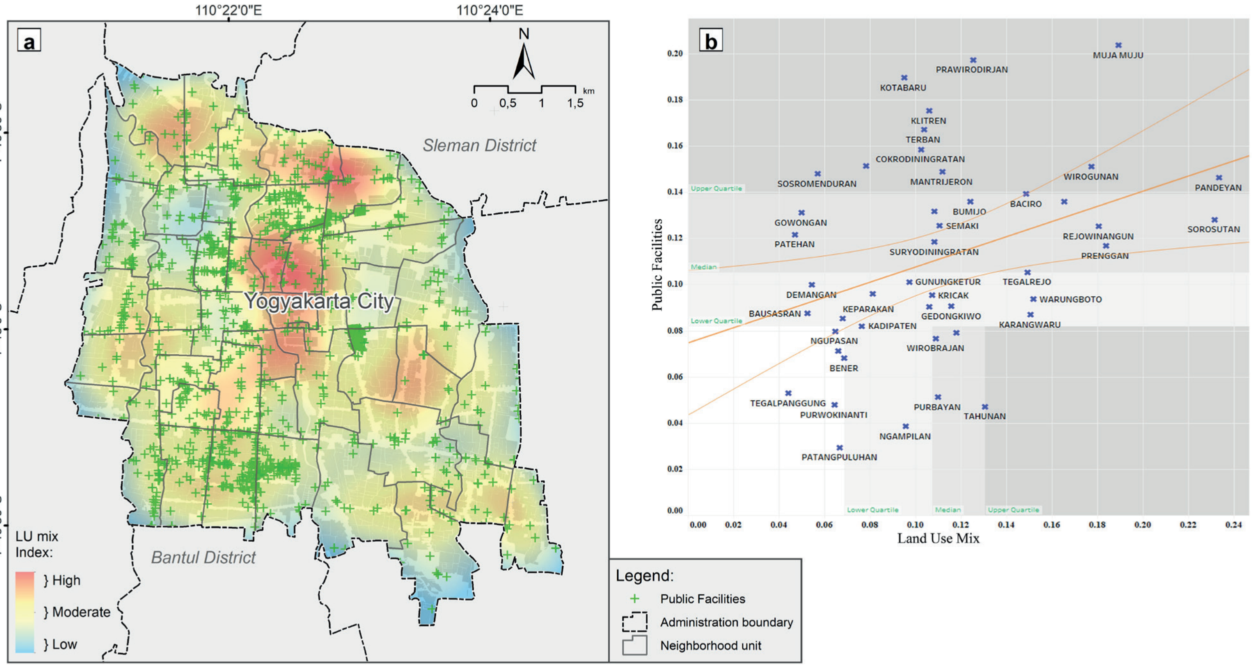

Fig. 6. The results of urban spatial heterogeneity show: (a) the spatial distribution of public facilities and land use mix, and (b) the statistical distribution of the entropy index

Table 4. Statistical summary of explanatory variables and diagnosis of the OLS model

Variables			Coefficient	Std_Error	t_Stat	Prob*	Robust SE	Robust_t	Robust Prob*
		Intercept	4.649763	0.978861	4.750178	0.000004	1.153647	4.030492	0.000074
Connectivity-Accessibility	Local integration	X_1	0.608993	0.187566	3.246816	0.001287	0.187514	3.247712	0.001283
	Global integration	X_2	-0.541646	0.346655	-1.562494	0.119044	0.338523	-1.600028	0.110463
	Local centrality	X_3	-0.856153	0.273999	-3.124663	0.001933	0.305744	-2.800229	0.005377
	Global centrality	X_4	1.699179	0.553574	3.069471	0.002314	0.451213	3.765798	0.000204
Spatial Density	Built-up area	X_5	-0.00198	0.00031	-6.391879	0.000004	0.000262	-7.549206	0.000004
	Settlement	X_6	-0.52968	1.006174	-0.52643	0.598916	1.199278	-0.441666	0.659003
	Population	X_7	-0.00749	0.010702	-0.699898	0.484428	0.011664	-0.642171	0.521161
Heterogeneity	Public facilities	X_8	6.822397	1.439608	4.739065	0.000004	1.283156	5.316889	0.000004
	Land use mixed	X_9	-7.40221	1.220654	-6.064137	0.000001	1.462142	-5.062578	0.000001
Diagnostic results		AIC	AICc	R^2	AdjR^2	F-Stat	F-Prob	Wald	Sigma^2
		968.6817	969.403	0.2173	0.1982	11.3522	0.0001	151.6488	0.7359

*statistical significance is indicated by the value ($p < 0.01$)

test yielded a value of 968.682, indicating relatively good model performance. The R^2 value of 0.217 (coefficient of determination) suggests that only a portion of the response variable can be explained by the explanatory variables. The F-Stat and Wald's test results indicate the overall significance of the model, while the Sigma^2 value represents the OLS estimate of the variance error in the explanatory variable. Although the coefficient of determination is not particularly high, the results indicate a significant relationship between the tested variables and the prevalence of COVID-19 cases in the study area. In other words, there is a general correlation between between urban form characteristics characteristics and the prevalence of COVID-19 cases.

Furthermore, most of the explanatory variables examined, particularly those related to accessibility and spatial connectivity (X_1, X_3, and X_4), showed statistical significance in the global model. However, in terms of density, only variable (X_5) was found to be significant. Additionally, the spatial heterogeneity aspect indicated that all the variables were significantly associated with the case prevalence rate.

Local Model Estimation using GWR:

To examine the relationship between the explanatory variables and the response variable, experiments were conducted using the GWR method with Poisson distribution configuration. The Poisson configuration was chosen because it best fits the nature of the response variable, considering that the case prevalence is discretely distributed. This means that the probability distribution of case prevalence varies across space and time within each observation unit. Table 5 summarizes the statistics from the GWR model's implementation.

The GWR model describes that certain explanatory variables have varying levels of significance. This indicates that not all variables can consistently explain the prevalence of COVID-19 cases across all observation units. According to the summary statistics in Table 5, the global centrality variable (x_3), which represents spatial accessibility, is significant, as well as the heterogeneity aspect, including public facilities (x_8) and land use mix (x_9). However, the density aspect does not show a significant correlation with the spatial distribution of COVID-19 cases. These findings differ slightly from the results of the global OLS model, where all three aspects of urban spatial form were found to be significant. In other words, the GWR model identifies specific variables from different aspects of urban form that are potentially related to the prevalence of cases in the study area.

Table 6 presents the statistical significance of each explanatory variable at the 95% confidence level for each observation unit. The significance of variables in the GWR model takes into account the unique locational attributes that reflect spatial variability. This highlights the importance of considering the location factor in understanding the spatial relationship of a phenomenon. It also indicates that certain characteristics and relationships may not be generalized across all spatial locations. Furthermore, Fig. 7 illustrates the spatial relationships of those variables within each observation area of the neighborhood units in the model.

DISCUSSION

The findings of this study highlight the intricate relationship between urban morphology and the prevalence of COVID-19 across diverse observation units. They reveal the varying impact of urban form elements on the spread of the disease. This research supports the hypothesis that the presence of urban form elements and their relationships with the surrounding spatial and social context significantly affect COVID-19 case numbers.

Table 5. Statistical summary of explanatory variables in GWR estimation along with model diagnostic test results

	Variables									
	Intercept	Connectivity-accessibility				Spatial density			Heterogeneity	
		X_1	X_2	X_3	X_4	X_5	X_6	X_7	X_8	X_9
Coefficient	-4.46	-0.059	-0.098	0.504	-0.181	0	0.103	0.003	1.491	-4.11
StdError	0.41	0.084	0.145	0.13	0.239	0	0.431	0.004	0.589	0.503
t_Stat	-10.87	-0.701	-0.675	3.882	-0.758	-1.206	0.239	-0.604	2.532	-8.17
p-value	0	0.483	0.5	0	0.449	0.228	0.811	0.546	0.011	0
Mean	-3.89	-0.151	0.062	0.334	-0.572	0	0.096	0.12	2.618	-5.978
Std.Dev	2.484	0.634	0.72	1.011	1.076	0.001	3.071	0.024	2.94	2.452
Min	-9.922	-2.472	-1.683	-1.543	-3.138	-0.003	-7.615	-0.069	-2.675	-12.316
Median	-4.286	-0.052	0.062	0.099	-0.549	0	0.315	-0.003	1.906	-5.499
Max	2.305	0.903	2.952	4.345	2.62	0.005	6.534	0.037	13.387	-1.475

Coordinate System	WGS 1984 UTM 49S (Lat, Long)
Diagnostic	Generated value
AIC	93.629
AICc	99.596
BIC	217.989
Optimum Badwidth (confidence 95%)	210
Degree of freedom (n - traces)	346.396
Deviance (goodness-of-fit)	30.421
Percent deviance explained	0.856
Adj. percent deviance explained	0.842
Adj. alpha (confidence 95%)	0.016
Adj. critical t value (confidence 95%)	2.424

Table 6. The significance of each variable (p-value) at the 95% confidence level is determined for each unit of observation

Neighborhood unit	*pX1*	*pX2*	*pX3*	*pX4*	*pX5*	*pX6*	*pX7*	*pX8*	*pX9*	Σ (significant)
Baciro	0.11254	0.43963	0.60634	0.03030	0.00002	0.46821	0.45756	0.74648	0.02607	3
Bausasran	0.31872	0.10461	0.97873	0.21707	0.05190	0.00909	0.00258	0.87477	0.00121	3
Bener	0.01628	0.02314	0.00004	0.00719	0.50403	0.43127	0.29016	0.04803	0.01136	6
Brontokusuman	0.34020	0.43211	0.21995	0.71698	0.26093	0.39812	0.39284	0.72752	0.00239	1
Bumijo	0.40294	0.45987	0.00038	0.18605	0.80357	0.12210	0.44313	0.08217	0.02387	2
Cokrodiningratan	0.27134	0.44551	0.00369	0.07721	0.63443	0.15639	0.40043	0.00516	0.06680	2
Demangan	0.17687	0.67195	0.00765	0.00617	0.00041	0.65011	0.29474	0.00237	0.03113	5
Gedongkiwo	0.05895	0.13442	0.99824	0.84214	0.03457	0.41390	0.41813	0.89379	0.00001	2
Giwangan	0.00777	0.11598	0.60430	0.05689	0.37387	0.16093	0.00421	0.02226	0.00021	4
Gowongan	0.42941	0.41833	0.00046	0.57911	0.62285	0.03206	0.15621	0.04642	0.01955	4
Gunungketur	0.70332	0.32613	0.87576	0.87513	0.10590	0.38609	0.24403	0.85640	0.00131	1
Kadipaten	0.32685	0.20892	0.19935	0.07530	0.15759	0.67374	0.36471	0.94196	0.00019	1
Karangwaru	0.31717	0.18098	0.00000	0.05667	0.22265	0.50602	0.75956	0.00208	0.07978	2
Keparakan	0.48595	0.62817	0.87448	0.82227	0.67010	0.55465	0.74009	0.81728	0.01858	1
Klitren	0.54091	0.72188	0.00158	0.01443	0.04377	0.34145	0.03140	0.00000	0.00481	6
Kotabaru	0.27375	0.30498	0.82777	0.96549	0.57319	0.00084	0.05207	0.00376	0.00039	3
Kricak	0.04122	0.02997	0.00002	0.01839	0.21669	0.63882	0.36099	0.03509	0.01488	6
Mantrijeron	0.36333	0.38400	0.99531	0.65975	0.27088	0.53834	0.19422	0.49678	0.00022	1
Muja Muju	0.41491	0.68873	0.96622	0.94362	0.04200	0.63868	0.70892	0.92128	0.03611	2
Ngampilan	0.79744	0.68861	0.04119	0.15372	0.43381	0.43255	0.28664	0.85977	0.01389	2
Ngupasan	0.37785	0.83887	0.16080	0.15255	0.41131	0.80786	0.72535	0.99263	0.05877	0
Notoprajan	0.37464	0.25883	0.15278	0.08240	0.23717	0.72088	0.37133	0.98580	0.00023	1
Pakuncen	0.51733	0.62773	0.06548	0.10328	0.68319	0.45253	0.48142	0.90499	0.19386	0
Pandeyan	0.35957	0.65999	0.98130	0.95926	0.46253	0.52589	0.42644	0.98981	0.07514	0
Panembahan	0.37950	0.56678	0.76980	0.06836	0.15035	0.69686	0.56361	0.95407	0.01495	1
Patangpuluhan	0.06714	0.05711	0.20733	0.18620	0.06739	0.36267	0.65335	0.86096	0.00003	1
Patehan	0.21595	0.10644	0.31797	0.09803	0.10067	0.59054	0.33403	0.99361	0.00007	1
Prawirodirjan	0.59360	0.52260	0.12496	0.84214	0.25341	0.44810	0.29894	0.98750	0.01516	1
Prenggan	0.25321	0.25229	0.37095	0.95801	0.61492	0.24773	0.19418	0.97026	0.09598	0
Pringgokusuman	0.30222	0.19018	0.03182	0.25180	0.84583	0.03577	0.14803	0.73214	0.07747	2
Purbayan	0.19750	0.16576	0.14723	0.95035	0.36185	0.10783	0.05278	0.91953	0.03702	1
Purwokinanti	0.50154	0.25321	0.42811	0.75152	0.32633	0.30508	0.37022	0.91442	0.03309	1
Rejowinangun	0.74407	0.60466	0.93871	0.91490	0.45710	0.57434	0.78480	0.98312	0.29303	0
Semaki	0.29887	0.55062	0.77764	0.18296	0.05123	0.69133	0.27787	0.82720	0.00054	1
Sorosutan	0.17211	0.50324	0.99656	0.20984	0.03945	0.39462	0.27789	0.99677	0.00679	2
Sosromenduran	0.26933	0.08601	0.01621	0.93395	0.69907	0.05421	0.02022	0.95100	0.01186	3
Suryatmajan	0.15895	0.02847	0.04714	0.56535	0.65708	0.00086	0.00840	0.78999	0.00670	5

Suryodiningratan	0.10799	0.21898	0.86277	0.98084	0.04445	0.52090	0.17996	0.66298	0.00002	2
Tahunan	0.60887	0.79059	0.76885	0.99324	0.09239	0.57384	0.27240	0.89086	0.00062	1
Tegalpanggung	0.22179	0.03786	0.28402	0.44341	0.44051	0.00375	0.00850	0.63464	0.00566	4
Tegalrejo	0.18526	0.40098	0.01263	0.07980	0.85887	0.12600	0.50275	0.03047	0.15961	2
Terban	0.46613	0.63422	0.56805	0.70384	0.69844	0.04186	0.03053	0.00002	0.05533	3
Warungboto	0.74419	0.82117	0.79805	0.99422	0.25571	0.53018	0.56895	0.96984	0.11884	0
Wirobrajan	0.21027	0.16935	0.15024	0.13002	0.16865	0.59731	0.51015	0.97606	0.00049	1
Wirogunan	0.72732	0.49266	0.82737	0.99805	0.31798	0.46680	0.68795	0.97549	0.02036	1
Σ (significant)	3	4	13	5	7	7	7	11	34	91

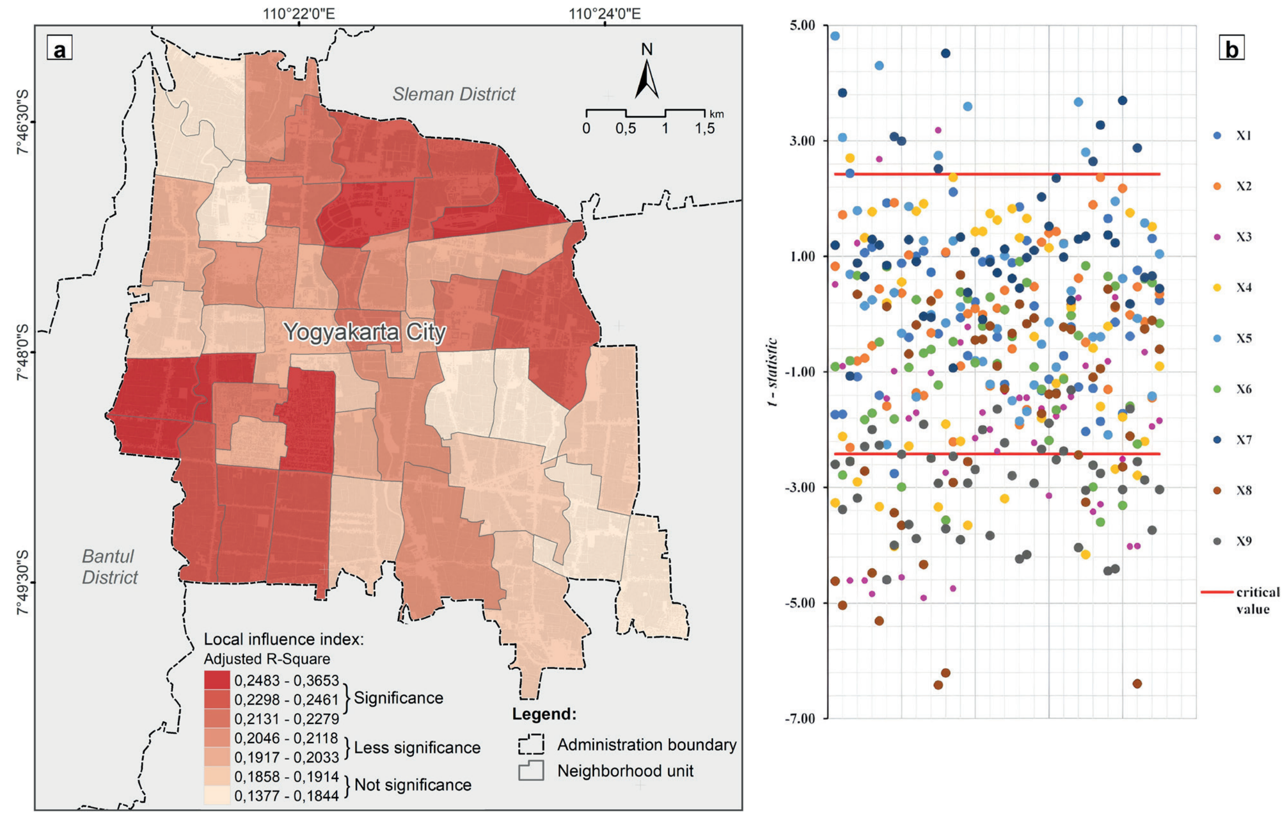

Fig. 7. The distribution of spatial relationships based on the GWR model is generated according to each neighborhood unit, including: (a) illustration of the local influence index adjusted by (R^2), and (b) distribution of significance level described by the tstatistic

This research reveals a significant link between urban connectivity, accessibility, and the spread of COVID-19. We found that areas with higher connectivity and accessibility tend to become hotspots for the virus spread, highlighting the crucial role of urban design in facilitating or mitigating disease transmission (Hamidi et al., 2020; Kwok et al., 2021). This pattern is particularly noticeable in our research location's central areas, which are adjacent to multiple districts. The urban configuration is characterized by a network of intersecting roads and a defined adjacent boundary, fosters extensive connectivity across the city. Such a layout significantly increases the opportunities for human interaction, elevating the virus transmission risk. These observations emphasize the importance of considering each location's unique characteristics and contexts when examining how urban form influences disease prevalence. This discussion is supported by the recent literature (Yechezkel et al., 2021), which indicates that urban connectivity can markedly affect the spread of infectious diseases by facilitating increased human movement and interaction.

Contrary to expectations, our study revealed that spatial density does not correlate strongly with COVID-19 case prevalence. This suggests that the mere concentration of buildings or population cannot predict outbreak severity, challenging prevalent notions within urban planning and public health domains. It indicates that other dimensions of urban form, such as the quality of public spaces or the nature of human activities within dense areas, may play more critical roles in disease spread dynamics (Wong & Li, 2020).

Furthermore, the heterogeneity of spatial functions within urban areas has shown significant associations with COVID-19 prevalence, highlighting the dual impacts of spatial arrangements. The concentration of public facilities correlates positively with COVID-19 cases. This suggests that areas with abundant public utilities may facilitate higher human interaction levels, increasing transmission risk (Yao et al., 2021). Otherwise, a diverse land use mix is inversely related to case numbers, possibly due to the dispersion of activities reducing crowding and direct contact between individuals. These findings point to the complexity of urban environments, where different configurations of space and function can either mitigate or exacerbate health risks.

Our research critically examines the current COVID-19 mitigation and preparedness policiesthat appear to overlook the valuable insights offered by urban science. Despite the deployment of numerous policies spanning science, technology, and innovation aiming to curb the virus's spread and strengthening socio-economic and community health resilience, there is an evident gap in incorporating urban scientific knowledge (Djalante et al., 2020; Putera et al., 2022). The case of Yogyakarta underscores the urgency of integrating urban science and spatial knowledge into virus mitigation strategies and preparedness planning. It enables the development of customized strategies considering the unique urban form and morphological characteristics of different city areas, such as informal settlements and kampungs (Wirastri et al., 2023).

Moreover, the disparity in urban forms across various city areas underscores the necessity for a nuanced approach to policy development, utilizing data on urban form elements to assess virus risk levels and determine the requisite medical support. This result ensures that all urban areas are adequately equipped to respond effectively to potential outbreaks, irrespective of their socio-economic status or regional characteristics. Our findings further highlight the complexity of urban environments in shaping the prevalence of COVID-19. The heterogeneity of spatial functions within urban areas reveals a dual impact on transmission rates, with the concentration of public facilities correlating positively with case numbers. At the same time, a diverse land use mix shows an inverse relationship, underscoring the importance of considering different spatial arrangements and their potential to mitigate or exacerbate health risks.

Additionally, understanding the spatial distribution of cases within a city is crucial for targeted interventions and resource allocation. Analyzing the relationship between urban forms and COVID-19 prevalence on finer spatial scale, such as at the neighborhood level, could provide more insights into local transmission dynamics. This detailed analysis could also identify specific urban form elements thar are most strongly associated with increased risk, enabling policymakers to prioritize interventions in areas where disease spread is most likely to occur.

However, the research limitations primarily stem from focusing on a specific urban area in Yogyakarta, which may limit the generalizability of findings to other urban contexts. Other factors influencing disease transmission dynamics, such as socio-economic conditions and cultural practices, still need to be further explored. Additionally, the study's cross-sectional design restricts the ability to determine causal relationships between urban form characteristics and COVID-19 prevalence. Despite these limitations, the research provides valuable insights into the spatial dynamics of disease transmission in cities. By integrating urban science and spatial knowledge into pandemic mitigation strategies and preparedness planning, cities can develop tailored approaches for unique urban form characteristics, ensuring equitable and effective responses to potential outbreaks.

CONCLUSIONS

In conclusion, our study provides compelling evidence supporting the hypothesis that urban form elements, particularly connectivity and accessibility, density, and spatial heterogeneity, play a crucial but underexplored role in shaping the spread of COVID-19. Our analysis of Yogyakarta City revealed clear associations between these urban morphological factors and the incidence of COVID-19 cases, reinforcing the importance of considering urban science and spatial knowledge when formulating effective pandemic mitigation and preparedness policies. By challenging the prevailing policy paradigm that often overlooks the intricate relationship between urban morphology and disease prevalence, our findings underscore the necessity of integrating urban science insights into public health strategies. This integration allows cities to better anticipate and mitigate the risks associated with future outbreaks. This research advocates for a multidisciplinary approach that combines urban planning and public health perspectives, emphasizing the need for detailed observation of urban form elements in order to develop resilient and healthy urban environments. The study thus contributes to the growing body of evidence that calls for a reassessment of how urban form considerations are integrated into disease mitigation and preparedness planning, aiming to enhance urban resilience in the face of ongoing and future health challenges.

REFERENCES

Aritenang, A. F. (2022). The impact of urban characteristics on the spread of Covid-19 in 2020: The case of Java Island cities, Indonesia. Regional Statistics, 12(3), 3–17. https://doi.org/10.15196/RS120301

Batty, M. (2008). Cities as Complex Systems: Scaling, Interactions, Networks, Dynamics, and Urban Morphologies. In The Encyclopedia of Complexity & System Science (Vol. 1, Issue 131, pp. 1–62). Springer Berlin.

Berghauser Pont, M. (2018). An analytical approach to urban form. In Urban Book Series. Springer International Publishing. https://doi.org/10.1007/978-3-319-76126-8_7

Berliner, L. M. (2015). Spatial Statistical Methods. In International Encyclopedia of the Social & Behavioral Sciences: Second Edition (Second Edi, Vol. 23). Elsevier. https://doi.org/10.1016/B978-0-08-097086-8.42174-4

Bhattacharjee, S., & Sattar, S. (2021). Pandemic and urban sustainability: Analyzing the COVID-19 scenario in Mumbai, India. Geography, Environment, Sustainability, 14(1), 17–24. https://doi.org/10.24057/2071-9388-2020-189

Brizuela, N. G., García-Chan, N., Pulido, H. G., & Chowell, G. (2019). Understanding the role of urban design in disease spreading. BioRxiv, 1–18. https://doi.org/10.1101/766667

Brunsdon, C., Fotheringham, S. A., & Charlton, M. E. (1996). Geographically Weighted Regression: A Method for Exploring Spatial Nonstationarity. Geographical Analysis, 28(4), 281–298. https://doi.org/10.1016/B978-008044910-4.00447-8

Clifton, K., Ewing, R., Knaap, G. J., & Song, Y. (2008). Quantitative analysis of urban form: A multidisciplinary review. Journal of Urbanism, 1(1), 17–45. https://doi.org/10.1080/17549170801903496

Cortes, P. (2005). Morphologies of Fragmentation and Continuity. In M. Barke (Ed.), Approaches in urban morphology (pp. 44–58). University of Northumbria.

da Silva, F. R., Câmara, S. F., Pinto, F. R., Soares, M., Viana, M. B., & De Paula, T. M. (2021). Sustainable development goals against COVID-19: The performance of brazilian cities in SDGS 3 and 6 and their reflection on the pandemic. Geography, Environment, Sustainability, 14(1), 9–16. https://doi.org/10.24057/2071-9388-2020-188

Djalante, R., Lassa, J., Setiamarga, D., Sudjatma, A., Indrawan, M., Haryanto, B., Mahfud, C., Sinapoy, M. S., Djalante, S., Rafliana, I., Gunawan, L. A., Surtiari, G. A. K., & Warsilah, H. (2020). Review and analysis of current responses to COVID-19 in Indonesia: Period of January to March 2020. Progress in Disaster Science, 6(March), 100091. https://doi.org/10.1016/j.pdisas.2020.100091

Fathi, S., Sajadzadeh, H., Sheshkal, F. M., Aram, F., Pinter, G., Felde, I., & Mosavi, A. (2020). The role of urban morphology design on enhancing physical activity and public health. International Journal of Environmental Research and Public Health, 17(7), 1–29. https://doi.org/10.3390/ijerph17072359

Getis, A., & Ord, J. K. (2010). The analysis of spatial association by use of distance statistics. In Advances in Spatial Science. https://doi.org/10.1007/978-3-642-01976-0_10

Ghishan, S., Al-Tal, R., & Aburamadan, R. (2023). COVID-19 causes and influences: rethinking neighborhood design in Jordan. Journal of Urbanism: International Research on Placemaking and Urban Sustainability, 1–23. https://doi.org/10.1080/17549175.2023.2181850

Gil, J. (2016). Street network analysis "edge effects": Examining the sensitivity of centrality measures to boundary conditions. Environment and Planning B: Urban Analytics and City Science, 44(5), 819–836. https://doi.org/10.1177/0265813516650678

Gross, B., Zheng, Z., Liu, S., Chen, X., Sela, A., Li, J., Li, D., & Havlin, S. (2020). Spatio-temporal propagation of COVID-19 pandemics. MedRxiv, 1–7. https://doi.org/10.1101/2020.03.23.20041517

Hamidi, S., Sabouri, S., & Ewing, R. (2020). Does Density Aggravate the COVID-19 Pandemic?: Early Findings and Lessons for Planners. Journal of the American Planning Association, 86(4), 495–509. https://doi.org/10.1080/01944363.2020.1777891

Hillier, B. (1988). Bill Hillier Mapping Method: Basis of Space Syntax Technique. Space Syntax, may 2008, 110–130.

Hillier, B., & Iida, S. (2005). Network and psychological effects: a theory of urban movement. International Conference on Spatial Information Theory, 1987, 475–490.

Hillier, B., Turner, A., Yang, T., & Park, H.-T. (2007). Metric and Topo-Geometric Properties of Urban Street Netrworks. 6th International Space Syntax Symposium, 1–22.

Jackson, L. E. (2003). The relationship of urban design to human health and condition. Landscape and Urban Planning, 64(4), 191–200. https://doi.org/10.1016/S0169-2046(02)00230-X

Kim, J., Zhang, J., Cha, Y., Kolitz, S., Funt, J., Chong, R. E., Barrett, S., Zeskind, B., Kusko, R., & Kaufman, H. (2020). Coronavirus Disease - 2019 (COVID-19). ChemRxiv, 2019(March). https://doi.org/10.26434/chemrxiv.12037416.v1

Kolosov, V. A., Tikunov, V. S., & Eremchenko, E. N. (2021). Areas of Socio-Geographical Study of The Covid-19 Pandemic In Russia and The World. Geography, Environment, Sustainability, 14(4), 109–116. https://doi.org/10.24057/2071-9388-2021-091

Kwok, C. Y. T., Wong, M. S., Chan, K. L., Kwan, M. P., Nichol, J. E., Liu, C. H., Wong, J. Y. H., Wai, A. K. C., Chan, L. W. C., Xu, Y., Li, H., Huang, J., & Kan, Z. (2021). Spatial analysis of the impact of urban geometry and socio-demographic characteristics on COVID-19, a study in Hong Kong. Science of the Total Environment, 764, 144455. https://doi.org/10.1016/j.scitotenv.2020.144455

Liu, L. (2020). Emerging study on the transmission of the Novel Coronavirus (COVID-19) from urban perspective: evidence from China. Cities, 103(April), 1–11. https://doi.org/10.1016/j.cities.2020.102759

Lu, C., Pang, M., Zhang, Y., Li, H., Lu, C., & Tang, X. (2020). Mapping Urban Spatial Structure Based on POI (Point of Interest) Data : A Case Study of the Central City of Lanzhou , China. International Journal of Geo-Information.

Marshall, S., Gil, J., Kropf, K., Tomko, M., & Figueiredo, L. (2018). Street Network Studies: from Networks to Models and their Representations. Networks and Spatial Economics, 18(3), 735–749. https://doi.org/10.1007/s11067-018-9427-9

Mollalo, A., Vahedi, B., & Rivera, K. M. (2020). GIS-based spatial modeling of COVID-19 incidence rate in the continental United States. Science of the Total Environment, 728, 138884. https://doi.org/10.1016/j.scitotenv.2020.138884

Nakaya, T., Fotheringham, A. S., Brunsdon, C., & Charlton, M. (2005). Geographically weighted Poisson regression for disease association mapping. Statistics in Medicine, 24(17), 2695–2717. https://doi.org/10.1002/sim.2129

Oshan, T. M., Li, Z., Kang, W., Wolf, L. J., & Stewart Fotheringham, A. (2019). MGWR: A python implementation of multiscale geographically weighted regression for investigating process spatial heterogeneity and scale. ISPRS International Journal of Geo-Information, 8(6). https://doi.org/10.3390/ijgi8060269

Ottensmann, J. R. (2018). On Population-Weighted Density. Florida 2012, 1–33.

Páez, A., & Scott, D. M. (2004). Spatial statistics for urban analysis: A review of techniques with examples. GeoJournal, 61(1), 53–67. https://doi.org/10.1007/s10708-005-0877-5

Putera, P. B., Widianingsih, I., Ningrum, S., Suryanto, S., & Rianto, Y. (2022). Overcoming the COVID-19 Pandemic in Indonesia: A Science, technology, and innovation (STI) policy perspective. Health Policy and Technology, 11(3). https://doi.org/10.1016/j.hlpt.2022.100650

Seungkoo Jo. (1998). Spatial configuration and built form. Journal of Urban Design, 3(3), 285–302. https://doi.org/10.1080/13574809808724430

Sharifi, A., & Khavarian-Garmsir, A. R. (2020). The COVID-19 pandemic: Impacts on cities and major lessons for urban planning, design, and management. Science of the Total Environment, 749, 1–3. https://doi.org/10.1016/j.scitotenv.2020.142391

Silalahi, F. E. S., Hidayat, F., Dewi, R. S., Purwono, N., & Oktaviani, N. (2020). GIS-based approaches on the accessibility of referral hospital using network analysis and the spatial distribution model of the spreading case of COVID-19 in Jakarta, Indonesia. BMC Health Services Research, 20(1), 1–21. https://doi.org/10.1186/s12913-020-05896-x

Subkhi, W. B., & Mardiansjah, F. H. (2019). Pertumbuhan dan Perkembangan Kawasan Perkotaan di Kabupaten: Studi Kasus Kabupaten Sleman, Daerah Istimewa Yogyakarta. Jurnal Wilayah Dan Lingkungan, 7(2), 105–120. https://doi.org/10.14710/jwl.7.2.105-120

UN-Habitat. (2021). Cities and Pandemics : Towards a More Just , Green and Healthy Future.

Van Nes, A., & Yamu, C. (2018). Space Syntax: a Method To Measure Urban Space Related To Social, Economic and Cognitive Factors. The Virtual and the Real in Urban Planning and Design: Perspectives, Practices and Application, January, 136–150.

Varoudis, T., Law, S., Karimi, K., Hillier, B., & Penn, A. (2013). Space syntax angular betweenness centrality revisited. 2013 International Space Syntax Symposium.

Wahid, W. W. C., & Setyono, J. S. (2022). The Urban Environment and Public Health: Associations between COVID-19 Cases and Urban Factors in Semarang City, Central Java, Indonesia. IOP Conference Series: Earth and Environmental Science, 1111(1). https://doi.org/10.1088/1755-1315/1111/1/012067

Wang, C., & Zhao, H. (2018). Spatial Heterogeneity Analysis: Introducing a New Form of Spatial Entropy. Entropy, 20(6). https://doi.org/10.3390/e20060398

Wheeler, J. O. (1971). Social Interaction and Urban Space. Journal of Geography, 70(4), 200–203. https://doi.org/10.1080/00221347108981620

Whitehand, J. W. R., Batty, M., & Longley, P. (1996). Fractal Cities: A Geometry of Form and Function. The Geographical Journal, 162(1), 113. https://doi.org/10.2307/3060277

Wirastri, M. V., Morrison, N., & Paine, G. (2023). The connection between slums and COVID-19 cases in Jakarta, Indonesia: A case study of Kapuk Urban Village. Habitat International, 134. https://doi.org/10.1016/j.habitatint.2023.102765

Wong, D. W. S., & Li, Y. (2020). Spreading of COVID-19: Density matters. PLoS ONE, 15(12 December), 1–16. https://doi.org/10.1371/journal.pone.0242398

Yao, Y., Shi, W., Zhang, A., Liu, Z., & Luo, S. (2021). Examining the diffusion of coronavirus disease 2019 cases in a metropolis: a space syntax approach. International Journal of Health Geographics, 20(1), 1–14. https://doi.org/10.1186/s12942-021-00270-4

Yechezkel, M., Weiss, A., Rejwan, I., Shahmoon, E., Ben-Gal, S., & Yamin, D. (2021). Human mobility and poverty as key drivers of COVID-19 transmission and control. BMC Public Health, 21(1), 1–13. https://doi.org/10.1186/s12889-021-10561-x

RESEARCH PAPER

A REGIONAL-SCALE ESTIMATE OF THE SOIL ORGANIC CARBON ISOTOPIC COMPOSITION ($\delta^{13}C$) AND ITS ENVIRONMENTAL DRIVERS: CASE STUDY OF THE BAIKAL REGION

Viktor A. Golubtsov*, Yulia V. Vanteeva, Anna A. Cherkashina
V.B. Sochava Institute of Geography, Siberian Branch of Russian Academy of Sciences, Ulan-Batorskaya 1, Irkutsk, 664033, Russia
*Corresponding author: tea_88@inbox.ru
Received: October 15th 2023/ Accepted: April 10th 2024 / Published: July 1st 2024
https://DOI-10.24057/2071-9388-2024-3091

ABSTRACT. Modern plants and surface soil $\delta^{13}C$ values from 95 sites in the Baikal region were obtained for the first time and were used to establish relationships with regional environmental factors. Studied sites were distributed along the elevation gradient from 403 to 2315 m, which defined a strong landscape and climatic gradients encompassing mountain tundra, subalpine grasslands, mountain taiga, subtaiga, and steppe. $\delta^{13}C$ values of soil organic matter (SOM) varied from −29.50 to −22.98‰. This result showed that the stable C isotopic composition of the surface soils was mainly determined by $\delta^{13}C$ values of C3 plants (vary from −33.0 to −24.5‰) and C isotope fractionation during stabilization of plant-derived C into SOM. The $\delta^{13}C$ values of modern plants and surface soils were negatively correlated with mean annual and growing season precipitation ($p<0.05$), confirming that precipitation is the primary factor determining SOM's stable C isotopic composition in the Baikal region. A distinct increase in the $\delta^{13}C$ values with decreasing mean annual and growing season precipitation was found with a slope of −0.42‰/100 mm and −0.97‰/100 mm, respectively. Temperature had no significant effect on the spatial distribution of SOM $\delta^{13}C$ values at the regional scale but played an important role in the severe environments of mountain tundra (the coldest and wettest) and steppes (the warmest and driest). Such conditions strongly impacted SOM $\delta^{13}C$ values by influencing plant species composition and soil microbiological activity. As a result, the organic matter of these soils is characterized by the highest $\delta^{13}C$ values. The SOM of taiga soils formed under a favorable combination of temperature and precipitation was characterized by the lowest $\delta^{13}C$ values.

KEYWORDS: carbon, $\delta^{13}C$, C3 plants, climatic conditions, mountain areas, Southeastern Siberia

CITATION: Golubtsov V. A., Vanteeva Y. V., Cherkashina A. A. (2024). A Regional-Scale Estimate Of The Soil Organic Carbon Isotopic Composition ($\delta^{13}c$) And Its Environmental Drivers: Case Study Of The Baikal Region. Geography, Environment, Sustainability, 2(17), 63-93
https://DOI-10.24057/2071-9388-2024-3091

ACKNOWLEDGEMENTS: The work was supported by the state assignment AAAA-A21-121012190055-7 (FWEM-2021-0002), AAAA-A21-121012190056-4. We are grateful to E.P. Zazovskaya and S.M. Turchinskaya, who kindly organized the laboratory work and stable isotopic measurements. Further special thanks to N.N. Voropay, E.A. Dukarev, M.Yu. Opekunova, M.A. Bronnikova, and T.I. Znamenskaya, who valuably supported us during the fieldwork.

Conflict of interests: The authors reported no potential conflict of interest.

INTRODUCTION

Understanding the spatio-temporal dynamics of soil organic carbon (SOC) and its driving factors is critical to assessing the feedback between the terrestrial C cycle and climate (Kudeyarov et al. 2007). This issue is especially relevant for mountain areas most affected by climatic changes (Pepin and Lundquist 2008). The overall impact of individual environmental factors on SOC dynamics is well-known. At the same time, analysis of the SOC dynamics in mountain regions is complicated by the high heterogeneity of bioclimatic conditions.

The Baikal region, where the fate of organic C in soils has been relatively poorly understood, is no exception. This circumstance brings to the fore the need to assess the main regional factors that determine soil C dynamics in various bioclimatic conditions. The problem is also relevant because the area under consideration is one of the planetary regions most prone to global warming (Shimaraev et al. 2002; Mackay et al. 2016). These climatic changes are bound to affect the C balance in regional ecosystems (Mackay et al. 2016).

Analysis of the stable C isotopic composition is an important approach to studying SOC dynamics (Dawson et al. 2002). Despite the significant potential of isotope studies, there are few examples of learning the $\delta^{13}C$ of SOM in the Baikal region and adjacent territories of Southeastern Siberia. Such studies cover individual soil types (Menyailo and Hungate 2006; Tsybenov et al. 2016; Golubtsov 2020; Tsybenov et al. 2022; Golubtsov et al. 2023a) as well as altitudinal profiles in depressions of the Baikal rift zone (Andreeva et al. 2013; Golubtsov et al. 2022; Andreeva et al. 2022; Golubtsov et al. 2023b). Most of the territory's soil remains unstudied regarding the geochemistry of stable carbon isotopes.

Filling this gap is also important in the context of the lack of knowledge about the soils in the vast inland regions of Northern Eurasia, which contain almost a fifth of the world's total soil carbon reserves (Kudeyarov et al. 2007; Schepaschenko et al. 2013). Most syntheses describing the global patterns of $\delta^{13}C$ value distribution in the SOM and organic matter-producing plants (Kohn 2010; Diefendorf et al. 2010; Rao et al. 2017; Cornwell et al. 2018) almost do not take into account data on the indicated region.

This study aimed to assess the spatial variability in SOC content and its stable C isotopic composition to identify the main factors controlling these variables in the Baikal region. We hypothesized that (1) climatic heterogeneity of the study area is one of the leading factors influencing variations in the $\delta^{13}C$ values of SOM; (2) precipitation has the main effect on the SOM $\delta^{13}C$ values; and (3) temperature has no significant effect on the spatial distribution of SOM $\delta^{13}C$ values at the regional scale but plays an important role in extreme climatic conditions.

This study could then provide clues on soil carbon dynamics in sharply continental regions and the potential feedbacks to climatic changes.

MATERIALS AND METHODS

Study area: geographical localization and orography

The Baikal region (Fig. 1) is a vast area in Southeastern Siberia that is strongly heterogeneous regarding physiographic conditions (Mikheev and Ryashin 1977).

The western part of the study area (Fore-Baikal region) is confined to the Siberian platform and its margins. The Eastern Sayan mountains' foothill plains and intermountain depressions, characterized by a predominance of hilly relief and absolute heights of 200-500 m, orographically represent this area (Plateaus… 1971). Deeply incised river valleys dissect this area.

The central part (Sayan-Baikal highlands) of the study area is characterized by extensive high plateaus and alpine-type mountain ranges with absolute heights up to 2300-3000 m or more, separated by deep depressions (Highlands… 1974).

The eastern part (Transbaikal region) is the area of ancient folding characterized by middle mountains, plateaus, and flat (in the southeast) relief. The territory is composed of deep intermountain depressions alternating with mountain ranges. Oriented from northeast to southwest, the mountain ranges are characterized by prevailing absolute heights of 1000-1500 m (Highlands… 1974). The northeast direction dominates the intermountain depressions, which are characterized by predominantly gently sloping terrain divided by hills and low ridges.

Climatic conditions, vegetation cover, and general patterns of pedogenesis

The heterogeneous topography of the study area has a significant impact on climatic conditions, which results in a high spatial diversity of landscapes (Plysnin et al. 2018), an altitudinal distribution of vegetation (Belov et al. 2018) and a diversity of soils (Koposov 1983; Kuz'min 1988). There is a wide range of vegetation types in the region, such as high-mountain (mountain-tundra and subalpine grasslands) and boreal (taiga and steppe) (Belov et al. 2018). Taiga forms the study area's main landscape background. Mountain tundra and steppe are localized as more, or less isolated areas confined to the most highly elevated surfaces (in the case of mountain tundra); high terraces and slopes of river valleys and the bottoms of depressions (in the case of steppes) (Mikheev and Ryashin 1977).

The climate of the study territory is sharply continental, characterized by large daily and annual (up to 30-45°C) temperature fluctuations. The amplitude of temperature fluctuations and degree of climate continentality increase from west (Fore-Baikal) to east (Transbaikal) (Zhukov 1965). The annual air temperature ranges from 0.5 to –4.2°C. The temperature of the coldest month (January) is from –18°C to –35°C, the warmest (July) is 10-15°C at altitudes of 1000-2000 m and 15-20°C in low-elevation sites (Scientific and Applied Handbook… 1989; 1991). The low annual radiation balance causes insufficient heat supply to landscapes (Zhukov 1965; Chimitdorzhieva 2016). The sum of active temperatures (above 10°C) varies from 600°C in the mountain tundra landscapes to 1500-2000°C on the plains and in basins, within the area of distribution of steppe and subtaiga (Zhukov 1965; Scientific and Applied Handbook… 1989; 1991).

The duration of periods with negative temperatures significantly exceeds those with positive ones, affecting the soil temperature regime (Trofimova et al. 2019). There is a strong cooling and deep freezing of soils during the winter and long-term preservation of negative temperatures in the soil profile (Koposov 1983; Abasheeva 1992).

Significant spatial heterogeneity in atmospheric precipitation is one of the most critical climatic features due to the complex topography of the study area (Trofimova et al. 2019). The predominantly northeastern orientation of the ridges and depressions, combined with the prevailing north-western flow of air masses, contribute to condensation and precipitation on the windward slopes. Due to mountain-barrier and basin effects, leeward slopes and intermountain basins are significantly less moistened (Zhukov 1965).

A heterogeneous distribution of precipitation is noted during the year. The first half of the vegetation season (May-June) is characterized by aridity; for July-August, moisture is optimal. At the same time, most precipitation falls in the summer (up to 75% of annually) (Scientific and Applied Handbook… 1989; 1991). The soil moisture fluctuates significantly during the vegetation season, and the soil is intensely dried in the first half (Koposov 1983).

Thus, there is a pronounced contrast between the dry and wet seasons of the warm period, which affects the short periods of optimal combination of positive temperatures and soil moisture for microbiological activity. This circumstance limits the intensity and degree of plant residue decomposition (Volkovintser 1978; Abasheeva 1992; Chimitdorzhieva 2016) and humification (Kuz'min 1988; Chimitdorzhieva 2016).

The most severe variants of the described regional specifics of soil temperature and water regimes are typical of the soils of the mountain tundra. It is also found in steppe soils in a somewhat milder form (Kuzmin 1988; Abasheeva 1992; Chimitdorzhieva 2016). Steppe landscapes are characterized by a dryness index (the ratio of the surface annual radiation balance to the amount of heat required to evaporate the annual amount of precipitation) in the range of 1.5-1.8 which indicates a large moisture deficit (Zhukov 1965). The forming conditions of soils in taiga landscapes are more favorable. Here, the dryness index ranges from 0.45 to 1.0 indicating sufficient and even excessive moisture (Budyko 1971). Such humidity contributes to the optimal water balance of plants that form SOM and high soil microbiological activity. At the same time, the temperature decrease with increasing altitude is often offset by temperature inversions, which are one of the essential features of the regional climate (Trofimova et

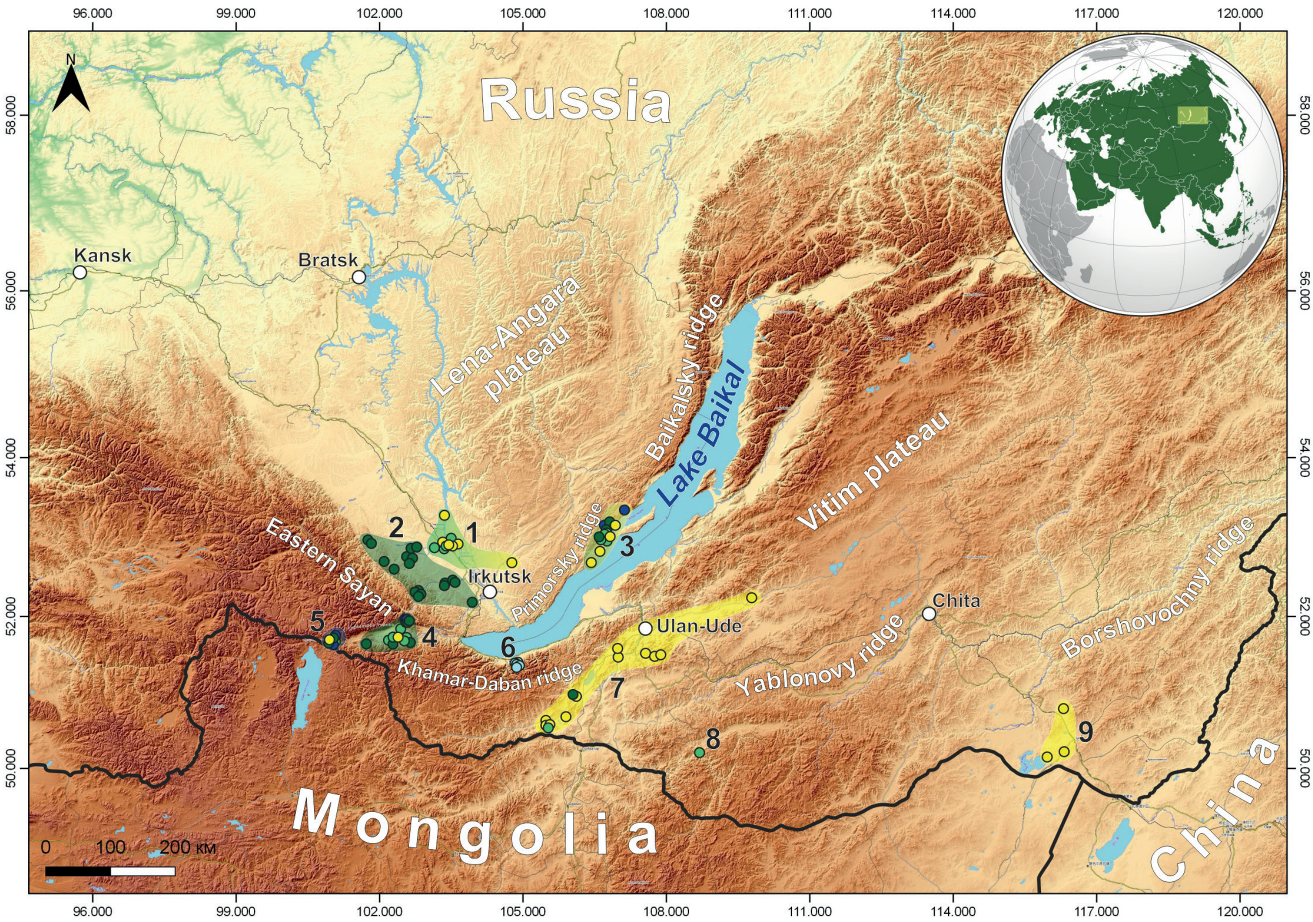

Fig. 1. Location of the study area and main sampling sites. Landscape types: yellow – steppes; dark green – mountain taiga; light green – subtaiga; light blue – subalpine grasslands; dark blue – mountain tundra

al. 2019). As a result, the period with positive temperatures in some taiga areas may exceed that even on the plains and in the bottoms of the depressions.

Study sites

The study sites include (Fig. 1; Table A): steppe and subtaiga of the Irkutsk-Cheremkhovo plain and Cis-Baikal depression (1); mountain taiga of the foothills of the Eastern Sayan mountains (2); mountain tundra, mountain taiga, subtaiga, and steppe of the Olkhon region and the southeastern side of the Primorsky ridge (3); Tunka (4) and Mondy (5) basins of the Baikal rift zone; subalpine grasslands of the Khamar-Daban ridge at the southern part of Lake Baikal (6); steppes and subtaiga of intermountain basins of the Selenga middle mountains (7) and the Chikoy river valley (8); steppes of the Southeastern Transbaikal region (9).

The study is based on SOM investigation data from 95 plots. Each plot (10 x 10 m) was characterized by a complex environmental description that includes the characteristics of phytocenoses, geomorphological conditions, and morphogenetic analysis of soils. Soil taxonomic affiliation was determined according to (IUSS Working Group WRB 2015). General information on the sampling sites is shown in Table A. A more detailed description of sites and soil characteristics can be found in previous works (Golubtsov et al. 2021; 2022; 2023 a, b).

Sampling scheme, sample preparation, and laboratory analyses

The fieldwork was carried out in July of 2020-2022. We collected fresh, mature leaves of the dominant species, constituting 80% of the biomass in each plot. Leaf and mineral soil samples were dried to an air-dry state and homogenized. Leaves were oven-dried at 70°C for 60 hours until weight constancy and ground. Samples of mineral soil horizons were sifted through a 1-mm sieve with the subsequent removal of fine roots and washed using 1M HCl to remove carbonates.

The total organic carbon (TOC) content was determined by pyrolysis of samples on an elemental analyzer CHNS Vario Isotope Cube (Elementar, Germany). The stable carbon isotopic composition ($\delta^{13}C$) was measured on a set of equipment CHNS-analyzer Vario ISOTOPE Cube mass spectrometer Isoprime precision IRMS (Elementar, UK) connected in continuous flow mode. The measurements were conducted at the Center for Collective Use "Laboratory of Radiocarbon Dating and Electron Microscopy" Institute of Geography of the Russian Academy of Sciences. The results were expressed in ‰ for the VPDB standard. The standard deviation for measurement of the $\delta^{13}C$ is less than 0.1‰.

Meteorological data

Climatic data for each sampling location were assessed both for the vegetation season (May-September) and for the year as a whole based on the WorldClim 2.0 database (spatial resolution 30") (Fick et al. 2017), monthly data of bias-corrected ERA5-Land reanalysis (reference period from 1981 to 2021) (Muñoz Sabater 2019) with spatial resolution 0.1°×0.1°, which approximately corresponds to 11.0 km in latitude and 7.2 km in longitude for Siberia. For each investigated site, the time series at the nearest mode of the reanalysis grid was used.

The data of microclimatic observations obtained using automatic recorders Elitech RC-51H and RC-4HC (Golubtsov et al. 2022; Golubtsov et al. 2023b) were used for sites located on altitude profiles within mountain-depression areas (Fig. 1, areas 3-5) where the climate changes noticeably at reasonably close distances that are beyond the spatial resolution of the reanalysis. The air temperature, relative humidity (at a height of 2 m above the surface), and soil surface temperature were measured. The temperature measurement accuracy is 0.1°C, and the relative humidity is 3%. The observations have been carried out at 1-hour intervals since 2013. In some cases, the data were corrected based on annual precipitation, taking into account data from the nearest meteorological stations (Scientific and Applied Handbook… 1989; 1991).

Data analysis

Data processing was performed using MO Excel and PAST 4.03 (Hammer et al. 2001). For each data set, a check was carried out for compliance with the normal distribution using the Shapiro-Wilk and Anderson-Darling tests, and according to this, parametric or non-parametric statistical methods were selected. For samples of less than 30 measurements, nonparametric methods and tests were used.

A one-way ANOVA with Tukey's HSD test was conducted for the estimation of differences in $\delta^{13}C$ values in the SOM of the surface horizons of soils in different landscape types. The Kruskal-Wallis H-test (a nonparametric analogue of ANOVA) with Dunn's post hoc test was used to estimate differences in $\delta^{13}C$ values in different life forms of plants and lichens. A paired correlation analysis with the Spearman correlation coefficient (Spearman's rs) was conducted to identify the main climatic factors (air temperature and precipitation for the year and the growing season, altitude) influencing the variation in $\delta^{13}C$ values in plant biomass of different life forms. To confirm the dependence of $\delta^{13}C$ values in the SOM of the surface horizons of soils on the amount of precipitation for the year and growing season, paired linear regressions were calculated. The linear regression residuals were close to a normal distribution.

RESULTS

Differences in climate

Both mean annual temperatures and mean temperatures of the growing season decreased in the direction from the steppes to the mountain tundra (Fig. 2). In many cases, temperatures are quite similar in a large group of steppe, subtaiga, and taiga plots, along with this general trend. In terms of temperatures, the mountain-taiga area was the most heterogeneous. The lowest temperatures here were recorded in high-elevated sites that form in the mountain-depression conditions of the Baikal rift zone (Primorsky ridge (3), the mountains surrounding Tunka (4) and Mondy (5) basins, the Khamar-Daban ridge (6)). A similar differentiation was also typical for the steppes, where low temperatures were observed in the highest-located steppes of the Olkhon region (3), the Mondy basin (5), and the Selenga middle mountains (7).

The studied sites were also heterogeneous in terms of atmospheric precipitation (Table A). The highest mean annual and growing season precipitation was observed in mountain tundra, subalpine grasslands, and high-elevated mountain taiga sites (Fig. 2), especially on the Khamar-Daban ridge (6), windward slopes, and foothills of the Eastern Sayan mountains (2). The leeward slopes and intermountain depressions were significantly drier due to the mountain barrier and basin effects. This was most clearly indicated in the mountain taiga on the southeastern slope of the Primorsky ridge (3) and the Tunka mountains (4). The lowest mean annual precipitation within the study area was observed in the steppe landscapes of the intermountain basins of the southern part of the Selenga middle mountains (7), the Mondy basin (5), and the western coast of Lake Baikal at the foot of the Primorsky ridge (3). Here, the annual precipitation often only slightly exceeds 200-250 mm.

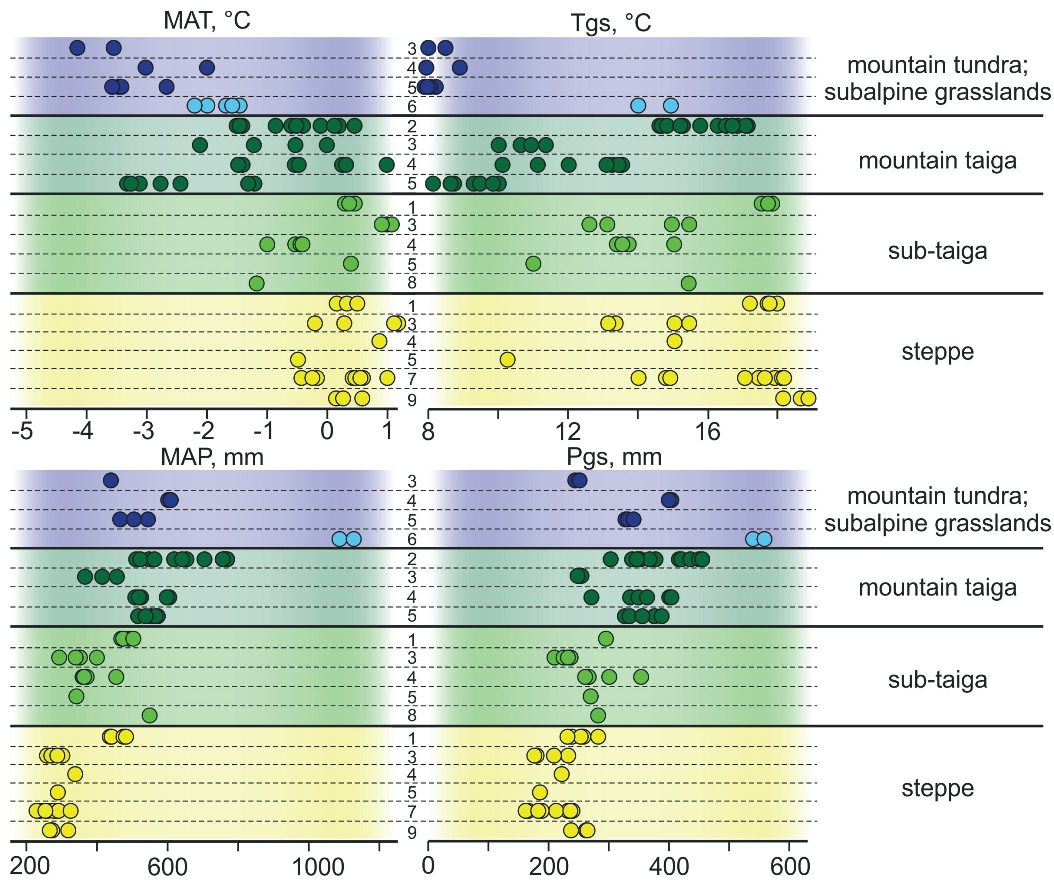

Fig. 2. Mean annual and mean growing season temperature and precipitation of landscapes in the Baikal region. The numbers in the center of the figure correspond to the areas on Fig. 1

Microclimatic observations within individual altitudinal profiles on the Primorsky ridge (3) (Golubtsov et al. 2022) and in the Tunka mountains (4) (Golubtsov et al. 2023b) indicated a linear increase in temperature, the duration of the growing season, and a decrease in precipitation from high to low-elevated sites. At the same time, local variations were associated with the density of the vegetation cover, the landform features, and local atmospheric circulation (Golubtsov et al. 2022; 2023b).

Differences in TOC

High-elevated mountain tundra and taiga soils were characterized by an increased TOC content in the surface mineral horizons compared to low-elevated steppe soils (Fig. 3). High TOC variation (from 2.5 to 45%) in mountain taiga soils was one of the most essential features. This feature is associated with the distribution of taiga landscapes in the Baikal region, both in terms of their vast area and the range of variations in environmental factors (temperature, precipitation, vegetation cover, etc.).

On the contrary, the TOC content in steppe soils is localized in rather narrow ranges (from 0.5 to 12%) (Fig. 3; Table A). The similarity of the steppe soils is probably due to their localization in the region, mainly within the basins, and the pronounced limitations of their areas in terms of precipitation.

The tundra and subalpine soils are very diverse in terms of TOC, which is largely due to the high heterogeneity in temperature and precipitation conditions in the mountains.

Variations in $\delta^{13}C$ values of plant organic matter

$\delta^{13}C$ values were determined for 38 species of higher vascular plants, two species of moss, and two species of lichen growing in the study area. Table 1 presents data only for the main plant species-edificators of landscape types. The $\delta^{13}C$ values in leaves and needles of higher vascular plants were low and varied from −32.6 to −25.5‰ (Fig. 4a).

The range of $\delta^{13}C$ values varied from −32.6 to −32.3‰ for mosses and −24.6 to −23‰ for lichens (Table 1). The mountain tundra and steppe plant species were the most enriched in ^{13}C (mean value −27.9 ± standard deviation 1.3‰ and −28 ± 0.8‰, respectively), the mean value $\delta^{13}C$ in taiga species was lower by 2.2 and 2.1‰.

Analysis of $\delta^{13}C$ values in various life forms of plants showed (Fig. 5) that the greatest range of values was observed in trees (a difference of 6.77‰) and shrubs (5.4‰), and the minimum (0.37‰) in mosses.

When comparing the mean $\delta^{13}C$ values in leaf samples, litter, and the SOM of the surface horizons of soils, it was revealed that the $\delta^{13}C$ value of organic matter became higher during the transition from plants to litter at 0.1-3.9‰, and from litter to the surface humic horizon at 0.3-2.0‰ (Fig. 6). The maximum difference in $\delta^{13}C$ values was observed mainly in the mountain taiga, which may be due to the mixed composition of the litter, including both coniferous and deciduous litter, as well as to varying degrees of their decomposition.

This pattern is not observed at several plots where the plant sample was enriched with ^{13}C compared to the litter, or $\delta^{13}C$ value of the humic horizon SOM was lower than that of the litter (Fig. 6). This difference from the general pattern is probably due to the fact that the soil on these plots was formed under conditions of changes in taiga and steppe landscapes, determined by the dynamics of climatic conditions. The disruption of the ecological balance between the litter and other components of the landscape as a result of the periodic expansion and contraction of the taiga area could be one of the factors that caused the observed differences in the stable carbon isotopic composition of the upper part of the soil organic profile (Golubtsov et al. 2022).

Variations in $\delta^{13}C$ values of SOM in regional soils

SOM of the study soils showed a considerable variation in $^{13}C/^{12}C$ isotopic ratios, covering a wide range of $\delta^{13}C$ values characteristic of C3 plants (O'Leary 1988) (Fig. 4). The topsoil organic matter had $\delta^{13}C$ values from −29.5 to −22.98 ‰ (Fig. 4; Table A).

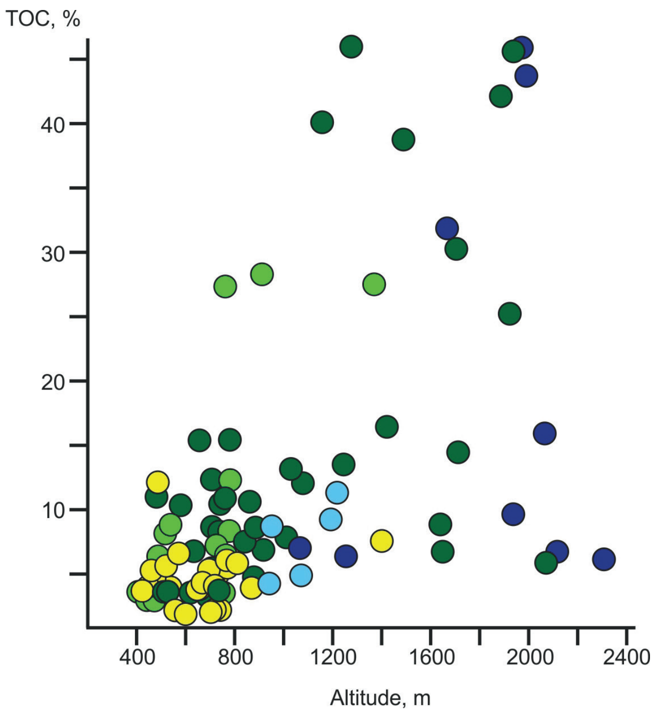

Fig. 3. Altitudinal variations in topsoil TOC content in different landscapes (yellow – steppes; dark green – mountain taiga; light green – subtaiga; light blue – subalpine grasslands; dark blue – mountain tundra)

Table 1. δ¹³C values of dominant species of vascular plants and lichens at sampling sites

№	Plant species	δ¹³C, ‰ (mean ± st. dev.)	Number of samples	Landscape type
Trees				
1	*Betula pendula* Roth	-31.04 ± 0.86	4	Taiga/subtaiga, successional stage
2	*Larix sibirica* Ledeb.	-28.12 ± 1.86	4	Light coniferous taiga
3	*Pinus sibirica* Du Tour	-29.14 ± 1.99	3	Dark coniferous taiga
4	*Pinus sylvestris* L.	-28.74 ± 1.49	9	Light coniferous taiga and subtaiga
5	*Populus tremula* L.	-29.69 ± 1.53	4	Taiga/subtaiga, successional stage
Shrubs				
6	*Betula fruticosa* Pall.	-29.57 ± 1.39	3	Mountain tundra
7	*Duschekia fruticosa* (Rupr.) Pouzar	-29.66 ± 1.26	3	Taiga
8	*Rhododendron parvifolium* Adams	-26.72	1	Mountain tundra
9	*Rhododendron dauricum* L.	-30.87 ± 0.94	3	Light coniferous taiga, subtaiga
Subshurbs				
10	*Dryas oxyodonta* Juz.	-29.63	1	Mountain tundra
11	*Empetrum nigrum* L.	-27.33	1	Mountain tundra
12	*Vaccinium vitis-idaea* L.	-30.50 ± 0.83	9	Taiga
13	*Vaccinium myrtillus* L.	-32.14 ± 0.55	4	Taiga
Herbs				
14	*Agropyron cristatum* (L.) Gaertn.	-28.57 ± 0.69	3	Steppe
15	*Artemisia frigid* Willd.	-28.43 ± 1.04	3	Steppe
16	*Koeleria cristata* (L.) Pers.	-28.16 ± 1.76	2	Steppe
17	*Maianthemum bifolium* (L.) F.W. Schmidt	-30.84 ± 0.42	2	Taiga
18	*Poa botryoides* (Trin. ex Griseb.) Kom.	-29.56 ± 0.52	2	Steppe
Mosses				
19	*Hylocomium splendens* (Hedw.) Bruch et al.	-32.46	1	Taiga
20	*Pleurozium schreberi* (Willd. ex Brid.) Mitt.	-32.45 ± 0.17	4	Taiga
Lichens				
21	*Flavocetraria nivalis* (L.) Kärnefelt et A. Thell	-23.03	1	Mountain tundra
22	*Cladonia rangiferina* (L.) F. H. Wigg.	-24.58	1	Mountain tundra

A non-linear distribution of δ¹³C values in the altitudinal profile was noted, which was strongly correlated with the landscape type (Fig. 4b). One-way ANOVA with Tukey's HSD test showed differences ($p \leq 0.0001$) in ¹³C/¹²C ratios in the surface horizons of steppe soils (Table 2) from subalpine grasslands, mountain taiga, and subtaiga forests. The differences between δ¹³C values in mountain tundra, subtaiga, and steppe soils have not been identified ($p > 0.05$, Table 2).

Even though subalpine grasslands like mountain-tundra soils were formed under rather severe climatic conditions, they were much lighter in stable C isotopic composition ($p = 0.001$) and were distinguished as an independent group.

The highest variations in δ¹³C values were observed in mountain taiga soils (from −27.06 to −24.72‰) associated with a reasonably wide taiga distribution under different climatic conditions (from wet dark-coniferous forests to drier pine forests). At the same time, differences were revealed between the soils of the mountain taiga and subtaiga ($p < 0.05$), which occupied a transitional position between the taiga and the forest-steppe zone (Fig. 4, Table 2).

DISCUSSION

Control of C3 and C4 plants on ¹³C/¹²C ratios of SOM

The ¹³C/¹²C isotopic ratio in the plant tissues is one of the main predictors of SOM's stable carbon isotopic composition (Ehleringer 2005). It is essential to pay

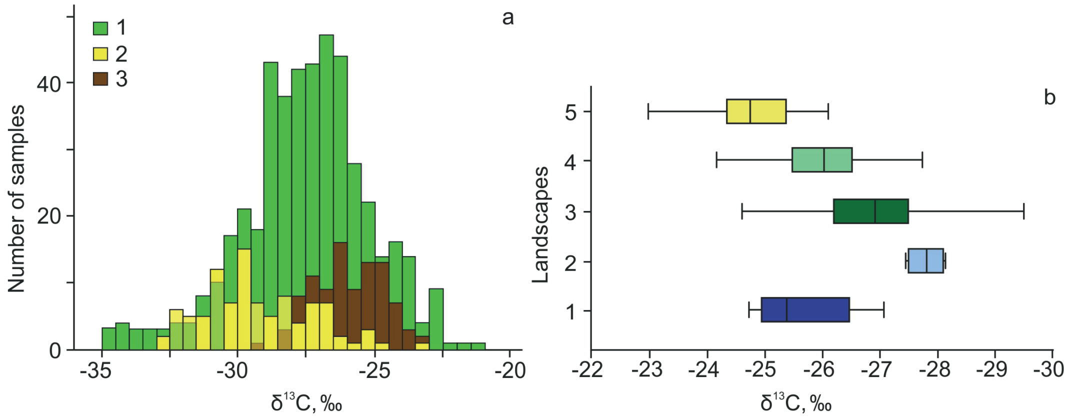

Fig. 4. Histogram of the $\delta^{13}C$ values of surface soils and plants in the Baikal region (a). Table of symbols: 1 – data of C3 plants come from O'Leary (1988); 2 – $\delta^{13}C$ values of study plant species; 3 – $\delta^{13}C$ values of surface humic soil horizons. The $\delta^{13}C$ values of surface soil samples in different landscape types in the Baikal region (b): 1 – mountain tundra; 2 – subalpine grasslands; 3 – mountain taiga; 4 – subtaiga; 5 – steppe

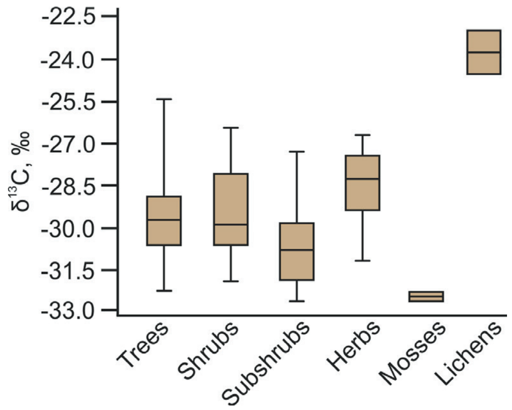

Fig. 5. $\delta^{13}C$ values in different life forms of higher vascular plants, mosses and lichens

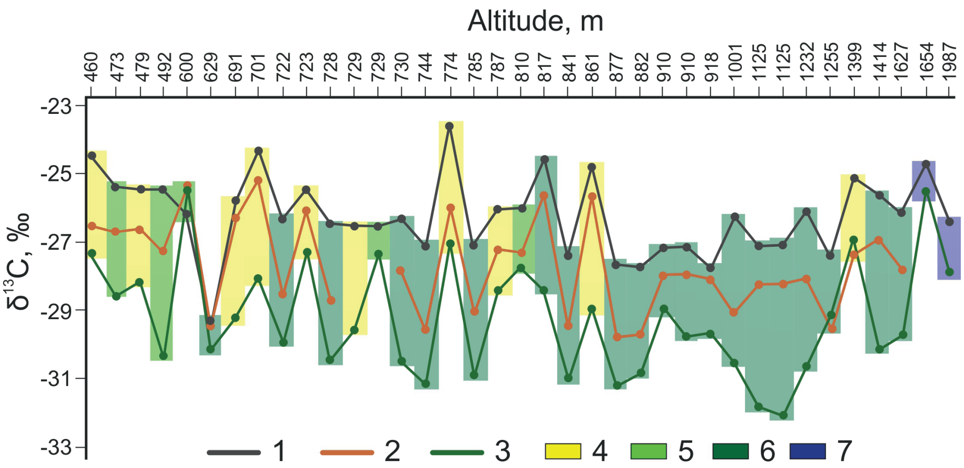

Fig. 6. The mean $\delta^{13}C$ values: 1 - in the SOM of the surface humic horizons of soils, 2 – in litter samples, 3 – in leaf samples. Landscape types: 4 – steppe, 5 – subtaiga, 6 – mountain taiga, 7 - mountain tundra

Table 2. The results of the estimation of differences in the $\delta^{13}C$ values of surface soil samples in different landscape types in the Baikal region by ANOVA

Landscape type	$\delta^{13}C$, ‰ (mean ± st. dev.)	Tukey's Q below the diagonal, p-value above the diagonal				
		mountain tundra	subalpine grassland	taiga	subtaiga	steppe
mountain tundra	–25.39 ± 0.82		0.001	0.005	0.912	0.051
subalpine grassland	–27.8 ± 0.32	5.7		0.231	0.002	< 0.0001
taiga	–26.8 ± 0.98	5.0	3.0		0.007	< 0.0001
subtaiga	–25.96 ± 0.84	1.3	5.4	4.9		0.0001
steppe	–24.7 ± 0.82	3.9	9.2	12.9	6.6	

attention to some issues, given the rather heterogeneous plant cover of the study area.

The first is the relative abundance of plants with different photosynthetic pathways (Ehleringer 2005; Rao et al. 2017). Higher terrestrial plants are divided into three main groups according to their photosynthetic pathways: C3 (Calvin-Benson), C4 (Hatch-Slack) and CAM (Crassulacean acid metabolism). CAM plants will not be considered in this paper because they are only present in highly specialized ecosystems (for example, deserts). C3 plants include almost all trees, shrubs, and cool-season grasses, while C4 plants comprise mainly warm-season grasses (Ehleringer 2005; Sage 2005; Rao et al. 2017). C3 and C4 plants have $\delta^{13}C$ values ranging from -20‰ to -32‰ and -10‰ to -17‰, respectively.

Plant phylogenetic lines that are common mainly in the tropics and subtropics tend to use C4 photosynthesis (Sage 2005). However, the flora of the study region has distinct boreal features (Belov et al. 2018). Nevertheless, according to various estimations, the relative abundance of C4 plants in the plant communities of arid and semi-arid areas of Central Asia can reach 30% (Ehleringer 2005).

The steppes presented in the study area had floristic similarities with the Central Asian and East Asian steppes and belonged to the Mongolian-Chinese florogenetic type (Belov et al. 2018). Several authors noted the presence of C4 plants in the steppe communities of the study area (Ivanova et al. 2019; Golubtsov et al. 2022). These findings agreed with the nature of C4 plants adapted to high-intensity photosynthesis at elevated temperatures and light, mainly due to the possibility of fixing CO_2 at high stomatal resistance under water stress conditions (Sage 2005).

However, an abundance of plants with C4 photosynthetic pathways in the steppes of the Baikal region was insignificant (Ivanova et al. 2019). For example, on several plots in the steppes of the Olkhon region (3), plants of this group were represented singly, or their projective cover did not exceed 1% (Golubtsov et al. 2022). Hence, C4 plants did not contribute to variations in the study area's $^{13}C/^{12}C$ isotopic ratios of SOM. The obtained $\delta^{13}C$ values of SOM supported this assumption since they indicated the C3 plant biomass as the primary source of SOM (Fig. 4).

Variations in the $\delta^{13}C$ values of SOM can also correlate with stable C isotope fractionation features in C3 plant tissues depending on their growing conditions (Dawson et al. 2002; Diefendorf et al. 2010; Rao et al. 2017). It was noted above that the SOM $\delta^{13}C$ values were distributed nonlinearly depending on the elevation. The SOM of low-elevated (steppe) and high-elevated (mountain tundra) sites was most enriched in ^{13}C. The lowest $\delta^{13}C$ values were observed in the SOM of mid-elevated mountain taiga landscapes (Fig. 4). A similar nonlinear distribution of $\delta^{13}C$ of plant biomass depending on altitude was observed (Fig. 6).

Significant height amplitudes caused pronounced changes in the air temperature and precipitation (Fig. 2), determining plant communities' species composition and growth conditions. It is also known that $\delta^{13}C$ can vary in C3 plants of different layers and life forms depending on moisture availability, temperature, and other factors (Dawson et al. 2002; Tiunov 2007). The results of the Kruskal-Wallis H-test ($H=35.71$, $p < 0.0001$) revealed statistically significant differences in the $^{13}C/^{12}C$ isotopic ratios between the different life forms of the studied plants and lichens (Table 3). Differences were observed between the upper and lower layers ($p < 0.05$): subshrubs and mosses were lighter in composition of stable C isotopes than trees and shrubs (Fig. 5). The observed isotopic differences could primarily be associated with the effect of the forest canopy when, in dense forest stands, the concentration of ^{13}C in plant leaves had a pronounced vertical gradient and was minimal in plants of the lower layers (Tiunov 2007). The effect was associated with the peculiarities of photosynthesis under shading conditions, as well as the fixation of ^{13}C-depleted carbon dioxide released by soil and litter by plants.

Higher $\delta^{13}C$-values were found for herbs (Table 1, Fig. 5) than for other groups of plants except lichens. This was because the herb sample was represented mainly by steppe species that grow in drier conditions and are unaffected by the forest canopy effect. Of the taiga species, the sample included *Maianthemum bifolium* (Table 1), which had the lightest isotopic composition among herbs.

A separate group with a high level of significance ($p < 0.05$) included lichens (Fig. 5, Table 3) that dominated the plant cover of the mountain tundra on the Primorsky ridge (3). The increase in ^{13}C content in lichens compared to vascular plants in the study area was associated with the peculiarities of C fractionation in this group of organisms (Byazrov et al. 2010). The $\delta^{13}C$ values we obtained indicated insufficiently favorable conditions for lichens in the mountain tundra and were consistent with the data obtained for *Flavocetraria nivalis* in the tundra in Western Yamal, where the $\delta^{13}C$ varied from –24.3 to –24.4 ‰ (Kuznetsova et al. 2020).

A paired correlation analysis was conducted to identify the main climatic factors influencing the variation in $\delta^{13}C$ values in plant biomass. It was revealed that $\delta^{13}C$ of coniferous tree species negatively correlates with annual precipitation (Spearman's rs is –0.77, $p = 0.0001$). For deciduous tree species, such a correlation has not been identified.

Table 3. The results of the estimation of differences in the $\delta^{13}C$ values between the different life forms of plants and lichens by Kruskal-Wallis H-test

Plant life form	$\delta^{13}C$, ‰ (mean ± st. dev.)	Dunn's post hoc test, raw p-value					
		Trees	Shrubs	Subshurbs	Herbs	Mosses	Lichens
Trees	–29.50 ± 1.63		0.68	0.02	0.02	0.001	0.02
Shrubs	–29.23 ± 1.68	0.68		0.02	0.11	0.0009	0.04
Subshurbs	–30.74 ± 1.38	0.02	0.02		< 0.0001	0.09	0.001
Herbs	–28.50 ± 1.19	0.02	0.11	< 0.0001		< 0.0001	0.15
Mosses	–32.45 ± 0.15	0.001	0.0009	0.09	< 0.0001		0.0001
Lichens	–23.81 ± 1.10	0.02	0.04	0.001	0.15	0.0001	

A strong positive correlation (Spearman's rs = 0.71, p = 0.002) with the absolute height of the area and an average negative correlation (Spearman's rs = –0.59, p = 0.02) with air temperature for the year and the growing season were found for shrubs. The shrub sample includes species from each studied landscape type except steppe. Therefore, this plant group demonstrates that under low-temperature conditions, processes of inhibition of photosynthesis occur, which, like dry conditions, led to the enrichment of plant tissues with ^{13}C. Subshrubs also showed similar correlations, although they were significantly less pronounced ($p > 0.05$). The lack of a reliable correlation of $\delta^{13}C$ with climatic parameters in subshrubs was because the sample was represented mainly by taiga species that grow in the low layer and were most susceptible to the forest canopy effect. Also, no significant correlation existed between $\delta^{13}C$ of herb biomass and climate parameters.

As a result of the analysis, it was established that for plants in taiga landscapes growing in subordinate layers, the effect of the forest canopy often overlapped with the influence of climatic factors on the $^{13}C/^{12}C$ isotopic ratios. However, the climatic conditions caused by altitudinal and latitudinal zonality largely determined the structure of plant communities. As a result, we considered the climatic heterogeneity of the study area to be one of the leading factors influencing variations in the composition of stable carbon isotopes of SOM.

Relationship between natural ^{13}C abundance in SOM and climate

With changing altitudes, the change of such climatic factors as temperature and precipitation were the most prominent. These climatic parameters were the main driving factors of C isotopic discrimination in C3 plant tissues during photosynthesis (Dawson et al. 2002; Diefendorf et al. 2010; Rao et al. 2017). These factors affected plant C isotope discrimination because they could control the intensity of CO_2 exchange between the plant and the atmosphere (Farquhar et al. 1989).

In conditions where the moisture in the air or soil is reduced or precipitation is decreased, the plants will close the stomata to decrease water evaporation, which can lower the stomatal conduction coefficient, followed by a decrease in the partial pressure of CO_2 in the leaf intercellular spaces (P_i) (Farquhar et al. 1989) which leads to a reduction in C isotope fractionation and an increase in $\delta^{13}C$ values of plants and SOM (Xu et al. 2015; Rao et al. 2017). Such a relationship has been found globally (Diefendorf 2010; Kohn 2010; Rao et al. 2017) and regionally (Chen et al. 2015; Lee et al. 2005; Zhang et al. 2020; Golubtsov et al. 2021; Golubtsov et al. 2022). There is a negative relationship between precipitation and the plant/SOM $\delta^{13}C$ values in which increased precipitation can result in a lighter carbon isotopic composition, especially in areas with water stress (Kohn et al. 2010; Diefendorf et al. 2010; Rao et al. 2017).

Previous studies have also reported that plant C isotope discrimination may be affected by temperature (Wang et al. 2013; Xu et al. 2015; Rao et al. 2017; Zhao et al. 2017; Zhang et al. 2020). The activity of enzymes in plants that assimilate CO_2 during photosynthesis is influenced by temperature. The activities increase as the temperature rises, then the photosynthetic rate increases, and the assimilation rate of CO_2 accelerates, and P_i is consequently lowered, which results in a decrease in the carbon isotope fractionation and an increase in the $\delta^{13}C$ values of plants (Farquhar et al. 1989).

However, when speaking about living organisms, it is necessary to consider the limitations beyond which C3 plants begin to experience physiological stress. An increase in annual temperatures is closely related to an increase in evaporation and can lead to the plant growing under water-stress conditions, the effect of which, in terms of $\delta^{13}C$ values, is described above. At the same time, plant growth at low temperatures will favor various physiological adaptations (for example, leaf morphology). Low temperatures may increase water viscosity, inhibit sapwood water movement, and thereby decrease plant water potential, resulting in partial stomatal closure and an increase in $\delta^{13}C$ values in plants and producing SOM as a consequence (Cernusak et al. 2013; Xu et al. 2015).

Thus, previous studies indicated a somewhat contradictory effect of temperature on the $^{13}C/^{12}C$ ratios in plant tissues and the SOM, which various factors can explain. The increase in SOM $\delta^{13}C$ values coinciding with the rise in annual temperatures was correlated with the relative abundance of C4 plants (Jia et al. 2016; Rao et al. 2017). It is well-known that C4 plants have a competitive growth advantage over C3 plants in high temperatures and aridity (Farquhar et al. 1989; Ehleringer 2005; Sage 2005). At the same time, no relationships between $\delta^{13}C$ values of SOM and temperature in C3-dominated plant communities or under pure C3 vegetation were found (Feng et al. 2008; Lee et al. 2005; Jia et al. 2016). This observation was supported by findings indicating an insignificant (in terms of $\delta^{13}C$ values) response of C3 plants to changes in mean annual temperatures compared to mixed C3/C4 phytocenoses (Rao et al. 2017).

Indeed, a linear regression analysis of the $\delta^{13}C$ SOM values driving factors showed a non-significant correlation for the average annual temperatures in the study area. Therefore, it would be most reasonable to search for the effect of temperature on the isotopic composition of soils and plants under ecologically unfavorable conditions. In our case, these included steppes with their relatively high temperatures and low moisture, and mountain tundra and subalpine grasslands that formed under conditions of low air temperatures (Fig. 2). As a result, SOM was most enriched in ^{13}C (Fig. 4).

At the same time, the optimal temperatures in combination with wet conditions in the taiga landscapes of the study area (Fig. 2) provided pronounced discrimination of ^{13}C in plant tissues during CO_2 fixation and caused the accumulation of ^{12}C in the SOM of taiga soils (Fig. 4). Low $\delta^{13}C$ values, both according to our data and according to (Andreeva et al. 2013) were found in the SOM on the northern slope of the Khamar-Daban ridge (Fig. 1, region 6) which is associated with favorable climatic conditions (Fig. 2), namely the combination of the highest precipitation and relatively high (for a given landscape belt and absolute heights) air temperatures.

Thus, the observed $\delta^{13}C$ variations reflected the impact of climatic factors on ^{13}C discrimination during the photosynthesis of C3 plants. Thus, the surface-soil $\delta^{13}C$ signatures in the study area were primarily dependent on the MAP ($r = 0.67$, $p < 0.0001$), and the dependency became a little stronger when only the vegetation season precipitation was considered ($r = 0.69$, $p < 0.0001$) (Fig. 7).

The pronounced response of regional soils to moisture conditions from the standpoint of the composition of stable carbon isotopes confirmed the point of view of previous authors (Koposov 1983; Kuzmin 1988) that one of the main predictors of soil and vegetation cover differentiation in the study area was the heterogeneous distribution of atmospheric precipitation. In addition, this response

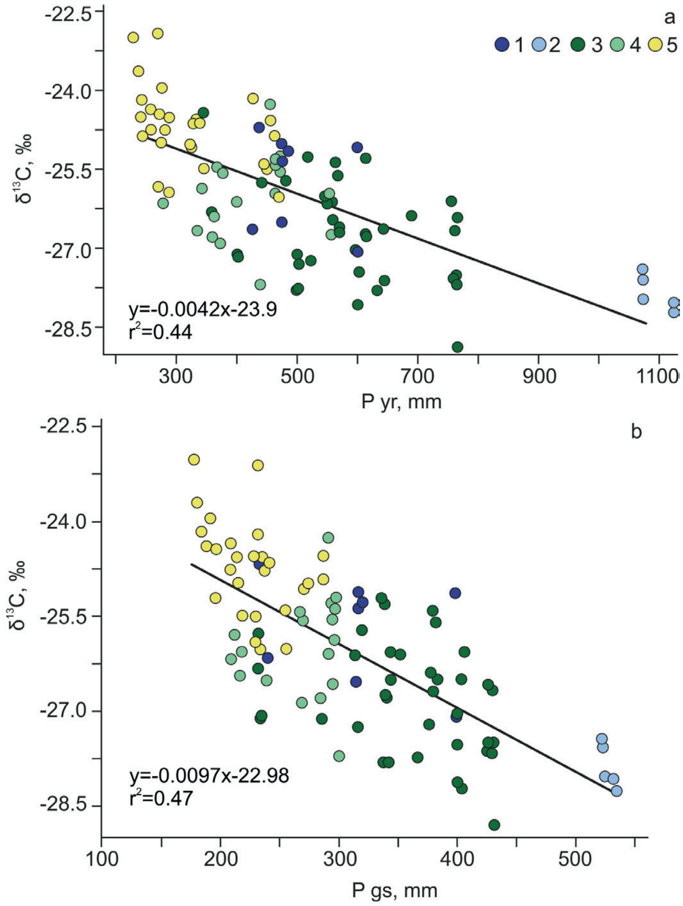

Fig. 7. Relationship between δ¹³C values of surface soils and mean annual precipitation (a) and mean precipitation of growing season (b). Landscapes: yellow – steppes; dark green – mountain taiga; light green – subtaiga; light blue – subalpine grasslands; dark blue – mountain tundra

agreed with global models (Kohn 2010), indicating that regions characterized by annual precipitation up to 800 mm (most of the soils we studied belong to this range) showed the greatest response to precipitation changes.

Linear regression analysis showed that MAP correlated with the soil $\delta^{13}C$ values in the Baikal region (Fig. 7, $p<0.05$) and the sensitivity of the $\delta^{13}C$ values response to MAP was –0.42 ‰/100 mm and to vegetation season precipitation was –0.97‰/100 mm. Such values indicated that the soils studied had a high sensitivity to changes in moisture conditions.

This relationship was comparable well with previous quantitative studies, which showed that the coefficient between soil $\delta^{13}C$ values and precipitation could be –1.16‰/100 mm in Mongolia (Feng et al. 2008) and varied from –0.3 to –0.8‰/100 mm in different regions of China (Zhang et al. 2020). In semiarid conditions in the northeastern part of China bordering the Transbaikal area, it was more pronounced in some places and amounts to –1.9‰/100 mm (Chen et al. 2015).

CONCLUSIONS

Variability of $\delta^{13}C$ in plants and surface soils was investigated in the Baikal region, which is strongly heterogeneous regarding physiographic conditions. The soil $\delta^{13}C$ varied by vegetation type and showed a high spatial diversity. At regional scale, the $\delta^{13}C$ values of modern plants and surface soils mainly responded to precipitation, with more negative values corresponding to greater precipitation.

Mean annual and mean growing season temperature were not significant factors to explain the spatial distribution of SOM $\delta^{13}C$ values at a regional scale. However, temperature was an essential plant growth-limiting factor that negatively affected soil microbial activity and C isotope discrimination in the unfavorable climatic conditions of mountain tundra (coldest) and steppe (warmest) landscapes. There was a powerful synergistic effect of temperature and precipitation in steppe landscapes where high temperature and water stress co-occurrences were found.

In fact, in some areas of the Baikal region, including mountain tundra and steppes, where extreme environmental conditions alternate throughout the year, biological activity was not especially favorable to SOM transformation. Under such conditions, the relative importance of abiotic constraints such as temperature and precipitation was critical for SOM formation.

REFERENCES

Abasheeva N.E. (1992). Agrochemistry of soils of Transbaikalia. Nowosibirsk: Nauka (in Russian).

Andreeva D.B., Balsanova L.D., Lavrent'eva I.N., Gonchikov B.N., Tsybikdorzhiev V.Ts., Glaser B. and Zech W. (2022). Variations in carbon and nitrogen isotopes in soils along the Barguzinsky Ridge, Eastern Baikal Region, Russia. Moscow Univ. Soil Sci. Bull, 77, 277–283, DOI: 10.3103/S0147687422040020.

Andreeva D., Zech M., Glaser B., Erbajeva M., Chimitdorgieva G., Ermakova O. and Zech W. (2013). Stable isotope ($\delta^{13}C$, $\delta^{15}N$, $\delta^{18}O$) record of soils in Buryatia, southern Siberia: Implications for biogeochemical and paleoclimatic interpretations. Quaternary International, 290–291, 82–94, DOI: 10.1016/j.quaint.2012.10.054.

Belov A.V., Bezrukova E.V. and Sokolova L.P. (2018). The evolutionary-genetic basis of structural-cenotic diversity of modern vegetation in Prebaikalia. Geography and Natural Resources, 39(1), 46–54, DOI: 10.1134/S1875372818010079.

Budyko M.I. (1971). Climate and life. Leningrad: Gidrometeoizdat (in Russian).

Byazrov L.G., Gongalsky K.B., Pelgunova L.A. and Tiunov A.V. (2010). Carbon isotope composition ($\delta^{13}C$) of lichen thalli in forests near the Chernobyl nuclear power plant. Radiation Biology. Radioecology, 50 (1), 98-105 (in Russian).

Cernusak L.A., Ubierna N., Winter K., Holtum J.A., Marshall J.D. and Farquhar G.D. (2013). Environmental and physiological determinants of carbon isotope discrimination in terrestrial plants. New Phytol, 200, 950–965, DOI: 10.1111/nph.12423.

Chen Y., Lu H., Zhang E., Zhang H., Xu Z., Yi S. and Wu S.-E. (2015). Test stable carbon isotopic composition of soil organic matters as a proxy indicator of past precipitation: Study of the and fields in northern China. Quaternary International, 372, 79–86, DOI: 10.1016/j.quaint.2014.10.062.

Chimitdorzhieva G.D. (2016). Organic matter of cold soils. Ulan-Ude: Buryat Scientific Centre SB RAS (in Russian).

Cornwell W.K., Wright I.J., Turner J., Maire V., Barbour M.M., Cernusak L.A., Dawson T., Ellsworth D., Farquhar G.D., Griffiths H., Keitel C., Knohl A., Reich P.B., Williams D.G., Bhaskar R., Cornelissen J.H.C., Richards A., Schmidt S., Valladares F., Körner C., Schulze E.-D., Buchmann N. and Santiago L.S. (2018). Climate and soils together regulate photosynthetic carbon isotope discrimination within C3 plants worldwide. Global Ecol. Biogeogr, 27, 1056-1067, DOI: 10.1111/geb.12764.

Dawson T.E., Mambelli S., Plamboeck A.H., Templer P.H. and Tu K.P. (2002). Stable isotopes in plant ecology. Annual Reviews of Ecology and Systematics, 33, 507–559, DOI: 10.1146/annurev.ecolsys.33.020602.095451.

Diefendorf A.F., Mueller K.E., Wing S.L., Koch P.L. and Freeman K.H. (2010). Global patterns in leaf ^{13}C discrimination and implications for studies of past and future climate. PNAS, 107, 5738–5743, DOI: 10.1073/pnas.0910513107.

Ehleringer J.R. (2005). The influence of atmospheric CO^2, temperature, and water on the abundance of C3/C4 taxa. In: I. Baldwin, ed., A history of atmospheric CO^2 and its effects on plants, animals and ecosystems. Ecological Studies. New York: Springer, 214-231, DOI: 10.1007/0-387-27048-5_10.

Farquhar G.D., Ehleringer J.R. and Hubick K.T. (1989). Carbon isotope discrimination and photosynthesis. Ann. Rev. Plant Physiol. Plant Molecul. Biol, 40, 503–537.

Feng Z.D., Wang L.X., Ji Y.H., Guo L.L., Lee X.Q. and Dworkin S.I. (2008). Climatic dependency of soil organic carbon isotopic composition along the S-N Transect from 34°N to 52°N in central-east Asia. Palaeogeography Palaeoclimatology Palaeoecology, 257, 335–343, DOI: 10.1016/j.palaeo.2007.10.026.

Fick S.E. and Hijmans R.J. (2017). WorldClim 2: New 1-km spatial resolution climate surfaces for global land areas. International Journal of Climatology, 37(2), DOI: 10.1002/joc.5086.

Golubtsov V.A. (2020). Stable carbon isotopic composition of organic matter of the Late Pleistocene and Holocene soils of the Baikal Region. Eurasian Soil Science, 53(6), 724-738, DOI: 10.1134/S1064229320060046.

Golubtsov V.A., Cherkashina A.A., Vanteeva Yu.V., Voropai N.N. and Turchinskaya S.M. (2023b). Variations in stable carbon isotopic composition of soil organic matter in mountain depressions of the Cis-Baikal region. Contemporary problems of ecology, 16(6), 776-789. DOI: 10.1134/S1995425523060094.

Golubtsov V.A., Vanteeva Yu.V., Bronnikova M.A., Cherkashina A.A. and Znamenskaya T.I. (2023a). Composition of stable carbon isotopes in organic matter of Cambisols of the Eastern Sayan foothills. Eurasian Soil Science, 56(2), 184-202, DOI: 10.1134/S1064229322602049.

Golubtsov V.A., Vanteeva Yu.V. and Voropay N.N. (2021). Effect of humidity on the stable carbon isotopic composition of soil organic matter in the Baikal region. Eurasian Soil Science, 54(10), 1463-1474, DOI: 10.1134/S1064229321100069.

Golubtsov V.A., Vanteeva Yu.V., Voropai N.N., Vasilenko O.V., Cherkashina A.A. and Zazovskaya E.P. (2022). Stable carbon isotopic composition ($\delta^{13}C$) as a proxy of organic matter dynamics in soils on the western shore of Lake Baikal. Eurasian Soil Science, 55(12), 1688-1701, DOI: 10.1134/S1064229322700041.

Hammer O., Harper D.A. and Ryan P.D. (2001). Past: Paleontological Statistics Software Package for Education and Data Analysis. Palaeontologia Electronica, 4(1), 4.

Highlands of the Fore-Baikal region and Transbaikalia (1974). Moscow: Nauka (in Russian).

IUSS Working Group WRB. World Reference Base for Soil Resources, 2015. International soil classification system for naming soils and creating legends for soil maps. World Soil Resources Reports. № 106. Rome.

Ivanova L.I., Ivanov L.A., Ronzhina D.A., Yudina P.K., Migalina S.V., Shinehuu T., Tserenkhand G., Voronin P.Yu., Anenkhonov O.A., Bazha S.N. and Gunin P.D. (2019). Leaf traits of C3- and C4-plants indicating climatic adaptation along latitudinal gradient in Southern Siberia and Mongolia. Flora, 254, 122-134, DOI: 10.1016/j.flora.2018.10.008.

Jia Y., Wang G., Tan Q. and Chen Z. (2016). Temperature exerts no influence on organic matter $\delta^{13}C$ of surface soil along the 400mm isopleth of mean annual precipitation in China. Biogeosciences, 13, 5057–5064, DOI: 10.5194/bg-13-5057-2016.

Kohn M.J. (2010). Carbon isotope compositions of terrestrial C3 plants as indicators of (paleo)ecology and (paleo)climate. PNAS, 107, 19691–19695, DOI: 10.1073/pnas.1004933107.

Koposov G.F. (1983). Genesis of mountain soils of Cisbaikalia. Nowosibirsk: Nauka (in Russian).

Kudeyarov V.N., Zavarzin G.A., Blagodatsky S.A., Borisov A.V., Voronin P.Yu., Demkin V.A., Demkina T.S., Evdokimov I.V., Zamolodchikov D.G., Karelin D.V., Komarov A.S., Kurganova I.N., Larionova A.A., Lopes de Gereny V.O., Utkin A.I. and Chertov O.G. (2007). Carbon pools and fluxes in terrestrial ecosystems of Russia. Moscow: Nauka (in Russian).

Kuz'min V.A. (1988). Soils of Cisbaikalia and Northern Transbaikalia. Nowosibirsk: Nauka (in Russian).

Kuznetsova A.O., Ivanova A.A., Slagoda E.A. and Tikhonravova Ya.V. (2020). Stable carbon isotopes in modern plants of the tracts of the key area of Marre-Sale (Western Yamal). Arctic and Antarctic, 1, 57-74, DOI: 10.7256/2453-8922.2020.1.32204 (in Russian).

Lee X., Feng Z., Guo L., Wang L., Jin L., Huang Y., Chopping M., Huang D., Jiang W., Jiang Q. and Cheng H. (2005). Carbon isotope of bulk organic matter: A proxy for precipitation in the arid and semiarid central East Asia. Global Biochem. Cycles, 19, GB4010, DOI: 10.1029/2004GB002303.

Mackay A.W., Seddon A., Leng M.J., Heumann G., Morley D.W., Piotrowska N., Rioual P., Roberts S. and Swann G. (2016). Holocene carbon dynamics at the forest–steppe ecotone of southern Siberia. Global Change Biology, 23(5), DOI: 10.1111/gcb.13583.

Menyailo O.V. and Hungate B.A. (2006). Carbon and nitrogen stable isotopes in forest soils of Siberia. Doklady Earth Sciences, 409(5), 747–749, DOI: 10.1134/S1028334X06050151.

Mikheev V.S. and Ryashin V.A. (1977). Landscapes of the south of Eastern Siberia. Moscow: GUGK (in Russian).

Muñoz Sabater J. (2019). ERA5-Land hourly data from 1981 to present. Copernicus Climate Change Service (C3S) Climate Data Store (CDS), DOI: 10.24381/cds.e2161bac.

O'Leary M.H. (1988). Carbon isotope in photosynthesis. Bioscience, 38, 328-336.

Pepin N.C. and Lundquist J.D. (2008). Temperature trends at high elevations: patterns across the globe. Geophys. Res. Lett, 35(14), L14701, DOI: 10.1029/2008GL034026.

Plateaus and lowlands of Eastern Siberia (1971). Moscow: Nauka (in Russian).

Plyusnin V.M., Bilichenko I.N. and Sedykh S.A. (2018). Spatio-temporal organization of mountain taiga geosystems of the Baikal natural territory. Geography and natural resources, 39, 130-139, DOI: 10.1134/S1875372818020051.

Rao Z., Guo W., Cao J., Shi F., Jiang H. and Li C. (2017). Relationship between the stable carbon isotopic composition of modern plants and surface soils and climate: A global review. Earth-Science Reviews, 165, 110–119, DOI: 10.1016/j.earscirev.2016.12.007.

Sage R.F. (2005). Atmospheric CO^2, environmental stress and the evolution of C4 photosynthesis. In: I. Baldwin, ed., A history of atmospheric CO^2 and its effects on plants, animals and ecosystems. Ecological Studies. 177. New York: Springer, 185-213, DOI: 10.1007/0-387-27048-5_9.

Schepaschenko D.G., Shvidenko A.Z., Mukhortova L.V. and Vedrova E.F. (2013). The pool of organic carbon in the soils of Russia. Eurasian Soil Science, 46(2), 107-116, DOI: 10.1134/S1064229313020129.

Scientific and applied handbook on the climate of the USSR (1989). Long-term data. Series 3. Part 1-6. Issue 23. Buryat ASSR, Chita region. Leningrad: Gidrometeoizdat (in Russian).

Scientific and applied handbook on the climate of the USSR (1991). Long-term data. Series 3. Part 1-6. Issue 22. Irkutsk region and western part of Buryat ASSR. Leningrad: Gidrometeoizdat (in Russian).

Shimaraev M.N., Kuimova K.N., Sinyukovich V.N. and Tsekhanovskii V.V. (2002). Manifestation of global climatic changes in Lake Baikal during the 20th century. Doklady Earth Sciences, 383(3), 288-291.

Tiunov A.V. (2007). Stable isotopes of carbon and nitrogen in soil ecological studies. Biology bulletin, 34 (4), 395-407. DOI: 10.1134/S1062359007040127.

Trofimova I.E., Osipova O.P. and Balybina A.A. (2019). Approaches to evaluating climate and ecological resources of Siberia. Contemporary problems of Ecology, 12(5), 444-452. DOI: 10.1134/S1995425519050111.

Tsybenov Y.B., Chimitdorzhieva G.D., Egorova R.A. and Gongal'skii K.B. (2016). The pool of organic carbon and its isotopic composition in cryomorphic quasi-gley chernozems of the Transbaikal region. Eurasian Soil Science, 49(1), 8-14, DOI: 10.1134/S106422931507011X.

Tsybenov Y.B., Chimitdorzhieva G.D., Egorova R.A. and Milkheev E.Yu. (2022). Isotope composition of carbon of plants and organic matter in Burozems of the southern Vitim Plateau. Moscow Univ. Soil Sci. Bull, 77, 266-270, DOI: 10.3103/S0147687422040135.

Volkovintser V.I. (1978). Steppe cryoaridic soils. Nowosibirsk: Nauka (in Russian).

Wang G.A., Li J.Z., Liu X.Z. and Li X.Y. (2013). Variations in carbon isotope ratios of plants across a temperature gradient along the 400 mm isoline of mean annual precipitation in north China and their relevance to paleovegetation reconstruction. Quaternary Science Reviews, 63, 83-90, DOI: 10.1016/j.quascirev.2012.12.004.

Xu M., Wang G., Li X., Cai X., Li X., Christie P. and Zhang J. (2015). The key factor limiting plant growth in cold and humid alpine areas also plays a dominant role in plant carbon isotope discrimination. Frontiers in Plant Science, 6, 961, DOI: 10.3389/fpls.2015.00961.

Zhang D., Yang Y. and Ran M. (2020). Variations of surface soil δ^{13}Corg in the different climatic regions of China and paleoclimatic implication. Quaternary International, 536, 92–102, DOI: 10.1016/j.quaint.2019.12.015.

Zhao Y., Wu F., Fang X. and Yang Y. (2017). Altitudinal variations in the bulk organic carbon isotopic composition of topsoil in the Qilian Mountains area, NE Tibetan Plateau, and its environmental significance. Quaternary International, 454, 45-55, DOI: 10.1016/ j.quaint.2017.08.045.

Zhukov V.M. (1965). Climate. In: I.P. Gerasimov, ed., Fore-Baikal region and Transbaikalia. Moscow: Nauka, 91-127 (in Russian).

APPENDICES

Table A. General information of the sampling sites and stable carbon isotopic composition ($\delta^{13}C$) of surface soil horizons

№	Section	Area	Coordinates	Lanscape	Soil type	Elevation, m	MAT, °C	Tgs, °C	MAP, mm	Pgs, mm	TOC, %	$\delta^{13}C$, ‰
1	Nizhniy Bulay-2-20	1	N 52°51'34.73" E 103°06'47.31"	subtaiga	Luvic Phaeozem	492	0.2	17.6	481	298	6.74	-25.52
2	Nizhniy Bulay-2-18		N 52°51'34.0" E 103°06'46.7"	subtaiga	Luvic Phaeozem	482	0.2	17.6	481	298	2.19	-25.25
3	Buret'		N 52°58'25.82" E 103°28'15.32"	subtaiga	Luvic Phaeozem	403	0.2	17.9	465	298	3.39	-24.15
4	Berezovyi		N 52°51'48.44" E 103°21'28.14"	subtaiga	Luvic Phaeozem	417	0.0	17.9	470	298	2.77	-25.85
5	Mikhailovka		N 52°59'25.9" E 103°18'01.8"	steppe	Luvic Chernozem	532	0.1	17.8	445	253	4.17	-25.45
6	Fedyaevskyi		N 53°15'41.7" E 103°21'54.1"	steppe	Calcic Chernozem	479	0.3	17.8	446	235	4.90	-25.50
7	Osinovyi-20		N 52°53'07.55" E 103°19'12.15"	subtaiga	Luvic Phaeozem	473	-0.4	17.8	474	298	2.89	-25.43
8	Osinovyi_18		N 52°53'05.6" E 103°19'12.2"	subtaiga	Cambic Calcisol (Loamic)	462	-0.4	17.8	474	298	2.36	-25.31
9	Taiturka-1		N 52°52'29.97" E 103°28'12.55"	steppe	Luvic Chernozem	429	0.4	18.0	467	290	4.11	-24.51
10	Taiturka-2		N 52°52'57.01" E 103°25'01.88"	steppe	Luvic Chernozem	436	0.4	18.0	470	290	5.30	-24.82
11	Belaya		N 52°50'06.8" E 103°20'31.8"	steppe	Pantofluvic Fluvisol (Arenic)	404	0.0	17.7	476	254	3.38	-25.98
12	Lastochkino Gnezdo-2		N 52°48'18.9" E 104°47'12.2"	steppe	Calcic Chernozem	514	0.1	17.2	418	236	5.56	-24.19
13	Onot-1	2	N 52°37'45.75" E 102°03'01.75"	mountain taiga	Folic Spodic Cambisol	1232	-2.6	14.5	769	403	13.78	-26.06
14	Onot-2		N 52°42'24.35" E 101°55'55.92"	mountain taiga	Sceletic Cambisol	1001	-1.8	14.6	771	402	7.67	-26.31
15	Yulinsk-1		N 52°41'44.0" E 102°21'22.7"	mountain taiga	Mollic Phaeozem	511	-1.0	16.3	608	340	3.66	-26.79
16	Yulinsk-3		N 52°42'34.5" E 102°23'01.3"	mountain taiga	Mollic Leptosol	591	-1.2	16.3	608	340	10.50	-26.81
17	Yulinsk-4		N 52°42'17.2" E 102°22'53.5"	mountain taiga	Leptic Luvisol	687	-1.3	16.3	608	340	2.72	-25.23
18	K1/20		N52°19'58.30" E102°51'17.98"	mountain taiga	Folic Cambisol	740	-0.7	15.4	692	375	10.86	-26.34
19	K3/20		N 52°28'14.34" E 103°06'50.92"	mountain taiga	Leptic Luvisol	722	-0.6	16.7	556	344	5.37	-26.43
20	Kitoy-2019		N 52°28'14.8" E 103°06'43.3"	mountain taiga	Leptic Luvisol	712	-0.6	16.7	556	344	5.81	-26.01
21	Mezhdurech'e		N 52°51'28.0" E 102°28'52.1"	mountain taiga	Leptic Luvisol	536	-1.2	17.1	509	339	3.63	-25.37
22	Novostroyka-1		N 52°57'33.0" E 101°47'38.3"	mountain taiga	Phaeozem	614	-1.8	15.8	632	425	6.59	-27.60
23	Novostroyka-2		N 52°57'30.55" E 101°47'36.90"	mountain taiga	Phaeozem	609	-1.8	15.8	632	425	3.25	-26.49
24	Bol'shaya Belaya		N 52°54'51.7" E 102°31'46.3"	mountain taiga	Cambic Phaeozem over Fluvisol	464	-1.0	17.1	509	364	11.13	-27.17

25	Irkut-2		N 52°08'48.3" E 103°53'47.1"	mountain taiga	Fluvisol	461	0.5	16.4	616	343	4.75	-27.76
26	2K/21		N 52°11'02.50" E 102°41'29.62"	mountain taiga	Folic Leptic Cambisol	841	-1.5	14.7	771	429	10.66	-27.47
27	4K/21		N 52°10'00.01" E 102°42'29.50"	mountain taiga	Folic Fluvisol (Arenic)	728	-1.1	14.7	771	429	3.23	-26.52
28	5K/21	2	N 52°09'53.90" E 102°41'58.70"	mountain taiga	Folic Cambisol	738	-1.1	14.7	771	429	10.34	-27.47
29	6K/21		N 52°10'34.21" E 102°41'28.30"	mountain taiga	Folic Cambisol	877	-1.4	14.7	771	429	8.65	-27.68
30	7K/21		N 52°19'34.32" E 102°50'59.60"	mountain taiga	Folic Fluvisol (Arenic)	629	-0.7	15.2	770	430	15.75	-29.50
31	12K/21		N 52°25'36.91" E 103°12'39.50"	mountain taiga	Folic Phaeozem over Fluvisol	520	-0.1	16.6	560	297	8.26	-26.51
32	C1		N 53°07'03.83" E 106°41'22.33"	mountain tundra	Folic Cryosol	1654	-4.6	7.9	429	235	32.08	-24.72
33	C2		N 53°07'09.20" E 106°42'49.00"	mountain taiga	Entic Folic Podzol (Differentic)	1414	-4.1	10.0	429	235	16.53	-25.61
34	C3		N 53°07'09.89" E 106°45'02.47"	mountain taiga	Entic Folic Podzol	1125	-3.2	10.5	400	235	12.29	-27.14
35	C5		N 53°06'17.60" E 106°46'21.08"	mountain taiga	Entic Folic Leptosol	910	-2.8	11.3	400	235	13.52	-27.18
36	C6		N 53°05'51.49" E 106°47'04.19"	subtaiga	Folic Leptosol	810	-2.0	13.1	400	216	12.71	-26.05
37	C8		N 53°05'32.02" E 106°48'02.94"	subtaiga	Calcaric Skeletic Phaeozem	600	-1.4	15.5	280	206	8.12	-26.22
38	C9		N 53°05'19.02" E 106°48'51.51"	steppe	Calcaric Mollic Leptosol	460	-1.0	13.4	290	215	12.69	-24.55
39	Ch1	3	N 52°58'07.43" E 106°48'37.26"	subtaiga	Folic Phaeozem over Skeletic Phaeozem	915	-1.6	12.5	340	216	28.51	-25.85
40	Ch2		N 53°02'23.82" E 106°40'10.74"	mountain taiga	Folic Phaeozem	1160	-1.8	10.9	364	235	40.49	-26.38
41	Ch3		N 53°01'07.74" E 106°40'44.10"	subtaiga	Hyperskeletic Leptosol	701	-2.8	14.8	360	216	8.50	-26.29
42	Sarma-1		N 53°06'32.0" E 106°48'52.90"	steppe	Sceletic Cambisol Protocalcic	626	-1.9	15.5	260	206	3.56	-24.75
43	Horga		N 53°04'32.80" E 106°47'29.70"	steppe	Cambic Skeletic Leptosol	564	-1.3	15.0	260	206	1.93	-24.34
44	Anga		N 52°47'31.70" E 106°34'10.80"	steppe	Calcaric Cambisol	570	-0.6	15.5	241	190	6.52	-24.42
45	Krestovyi		N 52°40'49.40" E 106°23'55.20"	steppe	Calcic Chernozem (Tonguic)	627	-0.5	13.3	280	190	3.33	-23.97
46	Trekhgolovyi		N 53°18'06.60" E 107°06'49.80"	mountain tundra	Lithic Skeletic Leptosol	1225	-3.7	8.3	407	235	5.50	-26.52
47	293	4	N 51°44'24.8" E 102°35'17.3"	subtaiga	Vitric Anthroumbric Leptic Entic Podzol (Loamic, Aric, Endoeutric)	763	-1.0	14.8	385	265	3.30	-25.47
48	357		N 51°40'54.95" E 102°13'42.11"	mountain taiga	Someriumbric Entic Podzols(Arenic, Albic)	744	-0.6	13.5	500	280	8.30	-27.12

49	Haribyaty	4	N 51°38'56.55" E 102°16'06.10"	mountain taiga	Someriumbric Entic Podzol (Arenic, Albic)	785	-1.4	13.3	500	320	15.60	-27.22
50	278		N 51°42'14.20" E 102°24'44.60"	steppe	Hypocalcic Chernozem (Arenic, Aric)	723	0.9	14.6	330	216	5.00	-25.50
51	Zaktui		N 51°41'19.60" E 102°40'52.39"	mountain taiga	Umbrisols (Siltic, Hyperdystric)	918	0.2	13.5	500	340	6.20	-27.79
52	501/1		N 51°44'22.25" E 102°19'44.40"	subtaiga	Entic Podzol (Arenic, Endoeutric)	764	-0.5	13.4	420	300	27.10	-27.74
53	185/1		N 51°49'24.63" E 102°29'18.85"	subtaiga	Vitric Skeletic Folic Leptic Entic Podzol (Loamic, Endoeutric)	773	0.4	13.8	380	265	8.10	-25.54
54	179		N 51°43'10.1" E 102°35'18.5"	subtaiga	Entic Podzol (Arenic, Endoeutric)	739	-0.4	13.6	385	365	7.00	-26.93
55	110		N 51°56'43.8" E 102°26'25.29"	mountain tundra	Hypereutric Somerimollic Orthoskeletic Leptosol	2063	-4.7	7.6	600	400	15.80	-24.91
56	113		N 51°56'31.77" E 102°26'25.04"	mountain tundra	Folic Sombric Leptosol (Protospodic)	1932	-4.0	8.6	600	400	9.30	-27.06
57	114		N 51°56'16.69" E 102°26'24.58"	mountain taiga	Skeletic Folic Leptic Entic Podzol	1712	-4.0	10.1	600	400	14.50	-27.02
58	114/1		N 51°56'06.27" E 102°26'15.86"	mountain taiga	Hypereutric Somerimollic Folic Skeletic Leptosol	1493	-4.0	11.1	600	400	39.10	-28.19
59	115/1		N 51°55'42.18" E 102°26'11.41"	mountain taiga	Somerirendzic Folic Skeletic Leptosol	1255	-3.0	12.0	600	400	48.00	-27.49
60	Turan		N 51°38'24.37" E 101°38'44.55"	mountain taiga	Histic Stagnic Eutric Gleysol (Arenic)	882	-1.5	13.1	500	360	29.36	-27.75
61	Mondy-1	5	N 51°41'10.42" E 100°55'45.10"	steppe	Cambic Leptic Calcisol	1399	-1.0	10.2	280	195	7.35	-25.14
62	Mondy-2		N 51°39'59.81" E 100°57'01.70"	subtaiga	Cambic Leptic Calcisol	1373	0.0	10.8	360	280	27.20	-26.84
63	Mondy-3		N 51°37'21.47" E 100°55'20.89"	mountain tundra	Folic Lithic Leptosol	1987	-3.5	8.1	490	311	47.16	-26.40
64	Mondy-4		N 51°39'27.05" E 100°54'38.97"	mountain taiga	Folic Albic Leptic Podzol	1672	-1.2	10.0	549	310	7.71	-26.17
65	98 p.		N 51°43'59.67" E 101°00'15.27"	mountain tundra	Umbric Leptosol	2315	-3.5	7.1	489	311	6.07	-24.98
66	99 p.		N 51°43'29.57" E 101°00'12.82"	mountain tundra	Umbric Leptosol	2156	-2.7	7.7	489	311	6.65	-25.39
67	100 p.		N 51°43'24.6" E 101°0'4.32"	mountain taiga	Cambic Leptosol	2078	-3.1	7.5	585	380	5.44	-26.46
68	101 p.		N 51°43'7.25" E 100°59'51.72"	mountain taiga	Umbric Leptosol	1932	-2.4	8.3	585	380	25.13	-25.59
69	102 p.		N 51°42'23.08" E 101°0'5.26"	mountain taiga	Histic Cryosol	1687	-3.4	9.4	585	380	30.20	-25.42
70	103 p.		N 51°37'21.68" E 100°55'20.03"	mountain tundra	Histic Eutric Turbic Cryosol	1990	-3.5	8.1	490	311	44.24	-25.35
71	104 p.		N 51°37'48.39" E 100°53'19.90"	mountain taiga	Histic Cryosol	1874	-2.8	8.5	490	311	42.15	-25.68

72	41 p.	5	N 51°42'21.60" E 101°00'5.06"	mountain taiga	Histic Cryosol	1996	-3.4	9.4	585	380	29.81	-26.65
73	43 p.		N 51°39'25.78" E 100°54'39.28"	mountain taiga	Eutric Leptosol	1627	-1.2	10.0	550	353	6.29	-26.10
74	506 (M1.1)	6	N 51°23'36.96" E 104°50'35.34"	subalpine grassland	Folic Umbrisol (Hyperdystric)	950	-1.6	14.7	1082	520	3.14	-27.65
75	507 (M1.2)		N 51°24'38.10" E 104°50'43.98"	mountain taiga	Folic Umbrisol (Hyperdystric)	1050	-1.8	14.7	1082	520	4.99	-27.92
76	508 (M1.3)		N 51°23'28.38" E 104°50'45.18"	subalpine grassland	Haplic Umbrisol (Hyperdystric)	950	-1.9	14.7	1082	520	7.59	-27.45
77	509 (M2.4)		N 51°22'52.44" E 104°51'31.56"	subalpine grassland	Cambic Umbrisol (Hyperdystric)	1200	-2.2	14.0	1120	532	11.53	-28.13
78	510 (M 2.5)		N 51°22'45.00" E 104°51'27.48"	subalpine grassland	Haplic Umbrisol (Hyperdystric)	1200	-2.1	14.0	1120	532	9.02	-28.01
79	2-Z-18	7	N 51°31'55.3" E 107°06'14.8"	steppe	Skeletic Cambic Leptic Calcisol Turbic	633	-0.5	17.9	224	177	0.85	-23.01
80	5-Z-18		N 50°38'02.8" E 105°23'09.1"	steppe	Skeletic Cambic Leptic Calcisol Hypercalcic Yermic	787	-0.9	17.3	293	239	5.65	-26.09
81	9-Z-18		N 50°36'21.1" E 105°25'52.3"	steppe	Skeletic Cambic Leptic Calcisol	691	-1.1	17.3	278	234	5.63	-25.90
82	11-Z-18		N 50°43'35.4" E 105°54'15.7"	steppe	Skeletic Cambic Leptic Calcisol Hypercalcic Yermic	861	-0.5	18.0	244	212	4.10	-24.82
83	1-Z-21		N 50°35'25.4" E 105°26'56.4"	subtaiga	Cambic Leptic Calcisol	729	-1.3	17.3	319	239	6.31	-26.58
84	1-Z-21 ovrag		N 50°35'31.70" E 105°26'51.70"	steppe	Cambic Leptic Calcisol	701	-1.2	17.3	293	239	1.56	-24.75
85	2-Z-21		N 50°58'30.6" E 106°05'03.8"	steppe	Luvic Chernozem	774	-0.6	18.1	224	177	5.57	-23.61
86	3-Z-21		N 50°58'45.1" E 106°04'11.1"	mountain taiga	Folic Albic Leptic Podzol	817	-0.6	18.1	325	176	7.62	-24.59
87	4-Z-21		N51°35'39.70" E107°03'17.94"	steppe	Cambic Leptic Calcisol	701	-1.2	17.6	278	198	1.40	-24.32
88	B.Kunaley-1		N 51°25'30.89" E 107°34'30.00"	steppe	Luvic Chernozem	735	-1.7	14.6	315	230	5.15	-24.49
89	B.Kunaley-2		N 51°25'6.61" E 107°36'11.97"	steppe	Luvic Chernozem	724	-1.7	16.9	315	230	1.51	-24.50
90	Khorinsk		N 52°13'41.98" E 109°49'51.16"	steppe	Cambic Leptic Calcisol	715	-1.9	14.0	236	187	0.83	-24.17
91	Pesterevo		N 51°30'41.5" E 107°29'16.7"	steppe	Calcic Chernozem	606	-1.7	14.6	315	230	0.64	-24.60
92	Ust'-Menza-1	8	N 50°13'28.90" E 108°37'33.10"	subtaiga	Fluvisol	734	-1.7	15.7	551	291	2.91	-26.03
93	16-Z-18	9	N 50°50'01.0" E 116°19'36.2"	steppe	Luvic Chernozem	679	0.2	18.2	312	261	4.27	-24.92
94	17-Z-18		N 50°10'36.5" E 116°17'26.7"	steppe	Leptic Chernozem	723	0.1	18.7	312	263	2.90	-24.84
95	19-Z-18		N 50°07'21.8" E 115°58'43.4"	steppe	Leptic Chernozem	650	0.5	19.0	283	238	2.61	-22.98

Note: MAT – mean annual air temperature, Tgs – mean air temperature of vegetation season, MAP – mean annual precipitation, Pgs - mean precipitation of vegetation season, TOC – total organic carbon

RESEARCH PAPER

INCIDENCE OF FORCING FACTORS ON LAND COVERS OF THE GUACHENEQUE PARAMO, COLOMBIA

Yulia Ivanova[1*], David H. Arenas, Julian G. Castellanos
[1] Universidad Militar Nueva Granada, Faculty Engineering, Cra. 11 # 101-80, Bogotá, 110221, Colombia
***Corresponding author:** yulia.ivanova@unimilitar.edu.co
Received: December 7th, 2023/ Accepted: May 29th 2024 / Published: July 1st 2024
https://DOI-10.24057/2071-9388-2024-3145

ABSTRACT. Paramo ecosystems are unique and are located in Ecuador, Colombia, and Venezuela. Although the Colombian government has made efforts for their preservation and sustainable use, several of the national paramos have experienced a change in their land cover as a result of climate variability, climate change, and the expansion of the agricultural and livestock frontiers. Changes in land cover can affect ecosystem integrity and its environmental services. Taking into account the regional importance of the Guachaneque paramo, it was analyzed whether its vegetation cover experiences any significant changes. This study was carried out by combining multi – temporal analysis of vegetation cover with climatic and statistical analyses. It was found that most land covers present a change mostly associated with human interventions (0.77–0.91). Climate variability and climate change also affect the landscape, but to a lesser extent (0.09–0.23). Water availability directly affects the expansion of all land covers, except paramo grassland, which indicates that an increase in rainfall associated with climate change will cause a contraction of this land cover. Currently, it is identified that anthropogenic pasture and crop surfaces replace the paramo grassland covers with an approximate change of 28.5 hectares per year. These results alert us to the need for monitoring and controlling the development of livestock and agricultural activities in order to preserve the integrity of the paramo landscape.

KEYWORDS: paramo, human activity, climate variability, water availability, Colombia

CITATION: Ivanova Y., Arenas D. H., Castellanos J. G. (2024). Incidence Of Forcing Factors On Land Covers Of The Guacheneque Paramo, Colombia. Geography, Environment, Sustainability, 2(17), 94-105
https://DOI-10.24057/2071-9388-2024-3145

ACKNOWLEDGEMENTS: The authors would like to thank the Universidad Militar Nueva Granada of Colombia for supporting the research project identified with the code INV - ING – 3790.

Conflict of interests: The authors reported no potential conflict of interest.

INTRODUCTION

Paramo ecosystem can be considered unique in the world both for their location and for the range of ecosystem services they support. According to recent statistics, 43% of the paramo area belongs to Colombia and this percentage is only surpassed by the 47% of the paramo area of Ecuador (Peyre et al. 2021). In relation to the distribution of paramo in the national territory, 24% of paramo areas in Colombia are found in the department of Boyacá[1] and, given their importance, in recent years these ecosystems have been prioritized for conservation and sustainable use.

However, the paramo provide different processes of anthropic pressure (Rey-Romero, Domínguez, and Oviedo-Ocaña 2022), (Etter et al. 2006), climate variability and climate change (Diazgranados et al. 2021) that can affect the ecological integrity of these. Often, evaluating these effects is not easy due to the lack of monitoring systems in high mountains. Knowing that some paramo present alterations due to different forcing factors, different actors have investigated the alteration of water supply (Cresso et al. 2020) and its quality (Rey-Romero et al. 2022), vegetation cover (Ross, Fildes, and Millington 2017), soil characteristics (Lis-Gutiérrez, Rubiano-Sanabria, and Usuga 2019), among others.

In Colombia, academic research is complemented by institutional initiatives that are responsible for delimiting and characterizing (IAvH 2013), generating mechanisms for its protection, conservation and sustainable management[2], (MADS 1993)[3,4]. The Regional Autonomous Corporations – CAR in Colombia is responsible for complying with the management of the territory under their jurisdiction, promoting its sustainable development. Thus, in 2016, one of the strategic paramo of the Departments of

[1] SIRAP. (2022, noviembre 25). Sistema regional de áreas protegidas. Retrieved from https://www.corpoboyaca.gov.co/sirap/areas-protegidas/paramos/ecosistemas-estrategicos/
[2] Presidencia de la República. (1974). Decreto 2811 de 1974. Retrieved from https://www.funcionpublica.gov.co/eva/gestornormativo/norma.php?i=86901/
[3] PND. (2023, February 28). National Development Plan 2021-2026. Retrieved from https://www.dnp.gov.co/Paginas/plan-nacional-de-desarrollo-2023-2026.aspx
[4] Presidencia de la República. (2018, Junio 14). Decreto 1008 de 2018. Retrieved from https://www.funcionpublica.gov.co/eva/gestornormativo/norma.php?i=86902

Cundinamarca and Boyacá[5], which is the Guacheneque paramo, was delimited, its conservation and preservation areas were established (Corpoboyacá 2016) are formulated its Environmental Management Plan (Corpochivor and IAvH 2018).

Although the actions mentioned above have managed to characterize different environmental and socio-economic aspects to the paramo, the ecosystem is exposed to the effects of climate variability, global climate change and some anthropogenic interventions (Fonseca 2022) that can impact the integrity of the paramo. The study uses the theory that anthropogenic activity (deforestation and agriculture) together with the effects of climate variability produce a transformation of vegetation cover – an effect hitherto unknown due to the absence of the monitoring system in the paramo. For this reason, the study will analyze the effect of these two forcing forces on the dynamics of plant cover and evaluate their impact on water availability.

METHODOLOGY

The Guacheneque paramo is located in the Eastern mountain range of Colombia (Fig. 1), between the departments of Cundinamarca and Boyacá and belongs to the municipalities of Villa Pinzon, Lenguazaque and Guachetá (Cundinamarca) and the municipalities of Ventaquemada, Samacá and Ráquira (department of Boyacá) (IAvH 2020).

The main importance of the paramo lies in its ecosystem services of water provision and regulation because different water currents arise in its territory. Among the main ones we can mention Guacheneque, Teatinos, Chital, Mojica, Honda and Chital streams (Fig. 1). The waters of the Guacheneque river are regulated by the two reservoirs with the same name and are used for irrigation districts for agricultural and mining production (Beltran 2018). The Teatinos river basin pours its waters into the reservoir named with the same name. The water regime of this stream drops significantly during the dry season, causing water scarcity for existing demands (Cr Sib 2018). This basin supplies the city of Tunja. The tributaries of the Honda and Mojica streams, located in the southern and southern western part of the paramo, pour their waters into the Fúquene lagoon, which is an important source of supply for agricultural and livestock activities (Blanco Garrido et al. 2020). The Chital stream, like other water sources in the paramo, is used for different rural aqueducts to supply domestic water needs. The paramo nourishes with its waters the La Esmeralda reservoir of the Chivor hydroelectric plant, which has national importance, since it produces about 6% of the country's energy (Caracol Radio 2022). In the territory of the paramo there are 47 wetlands that cover an approximate area of the 1,390 hectares (IAvH 2013). The waters forms the paramo basins irrigate approximately 1,000,000 hectares and supply water to nearly 300,000 inhabitants.

In addition to providing ecosystem services related to hydrology, watersheds in the paramos support biodiversity. For example, the flora in the paramo is represented by 155 genera and 61 families. The main types of vegetation are rosettes, grassland, moor meadows, cormophyte vegetation and frail Jones *Espeletia argentea*. The fauna population is scarce given the anthropogenic influence generated by the loss of fauna biodiversity. The least affected are the species of birds where 57 species were found. The river courses allow the presence of more than 13 species of frogs (IAvH 2013).

However, despite the conservation and protection actions carried out in recent decades, the paramo is under the influence of anthropogenic activities such as temporary agriculture and deforestation in the western and south – Eastern fringes. These activities, together with the effects of climate variability and global climate change, until now unknown, generate an impact on the vegetal cover of the paramo that can affect its ecosystem integrality. For this reason, in this research, climate studies are combined with

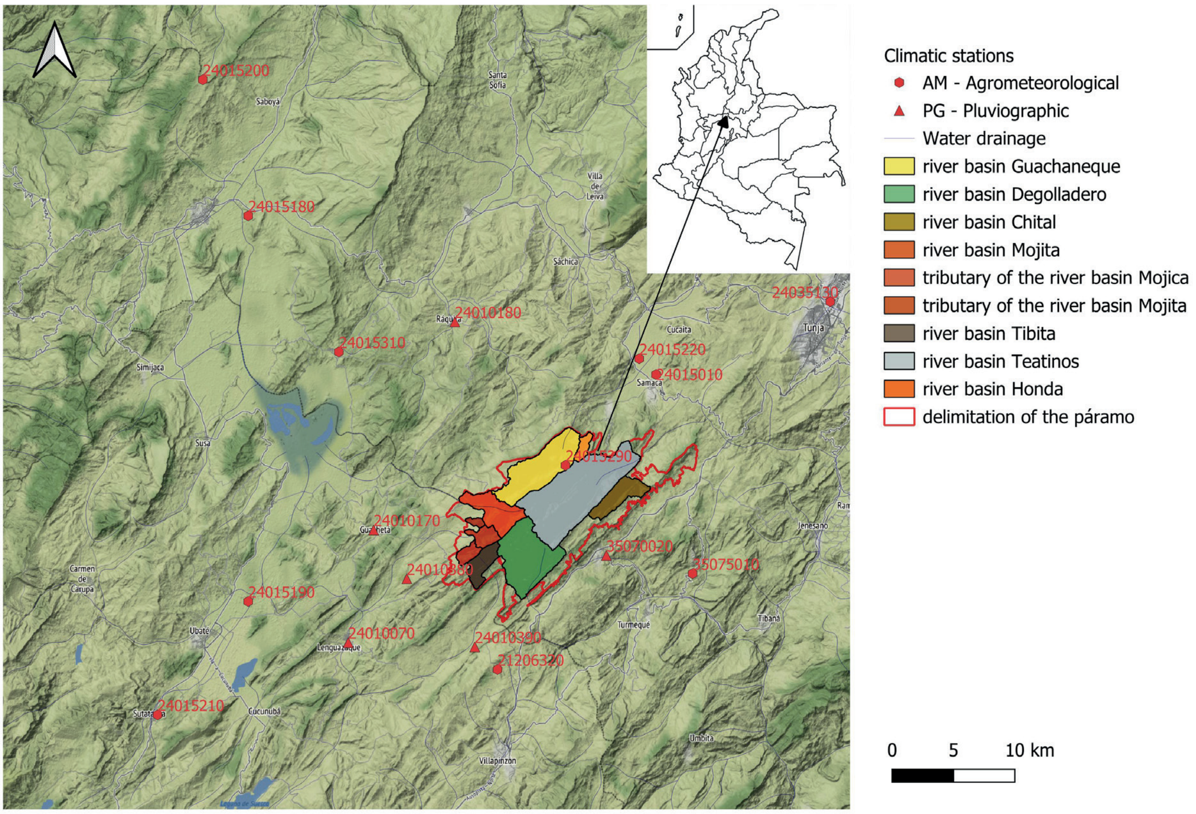

Fig. 1. Location of the paramo Guacheneque with its main hydrographic basins and meteorological stations

[5] MADS. (2016, Octubre 28). Resolución 1768. Retrieved from https://www.andi.com.co/Uploads/resolucion-1768-de-2016.pdf

remote sensing procedures in order to conclude whether significant changes in land cover occur in the paramo – a product of climate change and anthropogenic activities.

Understanding these dynamics makes it possible to evaluate the dynamics of land covers and generate proposals for their conservation.

The description of the methodology is presented below, and the flow diagram is presented in Fig. 2. The methodological steps were divided into three blocks, differentiated in the figure by color. The green color corresponds to the achievement of the inputs; the purple color – to the methodological development; and, finally, the yellow color – to the construction of the results and conclusions of the research.

The achievement of inputs is part of the first stage of the methodological framework. These can be divided into two large blocks: climatological and geospatial information. Among the climatic information are records of precipitation and average temperatures from the Institute of Hydrology, Meteorology and Environmental Studies (IDEAM, 2023) and the Regional Autonomous Corporation of Cundinamarca (CAR, 2023) and the geospatial information includes the land coverage map of the Earth at a scale 1:100,000 (IDEAM, 2021), which guides in the interpretation of satellite images, and the set of the Landsat satellite images, available on the United States Geological Survey website[6].

After collecting the inputs, we proceed to the methodological development that includes climate analysis (second stage), study of land covers (third stage) and, finally, integration of the two previous analyses in order to identify if the effects of climate variability, climate change, and anthropogenic activities can be considered as forcing factors in the change of land cover in the paramo (fourth stage).

The first step of the second stage consists of complementing the historical series of total monthly rainfall and average monthly temperatures. This procedure is done through regression analysis with the precipitation and temperature stations whose records are complete and present a statistically valid correlation with the station whose records are intended to be complemented (Rodríguez Morilla 2000). By complementing the series, the values of total annual temperature are calculated, considering the time scale of the analysis.

The trend analysis is carried out in the series of total annual rainfall and average annual temperatures through the Mann–Kendall test with the significance level of 0.05 (Mann Kendall 1938). The appearance of the statistically significant trend in the hydrometeorological series is normally associated with the incidence of global climate chang (Shi and Touge 2023), (Bayer-Altın 2023). The equations of the Mann–Kendall test is listed below (1-2):

$$S = \sum_{k-1}^{n_1-1} \sum_{j-k+1}^{n} sng\left(x_j - x_k\right) \tag{1}$$

$$sng\,(x) = \begin{cases} +1, x > 0 \\ 0, x = 0 \\ -1, x < 0 \end{cases} \tag{2}$$

where: x_j are the data of the analyzed climatic variables, sequence of values, n – time series size. The value of zero is assigned when $(x_j\text{-}x_k)=0$, -1 when $(x_j\text{-}x_k)>0$, and, finally, 1 when $(x_j\text{-}x_k)<0$. The null hypothesis is that the data has no trend. In this case, the value of S must have a normal distribution with zero mean and variance equal to $Var(S)=[n(n-1)(2n+5)]/18$. The result of S different from zero indicates some type of trend. The significance of the trend is evaluated through the Z statistic that is expressed through the following Eq. (3):

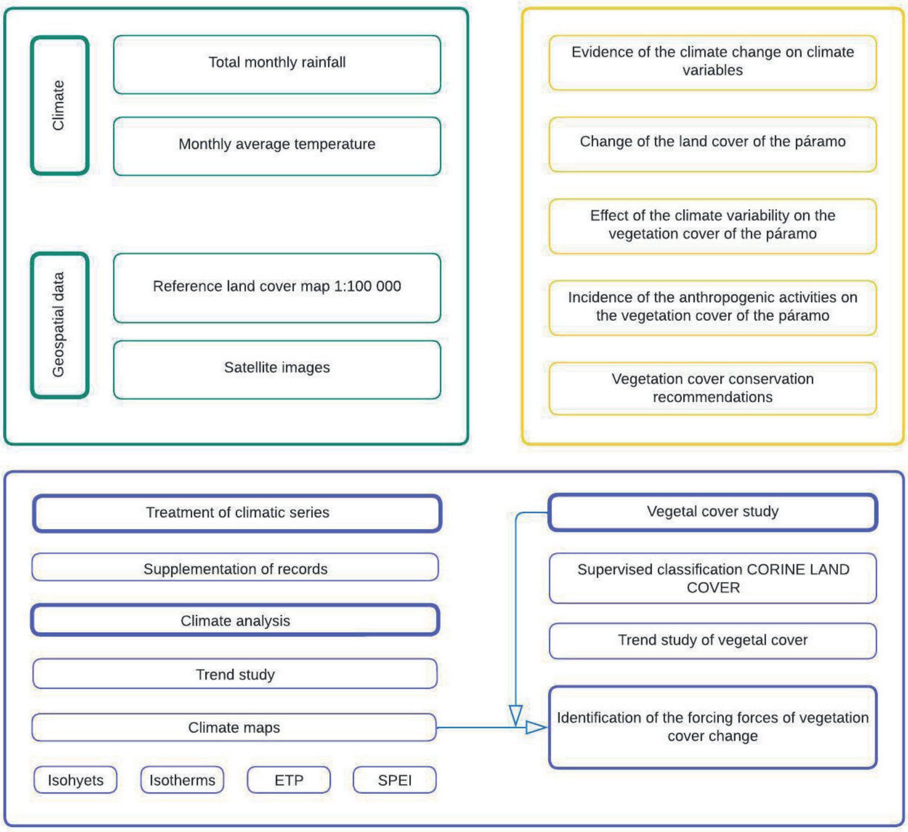

Fig. 2. Methodological steps to evaluate the incidence of forcing forces on the vegetation cover of the paramo

[6] USGS. (2023, Junio 4). Earth Explorer. Retrieved from https://earthexplorer.usgs.gov/

$$Z = \begin{cases} \dfrac{S-1}{\sqrt{Var(S)}} when\ S>0 \\ 0,\ when\ S=0 \\ \dfrac{S+1}{\sqrt{Var(S)}} when\ S<0 \end{cases} \quad (3)$$

The Z value indicates both the sign and significance of the trend. The positive value of Z statistic indicates an increasing trend and negative values – a decreasing trend. The significance of the trend is evaluated through the critical value, which for the significance level of 0.05 is 1.96. This, if the calculated value of the test is less than -1.96, the trend is significant negative and if it is greater than 1.96 if is significant positive. Z value in the range if -1.96 to 1.96 indicate a statistically non–significant trend (Mann Kendall 1945). The results of the Mann–Kendall test allow us to conclude whether the hydrometeorological series are under the influence of global climate change (Buyukyildiz 2023), (Sang et al. 2023).

The next step of the second stage consists of calculating the potential evapotranspiration – PET through the Turc method (Hurtado, Cadena, and IDEAM 2018).

The availability of historical records of average temperatures, total annual precipitation and PET makes it possible to construct annual maps of isotherms, isohyets and PET. Through the isohyet and PET maps, the SPEI index maps are constructed, which represents the relationship between precipitation and PET on an annual scale. This can be considered done of the indicators of water availability that are used in areas where there are no hydrological measurements (Ankrah, Monteiro, and Madureira 2023), (Nejadrekabi, Eslamian, and Zareian 2022). Thus, if the index values are greater than 1 (Shrivastava et al. 2022), there are surpluses of water resources, while these are less than one, the analyzed territory faces a water deficit. Specifically, the SPEI index ranges are as follows (Table 1):

Through the SPEI maps, built for the entire analysis period, the spatial-temporal variability of water availability can be identified.

The third methodological stage consists of studies of the vegetation cover in the paramo, which is carried out for the same period of observation of the climatic stations with the annual scale. For this purpose, temporal composites of medians for four consecutive years are generated from Landsat images using the GEE platform (Google Earth Engine 2023). The creation of these compositions is justified because the paramo is located under the passage of the Intertropical Confluence Zone (ITCZ) (Peréz Rendon, Ramírez Builes, and Peña Quiñones 2016), which generates high cloudiness that complicates the achievement of satellite images for each year of the study period. By making compositions of medians of the four consecutive years, the creation of a composite image for each period is achieved, practically without clouds. Additionally, the annual dynamics of vegetation cover may not be representative for this time scale because they would not be able to identify significant changes in these (González-M. et al. 2019), while the composition of the four – year images allow demonstrate this change.

To facilitate the interpretation of land cover, the vegetation cover maps of (IDEAM 2021) were used as a reference. The interpretation of the temporal composites of the satellite images is done through the Corine Land Cover methodology adapted for Colombia (IDEAM 2010), which can be considered as a national reference in the remote sensing processes of satellite images. Based on the multi – temporal classification of the images, the areas occupied by each of the paramo coverages are calculated. Based on these statistics, the trend analysis and its significance of the vegetation covers are carried out through the Mann–Kendall test (Mann Kendall 1945), mentioned above.

The dynamics of vegetation covers are sensitive to different forcing factors such as global climate change (Martínez-Retureta et al. 2022), (Kempf 2023), climate variability (Ogou et al. 2021), and the different socio-economic activities (Etter, Andrade, and Zuñiga 2020). The study aims to evaluate the incidence of each of the factors that make up the fourth part of the methodology.

It has been shown that the change in the areas of vegetation cover associated with climate variability can be evidenced through their trend analysis (Xue et al. 2022). The analysis of trends and their significance are analyzed through the Mann–Kendall test. The effect of socio-economic activities would represent the residual term between the observed and predicted values through the linear trend. Tre percentage contribution of the forcing factors mentioned above on the dynamics of vegetation covers and its relationship with the statistical analysis mentioned below can be presented through the following procedure:

The predicted values of the vegetation cover areas, which identify the effect of climate variability, are estimated

Table 1. Classification ranges of water availability according to the SPEI index

SPEI Index Range	Classification
≥ 2.0	Extremely humid
1.5 - 2.0	Very humid
1.0 - 1.5	Moderately humid
0.5 - 1.0	Incipient humidity
0.5 - 0.5	Normal
-0.5 - 1.0	Incipient drought
-1.0 -1.5	Moderately dry
-1.5 - 2.0	Very dry
≤ - 2.0	Extremely dry

Source: (Scordo, Piccolo, & Perillo 2018) through the regressive model with the hydroclimatic variables using the following Eq. (4):

$$A_{ki_{pro}} = a_1 P + a_2 PET + \varepsilon \tag{4}$$

where

$A_{ki_{pro}}$ - vegetation cover area – k (paramo grassland, forest, crops, among others) predicted through the trend line, km^2;

$a_1, a_2, ..., a_n, \varepsilon$ – regression parameters;

P, PET – hydroclimatological variable (precipitation, evapotranspiration) with which the regressive model is built. The statistical significance of the regressive model is built with the significance level of 0.05 and is tested through the student test.

The residual term, associated with the effect of anthropogenic activity, is calculated as the difference between the observed and predicted values through the following Eq. (5):

$$A_{ki_{res}} = A_{ki_{obs}} - A_{ki_{pro}} \tag{5}$$

where:

$A_{ki_{res}}$ – area of residual vegetation cover (paramo grassland, forest, crops, among others), associated with the influence of anthropogenic activities, km^2;

$A_{ki_{obs}}$ – area of vegetation cover (páramo grassland, forest, crops, among others), observed through remote sensing analysis, km^2.

Next, we will identify the extent to which climate variability and anthropogenic activities have influenced the dynamics of land cover in the paramo. This analysis is carried out through the relationships between the slopes with significant trends in the areas of one or another coverage of the observed, predicted, and residual values. The structure of the interpretation is presented below (Table 2).

In the previous step, the percentage contribution of climate variability and anthropogenic activities (residual series) to the dynamics of contraction and expansion of different coverages of the paramo was identified. Finally, in the fifth stage, the results were analyzed and conclusions were drawn about whether there was a change in the plant cover of the Guacheneque paramo associated with climate variability or anthropogenic activities.

RESULTS

To carry out the climatic analysis, information on total monthly precipitation and average monthly temperatures in the vicinity of the study area was collected. Incomplete historical records were complemented with complete historical series from nearby stations, considering the statistical significance of said correlations. As a result, complete records of precipitation and temperatures were obtained (period 1983-2021), whose location can be consulted in Fig. 1 and whose main data are found in Table 3. The selection of the study period is explained by the joint availability of climate records and satellite images in the paramo.

For the records of average temperatures and total annual precipitation, the trend analysis was constructed through the Mann – Kendall test, which yielded the results presented below.

As can be seen from the results of the temperature trend study, 38.5% of the stations affirm an increasing pattern of statistically significant trend. 7.6%, corresponding to a climatic station, confirm a decreasing trend, and 53.9% of the stations confirm a trend, but with the level of significance applied, it still cannot be confirmed as significant.

In terms of precipitation trends analysis, 3 stations confirmed a pattern toward a decrease in average values. One station confirmed a significant positive trend, and the other stations, corresponding to 58.3% of all stations, mostly confirmed a positive but still non-significant trend. From the aforementioned, it is concluded that in the study area, a trend pattern of precipitation cannot yet be identified through the Mann-Kendall test with a significance level of 0.05. However, taking into account that most stations confirm a non-significant positive trend, it is expected that in the coming years this will consolidate into a pattern.

In summary, the study area's climate series exhibit changes in their regime due to global climate change. Most stations confirm a trend towards increasing temperatures and decreasing precipitation. The historical series of precipitation, temperatures, and PET made it possible to construct climate maps of isotherms, isohyets, and the PET that not only allow us to characterize the climate but also serve as input for the calculation of the SPEI index that characterizes the availability of water resources in areas where hydrological monitoring is not carried out and when this is scarce. Below are examples of the constructed maps corresponding to the year 2021.

Table 2. Decision algorithm to identify the contributions of climate variability and anthropogenic activities on vegetation cover

A_{obs_i}	$A_{i\,pro}$	$A_{res\,i}$	Contribution		Conclusion
	Predicted area trend	Residual area trend	Climate variability	Human activities	
Increasing slope of the observed area	>0	>0	i_{pre}/i_{obs}	i_{res}/i_{obs}	All factors influence the increase in coverage area
	>0	<0	100	0	Climate variability and climate change influence the expansion of the vegetation cover area
	<0	>0	0	100	Human activities influence the growth on the vegetation cover area
Decreasing slope pf observed area	<0	<0	i_{pre}/i_{obs}	i_{res}/i_{obs}	All factors influence the decrease in coverage area
	<0	>0	100	0	Climate variability and climate change influence the contraction of the vegetation cover area
	>0	<0	0	100	Human activities influence the decrease in the area of vegetation cover
i	slope				

Table 3. General information about the climatic stations used in the study

Precipitation measuring stations		Temperature measuring stations	
Code	Name	Code	Name
24010170	Guachetá	24015120	Isla del Santuario
21206320	La Fortuna	24015220	Villa Carmen
24010380	El Puente	24015290	Gachaneca
24010070	Leticia	24035130	UPTC
24010180	Ráquira	35075010	Nuevo Colón
24010390	El Triángulo	24015310	San Miguel de Sema
24015120	Isla del Santuario	24015210	Sutatausa
24015200	Alto Saboya	24015130	Simijaca
24015310	San Miguel de Sema	21205570	Primavera La
24015010	Represa Gachaneca	24015190	Novilleros
35070020	Ventaquemada	21205610	Muña
35075010	Nuevo Colón	24015180	Esclusa Tolón

Table 4. Results of the trend analysis of average temperatures and total annual precipitation in the study area through the Mann – Kendall test (significance level 0.05)

Average annual temperature			Total annual precipitation		
Code	Type of trend	Z	Code	Type of trend	Z
24015120	Positive not significant	0.60	24010170	Significant negative	-2.56
24015220	Significant positive	2.77	24010180	Significant negative	-3.67
24015290	Positive not significant	0.48	24010070	Significant negative	-2.45
24035130	Non-significant negative	-2.44	21206320	Positive not significant	0.48
35075010	Significant positive	4.03	24010380	Positive not significant	1.44
24015310	Significant negative	-2.57	21010390	Positive not significant	0.95
24015210	Positive not significant	1.27	24015210	Positive not significant	1.33
24015130	Positive not significant	0.78	24015200	Significant positive	2.27
21205570	Significant positive	4.02	24015310	Non-significant negative	-1.03
24015190	Non-significant negative	-1.3	24015010	Positive not significant	0.35
21205610	Significant positive	2.00	35070020	Significant negative	-3.12
24015180	Significant positive	3.85	35075010	Positive not significant	0.23

As can be seen from the climate maps, the spatial variation of precipitation is quite homogeneous with greater rainfall in the eastern part of the paramo. The behavior of temperatures preserves a clear pattern in altitudinal variation, where higher altitudes correspond to lower values of average temperatures. For its part, the temperature regime directly affects the evapotranspiration rates. In relation to the spatial variation of the SPEI index, which defines water availability, its highest values are found in the central and Eastern part of the paramo, where a lower proportion of the precipitated water is spent in the evapotranspiration process. In the map presented, the SPEI index values range between 1.3 to 2.3, which characterizes the climate between very humid and extremely humid. However, in some hydrologically dry years, the SPEI index can reach values close to 1.0 that characterize dry climates. This temporal variability is due to the ENSO phenomenon, which significantly influences the interannual regime of water supply in Colombia (Díaz and Villegas 2022). Thus, in 1997 the average annual value of the index in the paramo reached 0.94, when a strong episode of the warm phase of the ENSO phenomenon occurred with the average annual value of the MEI index of 1.19, reaching its maximum value of 2.3 in the month of August[7].

In the second methodological stage, the land covers present in the paramo were classified. For this purpose, initially, coverage was identified with the support of the

[7] NOAA. (2023, Julio 13). Multivariate ENSO Index Version 2 (MEI.v2). Retrieved from https://psl.noaa.gov/enso/mei/

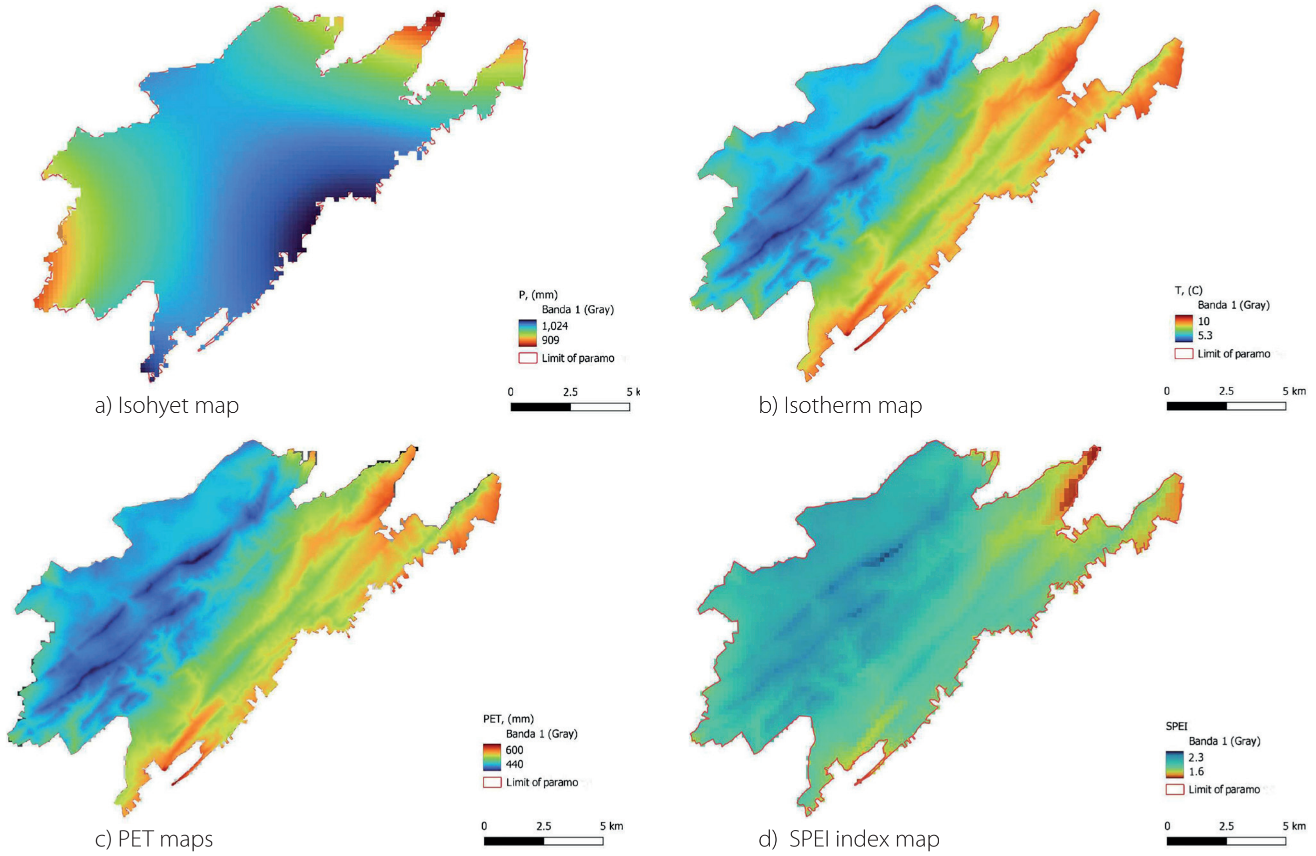

Fig. 3. Example of climate maps for the year 2021

coverage map of (IDEAM 2021). Among these are the following: dense bush dense forest, forest plantation, fragmented forest, crop mosaic, clean pastures, open forest, grassland dense, bodies of water, mosaic of pastures and natural spaces. The supervised classification of the satellite images was done following the Corine Land Cover methodology (IDEAM 2010) for the composites of medians of the satellite images corresponding to the following periods: 1983-1986, 1987-1990, 1991-1994, 1995-1998, 1999-2002, 2003-2006, 2007-10, 2011-14, 2015-18, 2019-21. Below, as an example, the graphic outputs for the periods 1983-86 and 2019-2021 are presented.

The previously provided land cover classification maps show remarkable preservation of natural areas during the period between 1983 and 1986. This conclusion is supported by contrasting these maps with the cartographic representation corresponding to the interval from 2019 to 2021. The comparison between these two temporalities reveals a significant increase in the extent of grassland during the 1983-1986 period, a phenomenon mainly attributed to the growth of anthropogenic activities in the southwestern part of the paramo and to the increase in the cover of clean grassland and shrubland for the 2019-2021 period. Examining the northern zone of the Rabanal paramo reveals changes in cover, with the forest plantation and fragmented forest occupying a smaller area during the 1983-1986 period. This suggests that, although in the 1983-1986 period, the conservation of grassland cover covered a larger area, for the 2019-2021 period, a slight increase in forest and shrub cover is observed

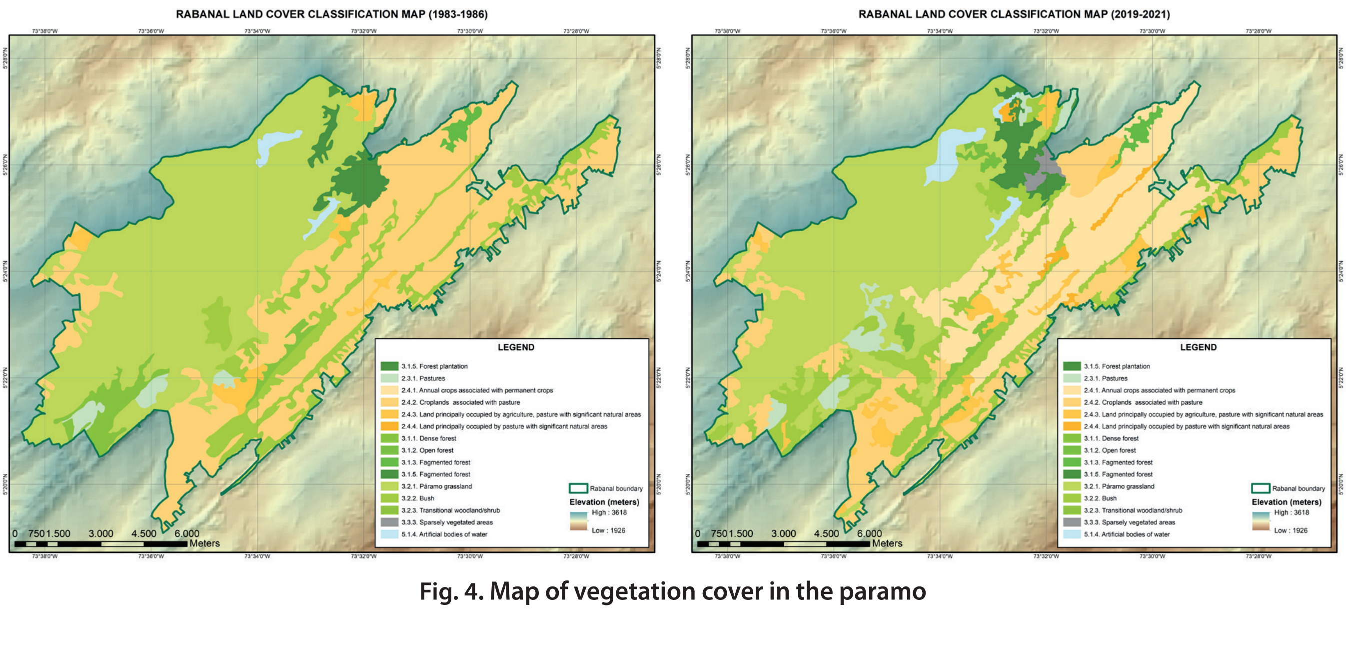

Fig. 4. Map of vegetation cover in the paramo

in this part of the paramo. This indicates that, although the coverage of paramo grassland is lower, forest and shrubland conservation has been increasing over time, thanks to better control over anthropogenic activities in this part of the paramo. This change suggests a more efficient and sustainable management of natural resources in the region, contributing to the conservation of natural vegetation cover.

Subsequently, forest covers (open forest, dense forest, fragmented and planted forest) and mosaic surfaces of crops, pastures, and natural spaces were grouped. For each type of vegetation cover, the areas were calculated. The graph of the temporal variation of the coverage is presented in Fig. 5.

Fig. 5 shows that land covers are not constant, and, visually, some of them tend to increase and others – to decrease. In order to confirm this fact, the Mann - Kendall test was applied to the coverage in order to identify if these changes are statistically significant. The results of this analysis are presented in Table 5.

As shown in the previous table, the forest cover does not present any type of trend. Although in the last period analyzed, in the northeastern part of the paramo in the area of the planted forest, a patch of forestry exploitation has appeared (about 85 hectares), this does not affect the trend dynamics of the forest cover. The coverage areas of crops, pastures, natural spaces, clean grasses, shrubs, and aquatic surfaces confirmed a trend towards their expansion, and paramo grassland is the only coverage that shows a decreasing trend in its area. The area of mosaics of crops, pastures, and natural surfaces gains 7.3 hectares per year; the areas of pastures – 4.8 hectares; bushland –12.6 hectares; and the water bodies increase annually by 3.2 hectares, while the paramo loses 28.5 hectares of paramo grassland.

To identify the percentage contribution of climate variability and anthropogenic activities to the change in land cover areas, the procedure described in Table 2 was applied. The regressive models built through Eq. 4 confirmed its significance for mosaics, paramo grassland, and shrub cover, while for clean pastures and water bodies the correlation is not statistically significant with a significance level of 0.05 through the t Student test. This result does not indicate an absence of correlation between the variables, but rather that there is no significant level of 0.05 and a limited number of data (10) that were used in the construction of regressive models. This result will be taken into account for the analysis of the percentage contribution of the forcing factors to the land coverage of the paramo.

The summary of the percentage contribution of the forcing factors to the vegetal cover of the paramo is presented in Table 6. Graphically, the results are presented in Fig. 6.

From the summary presented in Table 6, it is identified that the expansion of coverage associated with anthropogenic activity (mosaic of surface of crops, pastures and natural spaces and pastured) occurs mainly due to human interventions. This conclusion is consistent with several studies that confirm the expansion of agricultural and livestock activities towards the paramos (Ross et al. 2017), (Balthazar et al. 2015), (Tovar et al. 2012). Variations in the area of aquatic surfaces depend 86 % on anthropogenic activities related to the regulation of the water cycle and 14 % on interannual variations in water availability, although the regressive model did not show that this is not statistically significant. In all the coverages analyzed, the influence of human activities is more significant than that of climate variability and climate change. The area of the paramo grassland decreases by 82% due to the effect of human actions and by 18% due to climatic variation. This indicates that some anthropogenic covers displace this cover. This analysis is presented later.

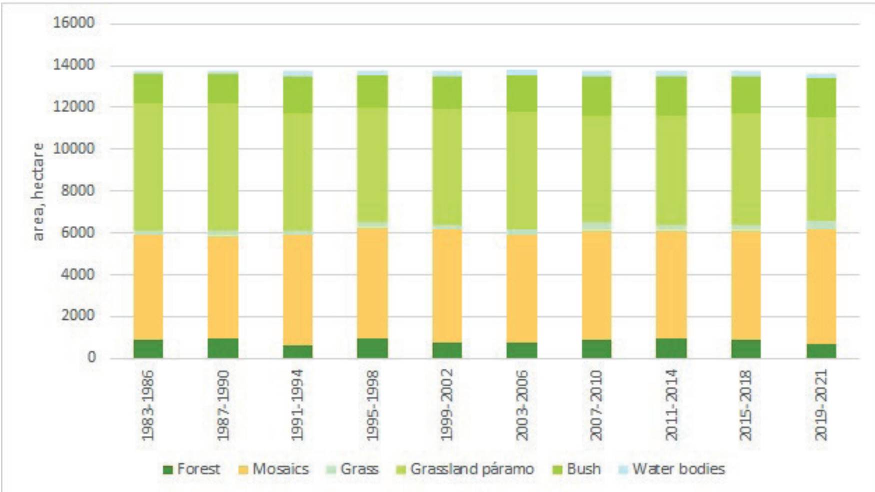

Fig. 5. Temporal variation of the plant cover in the paramo

Table 5. Results of the trend analysis of land cover through the Mann – Kendall test (significance level 0.05)

Land cover	Z	Conclusion
Forest	0.000	There is no trend
Surface of crops, pastures and natural spaces	2.078	Positive trend
Clean grass	4.157	Positive trend
Páramo grassland	-3.464	Negative trend
Bush	3.233	Positive trend
Artificial bodies of water	3.464	Positive trend

Table 6. Percentage contribution of climate variability and anthropogenic activities to the land covers of the paramo

Land cover	Slope per period			Relative proportions of the forcing factors	
	Slope of observed area	Predicted area slope	Residual area slope	Climate variability and climate change	Anthropogenic activity
Mosaic of crops, pastures and natural spaces	29.28	2.76	26.51	0.09	0.91
Clean grass	19.08	2.17	16.91	0.11	0.89
Páramo grassland	-113.85*	-20.18*	-93.68*	0.18	0.82
Bush	50.53	11.47	39.06	0.23	0.77
Water bodies	12.75	1.82	10.93	0.14	0.86

* Negative values indicate the contraction of the paramo grassland area.

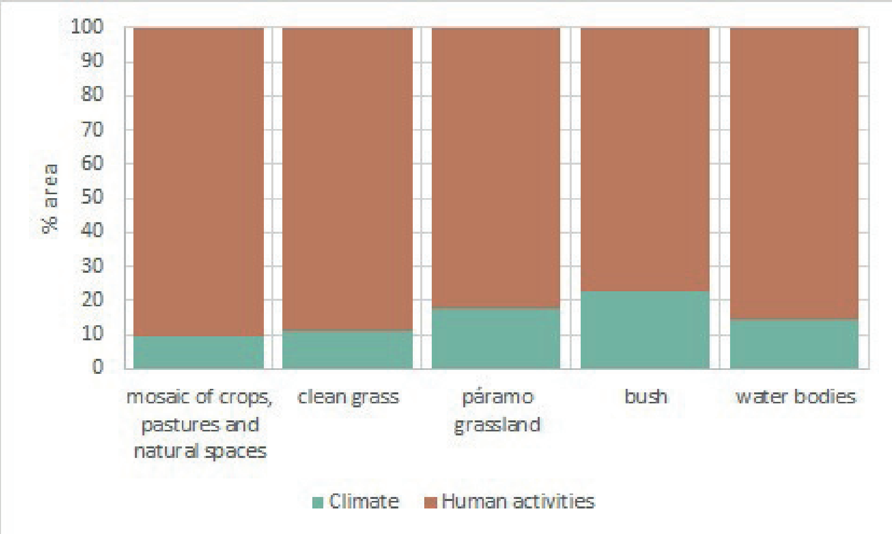

Fig. 6. Relative proportions of the forcing factors on the land covers of the paramo

Regardless of the fact that the change in the areas of most of the land cover of the paramo is associated with human activities, a percentage of the change occurs due to the effects of climate variability. For this reason, the land cover areas were correlated with the SPEI index that characterizes the availability of the water resource. It is recalled that in the study area an increase in rainfall and water supply is expected according to climate change scenarios (Mesa, Urrea, and Ochoa 2021). A positive correlation between the SPEI index and predicted coverage areas indicates that greater water availability favors the increase in the land coverage area and vice versa. Below are the graphical results of this analysis.

According to the results presented in Fig. 7, most of the variation in coverage responds directly to water availability. That is, the greater the amount of water available, the larger the area covered by pasture, crops, natural surfaces, and shrubs, while bushes and aquatic areas are reduced with increased water availability. The paramo grasslands are repressed by increased water availability as well.

If the forecast of increased rainfall in the paramo area comes true, in the coming years a decrease in the area of paramo grassland is expected due to the effects of global climate change. The contraction of the paramo area is also due to anthropogenic activities. This indicates that anthropic covers replace the grasslands of the paramo. For this reason, the multiple regression analysis was carried out between the grassland areas versus the mosaic of crops, pastures, and natural, which yielded a value of the coefficient of determination of 0.97 with a *P–value* of 0.0006. This result concludes with paramo grasslands being replaced by land cover of pastures and crops.

In addition to everything mentioned above, paramo grasslands are sensitive to the two forcing forces: climate variability and climate change, and anthropogenic activity. The first factor's influence is reflected in an increase in water availability, which causes a contraction of the grassland surface. The second factor has a greater impact on the area of paramo grassland, which is expressed in the replacement of the paramo vegetation cover by crops and pastures.

DISCUSSION

The methodology applied and the results obtained open a range of issues that deserve to be discussed in order to refine the methodology and deepen our knowledge about the dynamics and impacts generated by different interventions in the Colombian paramo ecosystems, which are important per se and for the ecosystem services they provide, such as: water provision and regulation, biodiversity support, raw material provision, climate regulation, among others.

Initially, the methodology developed was designed to evaluate the incidence of climate variability, climate change, and human activities on land cover under the scenario of limited availability of hydrometeorological and geospatial information. This is justified because the climate monitoring system in Colombia's high mountains is limited and, in most cases, water availability and variability are characterized through indirect methods of water balance. Furthermore, the study area is influenced by the Intertropical Influence Zone (Hastenrath 2002), which generates a high cloud cover that limits the selection of

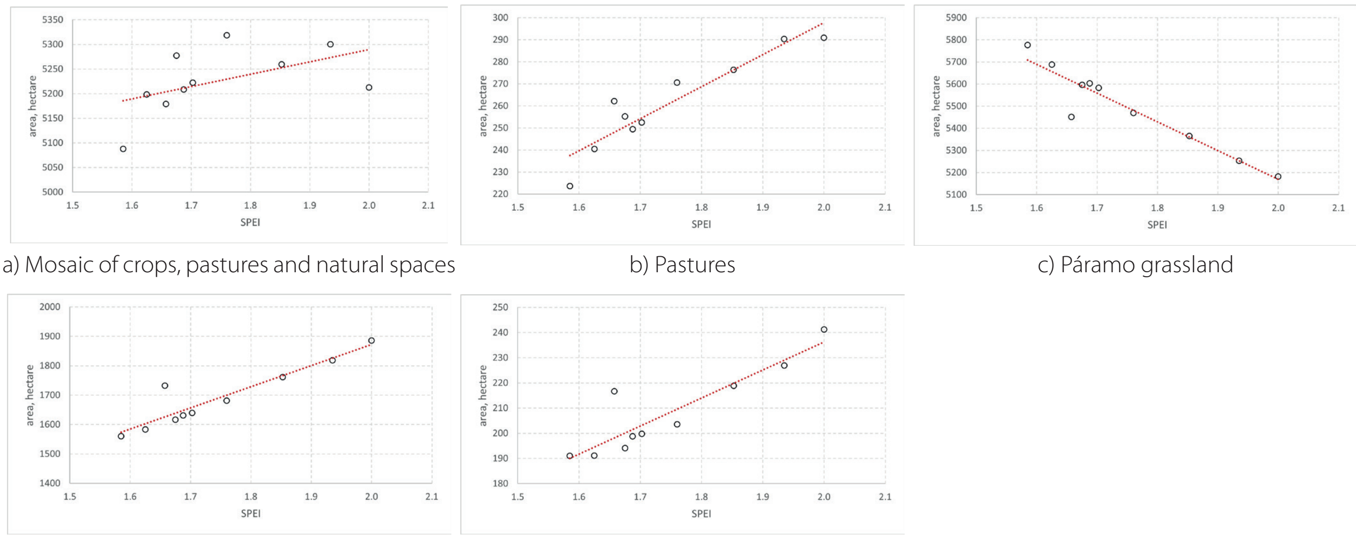

a) Mosaic of crops, pastures and natural spaces b) Pastures c) Páramo grassland

d) Bush e) Water bodies

Fig. 7. Temporal variation of the plant cover in the paramo

satellite images for remote sensing of vegetation cover. For this reason, in order to guarantee the availability of satellite images for the period from 1983 to 2021, median composites of 4-year satellite images were constructed, which made it possible to interpret the land covers of the paramo. Considering that paramo ecosystems are found in Colombia, Venezuela, and Ecuador and the availability of inputs for this type of study, it is important to take into account that the data were obtained from the data received from the satellite images of the paramo.

Although Colombia has expanded its hydro climatological monitoring network in recent decades, its three mountain ranges generate high climate variability that requires a greater density of climate stations.

Added to this high climate variability is the phenomenon of global climate change; however, the effects of global climate change on the climate regime are uncertain (Espinosa et al. 2023) and the rainfall regime does not respond to the climate signal in the same way. Some areas of the country face an increase in rainfall and others – a decrease in it (Arias et al. 2022). The effects of climate variability and climate change are added, and their individual contributions are not easy to distinguish. As a result, the study considered these two factors together.

Despite all the limitations in the inputs mentioned above, it was possible to identify that the vegetation covers of the Guacheneque paramo present a change, mostly associated with human activities, where the paramo grassland gives up about 28.5 hectares per year to clean and mosaics of pastures and crops.

CONCLUSIONS

In the study, the hypothesis was used that there are two factors that influence the change in land cover of the paramo, which are climate variability, climate change, and anthropogenic activity. Trend studies of climatological variables indicate that most temperature stations confirm a trend towards an increase in their mean values – the effect of global climate change – while in the trend analysis of precipitation, the pattern of change is not so certain but has a direction towards its increase. The multi-temporal analysis of satellite images shows a contraction of the paramo grasslands and an increase in anthropogenic coverage of pastures, crops, and water bodies.

The results obtained indicate that both climatic factors and anthropogenic activities motivate changes in the area of paramo coverage, such as clean pastures, mosaics of grasses, crops, and natural spaces, paramo grassland, and shrubs. Although each of these factors affects each type of vegetation in its own way, the predominance of human influence on climatic factors is preserved. Thus, the weight of anthropic factor on some land cover varies in a range from 0.77 to 0.91, while the weight of climate variability and climate change is between 0.09 and 0.23. The land covers that are most sensitive to climate variability and climate change are natural land covers, such as shrubs and paramo grasslands, whose surface area variations are 20% dependent on this forcing factor.

All paramo vegetation covers are sensitive to water availability, and all, except paramo grassland, have a direct relationship with water supply (SPEI index). This indicates that, if the climate change scenario towards increased precipitation is realized, these land covers will expand, replacing the paramo grassland.

From all of the above, it can be concluded that the vegetation cover of the Guacheneque paramo shows a change, in most cases, statistically significant. Although the effects of climate variability and climate change on vegetation cover cannot be controlled, it is possible to monitor and regulate the influence of human activities, which are the main causes of these changes, to ensure the conservation of the paramo's ecosystem services. One of the strategies could be multitemporal monitoring through satellite images that is being successfully applied in different parts of the world (Alberton et al. 2023, Ma et al. 2023). Another paramo protection strategy that seeks to generate employment and restore paramo coverage is the development of payment for environmental services projects, which are economic instruments that seek to ensure the provision of ecosystem services through contributions from the inhabitants of strategic ecosystems within the framework of conservation projects[8].

The methodology can be replicated in other countries such as Colombia, Ecuador, and Venezuela, to assess the impact of land cover as a result of climate variability and human activities.

[8] Presidencia de la República. (2018). Decreto 1007 de 2018. Retrieved from Regulación de los incentivos de pago por servicios ambientales: https://www.funcionpublica.gov.co/eva/gestornormativo/norma.php?i=86901

REFERENCES

Alberton, Bruna, Swanni T. Alvarado, Ricardo da Silva Torres, Geraldo Wilson Fernandes, and Leonor Patricia C. Morellato. 2023. "Monitoring Immediate Post-Fire Vegetation Dynamics of Tropical Mountain Grasslands Using Phenocameras." Ecological Informatics 78. doi: 10.1016/j.ecoinf.2023.102341.

Ankrah, Johnson, Ana Monteiro, and Helena Madureira. 2023. "Spatiotemporal Characteristics of Meteorological Drought and Wetness Events across the Coastal Savannah Agroecological Zone of Ghana." Water (Switzerland) 15(1). doi: 10.3390/w15010211.

Arias, Paola A., Laura D. Villegas, Oscar J. Mesa, José D. Pabón, Jacobo Arango, Santiago Arango-Aramburo, Dolors Armenteras, Lina Berrouet, Rolando Barahona, Janet Barco, Yuley Cardona, Yesid Carvajal-Escobar, Lina I. Ceballos-Bonilla, Wilmar L. Cerón, Jaime H. Escobar, Catalina González, Isabel C. Hoyos, Natalia Hoyos, Carlos Jaramillo, Giovanni Jiménez-Sánchez, J. Alejandro Martínez, Germán Poveda, Benjamín Quesada, Estela Quintero-Vallejo, Ángela M. Rendón, Daniel Ruiz-Carrascal, Alejandro Salazar, Juan F. Salazar, Adriana Sánchez, Sara C. Vieira, Juan Camilo Villegas, Clara Villegas-Palacio, and Manuel D. Zuluaga. 2022. "Methodological Implications and Inconsistencies of Colombia's Third National Communication on Climate Change." Revista de La Academia Colombiana de Ciencias Exactas, Fisicas y Naturales 46(180):769–94. doi: 10.18257/raccefyn.1705.

Balthazar, Vincent, Veerle Vanacker, Armando Molina, and Eric F. Lambin. 2015. "Impacts of Forest Cover Change on Ecosystem Services in High Andean Mountains." Ecological Indicators 48:63–75. doi: 10.1016/j.ecolind.2014.07.043.

Bayer-Altın, Türkan. 2023. "Long-Term Trends and Variability in Air Temperatures of Central Anatolia Region, Turkey, for the Period 1960–2021." Acta Geophysica 71(4):2031–47. doi: 10.1007/s11600-023-01077-6.

Beltran, Luis. 2018. "Effect of Climatic and Land Use Variables on the Water Supply of the Gachaneca River Basin, as a Scenario for the Comprehensive Management of Water Resources." Universidad de Ciencias Aplicadas y Ambientales U.D.C.A , Bogotá.

Blanco Garrido, Fabian, Laura Martínez Valdivieso, Juan Polo Ardila, Fredys Simanca, Miguel Hernandez, Liliana Patricia, Lozano Ayarza, and Julio Mojica. 2020. Strategies for the Conservation of the Fúquene Lagoon in the Departaments of Cundinamarca and Boyacá.

Buyukyildiz, Meral. 2023. "Evaluation of Annual Total Precipitation in the Transboundary Euphrates–Tigris River Basin of Türkiye Using Innovative Graphical and Statistical Trend Approaches." Applied Water Science 13(2). doi: 10.1007/s13201-022-01845-7.

Caracol Radio. 2022. "Ciencia y Medio Ambiente."

Corpoboyacá. 2016. Acuerdo 030. Retrieved from Be Means of Which the Regional National Natural Park Is Declared and Bounded, in the Municipality of Samacá in the Jurisdiction of the Regional Autonomous Corporation of Boyacá. Boyacá.

Corpochivor, and IAvH. 2018. Plan de Manejo Ambiental Del Distrito Regional de Manejo Integrado Del Páramo de Guacheneque.

Cr Sib. 2018. "Britófitos Reófilos Del Río Teatinos (Boyacá Colombia)." Retrieved June 4, 2024 (https://ipt.biodiversidad.co/cr-sib/resource.do?r=724_briofitos_20180903#:~:text=La%20microcuenca%20del%20r%C3%ADo%20Teatinos,elevaci%C3%B3n%20media%20de%202780%20m.).

Cresso, Matilda, Nicola Clerici, Adriana Sanchez, and Fernando Jaramillo. 2020. "Future Climate Change Renders Unsuitable Conditions for Paramo Ecosystems in Colombia." Sustainability (Switzerland) 12(20):1–13. doi: 10.3390/su12208373.

Díaz, Diana, and Nancy Villegas. 2022. "Wavelet Coherence between ENSO Indices and Two Precipitation Databases for the Andes Region of Colombia." Atmosfera 35(2):237–71. doi: 10.20937/ATM.52890.

Diazgranados, Mauricio, Carolina Tovar, Thomas R. Etherington, Paula A. Rodríguez-Zorro, Carolina Castellanos-Castro, Manuel Galvis Rueda, and Suzette G. A. Flantua. 2021. "Ecosystem Services Show Variable Responses to Future Climate Conditions in the Colombian Páramos." PeerJ 9. doi: 10.7717/peerj.11370.

Espinosa, Mónica, Juan S. Larrahondo, Juan F. Mendez-Espinosa, Denisse V. Cortés, Víctor F. Forero, and Juan F. Franco. 2023. "Perception of Climate Change in an Academic Community in Colombia—a Pilot Study in a Developing Country." Discover Sustainability 4(1). doi: 10.1007/s43621-023-00129-7.

Etter, Andrés, Angela Andrade, and Mateo Zuñiga. 2020. Ecosistemas Colombianos Amenazas y Riesgos Autores Andrés Etter Equipo de Investigación Ejecución de La Investigación Financiación Investigación.

Etter, Andrés, Clive McAlpine, Kerrie Wilson, Stuart Phinn, and Hugh Possingham. 2006. "Regional Patterns of Agricultural Land Use and Deforestation in Colombia." Agriculture, Ecosystems and Environment 114(2–4):369–86. doi: 10.1016/j.agee.2005.11.013.

Fonseca, Melisa. 2022. "Parque Natural Regional Rabanal, Mucho Más Que Una de Páramo." Retrieved June 4, 2024 (https://www.corpoboyaca.gov.co/noticias/parque-natural-regional-rabanal-mucho-mas-que-una-de-paramo/).

González-M., Roy, Natalia Norden, Juan M. Posada, Camila Pizano, Hernando García, Álvaro Idárraga-Piedrahita, René López-Camacho, Jhon Nieto, Gina M. Rodríguez-M, Alba M. Torres, Alejandro Castaño-Naranjo, Rubén Jurado, Rebeca Franke-Ante, Robinson Galindo-T, Elkin Hernández R., Adriana Barbosa, and Beatriz Salgado-Negret. 2019. "Climate Severity and Land-Cover Transformation Determine Plant Community Attributes in Colombian Dry Forests." Biotropica 51(6):826–37. doi: 10.1111/BTP.12715.

Hastenrath, Stefan. 2002. "The Intertropical Convergence Zone of the Eastern Pacific Revisited." International Journal of Climatology 22(3):347–56. doi: 10.1002/JOC.739.

Hurtado, S., M. Cadena, and IDEAM. 2018. "CARACTERIZACIÓN CLIMÁTICA DE LA EVAPOTRANSPIRACIÓN DE REFERENCIA (ETo) EN COLOMBIA: DISTRIBUCIÓN ESPACIO-TEMPORAL, VARIABILIDAD INTERANUAL Y AFECTACIÓN POR EL FENÓMENO EL NIÑOOSCILACIÓN SUR (ENOS)." Retrieved June 4, 2024 (chrome-extension://efaidnbmnnnibpcajpcglclefindmkaj/http://www.ideam.gov.co/documents/21021/21147/NotaT%C3%A9cnica+Evapotranspiracion+de+Referencia+en+Colombia/9f938590-ef96-4e6f-99dd-861ff6355b84).

IAvH. 2013. "Átlas de Páramos de Colombia." Retrieved (http://www.humboldt.org.co/es/buscar?q=paramo).

IAvH. 2020. "Páramo Guacheneque y Ecosistema de Vida." Retrieved June 4, 2024 (http://www.humboldt.org.co/es/i2d/item/559-paramos-y-sistemas-de-vida-rabanal).

IDEAM. 2010. "Leyenda Nacional de Coberturas de La Tierra. Metodología CORINE Land Cover Adaptada Para Colombia Escala 1 : 100 000."

IDEAM. 2021. "Mapa de Coberturas de La Tierra, Metodologia Corine Land Cover, Periodo 2018." Retrieved June 4, 2024 (http://www.ideam.gov.co/documents/10182/512130/Cobertura+de+la+tierra+100K+Periodo+2018.pdf/de4cdf86-49be-4825-83c0-5569355f9e2b?version=1.0).

Kempf, Michael. 2023. "Enhanced Trends in Spectral Greening and Climate Anomalies across Europe." Environmental Monitoring and Assessment 195(2). doi: 10.1007/s10661-022-10853-8.

Lis-Gutiérrez, Melissa, Yolanda Rubiano-Sanabria, and Juan Carlos Loaiza Usuga. 2019. "Soils and Land Use in the Study of Soil Organic Carbon in Colombian Highlands Catena." Acta Universitatis Carolinae, Geographica 54(1):15–23. doi: 10.14712/23361980.2019.2.

Ma, Zhiyuan, Jinyu Gong, Chen Hu, and Jingpin Lei. 2023. "An Integrated Approach to Assess Spatial and Temporal Changes in the Contribution of the Ecosystem to Sustainable Development Goals over 20 Years in China." Science of the Total Environment 903. doi: 10.1016/j.scitotenv.2023.166237.

MADS. 1993. Ley 99 de 1993. Bogotá D.C. Bogotá.

Mann Kendall. 1945. NONPARAMETRIC TESTS AGAINST TREND1.

Mann Kendall, G. 1938. "A NEW MEASURE OF RANK CORRELATION." Biometrika 30(1–2):81–93. doi: 10.1093/BIOMET/30.1-2.81.

Mann Kendall, Henry B. 1945. "Nonparametrics Tests against Trend. Econometrica." Econometrica 13(3):245. doi: 10.2307/1907187.

Martínez-Retureta, Rebeca, Mauricio Aguayo, Norberto J. Abreu, Roberto Urrutia, Cristian Echeverría, Octavio Lagos, Lien Rodríguez-López, Iongel Duran-Llacer, and Ricardo O. Barra. 2022. "Influence of Climate and Land Cover/Use Change on Water Balance: An Approach to Individual and Combined Effects." Water (Switzerland) 14(15). doi: 10.3390/w14152304.

Mesa, Oscar, Viviana Urrea, and Andrés Ochoa. 2021. "Trends of Hydroclimatic Intensity in Colombia." Climate 9(7). doi: 10.3390/cli9070120.

Nejadrekabi, M., S. Eslamian, and M. J. Zareian. 2022. "Spatial Statistics Techniques for SPEI and NDVI Drought Indices: A Case Study of Khuzestan Province." International Journal of Environmental Science and Technology 19(7):6573–94. doi: 10.1007/S13762-021-03852-8/TABLES/7.

Ogou, Faustin Katchele, Vincent Nduka Ojeh, Edward Naabil, and Chukwuemeka I. Mbah. 2021. "Hydro-Climatic and Water Availability Changes and Its Relationship with NDVI in Northern Sub-Saharan Africa." Earth Systems and Environment 6(3):681–96. doi: 10.1007/S41748-021-00260-3.

Peréz Rendon, Edna Paola, Victor Hugo Ramírez Builes, and Andrés Javier Peña Quiñones. 2016. "Variabilidad Espacial y Temporal de La Temperatura Del Aire En La Zona Cafetera Colombiana." Investigaciones Geográficas 89(89):23–23. doi: 10.14350/RIG.38707.

Peyre, Gwendolyn, Diego Osorio, Roman François, and Fabien Anthelme. 2021. "Mapping the Páramo Land-Cover in the Northern Andes." International Journal of Remote Sensing 42(20):7777–97. doi: 10.1080/01431161.2021.1964709.

Rey-Romero, Daniela Cristina, Isabel Domínguez, and Edgar Ricardo Oviedo-Ocaña. 2022. "Effect of Agricultural Activities on Surface Water Quality from Páramo Ecosystems." Environmental Science and Pollution Research 29(55):83169–90. doi: 10.1007/s11356-022-21709-6.

Rodríguez Morilla, Carmen. 2000. "Análisis de Series Temporales."

Ross, Cristina, Stephen Fildes, and Andrew C. Millington. 2017. "Land-Use and Land-Cover Change in the Páramo of South-Central Ecuador, 1979-2014." Land 6(3). doi: 10.3390/land6030046.

Sang, Jing, Baodeng Hou, Hejia Wang, and Xiaowen Ding. 2023. "Prediction of Water Resources Change Trend in the Three Gorges Reservoir Area under Future Climate Change." Journal of Hydrology 617. doi: 10.1016/j.jhydrol.2022.128881.

Shi, Ke, and Yoshiya Touge. 2023. "Identifying the Shift in Global Wildfire Weather Conditions over the Past Four Decades: An Analysis Based on Change-Points and Long-Term Trends." Geoscience Letters 10(1). doi: 10.1186/s40562-022-00255-6.

Shrivastava, Sourabh, R. Uday Kiran, P. K. Bal, and K. K. Singh. 2022. "Estimation of the Standardized Precipitation Evapotranspiration Index (SPEI) Using a Multilayer Perceptron Artificial Neural Network Model for Central India." Pure and Applied Geophysics 179(4):1461–73. doi: 10.1007/s00024-022-02969-2.

Tovar, Carolina, Joost F. Duivenvoorden, Isidoro Sánchez-Vega, and Arie C. Seijmonsbergen. 2012. "Recent Changes in Patch Characteristics and Plant Communities in the Jalca Grasslands of the Peruvian Andes." Biotropica 44(3):321–30. doi: 10.1111/j.1744-7429.2011.00820.x.

Xue, Lin, Martin Kappas, Daniel Wyss, Chaoqun Wang, Birgitta Putzenlechner, Nhung Pham Thi, and Jiquan Chen. 2022. "Assessment of Climate Change and Human Activities on Vegetation Development in Northeast China." Sensors 22(7). doi: 10.3390/s22072509.

RESEARCH PAPER

MODELING LAND USE CHANGE OF MID-SIZED CITIES IN THE PROCESS OF METROPOLIZATION. CASE STUDY LA SERENA-COQUIMBO CONURBATION, CHILE

Diana Mustelier[1*], Cristian Henríquez[1,2]
[1] Institute of Geography, Pontificia Universidad Católica de Chile, 7820436, Chile
[2] Interdisciplinary Centre on Global Change, Pontificia Universidad Católica de Chile, 8331150, Chile; Centre for Sustainable Urban Development ANID/FONDAP, 7520246 Chile
***Corresponding author:** dmustelier@uc.cl
Received: July 24th, 2023 / Accepted: May 29th 2024 / Published: July 1st 2024
https://DOI-10.24057/2071-9388-2024-2984

ABSTRACT. The current urbanization trend shows a large number of conurbated medium-sized cities growing and others that could be transformed into metropolises, especially in Latin America. This has led to disparities in the provision of urban services and amenities, as well as new territorial processes and spatial fragmentation. The objective of this study is to analyze the future changes in land use and land cover in the La Serena-Coquimbo conurbation, Coquimbo Region, Chile, under two different scenarios: Business-as-usual and Spatial Planning between 2020 and 2042. These different scenarios were simulated using the CLUMondo model based on the evolution of land use/cover between 1990-2020 in order to identify the main dynamics associated with urban growth in both cities. The simulation scenarios reflect how the urban area of the conurbation will expand towards the peri-urban area. In the first scenario, urban land shows an increase of 54%, and in the second one, 45% from 2020 to 2042, reinforcing the issues of the metropolization process in the conurbation, such as spatial segregation, infrastructure deficits, loss of ecosystems and natural landscapes, and fragmentation of rural areas. Spatially explicit models have proven to be a powerful tool for decision-makers tasked with projecting urban growth, particularly in conurbated cities undergoing metropolization.

KEYWORDS: mid-sized cities, land use change, modeling, scenario simulation, La Serena-Coquimbo, CLUMondo

CITATION: Mustelier D., Henríquez C. (2024). Modeling Land Use Change Of Mid-Sized Cities In The Process Of Metropolization. Case Study La Serena-Coquimbo Conurbation, Chile. Geography, Environment, Sustainability, 2(17), 106-118
https://DOI-10.24057/2071-9388-2024-2984

ACKNOWLEDGEMENTS: The authors thank public officials of the Regional Government of Coquimbo for their contribution of knowledge for the validation of the results. Also, we gratefully acknowledge the research support provided by ANID/Fondecyt Project No 1220688 and CEDEUS, ANID FONDAP 1522A0002.

Conflict of interests: The authors reported no potential conflict of interest.

INTRODUCTION

The current demographic trend shows a growing number of people living in urban areas. Although megacities contain a significant portion of the urban population, around 50% reside in medium-sized and intermediate cities with fewer than 500,000 inhabitants[1]. In this context, mid-sized cities are crucial in providing specialized services, goods, and infrastructure to both urban populations and rural areas. They occupy a strategic position between global and national metropolises, generated by globalization, which allows them to control important information and capital flows (Maturana et al. 2017). Their territorial organization in the form of networks promotes the integration and coordination of extensive areas, granting them a fundamental role in the structure and development of the territory (Llop and Cifuentes 2015).

Chile is among the most urbanized countries in Latin America with 87.7% in 2020[2]. The rapid expansion of Latin American cities reflects processes of metropolization among nearby urban centers, driven by economic dependence and the evolution of economic models in the context of globalization. This has resulted in inequalities in the quality of services and urban infrastructure, as well as new territorial processes and spatial fragmentation (Aguirre et al. 2018). Chilean cities have experienced a shift in their expansion pattern, transitioning from a relatively compact structure to diffuse urbanization towards peripheral areas, leading to a dispersed distribution (Hidalgo et al. 2009). This urbanization process includes not only the country's three major metropolitan areas (Santiago, Valparaiso, and

[1] United Nations, D. of E. and S.A.P.D. (2019). World Urbanization Prospects: The 2018 Revision. [online] https://population.un.org/wup/Publications/Files/WUP2018-Report.pdf [Accessed 03 Apr. 2023]
[2] UN-Habitat (2022). World Cities Report 2022. Envisaging the Future of Cities [online] https://unhabitat.org/wcr/ [Accessed 03 Apr. 2023]

Concepción) but also medium-sized cities that exhibit features of metropolization (Maturana et al. 2019). This process is no longer related to traditional models of Latin American cities (Borsdorf 2003) but rather involves the formation of conurbations among intermediate cities (Orellana 2020).

Many small and medium-sized cities in Latin America are growing rapidly and in the future, some may reach the level of a metropolis. However, there are no studies that allow exploring and forecasting these changes using spatially explicit urban simulation models. In this sense, the "new science of cities" provides a reference point for modeling and analysis of cities (Batty 2013). In this context, land use and land cover change (LUCC) models, are tools used to support the analysis of this type of change to understand the functioning of the complex earth system, which integrates socio-economic and biophysical dimensions (Verburg et al. 2004). Simulation models, according to Batty (2013), are crucial in the study of cities under different scenarios to represent, analyze and predict their behavior, which allows the assessment of decisions and policies for better development and management (Salazar et al. 2020).

From a geographic perspective, modeling land use changes uses Remote Sensing and Geographic Information Systems (GIS) in an integrated and systemic manner provides a spatially explicit view. The scale of study plays a significant role as it determines the information about the social organization of the territory and helps identify spatial factors that influence the patterns of LUCC (Henríquez 2014; Henríquez and Azócar 2007; Veldkamp and Lambin 2001; Verburg et al. 2004). Land use change (LUC) models, classified by (Mas et al. 2014) use different methodological approaches, theoretical foundations, and techniques, depending on the scientific discipline used (Henríquez 2014; Henríquez and Azócar 2007; Islam et al. 2021; Pokojska 2019).

Studies of this nature are widely developed in the United States, Europe, and Asia. In contrast in developing countries there is a little research regarding urban area expansion (Henríquez-Dole et al. 2018), intermediate and mid-sized cities (Azócar et al. 2003; Puertas et al. 2014; Romero and Vásquez 2009), with less representation of those in the process of metropolization (Maturana et al. 2021), which shows the importance of studying the issue in this field.

Consequently, it is imperative that urban modeling, particularly within the purview of urban planning and Strategic Environmental Assessment (SEA) proactively anticipates the demands of urban expansion and proposes alternative strategies for comprehensive and strategic development. The incorporation of a more explicit and sustainable vision into the formulation of urban alternatives through the projection of prospective scenarios using the CLUMONDO model (van Asselen and Verburg 2013), enables the integration of the strategic aspects outlined in the SEA as well as the possibility of calculating demand based on what is considered in the regulatory plans.

In light of the significance of the growth of intermediate cities in the metropolization process, the application of this approach represents an innovative contribution to the development of planning instruments. Thus, it provides a valuable tool for formulating and evaluating development options within the framework of the SEA and other planning instruments in Chile. Studies of future metropolization are scarce (Jande et al. 2020; Salazar 2020). Therefore, the novelty of this study lies in its contribution to understanding future metropolization through spatially explicit simulations, presenting the case of a mid-sized cities with accelerated growth under an explicit modeling approach, the results of which help decision-making processes.

In this regard, the following question is posed as a guiding principle: Can a mid-size city in the process of conurbation potentially evolve into a future metropolis? The objective of this study is to analyze the future changes in land use and land cover (LULC) in the La Serena-Coquimbo conurbation, Coquimbo Region, Chile, under two different scenarios: Business-As-Usual (BAU) and Spatial Planning (SP) between 2020 and 2042. These scenarios are determined using the CLUMONDO model, which is based on the evolution of LULC between 1990 and 2020. This analysis aims to identify the main dynamics associated with urban growth, which contributes to a more precise delineation of the boundaries of both mid-size cities, La Serena and Coquimbo, as well as future urban expansion areas. The projected configuration of the conurbation provides insight into how both cities will develop in their transition to becoming a future metropolitan area.

MATERIALS AND METHODS

Study area

The region is located in the southern section of the north of Chile, known as the "Norte Chico" and is bordered to the north by the Atacama Region, to the south by the Valparaiso region, to the west by the Republic of Argentina and to the east by the Pacific Ocean (Fig. 1). La Serena is the regional capital. According to the geographical characteristics, both municipalities comprise a series of longitudinal marine terraces that increase in height towards the east, crossed by ravines and river valleys. La Serena-Coquimbo conurbation is located in an area prone to natural hazards, such as earthquakes and tsunamis, tidal waves, and landslides (Ortiz et al. 2002).

The population distribution is heavily concentrated around the regional capital of La Serena and the port of Coquimbo. According to the last Census of the National Statistical Institute (INE in Spanish acronym) in 2017, the population at the regional level reached 757,586 inhabitants, of which 448,784 inhabitants are located in the municipalities of La Serena (221,054) and Coquimbo (227,730), which concentrates 59,2% of the regional population (INE 2019).

The conurbation La Serena-Coquimbo, since the mid-sized cities of La Serena and Coquimbo constitute a conurbation currently undergoing a process of metropolization (Hidalgo et al. 2009). The accelerated growth of La Serena-Coquimbo, as part of the expansion of mid-sized cities in Chile since the 1990s, exacerbates issues such as socio-spatial segregation, an increase in illegal land seizures, and poor urban transport planning. Residential expansion, driven by the demand for housing, raises urban land costs, contributing to the concentration of social housing in disadvantaged areas with inadequate services and accessibility. The growing preference for low-density housing results in the formation of numerous scattered nuclei, especially through the subdivision of rural land. As a consequence, pressure is generated on high-yield agricultural areas and threatens valuable ecosystems in the region, further complicating the metropolization process.

Datasets and processing

The classification of LULC was made using Google Earth Engine (GEE) cloud computing platform, which

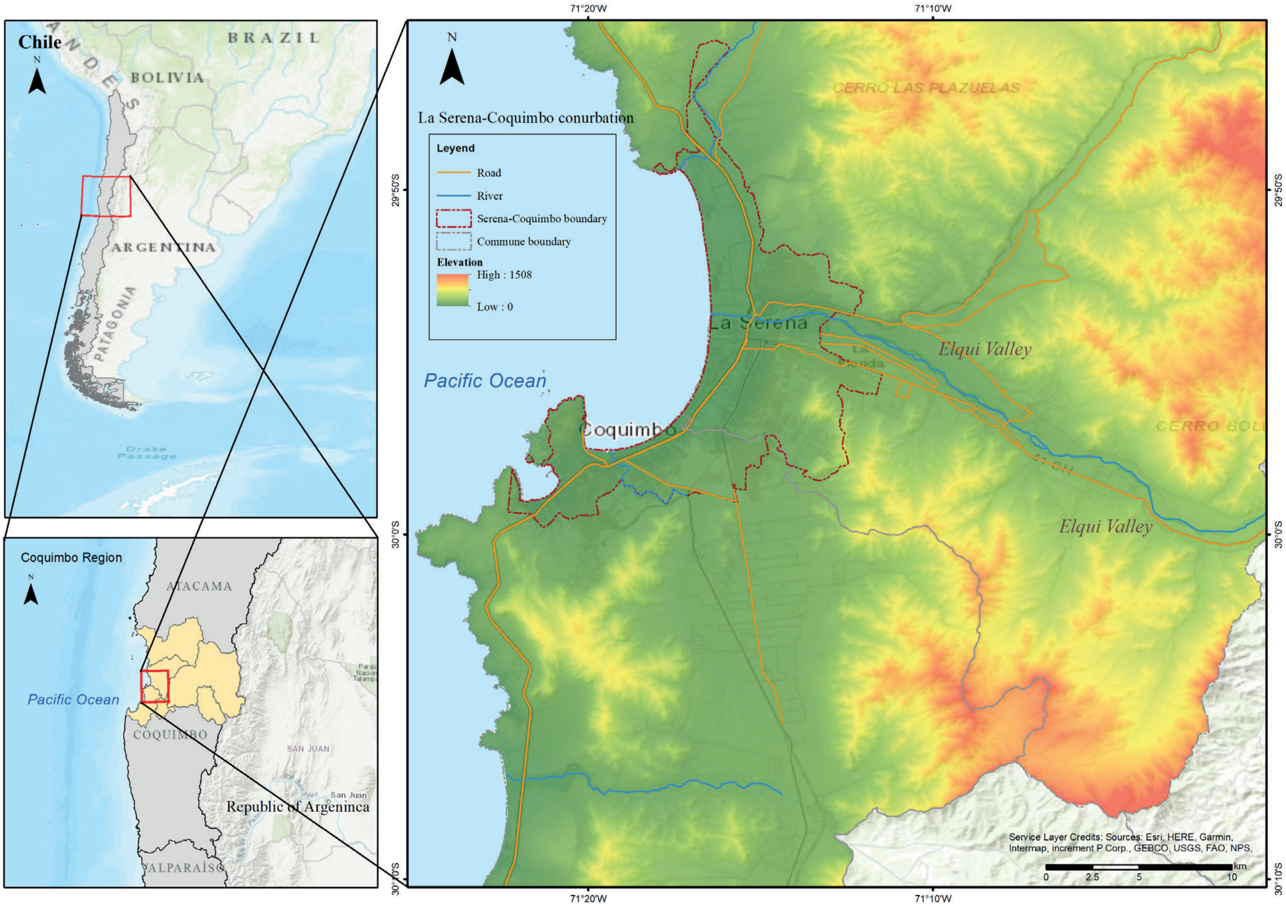

Fig. 1. Geographical location of the study area (La Serena-Coquimbo conurbation)

provides access to satellite images from the United States Geological Survey (USGS) Landsat. For the purpose of this study, we used Landsat Collection 1 Tier 1, because the images in this collection are orthorectified and have well-characterized radiometry, as well as inter-calibration across different Landsat instruments. The georegistration of Tier 1 scenes is consistent and complies with image-to-image tolerances of ≤ 12-meter radial root mean square error (RMSE) (USGS, n.d.). To determine land use for the years 1990, 2000, 2010, and 2020, Landsat 5 Thematic Mapper (TM), Landsat 7 Enhanced Thematic Mapper Plus (ETM+), and Landsat 8 Operational Land Imager (OLI) satellite images were used, with a spatial resolution of 30 meters and the World Geodetic System (WGS) 1984 reference system (Table 1).

Training points were generated by visual inspection of high-resolution imagery available in Google Earth Pro for 1990, 2000, 2010, and 2020. A random forest decision tree classification algorithm (Breiman 2001) was used to classify the satellite images. This algorithm is one of the most widely used for LULC classification (García-Álvarez et al. 2022; Huang et al. 2017; Midekisa et al. 2017) as it allows greater differentiation between different LULC given its multidimensional characteristics (Rodriguez-Galiano et al. 2012) The land use and land classification were based Anderson's system (Level 1) (Anderson 1976), of which seven categories were selected, according to the geographical characteristics of the study area: urban (U), agricultural land (A), water (W), wetland (We), barren land (B), rangeland (R), and forest land (F). For the validation process, 70% of the training points were randomly selected from each class to act as training data, and the rest (30%) was used as the validation dataset.

The challenge of collecting on-site training points necessary for the validation process, crucial for more accurate classification, is acknowledged as one of the limitations of this study.

The framework used in this work is shown in Fig. 2.

Accuracy assessment of the land use maps

For the accuracy assessment of the land use/cover maps for 1990, 2000, 2010 and 2020 confusion matrices were generated based on validation points, from which statistical accuracy measures such as overall accuracy, user's accuracy, and producer's accuracy were calculated (Olofsson et al. 2014). Additionally, the Kappa coefficient (κ) was derived to assess the level of spatial agreement between the classified map and the reference data. The producer's accuracy defines the probability that a reference pixel is correctly

Table 1. Imagery of study area

Sensor	Year	Date	Images	Bands
LANDSAT 5 /C01/T1_TOA	1990	07/09/1990-22/10/1990	3	B1-B7, except B6
LANDSAT/LE07/C01/T1_TOA	2000	12/07/2000-26/11/2000	5	B1-B7, except B6
LANDSAT/LT05/C01/T1_TOA	2010	11/09/2010-31/11/2010	5	B1-B7, except B6
LANDSAT/LC08/C01/T1_TOA	2020	01/07/2020-01/12/2020	2	B2-B7

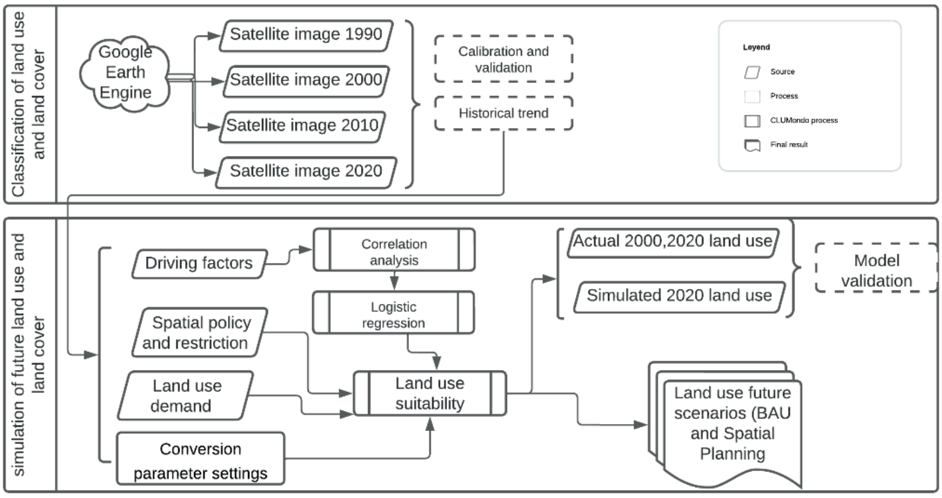

Fig. 2. Methodology flowchart to obtain future land use scenarios

classified (omission error). The user's accuracy defines the probability that a classified pixel in a map represents that category on the ground (commission error). All accuracy parameters have index values between 0 and 1, where 0 signifies low classification accuracy and 1 signifies strong classification accuracy or agreement (Jande et al. 2020).

Simulation of future land use and land cover

The CLUMondo (Conversion of Land Use on Mondial scale) model is an update to Dyna-CLUE that focuses on land systems (van Asselen and Verburg 2012), which makes it possible to model on a global scale by introducing macro-level demands (top-down) and at the same time to configure the model according to local factors (bottom-up) (van Asselen and Verburg 2013). Ornetsmüller et al. (2016) implement this new CLUMondo approach to model land use changes in the Lao People's Democratic Republic (Laos) based on three scenarios. This spatially explicit model integrates socioeconomic, demographic and environmental variables to simulate future land use changes (Arunyawat and Shrestha 2018; Malek and Verburg 2018).

Two scenarios were considered to simulate the future projection of LULC BAU and Spatial Planning (SP). The first one establishes a trend scenario where the current conditions of the territory do not change. It also incorporates the national protected areas as restriction zones for any change in land use. The second is based on the projected urban areas of the Intercomunnal Regulatory Plan of Elqui Province (PRI Elqui, in Spanish acronym) approved in 2019 (SEREMI 2013a; SEREMI 2013b), as well as restriction zones composed of green areas and protection zones at the district level of the municipalities of La Serena and Coquimbo (Municipality of Coquimbo 2014; Municipality of La Serena 2020) and at the intercommunal level (La Serena-Coquimbo conurbation).

The CLUMondo model (van Asselen and Verburg 2013) was used to project yearly time step land uses until 2042, coinciding with the PRI Elqui's projected year (SEREMI 2013a). Unlike other models, CLUMondo does not assume a hierarchy when allocating LULCs. Instead, it simultaneously addresses multiple demands (van Vliet and Verburg 2018).

The model requires four main inputs: location suitability, spatial policies and restrictions, land use demand, and land use conversion settings. In this study, the demand for goods and services is not used. Instead, the surface area demand for each land use type is predefined. As result, land system are allocates based on transition potential at time (t) and location (i) for each land system (LS) and the demand for that specific year (Eq. 1). The transition potential (*Ptrans t,i,LS*) is calculated as sum of local suitability (*Ploc t,i,LS*), the conversion resistance (*Pres LS*) and neighboorhood effect (*Pneigh t,i,LS)* as well as a competitive advantage of a land system (*Pcomp t,LS*) (van Vliet and Verburg 2018).

$$Ptrans\ t,i,LS = Ploc\ t,i,LS + Pres\ LS + \\ + Pneigh\ t,i,LS + Pcomp\ t,LS \qquad (1)$$

The local suitability of a location is estimated from the relationship between driving forces and land use. Logistic regression is used for each land category separately to estimate the probability of occurrence for each cell. Prior to the regression, Pearson's correlation analysis (R^2) was performed to discard highly correlated variables whose value exceeds 0.9.

A total of 17 variables were selected and grouped into three main categories: geographic, urban, and demographic (Table A.1). Altitude and slope variables were derived from the Digital Elevation Model (DEM) from Alos Palsar (2016) accessed through Alaska Satellite Facility - Distributed Active Archive Center (ASF-DAAC[3]).

The selection of the driving forces consists, firstly, of the researcher's knowledge of the study area and its territorial dynamics. Various bibliographic sources and case studies were reviewed to identify these driving forces (Geist and Lambin 2002; Verburg et al. 2021; Verburg et al. 2004; Zondag and Borsboom 2009). In addition, various regional and local stakeholders involved in the territorial planning process of the study area were consulted. Secondly, the significance value (less than 0.05), indicates how closely related the independent variable is to the specific land use. The accuracy of the logistic regression is calibrated from the Area Under the Curve value (AUC) (Pontius and Schneider 2001).

In terms of spatial policies and restrictions, the main sources of information to identify the policies that restrict urban development (restriction) and those that facilitate its expansion (location specific) were the territorial planning instruments corresponding to the study area, both at municipalities (Municipality of Coquimbo 2014; Municipality of La Serena 2020) and intercommunal scales (SEREMI 2013b, SEREMI 2013a). For the Spatial Planning scenario, location specific preferences were added as part of the spatial policies, corresponding to urban extension zones. These areas indicate the model's high probability for

[3] https://asf.alaska.edu

urban growth (preference), specified in the parameters by assigning weights to each land use.

Land use demands were calculated independently of the CLUMondo model and need to be specified for each scenario. In this study, the demand for goods and services is not used, but rather the demand for surface area is predefined for each land use type. This parameter restricts the simulation by defining a specific land use growth. The LULC demand for the two scenarios up to 2042 was calculated from a simple regression curve based on the observed area in the period from 1990 to 2020. For the Spatial Planning scenario, the demand for urban land use was calculated based on data from the PRI Elqui regarding urban and extension areas. The assumption was defined as "the water land use will maintain the same surface area as observed in 2020.

The conversion rules determine the temporal dynamics of the simulations and two sets of parameters: (1) conversion resistance and (2) land use transition sequences that must be specified before running the model. The conversion resistance parameter determines the strength or elasticity of one land use to change to another. The second set of parameters requires setting the conversion matrix and order. The first indicates the possible transitions between the land uses allowed in the model, while the second one tells the model the possibilities for land use change to satisfy demand.

Model validation

To validate the results, the methodological approach of Pontius et al. (2008) was applied in this research, which consisted of two phases. In the first phase, three maps were superimposed together: time reference map 1 (2000), time reference map 2 (2000), and time prediction map 2 (2020).

The results were entered into a three-dimensional table, where five possibilities were identified: correct for observing change and predicting change (hits); correct for observing persistence and predicting persistence (correct rejections); wrong for observing change and predicting change in the wrong category (wrong hits); wrong for observing change and predicting persistence (misses); and wrong for observing persistence and predicting change (false alarms) (Pontius et al. 2008). These results were used to calculate three proposed complementary statistical measures by Pontius et al. (2008): the figure of merit, producer's accuracy and user's accuracy.

RESULTS

Land use dynamics from 1990 to 2020

The spatio-temporal dynamics of the La Serena-Coquimbo conurbation over the observed period reveal significant transformations indicative of socio-economic and environmental dynamics, with changes measured in hectares (Fig. 3). The expansion of urban areas by 11,034 hectares highlights a notable trend towards urbanization. This growth reflects the increasing need for residential, commercial, and industrial spaces, raising concerns about the sustainability of such expansion in terms of ecosystem degradation and occupation of agricultural lands.

In this sense, agricultural land experienced a dynamic shift, with a net decrease of 6,396 hectares despite a gain of 8,103 hectares. This fluctuation is attributed to the conversion of previously non-agricultural lands to farming and the loss of agricultural areas to urban development, illustrating the complex balance between food security, urban expansion, and land use policy. Barren land shows the most significant decrease, with a loss of 18,748 hectares, indicating a shift toward more productive or developed land uses.

Given the dominance of rangelands in the study area, there was a net increase of 2,812 hectares, reflecting both losses and gains. The forest category loses 285 hectares, noting that this classification includes areas covered by natural trees and plantations. In this context, areas of crops previously classified as agricultural land were categorized under this one in the process of satellite image classification. The correction was made in the post-processing of the LULC classifications, leading to the observation that the forest exhibited the highest loss in the study area. In general, agricultural land, water, and rangeland maintained a positive balance during the analyzed period.

The remaining LULC, such as water and wetland experienced losses of 102 and 641 hectares, respectively, along with marginal gains. These changes emphasize the vulnerability of aquatic and semi-aquatic ecosystems to human activity and climatic fluctuations, necessitating enhanced conservation efforts to protect these ecologically significant areas.

The accuracy of the LULC classification shows that the overall accuracy of the classification is 0.91 (1990), 0.93 (2000), 0.97 (2010), and 0.99 (2020), which indicates a strong accuracy of the classification performed (Table A.1). The Kappa index result for the four years studied is above 0.8, which corresponds to a very good level of spatial agreement between the classified map and the reference data. The average values of

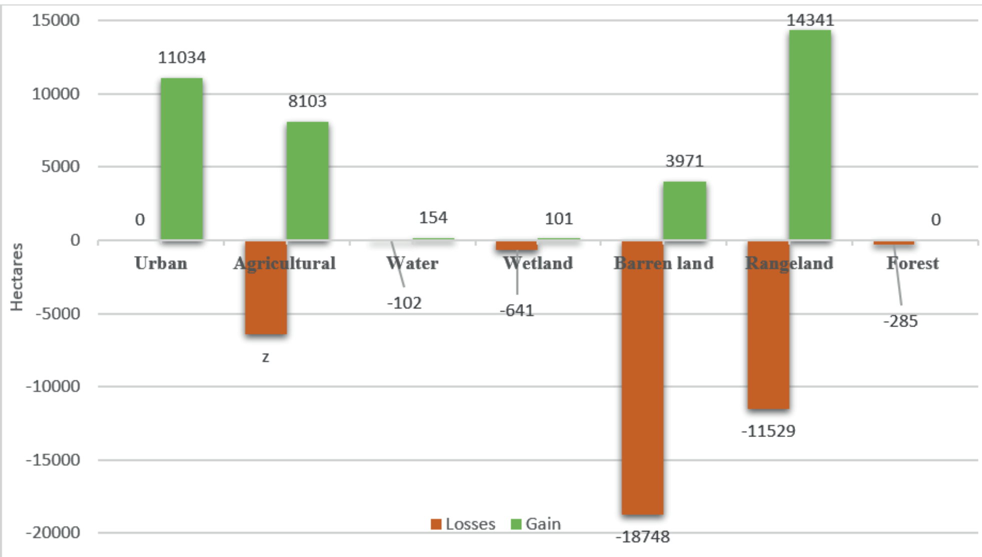

Fig. 3. Gains and losses of land use and land cover, 1990-2020

producer and user accuracy are higher than 0.9 so a good result is observed between commission and omission errors (Zhang et al. 2021).

The result of the evolution of land use change between 1990-2020 emphasizes the need to implement management and planning strategies for sustainable land use. These strategies should facilitate adaptation to urbanization demands, enhancing agricultural productivity, preserving ecosystems, and adapting to climate change.

Model result under two scenarios

BAU scenario. The increase in urban land use is caused by the displacement of other land cover and uses and extends both inside and outside the La Serena-Coquimbo conurbation. The urban land will cover 10% of the total area in 2042 and it will increase 54% between 2020 and 2042 (Fig. 4). The demand for urban land continues to exhibit an upward trend in both scenarios until 2042. In the BAU scenario, the demand for urban land will reach 21,610 ha by 2042, representing a 54% increase compared to 2020.

Agricultural land tends to disappear towards the coastal area of the conurbation due to the expansion of urban land, with some patches of barren land and wetland (Fig. 5a). The ratio of agricultural land is 12.6% of the total surface area of the study area, with the major concentration in the lower sector of the Elqui valley, where several urban areas are located close to the conurbation. The loss of wetland is 34.3% compared to the modeled year. Consequently, a large part of the wetland systems in the study area will disappear by 2042, and those that remain will react to the restrictions of this scenario.

The spatial distribution of urban land determines the configuration of a series of spatial patterns of urban land growth, which correspond to the form of urban sprawl. The first urban growth pattern can be seen in the advance of urban sprawl in the immediate proximity of the conurbation boundary, which is more evident towards the east of La Serena and south of Coquimbo. Likewise, urban sprawl increases towards the north of the conurbation. The second spatial pattern is identified around the study area's main communication axes and is characterized by a linear urban land expansion. The third pattern is presented as dispersed urban patches and focuses Elqui Valley's lower section and the study area's southeast. This type of growth is concentrated on higher terraces up to almost 300 m above sea level, with a slope steepness of more than 15°.

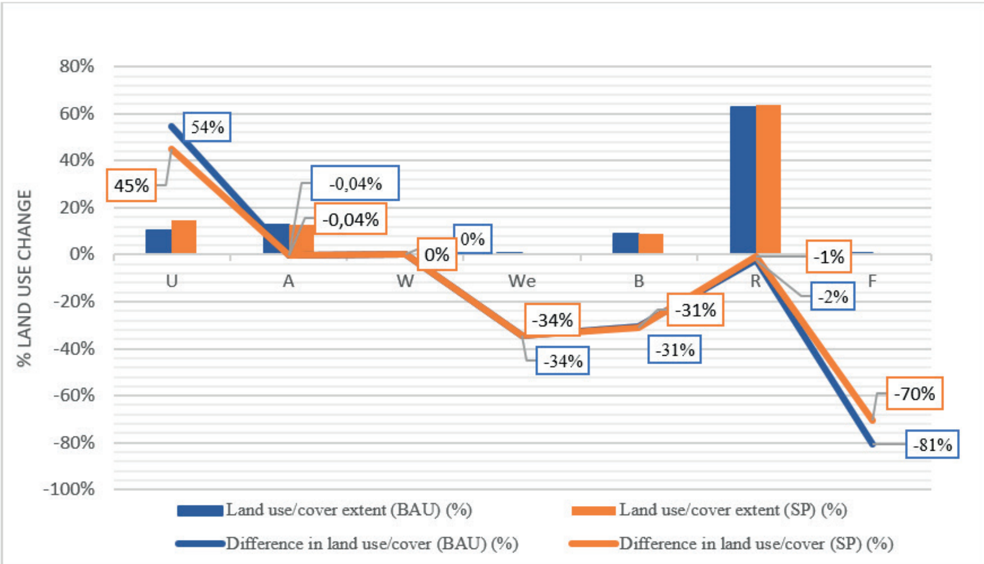

Fig. 4. Land use change between 2020-2042 for BAU and Spatial Planning (SP) scenarios according to the different land uses and land covers

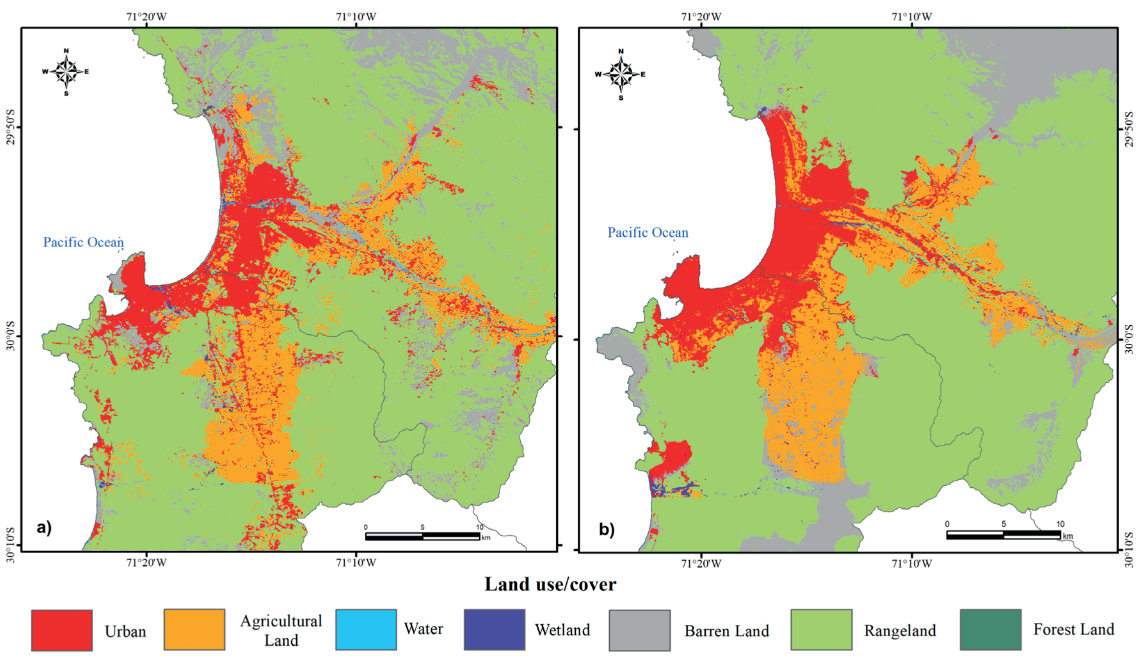

Fig. 5. Simulated scenarios of land use and land cover by 2042. a) BAU, b) Spatial Planning

Spatial Planning Scenario. The demand for urban land use in the Spatial Planning scenario is lower than in the previous one. Urban land growth is observed both in the coastal zone and in the urban extension areas proposed by the planning instruments. The projected urban land area for 2042 is 20,302 ha, a 45% increase from 2020, representing 14.6% of the total area. This figure aligns with the proposed 30% growth indicated by key stakeholders participating in the territorial planning process in the study area, as confirmed during interviews to validate the modeling results. The growth of the urban LULC area in 2042 is 45% compared to 2020 and its ratio reaches 15% of the total area (Fig. 5b).

Under this scenario, agricultural land use is better represented within the urban limits of the conurbation; however, its ratio is similar to that of the BAU scenario (13%) (Fig. 3). The permanence of agricultural land in these sectors is due to the fact that these areas concentrate important agricultural production at the regional level. Although the surface ratio of wetlands, such as agricultural land, is the same as in the BAU scenario (0.3%), the spatial representation is more evident and responds to restriction configuration to protect important ecosystems in the conurbation. However, the trend indicates a loss of almost 35% of wetland area by 2042. Forest land will experience the most significant losses by 2042, both in the BAU and SP scenarios.

In this scenario, three spatial urban growth patterns are evident, as in the BAU scenario. The expansion of urban land towards the periphery of the conurbation, where the change of urban land use over agricultural land is patent, and the growth around the main road axes of the conurbation. The third spatial pattern, corresponding to urban patches, is more prominent in this scenario and is concentrated in three specific sectors. First, toward the east of the study area (lower section of the Elqui Valley). Second, to the southeast of the conurbation, where patches are isolated among agricultural land. Third, to the west of Coquimbo, where urban land consolidation is observed by the merger of small urban patches and a strong urban land expansion to the south of the study area.

Analysis of the logistic regression results reveals that the most important variable is migration density, although in the reverse direction (Table A.2). This driving force is an important component of the demographic dynamics of La Serena-Coquimbo, as statistics show an exponential increase in migration at the regional level between 1992-2017, which corresponds to the census periods. Upon consulting with key actors on this aspect, it was found that, in the Coquimbo region, migration increased during the time of the COVID-19 pandemic in the period 2020-2022.

The second most important variable was the commercial value of land, which showed a strong relationship with urban and agricultural land use and land cover. This results from the neoliberal model installed in Chile since 1973, where urban land ceases to be a scarce resource and its profitability depends on market trends. In this context, the real estate industry represents a powerful actor that can generate land speculation and change the direction of urban land occupation, as well as tighten the problem of spatial segregation by presenting more significant opportunities for higher socio-economic groups.

Agricultural land, as opposed to urban land, has an inversely proportional relationship with the commercial value of land, as the price tends to rise within the urban boundary and fall as it moves away from it. Hence, there is an increase in the number of residential plots and an increase in interest in settling in these areas. This is consistent with the observed dynamics of the evolution of LULC in the La Serena - Coquimbo conurbation between 1990 and 2020.

The sensitivity analysis was carried out while interpretating collinearity and logistic regression of driving forces. In this regard, out of the 20 variables initially stipulated for the model, three (distance from commercial establishments, schools, and tourist attractions) were discarded as they did not show significant relevance for the change in urban land use according to the coefficient (β). The retained variables were those identified as the most important in the literature and those considered relevant at the local level, such as the commercial land value. This analysis is critical because it allows for refining and optimizing the model by eliminating variables that do not contribute significantly, thereby improving its accuracy and applicability in predicting changes in urban land use.

Integration of the model to metropolization

The results of the validation of the CLUMondo model by quantitative analysis determine the spatial agreement between an observed and a simulated image for the same period (Fig. 6). The observed image (time 1) corresponds to the year 2000 and the reference and prediction map (time 2) to 2020. The three-way comparison indicates that there is a 23% success rate for observing change and predicting change (hits). The rest is distributed among different types of errors, where the maximum value corresponds to false alarms with 34%, then misses with 29%, and finally, wrong hits with 14% of the total. The validation statistics variables record the results of a figure of merit of 23%, producer accuracy of 35% and user accuracy of 33%.

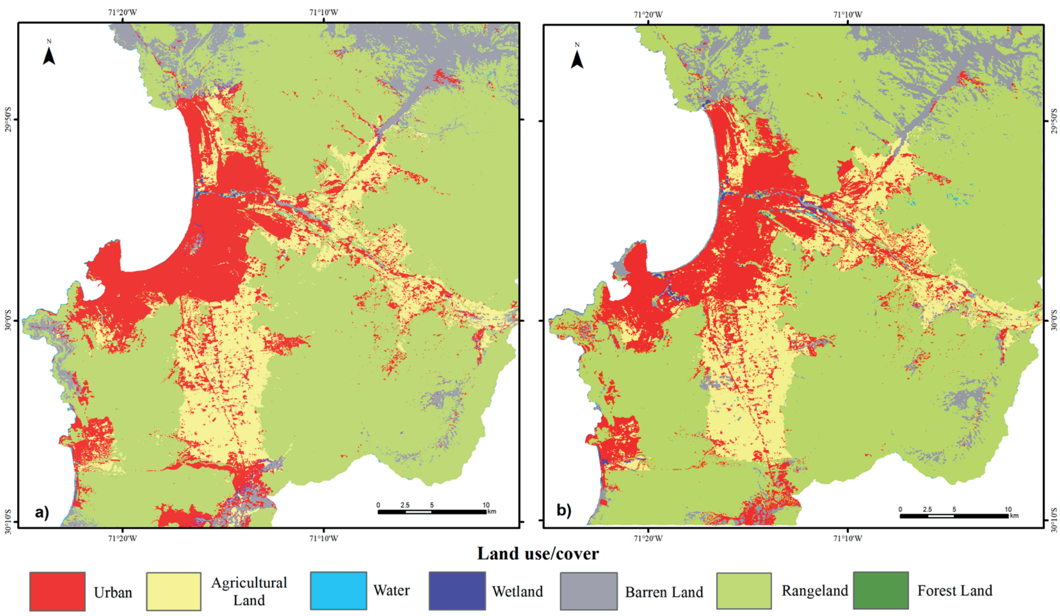

Fig. 6. Actual (a) and predicted (b) land use and land cover maps, 2020

The simulation models under the BAU and Spatial Planning scenarios using the CLUMondo model project change in LULC to 2042. The projection anticipates that the conurbation's growth will follow the trend of annexing territories at the edges of cities, which consolidate as urban areas due to pressure from changes in agricultural land use. This expansion is driven by the need to find available land at lower prices, contributing to the increase in informal settlements and illegal land occupations in Chile. The demand for urban land reflects on the one hand, a scenario that continues the trend of urban land growth without many obstacles and, on the other hand, a scenario that is in line with the proposal of the Intercommunal Regulatory Plan of the Elqui province. The demand for agricultural land remains stable, following a historical trend, as does the demand for rangeland. In contrast, the rest of the land uses show a decreasing trend in surface area. Under the BAU scenario, wetland and forest show the highest loss of land area, while agricultural land, water, and rangeland are the least affected by 2042.

The simulation result under the BAU and Spatial Planning scenarios shows a very similar spatial distribution. However, the first scenario contemplates a higher dispersion of urban patches throughout the study area, while in the second scenario, urban land expansion is more confined and controlled. Under this logic, the Spatial Planning scenario is identified as the most likely as it integrates the urban extension zones proposed by PRI Elqui. Therefore, it indicates to the model the areas of preference for change for urban land. This scenario also contemplates green and protected areas based on territorial instruments at the district and inter-communal levels in order to restrict future land use change.

In this context, it is expected that in the future La Serena-Coquimbo conurbation will be established as a metropolitan area, which answers the research question posed. The legal conditions set out in Article 4 of Decree 98 (2019[4]) are fundamental for establishing metropolitan areas in Chile. These areas must be formed by two or more municipalities of the same region and each of these municipalities must have a population of more than 250,000 inhabitants. Furthermore, it is important to have a spatial continuity in the urban fabric that facilitates mobility and accessibility between the different municipalities within the metropolitan area. This promotes greater connectivity and a better distribution of urban services and complements the functions between the municipalities that form them.

DISCUSSION

Patterns and modeling

The spatial and temporal evolution of the La Serena-Coquimbo conurbation from 1990-2020, according to its LULC configuration, presents the characteristics of the contemporary Latin American city model in its last phase of development: the fragmented city identified by a sectorial-linear tendency and a marked cellular growth of cities (Bähr and Borsdorf 2005).

The growth of the intermediate conurbation cities of La Serena and Coquimbo occurs in a fragmented manner, which responds to a historical process of territorial occupation by separate sectors (Orellana 2020). Urban sprawl occurs progressively between 1990 and 2020, where urban land spreads over other land uses and extends urban sprawl by the annexation of these areas to the boundaries of the agglomeration (Nasar et al. 2021). The road infrastructure of the conurbation, as well as geographical elements such as the Elqui River and the mountain range, are elements that affect the problem of fragmentation of the conurbation system, as they inevitably divide the territory into consolidated and physically separated centers.

While the trend between 1990-2020 shows that fragmentation appears to be less and less intense within the La Serena-Coquimbo conurbation, the increase in the number of isolated urban patches exacerbates the problem of socio-spatial segregation in both cities, as the residential plots are upper-middle and high socio-economic housing, while those living in camps are generally below the poverty or extreme poverty line (Hidalgo et al. 2009).

The result of the spatial evolution of land cover and land use from 1990 to 2020 is consistent with the multi-temporal study of land use variation in the La Serena-Coquimbo conurbation conducted by the Directorate of Extension and External Services (DESE in Spanish acronym) of the Faculty of Architecture at the Pontifical Catholic University of Chile (DESE 2016).

Linear interpolation based on the historical trend from 1990-2020 was used to calculate future demand in this study, and then demand was calibrated based on the information obtained from the sources consulted. Yang et al. (2022) applied the same method for a land use modeling study in the Yanhe watershed, China using CLUMondo under three different scenarios. In contrast to the results obtained using other models, such as the Land Change Modeler module used by Henríquez and Hidalgo (2023) to model the growth of mid-sized Chilean cities, the projection of future demand in CLUMondo allows more control over possible land use changes by projecting demand for the entire land classification system.

The comparison with Waiyasusri and Chotpantarat's study of Koh Chang, Thailand (2022) reveals similarities in the behavior of selected variables like population density, altitude, and slope. However, in the case of La Serena-Coquimbo, the most important demographic variable is migration density. The logistic regression result emphasizes the significance of the local context in each territory. Although both studies focus on tourist cities, the authors do not include the perspective of key actors in their variable selection stage which enriches the variable selection and adds an additional layer of contextualization.

The urban expansion of La Serena-Coquimbo, according to the urban growth patterns observed in the simulation, resembles the situation observed in the city of Temuco, where the real estate industry plays a decisive role in the diffuse and fragmented configuration of the conurbation (Maturana et al. 2021). In the case of the metropolization of Quito (Salazar et al. 2020), a similar model (Dyna-CLUE) was used considering driving forces associated with proximity to urban equipment and infrastructure, transportation, and slope.

Strengths and weaknesses of the model approach

The prospective modeling of land use changes using the CLUMondo model proves to be effective in projecting spatially explicit scenarios, as it considers a series of parameters such as spatial policies and growth restrictions that can be configured according to the sustainability

[4] Ministry of The Interior and Public Security. Undersecretary of Regional and Administrative Development. Decree number 98 of 2019. Approves the regulation that sets the minimum standards for the establishment of metropolitan areas and establishes rules for their constitution.

criteria established in the process of the SEA within the framework of the PRI Elqui.

It is important to highlight that the CLUMONDO model allows the introduction of no more than seven variables for each land category, which can be considered a limitation in its methodology. The precision required to select the most pertinent driving forces for LULC necessitates meticulous consideration by the researcher. Another limitation to highlight is the difficulty of collecting spatial data for all the analyzed years, so it was decided to use the data closest to the year 2020, such as demographic and urban data, as well as land use capability.

On the other hand, although the model allows the user to control and anticipate territorial conflicts between various land uses through spatial policies, its effectiveness depends largely on the quality of the base information and the precision with which spatial policies are configured. Furthermore, the model´s capacity to anticipate the transition between land use and land cover may be limited by the complexity and dynamics of territorial processes, as well as by the uncertainty in future projections.

Another limitation is that, while the simulated scenarios can provide future trends for the territory, they cannot anticipate all the potential changes and events that may occur in the future. This limitation can restrict their utility in the formulation of territorial planning instruments. Therefore, it is necessary to complement modeling with other approaches and consider its results as one of the many tools in decision-making rather than an exact prediction of the future.

The utility of modeling through the CLUMONDO model for the planning process and the evaluation of development options within the framework of the SEA lies in its ability to comprehensively incorporate parameters based on the objectives and environmental factors of the EAE of the PRI Elqui. These objectives include the conservation of soils with high agroecological value, the preservation of biodiversity, and the safeguarding of the coastal landscape. Including these elements strengthens the representation of relevant environmental, social, and economic factors. Additionally, this tool allows for the rapid incorporation of changes in demand and future projects that may be reflected in the proposed plan for the sustainable growth of the study area.

The participation of key stakeholders in the construction and validation of the model reinforces its robustness and relevance (Henríquez et al. 2022). This ensures that regional and local perspectives are duly considered, thereby contributing to more informed decision-making and the design of development strategies that align effectively with sustainability goals and territorial planning.

Future metropolization

The projected modeling scenarios show the future trend of urban expansion, configured from the analysis of the spatial evolution of LULC, which evidences a future conformation of the fourth metropolis in the country. Thus, the growth of urban land continues to move towards other uses, which generates the loss of land of high agro-ecological value, both inside and outside the urban boundary, and a substantial decrease in natural environments, such as the wetland systems present in the study area.

Henríquez and Hidalgo (2023) estimate that the La Serena-Coquimbo conurbation population will grow to over 650,000 inhabitants and the surface of the urban area will be around 14,000 ha by the year 2065. The research results project that the consolidated area will be 9,935.65 ha for the BAU scenario and 9,376.29 ha for the Spatial Planning scenario by 2042. If the trend of population and urban area growth in the conurbation continues at the same rate as in the last three decades, it can be expected that by 2065 the size of the urban area will be close to the results of Henríquez and Hidalgo (2023), and the conurbation will be considered a metropolitan area with more than 500,000 inhabitants. These conditions ensure that such areas are adequately equipped to address the challenges of urbanization, promote regional development, and provide better living conditions for their residents. By meeting these criteria, metropolitan areas can play a vital role in fostering sustainable and integrated urban development in the country.

The various urban forms identified in this study as spatial patterns of urban growth, as well as the spatial dynamics of the territory, react differently to the processes of metropolization, some being more resistant than others, as it presented in a study case of the city of Algiers (Mezoued 2022). The author states that the new transport infrastructure, particularly tramway routes, aimed to reduce the spatial fragmentation of the city, reveals a transformation in the urban fabric and its adaption to change. This case study contrasts with La Serena-Coquimbo, which undergoing metropolization.

However, in order to establish itself as a metropolitan system, La Serena-Coquimbo conurbation faces major challenges at a different scale, either as mid-sized cities at the district level or as a common urban area recognized by the PRI Elqui. The geomorphology of the territory presents natural barriers to urban development and contributes to a high vulnerability to tsunamis, while the real estate dynamism and the fluctuation of the seasonal floating population exacerbate the problem of road congestion (Aguirre, Olivares and Orellana 2018).

The analysis of spatial dynamics in the La Serena-Coquimbo conurbation provides not only a methodology but also valuable information about spatial patterns and future urban expansion. These results, obtained from spatially explicit models like CLUMondo, offer valuable insight and allow the anticipation and mitigation of potential environmental impacts and challenges. Using a spatial modeling perspective, it is possible to enrich the understanding of similar processes in intermediate cities undergoing metropolization globally. In this sense, the simulation can help decision-makers identify areas suitable for urban growth while preserving natural ecosystems, aiding in the development of sustainable urban development strategies.

CONCLUSIONS

Spatially explicit models have proven to be a powerful tool for decision-makers tasked with projecting urban growth, particularly in conurbated cities undergoing metropolization. These future metropolises will demand substantial coordination and governance efforts to address complex management issues, which the simulation model helps to visualize to achieve more articulated and sustainable cities. The integration of CLUMondo´s results into policymaking can lead to more informed decisions regarding sustainable urban development, infrastructure planning, and climate change adaptation. Ultimately, it contributes to strengthening the knowledge base in the field of sustainable urban development. Thus, it is possible to avoid processes of fragmentation, dispersion, and diseconomies in the governance of a metropolitan area, contributing to the creation of more resilient and efficient cities.

For a more accurate projection of future scenarios and further development of a research topic, it is essential to enrich the CLUMondo model with a broader perspective, including economic variables such as agricultural and livestock production. These variables are crucial for understanding the interactions between economic development and land use, which allows to evaluate how the economy affects urban expansion and the transformation of rural areas. Likewise, incorporating dynamic variables such as demographics, migration, and urban development is fundamental. These factors, reflecting population changes and infrastructure demands, are key to modeling how population movements and demographic growth foster urban expansion and land demand, influencing land planning and environmental sustainability. Such an approach not only improves the analysis of future scenarios but also strengthens decision-making in urban planning and land management, facilitating the anticipation and mitigation of conflicts between socioeconomic development and environmental protection.

REFERENCES

Aguirre, C., Olivares, R., and Orellana, A. (2018). Patrones de crecimiento urbano en la metropolización de sistemas urbanos intermedios. El caso de la conurbación La Serena-Coquimbo. Congreso Internacional Ciudad y Territorio Virtual (CTV), DOI: 10.5821/ctv.8234.

Anderson, J. (1976). A Land Use and Land Cover Classification System for Use with Remote Sensor Data. Washington: US Government Printing Office, DOI: 10.3133/pp964

Arunyawat, S. and Shrestha, R.P. (2018). Simulating future land use and ecosystem services in Northern Thailand. Journal of Land Use Science, 13(1–2), 146–165, DOI: 10.1080/1747423X.2018.1496157.

van Asselen, S. and Verburg, P. (2013). Land cover change or land-use intensification: simulating land system change with a global-scale land change model. Global Change Biology, 19(12), 3648–3667, DOI: 10.1111/gcb.12331.

Bähr, J., and Borsdorf, A. (2005). La ciudad latinoamericana. La construcción de un modelo. Vigencia y perspectivas. Urbe. Revista de ciudad, urbanismo y paisaje (Lima), 2(2), 207-222.

Batty, M. (2013). The New Science of Cities. Cambridge: MIT press, DOI: 10.7551/mitpress/9399.001.0001

Borsdorf, A. (2003). Cómo modelar el desarrollo y la dinámica de la ciudad latinoamericana. EURE. Revista latinoamericana de estudios urbano regionales, 29, 37–49, DOI: 10.4067/S0250-71612003008600002.

Breiman, L. (2001). Random Forests. Machine Learning, 45(1), 5–32, DOI: 10.1023/A:1010933404324.

DESE (2016). Desarrollo Urbano y El Cambio Climático: Huella Actual e Histórica, Escenarios de Crecimiento Urbano y Estudios Básicos Sobre Mitigación y Adaptación al Cambio Clima Tico En La Conurbación La Serena/Coquimbo.

García-Álvarez, D., Lara Hinojosa, J., Jurado Pérez, F.J., and Quintero Villaraso, J. (2022). Global General Land Use Cover Datasets with a Time Series of Maps. In: D. García Álvarez and M. Camacho Olmedo, M. Paegelow and J. Mas, eds. Land Use Cover Datasets and Validation Tools: Validation Practices with QGIS. Cham: Springer International Publishing, 287–311, DOI: 10.1007/978-3-030-90998-7.

Geist, H. and Lambin, E. (2002). Proximate Causes and Underlying Driving Forces of Tropical Deforestation: Tropical forests are disappearing as the result of many pressures, both local and regional, acting in various combinations in different geographical locations. BioScience, 52(2), 143–150, DOI: 10.1641/0006-3568(2002)052[0143:PCAUDF]2.0.CO;2.

Henríquez, C. (2014). El problema ambiental de la urbanización. In: C. Henríquez, Modelando El Crecimiento de Ciudades Medias Chilenas, 1st ed. Santiago de Chile: Ediciones UC, 29–94.

Henríquez, C. and Azócar, G. (2007). Propuesta de modelos predictivos en la planificación territorial y evaluación de impacto ambiental. Scripta Nova. Revista Electrónica de Geografía y Ciencias Sociales, [online] Volume 11. Available at: https://www.ub.edu/geocrit/sn/sn-24541.htm. [Accessed 10 april 2022].

Henríquez, C. and Hidalgo, R. (2023). Escenarios de crecimiento en ciudades medias chilenas: lectura de trayectorias futuras para diferentes tipologías urbanas. In: C. Henríquez, W. Ribeiro, V. Aprigliano, and G. Salazar, eds., Urbanización y Ciudades Medias. Territorios y Espacialidades En Cuestionamiento. Santiago de Chile: Impresión Gráfica LOM, 135-154.

Henríquez, C., Morales, M., Qüense, J., and Hidalgo, R. (2022). Future land use conflicts: Comparing spatial scenarios for urban-regional planning. Environment and Planning B: Urban Analytics and City Science, 50(2), 332-349, DOI: 10.1177%2F23998083221111404.

Henríquez-Dole, L., Usón, T., Vicuña, S., Henríquez, C., Gironás, J., and Meza, F. (2018). Integrating strategic land use planning in the construction of future land use scenarios and its performance: The Maipo River Basin, Chile. Land Use Policy, 78, 353–366.

Hidalgo, R., Arenas, F., and Monsalve, R. (2009). La conurbación La Serena-Coquimbo: problemas y desafíos de su transformación metropolitana. In R. Hidalgo, C. De Mattos, F. Arenas, eds., Chile: del país urbano al país metropolitano. Santiago de Chile: GEOlibros & EURE-Libros, 161–187.

Hidalgo, R., Borsdorf, A., and Plaza, F. (2009). Parcelas de agrado alrededor de Santiago y Valparaíso: ¿Migración por amenidad a la chilena? Revista de geografía Norte Grande, (44), 93–112, DOI: 10.4067/S0718-34022009000300005.

Hidalgo, R., De Mattos, C., and Arenas, F. (2009). Chile: Del País Urbano al País Metropolitano. Santiago de Chile: GEOlibros & EURE-Libros.

Huang, H., Chen, Y., Clinton, N., Wang, J., Wang, X., Liu, C., Gong, P., Yang, J., Bai, Y., Zheng, Y., and Zhu, Z. (2017). Mapping major land cover dynamics in Beijing using all Landsat images in Google Earth Engine. Remote Sensing of Environment, 202, 166–176, DOI: 10.1016/J.RSE.2017.02.021.

INE (2019). Análisis Del Censo de La Población y Vivienda. Región de Coquimbo.

Islam, S., Li, Y., Ma, M., Chen, A., and Zhongxi, G. (2021). Simulation and Prediction of the Spatial Dynamics of Land Use Changes Modelling Through CLUE-S in the Southeastern Region of Bangladesh. Journal of the Indian Society of Remote Sensing, 49, 2755–2777, DOI: 10.1007/s12524-021-01402-w.

Jande, J., Nsofor, G., and Abdulkadir, A. (2020). Modelling of Urban Growth with Land Change Modeler in Otukpo Metropolis of Benue State, Nigeria. International Journal of Engineering Applied Sciences and Technology, 4(9), 26–40.

Llop, J.M. and Cifuentes, P.A. (2015). Repensando la ciudad: estrategias de desarrollo urbano sostenible de las ciudades intermedias de América Latina. Nodo: Arquitectura. Ciudad. Medio Ambiente, 10(19),73–83.

Nasar-u-Minallah M., Zia S., Rahman A., Riaz O. (2021). Spatio-Temporal Analysis of Urban Expansion and Future Growth Patterns of Lahore, Pakistan. Geography, Environment, Sustainability, 14(3), 41-53, DOI: 10.24057/2071-9388-2020-215.

Malek, Ž. and Verburg, P.H. (2018). Adaptation of land management in the Mediterranean under scenarios of irrigation water use and availability. Mitigation and adaptation strategies for global change, 23(6), 821–837, DOI: 10.1007/S11027-017-9761-0.

Maturana, F., Morales, M., Peña-Cortés, F., Peña, M., and Vielma, C. (2021). Urban Growth, Real Estate Development and Indigenous Property: Simulating the Expansion Process in the City of Temuco, Chile. ISPRS International Journal of Geo-Information, 10(2), 101, DOI: 10.3390/IJGI10020101.

Maturana, F., Peña Cortés, F., Morales, M., and Vielma López, C. (2021). Crecimiento urbano difuso en ciudades intermedias. Simulando el proceso de expansión en la ciudad de Temuco, Chile. Urbano (Concepción), 24, 62–73, DOI: 10.22320/07183607.2021.24.43.06.

Maturana, F., Peña-Cortés, F., Carrasco, F., and Telias, M. (2019). Dinámicas urbanas y transición hacia espacios metropolitanos: el caso de Valdivia y la Región de Los Ríos, Chile. Urbe. Revista Brasileira de Gestão Urbana, 11, DOI: 10.1590/2175-3369.011.e20180143.

Maturana, F., Sposito, M., Bellet, C., and Henríquez, C. (2017). Sistemas Urbanos y Ciudades Medias En Iberoamérica. Santiago de Chile: Impresión gráfica LOM.

Mezoued, A.M. (2022). Fragmentation, metropolization and resilience of urban forms in Algiers. CyberGeo: European Journal of Geography, DOI: 10.4000/cybergeo.38150.

Midekisa, A., Holl, F., Savory, D.J., Andrade-Pacheco, R., Gething, P.W., Bennett, A., and Sturrock, H.J.W. (2017). Mapping land cover change over continental Africa using Landsat and Google Earth Engine cloud computing. PloS ONE, 12(9), DOI: 10.1371/journal.pone.0184926.

Municipalidad de Coquimbo (2014). Plan Regulador Comunal de Coquimbo (Actualización). Informe Ambiental.

Municipalidad de La Serena (2020). Plan Regulador Comunal de La Serena (Actualización). Memoria Explicativa. La Serena.

Olofsson, P., Foody, G., Herold, M., Stehman, S., Woodcock, C., and Wulder, M. (2014). Good practices for estimating area and assessing accuracy of land change. Remote Sensing of Environment, 148, 42–57, DOI: 10.1016/j.rse.2014.02.015.

Orellana, A. (2020). Conformación metropolitana desde la fragmentación. El proceso de conurbación del Gran La Serena. Urbano (Concepción), 23(41), 58–83, DOI: 10.22320/07183607.2020.23.41.04.

Ornetsmüller, C., Verburg, P., and Heinimann, A. (2016). Scenarios of land system change in the Lao PDR: Transitions in response to alternative demands on goods and services provided by the land. Applied Geography, 75, 1–11, DOI: 10.1016/j.apgeog.2016.07.010.

Ortiz, J., Castro, C.P., and Escolano, S. (2002). Procesos de reestructuración urbana y niveles de vulnerabilidad a amenazas naturales en una ciudad de tamaño medio: La Serena, Chile. Investigaciones Geográficas, 36, 17-42, DOI: 10.5354/0719-5370.2002.27744.

Pokojska, P. (2019). Simulating land use change in the southern part of warsaw metropolitan area with application of dyna-CLUE model. Geografie-Sbornik CGS, 124(1), 57–82, DOI: 10.37040/geografie2019124010057.

Pontius, R.G. and Schneider, L.C. (2001). Land-cover change model validation by an ROC method for the Ipswich watershed, Massachusetts, USA. Agriculture, Ecosystems & Environment, 85(1), 239–248, DOI: 10.1016/S0167-8809(01)00187-6.

Puertas, O.L., Henríquez, C., and Meza, F.J. (2014). Assessing spatial dynamics of urban growth using an integrated land use model. Application in Santiago Metropolitan Area, 2010–2045. Land Use Policy, 38, 415–425, DOI: 10.1016/J.LANDUSEPOL.2013.11.024.

Rodriguez-Galiano, V., Ghimire, B., Rogan, J., Chica-Olmo, M., and Rigol-Sanchez, J. (2012). An assessment of the effectiveness of a random forest classifier for land-cover classification. ISPRS Journal of Photogrammetry and Remote Sensing, 67, 93–104, DOI: 10.1016/j.isprsjprs.2011.11.002.

Salazar, E., Henríquez, C., Sliuzas, R., and Qüense, J. (2020). Evaluating spatial scenarios for sustainable development in Quito, Ecuador. ISPRS International Journal of Geo-Information, 9(3), 141, DOI 10.3390/ijgi9030141.

SEREMI (2013a). Plan Regulador Intercomunal de Elqui. Informe Ambiental de La Evaluación Ambiental Estratégica. Etapa de Proyecto. Regi[online] Available at: https://eae.mma.gob.cl/storage/documents/02_1er_IA_PRI_Elqui.pdf.pdf [Accessed 10 Aug. 2022]

SEREMI (2013b). Plan Regulador Intercomunal de Elqui. Memoria Explicativa. [online] Available at: https://eae.mma.gob.cl/storage/documents/04_Anteproyecto_PRI_Elqui.pdf.pdf [Accessed 10 Aug. 2022]

van Asselen, S., and Verburg, P. (2012). A Land System representation for global assessments and land-use modeling. Global Change Biology, 18(10), 3125-3148, DOI: 10.1111/j.1365-2486.2012.02759.x

Van Asselen, S., and Verburg, P. (2013). Land cover change or land-use intensification: simulating land system change with a global-scale land change model. Global change biology, 19(12), 3648-3667, DOI: 10.1111/gcb.12331

Veldkamp, A. and Lambin, E. (2001). Predicting land-use change. Agriculture, Ecosystems & Environment, 85(1), 1–6, DOI: 10.1016/S0167-8809(01)00199-2.

Verburg, P., Malek, Ž., Goodwin, S., and Zagaria, C. (2021). The Integrated Economic-Environmental Modeling (IEEM) Platform, IEEM Platform Technical Guides: IEEM Mathematical Statement. Inter-American Development Bank Technical Note.

Verburg, P., Soepboer, W., Veldkamp, A., Limpiada, R., Espaldon, M., and Mastura, S. (2002). Modeling the Spatial Dynamics of Regional Land Use: The CLUE-S Model. Environmental Management, 30, 391-405, DOI: 10.1007/s00267-002-2630-x.

Verburg, Schot, P., and Dijst, M.J. (2004). Land use change modelling: current practice and research priorities. GeoJournal, 61(4), 309–324, DOI: 10.1007/s10708-004-4946-y.

van Vliet, J. and Verburg, P.H. (2018). A Short Presentation of CLUMondo. In: M. Camacho Olmedo, M. Paegelow, J. Mas, F. Escobar, eds., Geomatic Approaches for Modeling Land Change Scenarios. Cham: Springer, 485–492, DOI: 10.1007/978-3-319-60801-3_34.

Yang, S., Zhao, W., and Pereira, P. (2022). Land-use modelling by CLUMondo under contrasting scenarios: a case study in the Yanhe watershed (China). In: P. Pereira, E. Gomes, and J. Rocha, eds., Mapping and Forecasting Land Use. Amsterdam: Elsevier, 173–192, DOI: 10.1016/B978-0-323-90947-1.00010-7.

Waiyasusri, K., and Chotpantarat, S. (2022). Spatial evolution of coastal tourist city using the Dyna-CLUE model in Koh Chang of Thailand during 1990–2050. ISPRS International Journal of Geo-Information, 11(1), 49, DOI: 10.3390/ijgi11010049

Zondag, B. and Borsboom, J. (2009). Driving forces of land-use change. Paper Prepared for the 49th ERSA Conference, [online] p. 1–16. Available at: https://www.researchgate.net/publication/285854006_Driving_forces_of_land-use_change [Accessed 20 Nov. 2022]

APPENDICES

Table A.1. List of Driving forces

Category	Driving forces	Variable code	Unit of measure	Information source
Geographic	Elevation	V1	m	Alos Palsar, 2016
	Slope	V2	Grades	Alos Palsar, 2016
	Distance to hydrographic network	V3	m	Geospatial Data Infrastructure of Chile (IDE), 2021
	Land use capacity	V4	Classes (I - VIII)	Natural Resources Information Center (CIREN), 2014
		V5		
Urban	Distance to operational drinking water territory	V6	m	Superintendence of Sanitation Services (SISS), 2020
	Faucets	V7	m	SISS, 2020
	Distance to irrigation channels and wells	V8	m	IDE, 2022
	Distance to urban centers	V9	m	Ministry of Urbanism and Constructions (MINVU), 2020
	Distance to road network	V10	m	IDE, 2022
	Distance to airports and ports	V11	m	Google Map, 2022
	Distance to camp areas	V12	m	National Registry Camps of MINVU, 2022
	Commercial land value	V13	Uf/pixel	Internal Revenue Service, 2020
	Rural property size P	V14	hectares	CIREN, 2014
Demographic	Population density	V15	Pob/hectares	IDE Chile, 2017
	Housing density	V16	Housing/ hectares	IDE Chile, 2017
	Migration density	V17	Mig/hectares	IDE Chile, 2017

Table A.2 Logistic regression coefficient results of land use and land cover in La Serena-Coquimbo conurbation

Driving force	Urban	Agricultural	Water	Wetland	Barren Land	Rangeland	Forest
Constant	-0.91074	0.07242	-4.00874	-1.74695	-2.11176	-0.84544	-6.05188
Elevation	-0.00502	0.00026	-0.01567	-0.01588	-0.00124	0.00203	-
Slope	-	-0.12368	-0.12992	-0.0287	-0.04794	0.07712	0.13289
Distance to hydrographic network	-	0.00013	-0.00014	-0.00045	0.00004	-0.00011	-
Land use capacity (I-IV)	-	0.00013	-	-	-	-	-
Land use capacity (VI-VIII)	-	-	-0.00021	0.00026	-	-0.00013	0.00057
Distance to operational drinking water territory	-	-	-	-	-	-	-0.00033
Distance to irrigation channels and wells	-	-0.00033	-	-	0.00015	-0.00004	-0.00053
Distance to urban centers	-	-	-	-0.00011	-0.00001	-	0.00036
Distance to road network	-0.0001	-	-	-	-0.00011	-	-
Distance to airports and ports	-	-	-	-	0.00009	-	-
Distance to camp areas	-0.00003	-	-	-	-	-	-
Commercial land value	0.31835	-0.38208	-	-0.05533	-	-	-
Rural property size	-	-0.00013	-	-	-	-	-
Population density	-0.93248	-	-	-	-	-	-
Housing density	0.02734	-	-	-	-	-	-
Migration density	0.04943	-	-	-	-	-	-
AUC	0.906183	0.912179	0.902306	0.93791	0.770421	0.936038	0.927431

RESEARCH PAPER

THE 3Ps (PROFITS, PROBLEMS & PLANNING) OF DAMS AS INEVITABLE DEVELOPMENTAL SOURCE: A REVIEW

Nidhi Jasrotia[1], Ripudaman Singh[2*]

[1] Department of Geography, Lovely Professional University, Punjab, 144011, India

[2] AISS, Amity University, Noida, Uttar Pradesh, 201313, India

*Corresponding author: ripudaman1@hotmail.com, rsingh29@amity.edu

Received: November 13th, 2022 / Accepted: May 29th 2024 / Published: July 1st 2024

https://DOI-10.24057/2071-9388-2024-2661

ABSTRACT. Since the beginning of river valley civilizations, humans have sought to harness the potential of flowing waters. The monumental structures of dams have been instrumental in damming these flowing waters and providing a wide range of benefits to society, including irrigation, drinking water, and generating clean energy. The present paper reviews in detail the hydropower reservoirs (dams) and presents a broader depiction of the 3Ps associated with their profits, problems, and planning. A literature review pertaining to dam construction and their impacts has been undertaken to analyze various approaches involving studies on socio-economic and environmental indicators and sustainability/risk factors related to dams. Various online search engines have been used to identify the desired studies and research for review. The first section of the paper gives a detailed account of the contribution (i.e., profits) made by dams to the economic development of humanity. The second part presents the negative social and environmental impacts (i.e., problems) of dams. As the paper proceeds, numerous tools/models analyzed during the literature review are presented that can be used to mitigate the negative fallouts of these dams (i.e., planning). However, it has been found that all these methods provide fragmented information with no certainty regarding which essential aspects require more emphasis while planning for these superstructures. Thus, a basic uniform frame is suggested, showcasing the fundamental and most critical aspects to be considered while planning a dam structure, which are described according to the three phases of dam construction, i.e., pre-construction, construction, and post-construction phases. While presenting the 3Ps (profits, problems and planning) of dams and analyzing their pitfalls, the 3Is (innovative keys) are recommended, emphasizing innovative technologies, innovative planning, and innovative solutions, which are needed in making these dams more optimal, judicious, and sustainable.

KEYWORDS: environment, hydropower, innovative, planning, reservoirs, sustainable

CITATION: Jasrotia Nidhi, Singh Ripudaman (2024). The 3Ps (Profits, Problems & Planning) Of Dams As Inevitable Developmental Source: A Review. Geography, Environment, Sustainability, 2(17), 119-130
https://DOI-10.24057/2071-9388-2024-2661

ACKNOWLEDGEMENTS: No funding has been received for this study. The authors are thankful for the constructive feedback from peers and colleagues. The anonymous reviewers' comments and advices are gratefully acknowledged.

Conflict of interests: The authors reported no potential conflict of interest.

INTRODUCTION

Earth is known as the blue planet (Byatt et al. 2001) as its surface has around 71% of water and 29% of land. Out of all water, oceans constitute around 96.5% of the remaining fresh water in the form of rivers, lakes, ice caps, glaciers, underground aquifers, and so on. However, the irony is that water resources are unevenly distributed over the land. These spatial variations in water distribution are the reasons why people in many parts of the globe still do not have enough water for drinking, sanitation, and irrigation. At some places, there are floods, while other regions experience droughts. To overcome the problem of regional variations in water availability, humans relied on dams not only in modern times but also in antiquity (Castelan 2002). Going back into history, the first dam was constructed in Jordan around 4000 BCE, and Sadd El-Kafara dam construction dates back to 2600 BCE in Egypt (Schhnitter 1994). In modern times, the Spanish were the leaders in dam construction around 1600 CE (Tullos et al. 2009). At present, there are around 800,000 dams constructed and operating on the earth, of which 50,000 are large dams (Kornijowl 2009). The International Commission on Large Dams (2022) describes dams with a height greater than 15 m as falling into the category of large dams. Whatever the size, whether small, large, or medium, all dams are the need of the hour all over the world, where the top three most populous countries, i.e., China, India, and the USA, are also the top-ranking countries with the largest number of dams (World Register of Dams 2020a), viz., China, which has 23,841 dams, followed by the USA (9263) and India (4407) (Fig. 1).

These hydropower reservoirs become inevitable, especially in developing countries, as they find no better option than dams to meet the demands of water supply, electricity, changing and urbanizing lifestyles of burgeoning populations, along with the mounting pressure to mitigate carbon emissions in the scenario of climatic change (Biswas 2012).

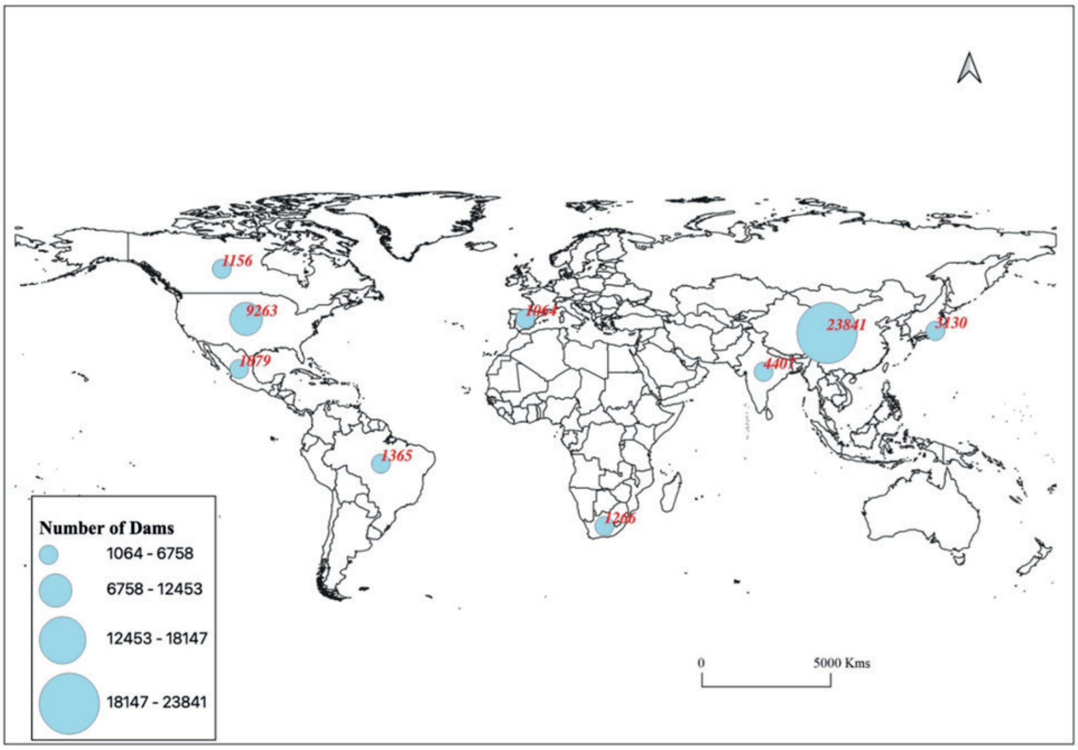

Fig. 1. Top Nine Countries with Largest Number of Dams in the World

Need for Dams. To mitigate and overcome the problems faced by emerging and developing countries and to address the growing needs of power, water, irrigation, food production, etc., dams play a vital role. Table 1 summarizes some facts that answer the question, why are these dams needed or and why do we need dams?

Considering these facts, countries all over the world are shifting their dependence from fossil fuels to more renewable and clean sources of energy (Fig. 2) (International energy agency, market report July 2021www.iea.org.electricity). Among the renewables, hydropower dominates, with more than half a share of power generation (International Hydropower Association 2020). In the year 2016, hydropower contributed 16-17% of the world's power, which was 70% of all renewable sources of energy (Alam et al. 2017).

MATERIALS AND METHODS

We conducted a literature review based on peer-reviewed journal articles pertaining to the construction of the dam's reservoir and their socio-economic and ecological impacts, both positive and negative. Further, we reviewed the articles pertaining to various approaches involving studies on social indicators, environmental indicators, sustainability indicators, and risk factors. For deriving the desired studies and literature, we used the online search engines Research Gate, Scopus, and Google Scholar and the National Digital Library of India, using the search terms viz., large dams, impacts of dams, hydropower, and dam construction-specific impacts on socio-economics and the environment (Fig. 3). A combination of all these could result in a limited number of selected studies. In total, 82 research papers have been reviewed, out of which 26 were reviewed for problems associated with major dams constructed in the world, 25 were reviewed for positive impacts of large dam construction, and 25 were reviewed for different approaches used to study various impacts of dams, respectively. The remaining papers were reviewed to analyze the innovative solutions recommended in the findings.

For exclusion criteria, we did not include papers related to run-of-river, small hydropower projects, or dam removal impacts, stipulating that impacts of dams and reservoirs must be based at least partially on large dams' construction. Fig. 3 depicts the flow diagram that shows the search engines used to select the studies for review using select terms and exclusion criteria.

Table 1. Summary of facts: why do we need dams?

Facts regarding dams	Measures and numbers
Aggregate storage capacity	7714 km^3 (World Register of Dams 2020b)
Hydropower	2.3 trillion kilowatt hours of electricity each year (World Register of dams 2020c)
Number of people dying of hunger	25000 /day (United Nations 2022)
Number of hungry people in the world	828 million people sleep hungry every night globally (World Food Program 2022)
Number of people without access to clean Cooking	2.6 billion people globally (IRENA 2021)
Number of people without access to drinking Water	1.5 billion people globally (IRENA 2021)
Number of people without electricity	759 million people globally (IRENA 2021)

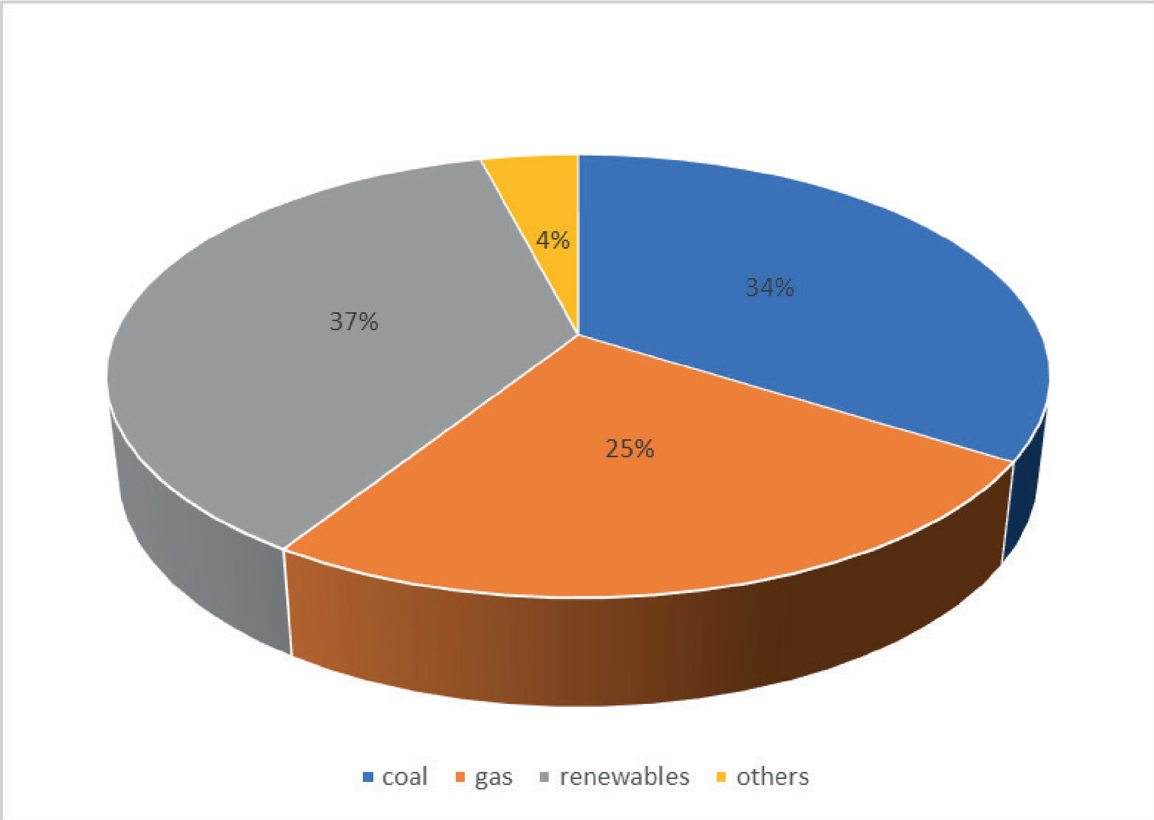

Fig. 2. Global share of fossil fuels and low carbon renewables in electricity generation, 2020

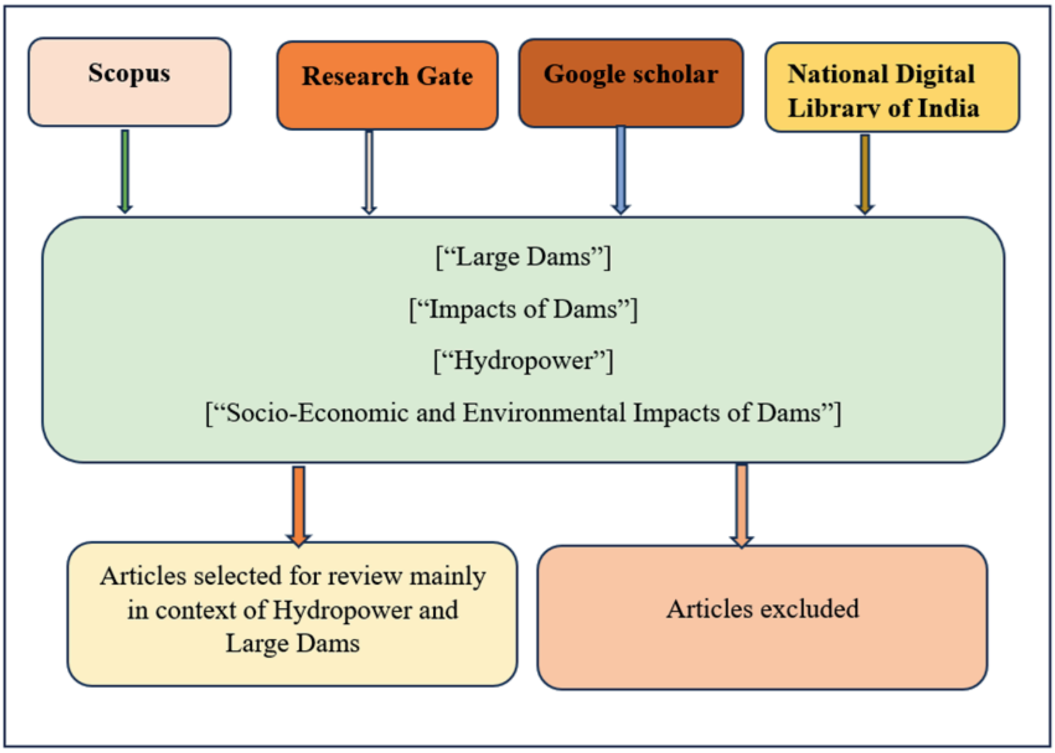

Fig. 3. Methodology for selection of articles on Large Dams

RESULTS AND DISCUSSION

The present paper analyzes the 3Ps associated with the profits, problems, and planning aspects of dams in a comprehensive and detailed manner. Firstly, the major profits of dams are discussed, followed by the problems that dams bring with them, and finally, the most significant planning perspective is scrutinized, which can maintain a balance between profits and problems of dams to make the dams more environmentally friendly and sustainable.

Profits (of Dams): without the exploitation of rivers, the world would be a much different place with cycles of droughts, floods, and famines (Altinbilek 2002). The International Energy Agency (2021) has found that energy produced by hydroelectric installations throughout the world provides approximately 1/5th of the world`s total electrical energy. As per the Hydropower Status Report (2022) for the year 2021, the total hydropower installed capacity reached 1360 GW, with the top six countries being China, Brazil, the USA, Canada, Russia, and India (Fig. 4) (International Hydropower Association 2022). The

International Renewable Energy Agency (IRENA 2021) reported that the world's existing hydropower capacity needs to grow by around 60% by 2050 to reach 2150 GW to help limit the rise in global temperature to well below 2°C. Considering their overall utility, dams are known for their multipurpose roles and benefits. Primarily, dams are constructed for four major profits, as listed below:

- to meet the increasing demand of water (Eiriksdottir et al. 2017);
- to provide electrical energy to expanding urban and industrial centers (Altinbilek 2002);
- to irrigate the agricultural regions (Brown 2009);
- to control floods and divert the excessive river waters to arid regions (Brown 2009).

The World Commission on Dams categorizes the purposes of dams in nine categories (Table 2). According to the study conducted by the United States Committee on Large Dams (USCOLD) (1997), the living conditions of people today are certainly improved by the construction of dams. For managing the finite water resources in a sustainable manner and to fulfil the potable and industrial water demand and the ever-increasing energy demand, dams are indeed considered to be an effective tool in this regard (Altinbilek 2002).

The large amount of water that can be stored in reservoirs makes dams more useful as they can generate power instantly according to the varied electricity demand, which is otherwise not possible with other sources of power generation, such as thermal and nuclear sources (Egrea & Milewskib 2002). Dams are considered large social investments as they have a great role in the future prospects of both urban and rural populations, especially

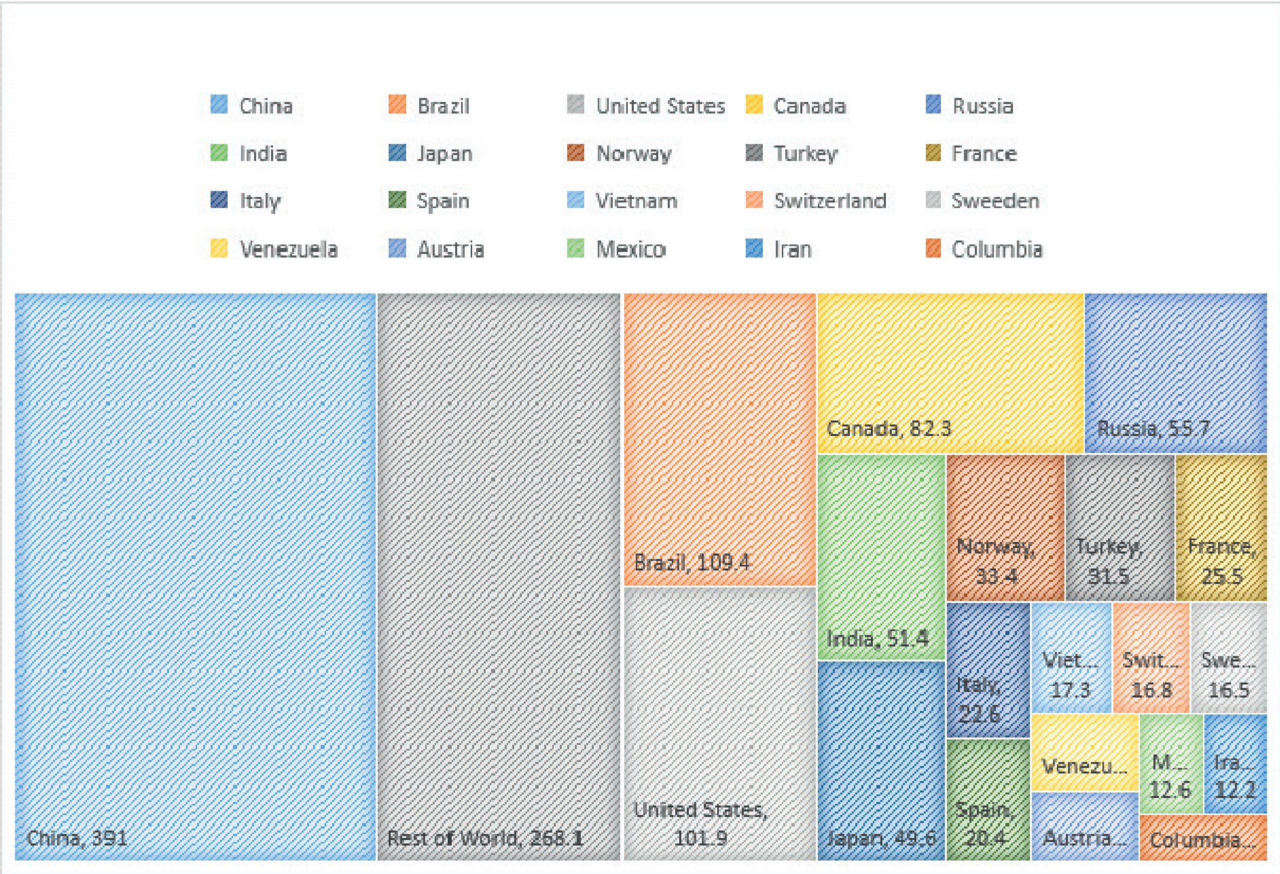

Fig. 4. Countrywise hydropower installed capacity, 2021: 1360GW

Table 2. Categorization of Dams based on Purposes

Code	Description	Dams with sole purpose	Multiple-purpose dams
C	Flood control	2539	4911
F	Fish farming	42	1487
H	Hydropower	6115	4135
I	Irrigation	13580	6278
N	Navigation	96	579
R	Recreation	1361	3035
S	Water supply	3376	4587
T	Tailing	103	12
X	Others	1579	1385

in developing countries (Dixon et al. 1989). Dams control flood hazards and support flood plain agriculture (Poff & Hart 2002). IPCC (2007), in its report, predicted that due to the increased frequency of precipitation events, the areas affected by droughts and floods will be augmented, the effects of which can be controlled by dams (Tullos et al. 2009).

Dams contribute much more than the above-explained benefits, such as low carbon emissions and adding very few impurities to the air (Jumani et al. 2017). Thus, hydropower can be a major bridge to the urgently needed transition to sustainable energy (Goodland 1995). Dams raise the socio-economic status of people by providing modern infrastructure and employment to them (Brown et al. 2009). For example, Bui Dam in Ghana led to improvements in road networks, drinking water, health, and education (Mortey 2017). Dams also provide recreational and navigational facilities as well as income to society (Brown et al. 2009).

The benefits and contributions of some of the major dams in the world are summarized in Table 3 and Fig. 5. Clean and affordable energy and zero hunger are two of the 17 Sustainable Development Goals adopted in 2015 by 193 countries to end extreme poverty, reduce inequality, and protect the planet through its Agenda 2030 (United Nation 2021).

Certainly, the path to reach these goals goes through hydropower if the problems associated with dams are reviewed and eradicated using proper planning and policies. There is a dire need to shed some light on the problematic side of dams, which is being done in the following section.

Problems (associated with dams): World Commission on Dams (2000) reports that "shortfalls in technical, financial and economic performance have occurred and are compounded by significant social and environmental impacts of dams, the costs of which are often disproportionately borne by poor, indigenous people and other vulnerable groups". Dixon et al. (1989), found that dams have direct benefits, but there are many associated environmental and social effects, most of which are likely to be costs. Globally, the major issues arising due to dam construction can be grouped as socio-economic impacts of dams (Rao 1989; Pinho et al. 2007; Sharma and Thakur 2017) and environmental impacts (Richter et al. 2010; Pinho et al. 2017). These negative impacts often lead to undue cost/schedule overruns of dams (Fig. 6).

Table 3. Benefits of some major dams in the world

Country (Dam)	Benefits
Mexico (Chicoasén Dam)	42% for agriculture, 39% for hydropower, 9% for water supply,10% for water supply (Castelan 2002).
Turkey (Ataturk)	irrigates 882,000 ha land which is about 56% of the total irrigated land, generate 8900 GWh/year energy and contributes about 3.8 billion US$/year to its economy (Altinbilek 2002).
Switzerland (Grande Dixence Dam)	59.6% of electricity comes from hydropower (Kellner 2019).
India (Sardar Sarovar)	Irrigates 18.45 lac ha land in Gujarat, provide drinking water to 173 Urban centers and 9490 villages, flood protection to 4 lac population of Gujarat, has two power houses of 1200 MW & 250 MW each (Sardar Sarovar Narmada Nigam Ltd. 2021).
China (Three Gorges)	It protects about 15 million residents and 3.7 million acres in the Lower Yangtze floodplain (Earth observatory 2007).
Brazil (Tucurui)	Supplies power to 13 million people (La Rovere and Mendes 2000).

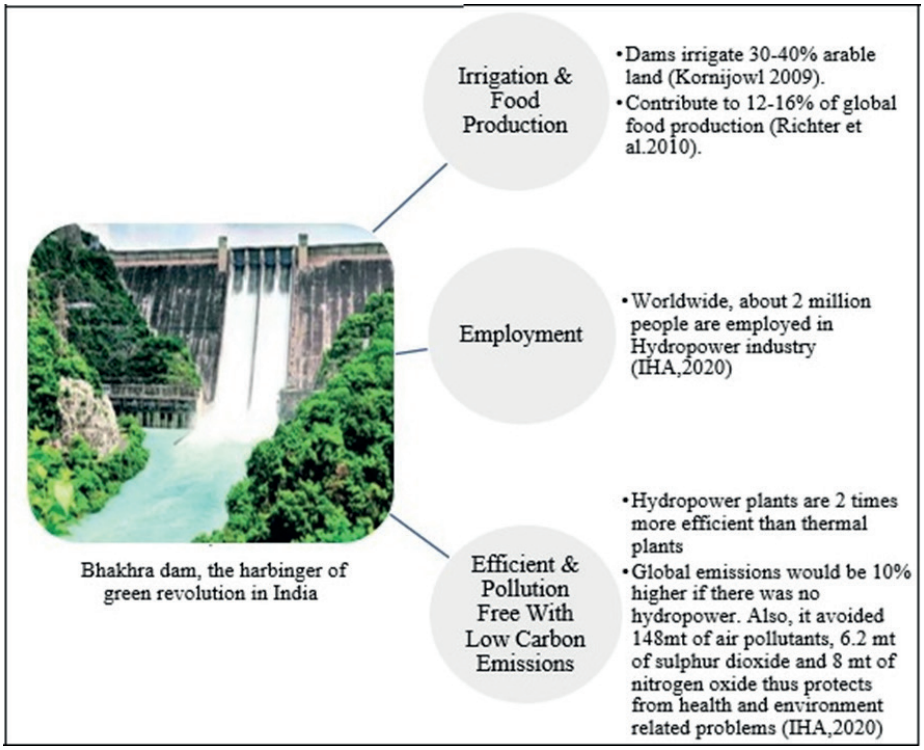

Fig. 5. Worldwide contributions of Dams

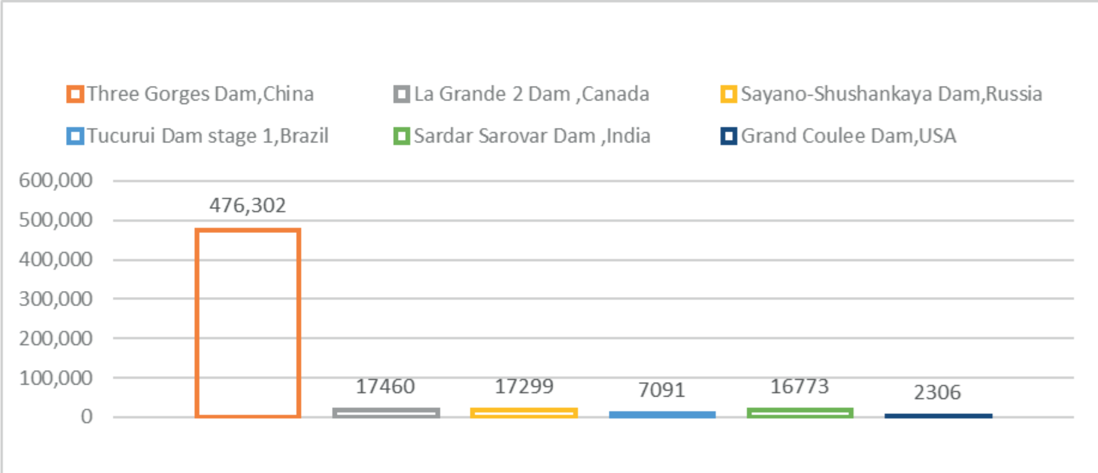

Fig. 6. Cost overruns of hydroprojects in million US dollar
(Shaktawat & Vadhera 2021)

Impoundment and presence of reservoirs in dam construction are the major causes of negative socio-economic as well as environmental impacts of dams (Egrea and Milewskib 2002; Sokolov et al. 2020). Also, global climatic changes and the growing demand for electricity intensify the negative impact of dams (Tullos et al. 2009). The intensity and magnitude of socio-economic impacts are vast in time and space and are explained below:

• Involuntary displacement and resettlement are the most dreadful of the socio-economic impacts (Mcnally et al. 2008; Gutman, 1994) leading to adulteration in social networks (Brown 2009). For example, over 10 million people were displaced by dam construction between 1950-1990 in China alone, and many more in other Asian developing countries (Kiik 2023). Similarly, in Poland, during the filling of Czorsztyn Reservoir, over 300 households were drowned in the village Maniowy (Kornijowl 2009). Gorshkov et al. (2013) discussed the problems of ponds and dam reservoirs in Russia.

• Profound direct and indirect negative impacts on the livelihood of displaced populations are found (Aung et al. 2021). Moreover, locals are cheated in the name of employment and electrification (Jumani et al. 2017). Forest and agricultural land are inundated (Mcnally et al. 2008), resulting in food insecurity (Richter et al. 2010), increased water conflicts (Rao 1989; Moller 2005), changes in resource allocation and resource use patterns (Gutman 1994). Sikka (2020) analyzed the large displacements caused by the Sardar Sarovar Dam in India. Chandy et al. (2012) found that due to dam construction in Sikkim, India, changes in land use and occupation of people could adversely impact their livelihoods. Also, there is immigration to host places, and thus relocation results in higher densities and greater struggles over resource access (Tullos et al. 2009) by altering the land-man ratio. Worldwide, about 1249 large dams have been constructed in protected areas, which adversely affect the health of protected areas; thus, dam construction within or near protected areas should be avoided (Thieme et al. 2020). The World Commission on Dams, in its seminal report, noted that dams are spatially significant, locally disruptive, and come along with lasting and often irreversible effects (Tullos et al. 2009). The World Register of Dams (2020d), illustrates the magnitude of displaced people through some of the largest dams (Fig. 7). The negative impacts of dams are summarized in Table 4. These problems can be tackled with the numerous tools/methods mentioned below in the planning section.

Planning (of dams). As numerous sectors such as water, food, and energy supply get affected by water resource projects, the framework of optimal designs for proper operation and maintenance of these projects and existing water resource–related curricula need to be improved and updated (Singh 2023). The sustainability of a dam depends on

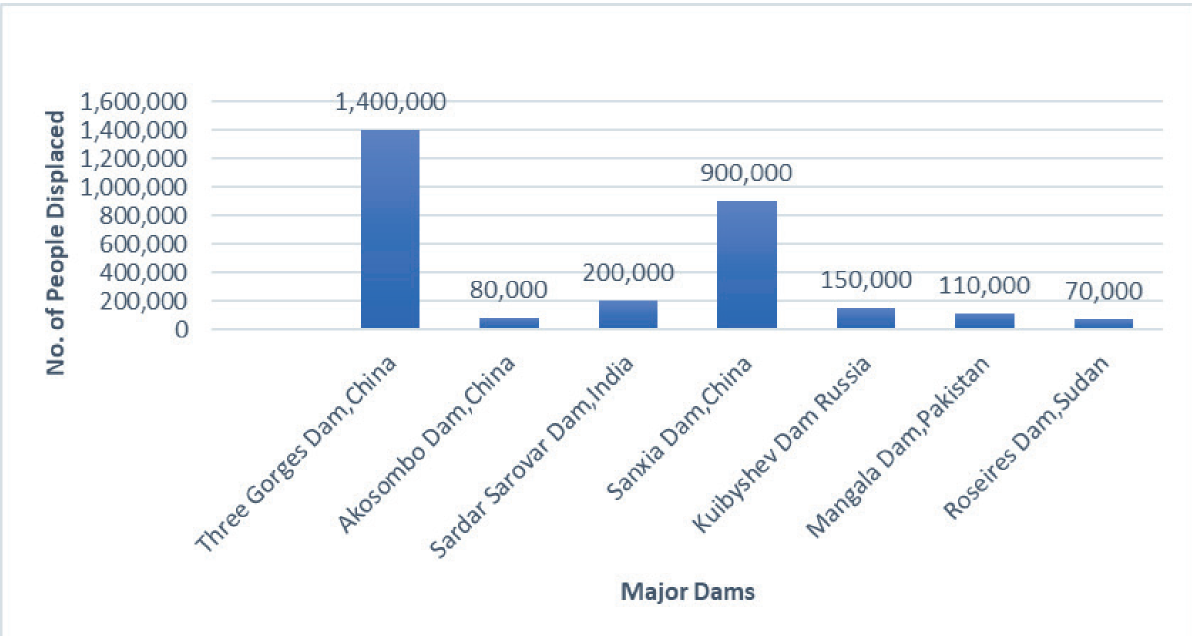

Fig. 7. Resettled persons due to major dam construction
(Shaktawat & Vadhera 2021; World Register of Dams, 2020d)

the policy, its planning, and its proper implementation. A well-crafted plan integrates policymakers, the scientific community, and the people who will share the costs and benefits. Public involvement in planning and decision-making processes is an important aspect (Gogoi 2023). A lack of involvement from any one of these three factors often results in the construction of controversial dams. Considering the negative impacts of dams and reservoirs, many countries in the west (including USA and European countries) have initiated dam and reservoir removal projects as well (Habel 2020).

Water resource management through dam construction is such a dynamic process as it involves the entangled web of society, environment, climate change, and sustainability. These four aspects are so interrelated that a minor imbalance in one can derail the entire development process initiated through dams. An innovative hydropower development model is one that can coordinate environmental protection and resettlement while boosting economic and social development and is needed the most (Sun et al. 2020). Such an innovative model is the precursor to the 'innovative technology' required for making sustainable dams. In the last 20 years, as dam construction has picked up mainly in developing countries, there has been an urgent need to address the issues related to the various impacts of dams. After the WCD (2002) report, new areas of research in the context of dams have emerged, namely climate change and dams, downstream impacts of dams, and gender-based studies in dam impacts (Schulz & Adams 2019). We recommend the 3Is (innovative keys) which emphasize the need for innovative technologies, innovative planning, and innovative solutions to enhance the optimization, judiciousness, and sustainability of dams. To begin with, getting acquainted with innovative technologies, some of the approaches/models for planning and sustainability assessment of dams (Tables 4-7) are summarized and presented here.

Table 4. Studies/approaches involving risk factor

Tools/Model	Indicators Used	Main Findings
Fuzzy Topsis (Agarwal & Kansal 2020)	Risk Index based initial cost interval assessment by using Multi criteria decision making methodology	The result of case study matches the actual values of project
Fuzzy Logic (Kucukali 2011)	Fuzzy rating tool to calculate Risk Index (R)	Site geology and Environment issues were the most important risks
Fuzzy Hybridized with ANN and genetic Algorithm (Shaktawat & Vadehra 2021)	Sensitivity analysis to evaluate Risk factor is a primary method	Study found that construction phase is the most critical and Life cycle risk assessment is required for sustainable growth
Risk Framework (Cleary et al. 2015)	Consequences of failure modes of Earth dams	Earth dams are more vulnerable to failures due to Overtopping, Piping and Landslip failures
Hydro Informatic (Approach Maan et al. 2020)	Estimation of design flash flood	Flood hydrographs are more important in flood-risk management.

Table 5. Studies/approaches involving environmental indicators

Tools/Model	Indicators Used	Main Findings
Greenhouse Gases Risk Assessment Tool (GRAT) (Kumar et al. 2019)	Life cycle GHG emissions of reservoirs using age of reservoirs, annual mean temperature, annual mean precipitation and runoffs	Three Gorges reservoir was found under high risk of CH_4.
Dam Environment Vulnerability Index (DEVI) (Latrubesse et al. 2017)	The Basin Integrity Index, The Fluvial Dynamics Index, the Dam Impact Index	The study found that the Maderia River watershed in Amazon River basin is the most vulnerable with high value of DEVI (80-100).
Artificial Neural Network (ANN) (Xu et al. 2019)	Quantification of plant biodiversity indicators related to Hydropower ANN was used to maintain a balance between hydropower and biodiversity targets by developing an optimization model	Recommended to use Pareto-Optimal solutions to optimize the human as well as ecosystem Objectives.
Life Cycle Impact Assessment (LCIA) (Gracey et al. 2016)	Quantification of environmental Impacts of hydropower on Biodiversity.	Study found that main impacts being, freshwater habitat alteration, water quality degradation, land use impact.
Multi - criteria scoring tool to assess the environmental risks of SHPs (Kucukali 2014)	Environmental flow, water quality, fish passage and protection, watershed protection, threatened and endangered species, selected on basis of EBRD*	The hydropower plant under case study failed in all criteria of EBRD.
Hierarchical Framework (Burke et al. 2009)	Quantification of First order, 2nd order and 3rd order impacts of multiple dams within the study area.	Recommended alternative River management Strategies using Hierarchical framework over space and time.
Environmental Impact Assessment (EIA), a Comparative analysis (Abdul-Sattar 2007)	Legislative and implementation deficiencies in developed and developing countries.	Case study in Pakistan shows deficiencies even after the implementation of EIA

Table 6. Studies/approaches involving social indicators

Tools/Model	Indicators Used	Main Findings
Social impact Assessment of three large Hydro Projects *Egre & Senecal 2003*	Resettlement issues and Resettlement Action Plan	Pre-project SIA is useful if resettlement plans' implementation is based on its findings
Social Life Cycle Assessment (SLCA) *Aung et al. 2021*	Multiple social stressors, Different impact Categories within Potentially disturbed communities	Shweli Dam has more negative impacts than benefits to locals.
Integrative Dam Assessment Model (IDAM) *Brown et al. 2009*	Objective and subjective Cost/benefit analysis using 27 impacts of dams	Policy makers can use it to find alternatives and priorities in dam construction
Comparison of SIA in two dams *Tilt et al. 2009*	Migration and resettlement, changes in rural economy, employment, infrastructure, cultural aspects, health and gender relations	Policy makers can know which interventions to be taken and how by identifying the dams' impacts
Hydraulic Modelling *Wyrick et al .2009*	Social impacts of dam removals	The study recommends Interaction between all stake holders
Matrix Framework-A Review *Kirchherr & Charles 2016*	Unification of existing frameworks for social impacts into a single Framework	A holistic way to assess the complex and multi-dimensional social impacts of dams
Resettlement and Livelihood adaptation-A Case study *Sayatham & Sudhardiman 2015*	Farming households with different assets and resources	Insufficient agricultural land is the major obstacle in livelihood adaptation after dam construction
Four stages planning for Resettlement *Scudder 2005*	Socio-economic status of displaced people	Handing over a Sustainable Resettlement to 2nd generation

Table 7. Studies/approaches involving sustainability criteria

Tools/Model	Indicators Used	Main Findings
Hydropower Sustainability Assessment Protocol *Hartmann et al. 2019*	Good and best practices at each stage of lifecycle of a hydropower project for 24 topics	Teesta-v project meets proven best practice on 6 out of 20 topics. It exceeds basic good practice on 9 topics and meets basic good practice on 5 topics
PROMETHEE & Analytical Network Process *Wu et al. 2017*	Firstly, HELTS* is used to rank social sustainability of each alternative. Then Analytical Network Process is used to measure Correlation between indicators	Public recognition is discovered as key indicator by Comparative analysis
Multi-Criteria Analysis *Morimoto 2013*	Quantitative relationship between economic, environmental and social indicators	Economic indicator has biggest impact (.324) followed by environment impact (.0102)
Emergy Analysis *Zhang et al. 2014*	Environment loading and Sustainability of energy Systems	Environment loading ratio is acceptable when 2.04.
Causal Diagrams to show Impact Pathways *Voegeli et al. 2019*	Series of 10 casual Diagrams each showing specific topic	Stakeholders' perspective with proper understanding of pathways to know the main reason of conflicts.
Sustainability Assessment -A Review *Nautiyal & Goel 2020*	Hydropower, development, society, environment, economy is interlinked	Sustainability prediction of HPPs is incomplete without considering all biophysical impacts.

Undoubtedly, there are numerous models/approaches being developed from time to time for assessing the impacts of dams based on different aspects; however, it has been found that whenever dam impact assessment is done, it is focused on only a single aspect, and there is a lack of a unified basic frame that can give a comprehensive understanding to policymakers (Schultz & Adams 2019), so that whatever method or tool they are applying to plan a proposed dam construction should be focused on some fundamental aspects to make dams more judicious and optimal development devices (Shafa et al. 2023). To fill this gap, phase-wise essential aspects for the planning of dam construction are being suggested here as 'innovative planning' (Table 8). Taking these planning phases as a uniform code for all dam construction, any method can be used to assess these aspects, on the basis of which policies, decision-making, and planning can be done accordingly.

Also, it is necessary to involve planners and policymakers, keeping in view the interdisciplinary approach. Apart from the above-mentioned aspects, there is a need for some 'innovative solutions' for redressing the negative impacts of dams, which are discussed as follows:

• To use dams' infrastructure for installing the solar panels, this way enhances energy production (Rauf et al. 2020; Vella 2021).

• To focus on developing new technologies to capture methane from hydroelectric reservoirs before it enters the atmosphere and convert it into energy (Hirsch 2007).

• As methane is a much more potent greenhouse gas than CO_2, you can control methane emissions by planting trees like pines, spruce, etc. that can absorb methane emissions (Yoneda 2013).

• To control reservoir siltation, detailed statistical analysis of the morphometric parameters at the micro-

Table 8. Phases of dam construction planning

Phase -I	Phase-II	Phase-III
Pre-construction Planning 1. Socio-economic equality and inclusion 2. Awareness among all the stakeholders about their roles in making dams sustainable 3. Site geology 4. Cost/schedule over runs 5. Environment safety and conservation 6. Climate change, hungry water and gender impacts of dams and vice-versa 7.Potential of dam reservoir for GHG emissions burden	Construction Planning 1.Dam failure risks and safety measures assessment 2.Assessing the burden of infrastructure on local as well as outsourced resources	Post-construction Planning 1.Re-checking and evaluating what has been achieved and what is the lacking? 2. Measures and solutions to mitigate the remaining problems

watershed scale is essential (Singh & Singh 2020) and the most severe impacts of sedimentation can be prevented if sedimentation management begins within a decade of reservoir construction (Anari et al. 2023).

• To use dam water for hydroponics, there is a benefit to the locals (Sharma et al. 2019).

• To use 'optimization model' for allocating reservoir water efficiently for irrigation to different cropping zones (Alfaisl et al. 2023).

• To use various 'Non-Revenue Water (the amount of water produced and lost before it reaches customers) Reduction Strategies' (Farouk et al. 2023). In this way, water theft and other water losses (losses due to leaks, bursts, overflow from water mains, service connections) in developing and developed countries can be reduced.

CONCLUSION

Dams have numerous profits along with various problems associated with them, for which these inevitable developmental tools attract criticism. However, one thing that needs to be mentioned here is that hydropower and dams cannot be ignored at all. Out of eight lac dams constructed in the world, more than 50,000 are large dams, which have an impact on more people. Although western countries have moved into the phase of decommissioning and the removal of dams, most developing countries are rapidly constructing more and more dams to tap their water resources. China and India, which have around 40% of the world population, are also home to more than 50% of the largest dams in the world. So efficient and sustainable dams are needed more to serve humanity and achieve sustainable development. Furthermore, without such dams, our shared sustainable future is incomplete. So, its high time to realize the truth: only counting the problems associated with dams is not going to work. More collaborative efforts from science, policy, governance, and people's inclusion are required to advance the 3Is of 'Innovative Technologies, Innovative Planning, and Innovative Solutions', aiming to enhance the efficiency of existing dams and create more optimal and sustainable future dams.

REFERENCES

Abdul-Sattar N. (2007). Comparative analysis of the EIA system of developed and developing countries: Cases of hydroelectric power plants. Gothenburg: Environmental System Analysis, Chalmers University of Technology. Available at: https://publications.lib.chalmers.se/records/fulltext/43366.pdf [Accessed 30 Mar. 2022].

Agarwal S.S. and Kansal, M.L. (2020). Risk based initial cost assessment while planning a hydropower project. Energy Strategy Reviews, 31, 100517, 1-12, DOI: 10.1016/j.esr.2020.100517.

Alam F., Alam Q., Reza S., Khurshid-ul-Alam S. M., Saleque K. and Chowdhury H. (2017). A review of hydropower projects in Nepal. Energy Procedia, 110, 581-585, DOI: 10.1016/j.egypro.2017.03.188.

Alfaisal F.M., Alam S., Alharbi R.S., Kaur K., Khan M. A., Athar M.F., and Rahin S. A. (2023). Application of an Optimization Model for Water Supply Chain Using Storage Reservoir Operation for Efficient Irrigation System. Discrete Dynamics in Nature and Society, 2023, 7932653, 1-13, DOI: 10.1155/2023/7932653.

Altinbilek D. (2002). The role of dams in development. Water Science & Technology, 45(8), 169-180, DOI: 10.2166/wst.2002.0172.

Anari R., Gaston T. L., Randle T. J., and Hotchkiss R. H. (2023). New Economic Paradigm for Sustainable Reservoir Sediment Management. Journal of Water Resources Planning and Management, 149(2), 04022078-1-13, DOI: 10.1061/(ASCE)WR.1943-5452.0001614.

Aung T.S. et al. (2021). Social impacts of large-scale hydropower project in Mynamar: A social life cycle assessment of Shweli hydropower dam. The International Journal of Cycle Assessment, 26, 417-433. DOI: 10.1007/s11367-021-01868-3.

Biswas A.K. (2012). Impacts of Large Dams. In: C. Tortajada, A. Dogan and A.K. Biswas eds., Impacts of Large Dams: A global assessment. New York: Springer, 1-18. Available at: http://ndl.ethernet.edu.et/bitstream/123456789/7406/1/Impacts%20of%20Large%20Dams%20A%20Global%20Assessment.pdf [Accessed Apr. 2022].

Brown P.H., Tullos D., Tilt B., Magee D. and Wolf A. T. (2009). Modelling the costs and benefits of dam construction from multidisciplinary perspective. Journal of Environmental Management, 2009 Jul, 90, S303-S311, DOI: 10.1016/j.jenvman.2008.07.025.

Burke M., Jorde K., and Buffington J.M. (2009). Application of a hierarchical framework for assessing environmental impacts of dam operation: changes in streamflow, bed mobility and recruitment of riparian trees in a western North American river. Journal of Environmental Management, 2009 Jul, 90 S3, S224-S236 DOI: 10.1016/j.jenvman.2008.07.022.

Byatt A., Fathergill A., Holmes, M. and Allenborough D. (2001). The Blue Planet, a natural history of the Oceans. New York: DK Publishing.

Castelan E. (2002). Role of large dams in the socio-economic development of Mexico. International Journal of Water Resources Development, 18(1), 163-177, DOI: 10.1080/07900620220121729.

Chandy T. et al. (2012). Impacts of hydropower development on rural livelihood sustainability in Sikkim, India: Community perceptions. Mountain Research and Development, 32(2), 117-125, DOI: 10.1659/MRD-JOURNAL-D-11-00103.1.

Cleary P. W. et al. (2015). A scenario-based risk framework for determining consequences of different failure modes of Earth dams. Natural Hazards, 75(2), 1489-1530, DOI: 10.1007/s11069-014-1379-x.

Dixon J.A., Talbot L.M. and Lemoigne, J.M. (1989). Dams and the Environment: Considerations in World Bank Projects. World Bank Technical Paper Number 110. Washington, D.C.: The World Bank. Available at: https://documents1.worldbank.org/curated/en/300561468782146320/pdf/multi-page.pdf [Accessed 30 Mar. 2022].

Earth Observatory. (2007, 15 July). Three Gorges Dam, China. [online], Maryland: NASA Earth Observatory. Available at: https://earthobservatory.nasa.gov/images/7769/three-gorges-dam-china [Accessed Apr. 2022].

Egrea D. and Milewskib J. C. (2002). The diversity of hydropower projects. Energy Policy, 30(14), 1225-1230, DOI: 10.1016/S0301-4215(02)00083-6.

Egre D. and Senecal P. (2003). Social impact assessment of large dams throughout the world: Lessons learned over two decades. Impact Assessment and Project Appraisal, 21(3), 215-224, DOI: 10.3152/147154603781766310.

Eiriksdottir S.E., Oelkers H.E. and Hardardottir, J. (2017). The impact of damming or riverine fluxes to the ocean: a case study from Eastern Iceland. Water Research, 113, 124-138, DOI: 10.1016/j.watres.2016.12.029.

Farouk A.M., Rahman R.A. and Romali N.S. (2023). Non-revenue water reduction strategies: a systematic review. Smart and Sustainable Built Environment, 12(1), 181-199, DOI: 10.1108/SASBE-04-2021-0071.

Gogoi T. (2023). Anti-Dam Discourse: Stakeholder Engagement and Decision-Making. In: P. Singh et al., eds., The Route Towards Global Sustainability: Challenges and Management Practices. Cham: Springer International Publishing, 379-393, DOI: 10.1007/978-3-031-10437-4_19.

Goodland R. (1995). How to distinguish better hydros from worse: the sectoral approach to environmental analysis of Hydroprojects. Washington D.C.: Environment Department, The World Bank. Available at: https://documents1.worldbank.org/curated/ru/864871555087210530/pdf/Environmental-Sustainability-Ranking-of-Hydroprojects-How-to-Distinguish-Better-Hydros-from-Worse.pdf [Accessed Apr. 2022].

Gorshkov S., Touchart L., Mochalova O., Ozerskiy A. and Evseeva, L. (2013). From Ponds to Man-made Seas in Russia. Geography Environment Sustainability, 6(4), 65-76, DOI: 10.24057/2071-9388-2013-6-4-65-76.

Gracey E.O. and Verones F. (2016). Impacts from hydropower production on biodiversity in a LCA framework- review and recommendations. The International Journal of Life Cycle Assessment, 21(3), 412-428, DOI: 10.1007/s11367-016-1039-3.

Gutman P.S. (1994). Involuntary resettlement in hydropower projects. Annual Review of Energy and Environment, 19, 189-210, DOI: 10.1146/annurev.eg.19.110194.001201.

Habel M., Mechkin K., Podgorska K., et al. (2020). Dam and reservoir removal projects: a mix of socio-ecological trends and cost-cutting attitudes. Scientific Reports, 10, 19210, 1-16, DOI: 10.1038/s41598-020-76158-3.

Hartmann J., Locher, H. and Khandkal Z. (2019). Hydropower sustainability assessment protocol-Teesta V Power Station, India, Official Assessment NHPC limited. [online] www.hydrosustainability.org Available at: https://static1.squarespace.com/static/5c1978d3ee1759dc44fbd8ba/t/5d8c752237aac41d409a4923/1569486263861/Teesta-V+Assessment+Report_Sept+19+2019_final.pdf [Accessed 30 Jun. 2022].

Hirsch T. (10 may, 2007). Project aims to extract dam methane. [online] BBC News. Available at: http://news.bbc.co.uk/2/hi/science/nature/6638705.stm [Accessed 31 Mar. 2022].

International Energy Agency (2021, July). Electricity Market Report. International Energy Agency, [online]. Available at: https://www.iea.org/reports/electricity-market-report-july-2021 [Accessed 10 Aug. 2021].

International Commission on Large Dams. (2022). Position Paper. [online] International Commission on Large Dams. Available at: www.icold-cigb.org [Accessed 31 Dec. 2022].

International Hydropower Association (2020). Facts about Hydropower. [online] International Hydropower Association. Available at: https://www.hydropower.org/iha/discover-facts-about-hydropower [Accessed 15 Dec. 2020].

International Hydropower Association (2022). Hydropower Status Report: 2021. [online] International Hydropower Association. Available at: https://assets-global.website-files.com/64f9d0036cb97160cc26feba/64f9d0036cb97160cc2711ef_IHA20212405-status-report-02_LR.pdf [Accessed 12 Dec. 2022].

International Renewable Energy Agency (2021). IRENA Members commit to top up global hydropower fleet. [online] International Renewable Energy Agency. Available at: https://www.irena.org/newsroom/articles/2021/May/IRENA-Members-Commit-to-Top-Up-Global-Hydropower-Fleet [Accessed 15 Jul. 2022].

Jumani S., Rao S., Machado S. and Prakash A. (2017). Big concerns with small projects: Evaluating the socio-ecological impacts of small hydropower projects in India. Ambio, 46, 500-511, DOI: 10.1007/s13280-016-0855-9.

Kellner E. (2019). Social Acceptance of a multipurpose reservoir in a recently deglaciated landscape in the Swiss Alps. Sustainability, 11(14), 3819, 1-22, DOI: 10.3390/su11143819.

Kiik L. (2023). Inter-national conspiracy? Speculating on the Myistone Dam controversy in China, Burma, Kachin, and a displaced village. Geopolitics, 28(1), 72-98, DOI: 10.1080/14650045.2020.1808886.

Kirchher J. and Charles K.J. (2016). The social impacts of dams: A new framework for scholarly analysis. Environmental Impact Assessment Review, 60, 99-114, DOI: 10.1016/j.eiar.2016.02.005.

Kornijowl R. (2009). Controversies around dam reservoirs: Benefits, Costs and future. Ecohydrology and Hydrobiology, 9(2-4), 141-148, DOI: 10.2478/v10104-010-0001-4.

Kucukali S. (2011). Risk assessment of river type hydropower plants using fuzzy logic approach. Energy Policy, 39(10), 6683-6688, DOI: 10.1016/j.enpol.2011.06.067.

Kucukali S. (2014). Environmental risk assessment of small hydropower (SHP) plants: A case study for Tefen SHP plant on Filyos river. Energy for Sustainable Development, 19(1), 102-110, DOI: 10.1016/j.esd.2013.12.010.

Kumar A., Yang T. and Sharma M.P. (2019). Long Term Prediction of greenhouse gas risk to the Chinese hydropower reservoirs. Science of Total Environment, 646, 300-308, DOI: 10.1016/j.scitotenv.2018.07.314.

Latrubesse E.M. et al. (2017). Damming the rivers of the Amazon Basin. Nature, 546, 363-369, DOI: 10.1038/nature22333.

La Rovere E.L. and Mendes F.E. (2000). Tucuruí Hydropower Complex Brazil, Final Report: November 2000. Cape Town: World Commission on Dams. Available at: https://archive.internationalrivers.org/sites/default/files/attached-files/csbrmain.pdf [Accessed 17 Dec. 2021].

Maan G.S., Patra J.P. and Singh R. (2020). A Hydro-Informatic Approach for Estimation of Design Flash Flood in Bargi Dam Cross-Section of Narmada River, India. Geography Environment Sustainability, 13(2), 104-114, DOI: 10.24057/2071-9388-2019-178.

McCully P. (2001). Silenced rivers: the ecology and politics of large dams. London: Zed Books. Available at: https://theswissbay.ch/pdf/Books/Survival/Farming%2C%20Animalraising%2C%20Homesteading/Farming%2Bgardening/water%20management/Silenced%20Rivers%20Complete%20.pdf [Accessed 15 Dec. 2021].

McNally A., Magee D. and Wolf A.T. (2008). Hydropower and sustainability: Resilience and Vulnerability in China's power sheds. Journal of Environmental Management, 90 (S3), S286-S293, DOI: 10.1016/j.jenvman.2008.07.029.

Moller L.C. (2005). Transboundary Water conflicts over hydropower and Irrigation: Can Multilateral Development Banks Help? CREDIT Research Paper No. 05/09. Nottingham: Centre for Research in Economic Development and International Trade, University of Nottingham. Available at: https://www.nottingham.ac.uk/credit/documents/papers/05-09.pdf [Accessed 20 Jul. 2021].

Moran E.F., Lopez M.C., Moore N., Muller N. and Hyndman D.W. (2018). Sustainable hydropower in the 21st century. Proceedings of National Academy of Sciences of United States of America, 115(47), 11891-11898, DOI: 10.1073/pnas.1809426115.

Mortey E.M., Ofosu E.A., Kolodko D.V. and Kabobah A.T. (2017). Sustainability assessment of the Bui hydropower System. Environments, 4(2), 1-25, DOI: 10.3390/environments4020025.

Morimoto R. (2013). Incorporating socio-environmental considerations into project assessment models using multi-criteria analysis: A case study of Sri Lankan hydropower projects. Energy policy, 59, 643-653, DOI: 10.1016/j.enpol.2013.04.020.

Nautiyal H. and Goel V. (2020). Sustainability assessment of hydropower projects. Journal of Cleaner Production, 265(1), 121661, DOI: 10.1016/j.jclepro.2020.121661.

Pinho P., Maia R. and Monterroso A. (2007). The quality of Portuguese environmental impact studies: The case of small hydropower projects. Environmental Impact Assessment Review, 27(3), 189-205, DOI: 10.1016/j.eiar.2006.10.005.

Poff N.L. and Hart D. (2002). How dams vary and why it matters for the emerging science of dam removal? [online], Bioscience, 52 (8), 659-688. Available at: https://pofflab.colostate.edu/wp-content/uploads/2019/08/Poff_2002_howdamsvaryandwhyitmatters.pdf [Accessed 10 Dec. 2022].

Rao R.V. (1989). Large and small dams. International Journal of Water Resources Development, 5(2), 135-142, DOI: 10.1080/07900628908722425.

Rauf H., Gull M.S. and Arshad N. (2020). Complementing hydroelectric power with floating solar PV for daytime peak electricity demand. Renewable Energy, 162, 1227-1242, DOI: 10.1016/j.renene.2020.08.017.

Richter B.D., Postel S., Revenga C., Scudder T., Lehner B., Churchill A. and Chow M. (2010). Lost in development's shadow: The downstream human consequences of dams. [online], Water Alternatives, 3(2), 14-42. Available at: https://www.water-alternatives.org/index.php/volume3/v3issue2/80-a3-2-3/file [Accessed 25 Nov. 2022].

Sardar Sarovar Narmada Nigam Ltd. (2021, 23 August). Benefits of Projects. [online], www.sardarsarovardam.org Available at: https://www.sardarsarovardam.org/benefits-of-project.aspx [Accessed 10 Dec. 2022].

Sayatham M. and Suhardiman D. (2015). Hydropower resettlement and livelihood adaptation: The Nam Mang 3 project in Laos. Water Resources and Rural Development, 5, 17-30, DOI: 10.1016/j.wrr.2015.01.001.

Schultz C., and Adams W.M. (2019). Debating dams: The World Commission on Dams 20 years on. Wiley Interdisciplinary Reviews: Water, 6(5), e1396, DOI: 10.1002/wat2.1369.

Scudder T.T. (2005). Future of Large Dams: Dealing with Social, Environmental, Institutional and Political Costs. London: Earthscan, Routledge, DOI: 10.4324/9781849773904.

Shafa N.S., Babzadeh H., Aghayari F., and Saremi A. (2023). Multi-objective planning for optimal exploitation of surface and groundwater resources through development of an optimized cropping pattern and artificial recharge system. Ain Shams Engineering Journal, 14(2), 101847, DOI: 10.1016/j.asej.2022.101847.

Shaktawat A. and Vadhera S. (2021). Risk management of hydropower projects for sustainable development- a review. Environment, Development and Sustainability, 23, 45-76, DOI: 10.1007/s10668-020-00607-2.

Sharma A.K. and Thakur N.S. (2017). Assessing the impact of small hydropower projects in Jammu and Kashmir: A study from north-western Himalayan region of India. Renewable and Sustainable Energy Reviews, 80, 679-693, DOI: 10.1016/j.rser.2017.05.285.

Sharma N., Acharya S., Kumar K., Chaurasia O.P. and Singh N. (2019). Hydroponics as an advanced technique for vegetable production-an overview. Journal of Soil and Water Conservation, 17(4), 364-371, DOI: 10.5958/2455-7145.2018.00056.5.

Singh, R. (2023). Water Resources Planning Under (Deep) Uncertainty. [online], Oxford Research Encyclopaedia of Environmental Science, www.oxfordre.com. Available at: https://doi.org/10.1093/acrefore/9780199389414.013.628 [Accessed 15 Mar. 2023].

Singh S., and Singh R. (2020). Geo-spatial topology based morphometric analysis for soil and water conservation in Dholbaha watershed of Kandi region. Journal of Physics: Conference Series, 1531 (2020) 012087, 1-14, DOI: 10.1088/1742-6596/1531/1/012087.

Sikka G. (2020). Moving beyond Economic Analysis: Assessing the socio-cultural impacts of displacement and resettlement by Sardar Sarovar Project, India. Geography Environment Sustainability, 13(3), 90-101, DOI: 10.24057/2071-9388-2019-165.

Sokolov D.I., Erina O.N., Tereshina M.A. and Puklakov V.V. (2020). Impact of Mozhaysk Dam on the Moscow River Sediment Transport. Geography Environment Sustainability, 13(4), 24-31, DOI: 10.24057/2071-9388-2019-150.

Sun L, Dongxiao N., Wang K. and Xu X. (2020). Sustainable development pathways of hydropower in China: Interdisciplinary qualitative analysis and scenario-based system dynamics quantitative modelling. Journal of Cleaner Production, 287, 125528, DOI: 10.1016/j.jclepro.2020.125528.

Thieme M.L., Khrystenko D., Qin S., Golden Kroner R.E., Lehner B., Pack S., ... and Mascia, M.B. (2020). Dams and protected areas: Quantifying the spatial and temporal extent of global dam construction within protected areas. Conservation Letters, 13(4), e12719, 1-8. DOI: 10.1111/conl.12719.

Tilt B., Barun Y. and He D. (2009). Social impacts of large dam projects: a comparison of international case studies and implications for best practice. Journal of Environmental Management, 90(Supplement 3), S249-S257, DOI: 10.1016/j.jenvman.2008.07.030.

Tullos D., Tilt B. and Liermann C.R. (2009). Introduction to the special issue: Understanding and linking the biophysical, socioeconomic and geopolitical effects of dams. Journal of Environmental Management, 90(Supplement 3), S203-S207, DOI: 10.1016/j.jenvman.2008.08.018.

United Nations (2021). Sustainable Development. New York: Department of Economic and Social Affairs, United Nations. Available at: https://sdgs.un.org/goals [Accessed 23 Jan. 2022].

United Nations (2022). Losing 25,000 to Hunger Every Day. [online], UN Chronicle. Available at: https://www.un.org/en/chronicle/article/losing-25000-hunger-every-day [Accessed 25 Dec. 2022].

Vella H. (12 January, 2021). Inside the world's largest dam - based floating solar power project. [online], Power Technology. Available at: https://www.power-technology.com/features/inside-the-worlds-largest-dam-based-floating-solar-power-project/ [Accessed 15 Mar. 2022].

Voegeli G., Hediger W. and Romerio F. (2019). Sustainability assessment of hydropower: Using Causal diagram to seize the importance of impact pathways. Environmental Impact Assessment Review, 77, 69-84, DOI: 10.1016/j.eiar.2019.03.005.

World Commission on Dams. (2000). Dams and Development; a new framework for decision-making: The Report of World Commission on dams. London: Earthscan Publications Ltd. Available at: https://archive.internationalrivers.org/sites/default/files/attached-files/world_commission_on_dams_final_report.pdf [Accessed 20 Nov. 2022].

World Food Program. (2022). Global Food Crisis- 2022: A year of unprecedented hunger. [online], World Food Program. Available at: https://www.wfp.org/global-hunger-crisis [Accessed 31 Dec. 2022].

World Register of Dams. (2020a). Number of dams by member countries. [online], International Commission on Large Dams. Available at: https://www.icold-cigb.org/article/GB/world_register/general_synthesis/number-of-dams-by-country-members [Accessed 31 Dec. 2020].

World Register of Dams. (2020b). General Synthesis. [online], International Commission on Large Dams. Available at: https://www.icold-cigb.org/GB/world_register/general_synthesis.asp [Accessed 31 Dec. 2020].

World Register of Dams. (2020c). Role of dams. [online], International Commission on Large Dams. Available at: https://www.icold-cigb.org/GB/dams/role_of_dams.asp [Accessed 31 Dec. 2020].

World Register of Dams (2020d). Classification by resettled persons. [online], International Commission on Large Dams. Available at: https://www.icold-cigb.org/article/GB/world_register/general_synthesis/classification-by-resettled-persons [Accessed 31 Dec. 2020].

Wu Y., Wang Y., Chen K., Xu C. and Li L. (2017). Social sustainability assessment of small hydropower with hesitant PROMETHEE method. Sustainable Cities and Society, 35, 522-537, DOI: 10.1016/j.scs.2017.08.034.

Wyrick J.R., Rischman B.A., Burke C.A., McGee C. and Williams C. (2009). Using Hydraulic modelling to address social impacts of small dam removals in southern New Jersey. Journal of Environmental Management, 90(Supplement 3), S270-S278, DOI: 10.1016/j.jenvman.2008.07.027.

Xu C., Xu Z. and Yang Z. (2019). Reservoir operation optimization for balancing hydropower generation and biodiversity conservation in a downstream wetland. Journal of Cleaner Production, 245, 118885, DOI: 10.1016/j.jclepro.2019.118885.

Yoneda Y. (18 December, 2013). Study shows Christmas trees suck up super potent greenhouse gas. [online], INHABITAT. Available at: https://inhabitat.com/new-study-shows-christmas-trees-suck-up-super-potent-greenhouse-gas/ [Accessed 30 Dec. 2022].

Zhang L., Pang M. and Wang C. (2014). Emergy Analysis of a small hydropower plant in South-western China. Ecological Indicators, 38, 81-88, DOI: 10.1016/j.ecolind.2013.09.037.

RESEARCH PAPER

GIS MAPPING OF THE SOIL COVER OF AN URBANIZED TERRITORY: DRAINAGE BASIN OF THE SETUN RIVER IN THE WEST OF MOSCOW (RUSSIAN FEDERATION)

Maria I. Gerasimova[1], Olga V. Chernitsova[1*], Jessica Yu. Vasil'chuk[1], Natalia E. Kosheleva[1]
[1] Lomonosov Moscow State University, Faculty of Geography, GSP-1, Leninskie Gory, Moscow, 119991, Russian Federation
*Corresponding author: olchernitsova@mail.ru
Received: December 5th, 2023 / Accepted: May 29th 2024 / Published: July 1st 2024
https://DOI-10.24057/2071-9388-2024-3136

ABSTRACT. Soil mapping of urban areas is required for solving many applied problems. However, its methodology is still under development. The lack of information about urban soils and the inconsistence of their classifications are the main difficulties, as well as the intricate soil cover patterns in cities and towns. The research was aimed to compile the soil map for the drainage basin of the small urban river Setun at a scale that could reflect its soil cover heterogeneity. Some new approaches to the differentiation of urban and semi-urban soils in accordance with recent ideas on their systematic and land use variants have been proposed. The concept of pedo-urbo-mosaics, which implements the soil cover pattern theory in relation to urbanized territory, has been used for delineating mapping units. The compilation methodology involved the use of open spatial data and GIS technologies. The subdivision of the basin into mapping units was performed using ©OpenStreetMap data and Yandex Maps Web mapping service. Spatial analysis in GIS allowed for mapping the territory with a moderate urbanization rate on a large scale, obtaining a more adequate and detailed spatial representation of the area than in the case of applying the traditional approach. The map, at a scale of 1:60,000 contains 16 natural/semi-natural soils and technogenic superficial formations, as well as 11 pedo-urbo-mosaics. The study may be of methodological interest as an experience in soil mapping of urbanized areas using GIS.

KEYWORDS: urban soils, soil classification, open spatial data, geoprocessing

CITATION: Gerasimova M. I., Chernitsova O. V., Vasil'chuk J. Yu., Kosheleva N. E. (2024). GIS Mapping Of The Soil Cover Of An Urbanized Territory: Drainage Basin Of The Setun River In The West Of Moscow (Russian Federation). Geography, Environment, Sustainability, 2(17), 131-138
https://DOI-10.24057/2071-9388-2024-3136

ACKNOWLEDGEMENTS: The work was supported by the Russian Science Foundation (project No. 19-77-30004-P).

Conflict of interests: The authors reported no potential conflict of interest.

INTRODUCTION

Mapping of urban areas is a relevant and important sphere of thematic mapping, required for solving applied problems, forecasting, and monitoring both the state of the environment as a whole and individual components of landscapes (Maantay and Ziegler 2006; Makarov et al. 2002), soils, and soil properties in particular (Gerasimova et al. 2003; Van De Vijver et al. 2020). The methodology for mapping the soil cover of cities, towns, and urbanized areas is currently still being formed.

The development of this particular sphere of GIS mapping faces certain difficulties. The amount of specific information concerning urban soils, their properties, and mapping units is insufficient; the very definition of urban soils and their separation from the natural ones depends on the concept of the map compilers (Charzyński and Hulisz 2017a; Prokof'eva et al. 2014). Classifications of urban soils are inconsistent, as they are based on different principles, on the one hand, and are considered as parts of the national basic classification systems, or as a classification of urban soils only, on the other hand (Aparin and Sukhacheva 2015; Burghardt et al. 2022; Charzhyński et al. 2013; Charzhyński et al. 2017b; IUSS Working Group WRB 2022; Lehman and Stahr 2007; Prokof'eva et al. 2014; Stroganova et al. 2005).

Urban landscapes comprise both human-made and natural elements. However, the city is a single spatial system, and its territory should be mapped following the same principles for all soils forming a virtual and spatial continuum from conventionally natural, urban-natural soils to urban soils sensu stricto and technogenic superficial formations (TSFs) perceived as "non-soils" (Tonkonogov 2001; Shishov et al. 2004), but occupying space in towns and cities. Urban-natural soils are those modified by urban impacts and having preserved initial natural properties, as well as soils on technogenic (urban) material with current pedogenesis governed by "natural rules".

Soils and soil units for urban maps. Within urban areas, most researchers identify several soil mapping units. Some of them are regarded as actually natural soils, considered background or reference soils. These are soils of green urban infrastructure – protected areas, parks, forests, and gardens (Klimanova and Illarionova 2020). However, in large cities and their suburbs, it seems hardly possible, since such soils are more or less subject to aerial pollution. Furthermore, the soil cover is composed of both undisturbed and slightly disturbed natural soils. Recreational impacts in such areas are insignificant and include compaction of some soils, changes in vegetation, and additions of organic materials, mostly urban waste. Occasionally, local mechanical disturbances can occur in the course of arranging paths, trails, and digging trenches for various cables, as well as due to the construction of infrastructural and sports facilities (Kuznetsov et al. 2017; Paramonova et al. 2010). Therefore, we name such soil mapping units "conventionally natural" soils.

The next (opposite) group includes artificial soils, purposefully constructed for the creation and/or maintenance of green infrastructure (Klimanova and Illarionova 2020; Mankiewicz et al. 2017) or for outdoor sports facilities. Examples of the latter are football fields (Zamotaev and Shevelev 2012), golf courses (Charzyński et al. 2017b), as well as rolled lawns in city parks and boulevards. There are also botanical gardens and even urban vegetable gardens or urban agriculture in cities, where soils are improved – prograded (Lal 2017).

Soils, most typical for the urban environment, were defined in publications as urbanozems (Gerasimova et al. 2003; Stroganova et al. 1998; Stroganova et al. 2005), later urbostratozems (Prokof'eva et al. 2014). They are specified by the presence of urbic diagnostic horizon in their profile. This horizon is composed of natural materials (sands, loams, clay, and fragments of initial soil horizons) mixed with any kind of urban additions (municipal wastes, construction blocks, dust, cultural layer, etc.). The urbic horizon is easily identified by the presence of rather numerous artefacts, and it is growing upward due to the additions of these and similar materials. It may occur either on a buried original soil profile that existed prior to city/town construction, or on the remnants of such profile, or on filled sediments. The name "urbostratozem" was proposed to emphasize additions that form strata and for correlating terminology when adjusting urban soils in the Russian soil classification system (Prokof'eva et al. 2014). In case of a lower thickness of the urbic horizon (< 40 cm) that overlays the identifiable remains of a natural soil, the term "urbo-soil" is used. These remains, mostly middle horizons, permit to identify the original soil and give a name to the urbo-soil, i.e., urbo-soddy-podzolic soil.

Quite special soils are those under highways, roads, squares, parking lots, and courtyards: they are covered or sealed with almost impermeable materials: paving stones, tiles, asphalt, and concrete. Sealed may be initial native soils or their remains, more commonly, special filled grounds – subbase and subgrade layers (sand, gravel) used for drainage, good trafficability, stability of covers and other engineering reasons (Kawahigashi 2017). In all cases, they are more or less strongly isolated from the surface impacts and named ekranozems (Prokof'eva 1998) or Ekranic Technosols (IUSS Working Group WRB 2022).

The non-soils, or technogenic superficial formations, are filled or cut sediments (strata or outcrops, respectively) lacking any genetic soil horizons.

The summarized current knowledge on soils in urban environment is presented in Fig.1.

Spatial units in cities and towns as identified in the current research. The intricate land use patterns and high heterogeneity of the soil cover in cities and towns are reasons to substitute the traditional approach to soil mapping with a more adequate one. Instead of delineating areas of individual soils, mapping units with similar compositions of soils – their ingredients – should be shown on the map. They should comprise two-four soils and TSF, if any. Thus, Aparin and Sukhacheva (2014) proposed the idea of "urbopedocombinations within the framework of the urbanized soil space", i.e., combinations, based on the geometry and composition of the polygons (areas) of soils, either natural, or human-modified, with non-soil formations in various proportions. Urban pedological combinations have regular geometric shapes, which distinctly separate them from the areas of almost all natural soils (Aparin and Sukhacheva 2014). Combinations of soils and TSF confined to certain land use zones on the same parent material were named by Shestakov et al. (2013) "urban pedological complexes". Similar concepts can be found in recent publications by foreign authors: pedo-urban complexes (Sobocká et al. 2020), urban pedotopes (Pindral et al. 2020). They were characterized as geographic and cartographic units for displaying the system of abiotic, biotic, and socio-economic components of an urban ecosystem. When identifying mapping units for the soil map of the city of Toruń, Poland, Charzyński and Hulisz (2017a) used the notion of mosaic pattern.

In cities and towns, the shapes of mapping units of almost all ingredients of the soil cover, that is, soil combinations, are determined by anthropogenic factors.

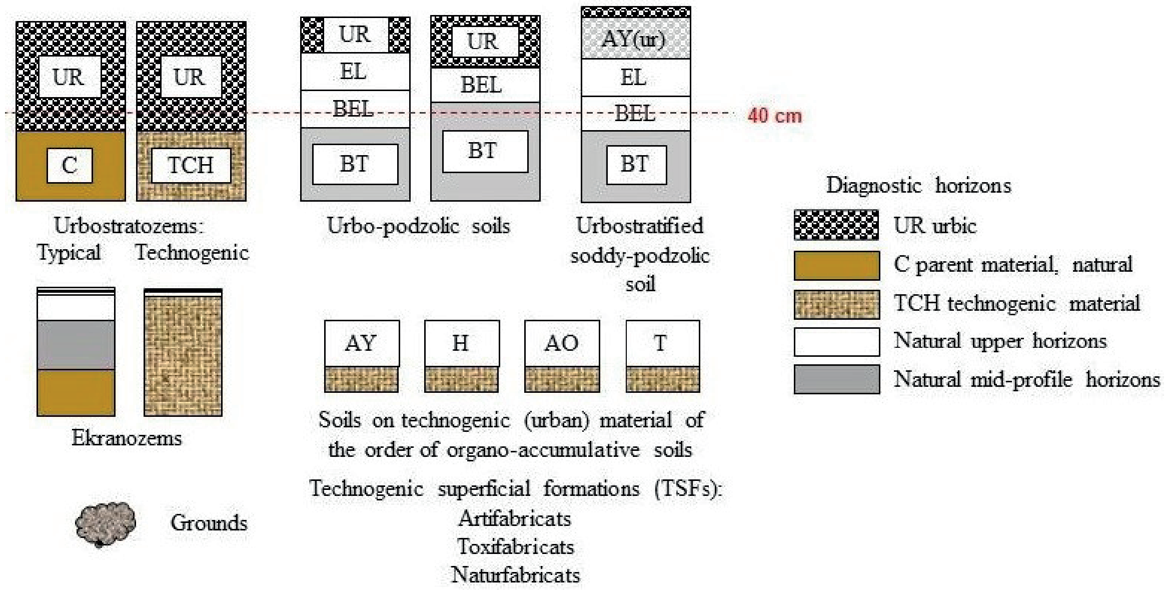

Fig. 1. Schemes of urban soil profiles within the Setun River drainage basin in terms of soil classification of Russia, with additions by Prokof'eva et al. (2014)

Consequently, the boundaries between them are usually sharp, irregular or winding, unnatural, and there are no genetic bonds between them. In the theory of soil cover pattern (Fridland, 1972), soil combinations of this type are defined as mosaics, since their components are casual, not related to each other, and quite contrasting. This is exactly how the soil cover in cities is arranged, since its configuration is mostly determined by historical and socio-economic factors, implemented in land use types. Following the criteria for identifying soil combinations in Fridland's theory of soil cover pattern, the soil cover of a city can be defined as composed of *pedo-urbo-mosaics*.

In most projects of large-scale urban soil mapping for delineating the spatial units, remote sensing (RS) data of high spatial resolution were used (for example, Aparin and Sukhacheva 2014; Kulik et al. 2015; Shestakov et al. 2013). For deriving boundaries of pedo-urban complexes, Sobocká et al. (2020, 2021) used open spatial data on land cover/ land use units of the Extended Nomenclature Urban Atlas 2012, which integrates information from different sources, mainly topographic maps and RS data of high and medium spatial resolution (Mapping guide… 2011). The efficiency of using GIS technologies for soil mapping of urban areas is also supported by the possibility of obtaining additional information about soil-forming agents, primarily relief and vegetation, through the analysis of digital terrain models and processing the RS data.

OpenStreetData (OSM), the volunteered spatial database, distributed under the Open Data Commons Open Database License[1], is widely used in large-scale thematic mapping of cities for outlining urban land use categories (Chen et al. 2021; Klimanova et al. 2020; Patriarca et al. 2019), urban greenery (Bobáľová et al. 2024) and classification of local climate zones (Fonte et al. 2019), but for urban soil mapping OSM data are currently undervalued. However, the positional accuracy and quality of OSM data, especially for urban areas, are estimated to be rather high (Borkowska and Pokonieczny 2022; Zheng and Zheng 2014).

The question of selecting the scale for soil maps of urbanized areas remains open. The limited experience in soil mapping of urban areas shows that the relevant cartographic scales for adequately representing the soil cover in cities are 1:25,000-1:75,000, or a larger one (up to 1:5,000) for particular sites of interest (Aparin and Sukhacheva 2014; Charzyński and Hulisz 2017a; Hernandez et al. 2017; Kulik et al. 2015; Shestakov et al. 2013; Sobocká et al. 2020; Vlasov et al. 2017). To our opinion, the most adequate approach for determining the scale of the soil map of urbanized areas is to rely on the average size of the identified soil units, taking into account the standards of traditional soil mapping in Russia in relation to meso- and micro-combinations identified in Fridland's theory of soil cover pattern (Fridland, 1972).

The purpose of this study was to develop methodological approaches to mapping the soil cover of an urbanized area based on GIS technologies, open spatial data, and current concepts on urban soils, as well as to compile the soil map of the urbanized drainage basin of a small urban river.

MATERIALS AND METHODS

The study area

The study was performed on the drainage basin of the small urban Setun River, which is the right tributary of the Moskva River. Its catchment area is about 190 km^2. There are two urban protected areas in the drainage basin: the Setun River Valley and Tepliy Stan.

The Setun drainage basin is located in the northwestern part of the Teplostan Upland, formed by a protrusion of bedrocks composed of sandy-clay strata from the Jurassic and Lower Cretaceous periods. Bedrocks are overlain by loams, which are underlain by the Dnepr loamy moraine and, less commonly, glaciofluvial sands (State Geological Map 1997). Due to urbanization, the relief has undergone significant changes: ravines and gullies have been filled in, and some parts of the Setun River floodplain have been elevated above the water level by 3-4 m by adding ground. Zonal soils, soddy-podzolics (Albic Retisols), are preserved fragmentarily in green urban areas, although they are somewhat changed by human impact.

Most of the study area is highly urbanized. The density of car roads with high transport intensity is about 2.6 km/km^2. There are also several railway lines, the total length of which is about 35 km. The majority of industrial emissions originate from heat and power supply facilities. Among non-industrial sources, facilities related to car repairs, car washes, and tire service, as well as gas stations, predominate (Bityukova and Akynzhanov 2023). Near the river source there is a closed municipal solid waste landfill Salar'yevo, the reclamation of which was implemented in 2018-2020.

The Setun River basin's soil mapping was performed using GIS. The published thematic maps (Ecological atlas of Moscow 2002; Grand comprehensive atlas of Moscow 2012; State Geological Map 1997), and the results of terrain studies have been systematized and organized as a GIS project implemented in the ArcGis™ software. The following OSM standard layers have been used for extracting information about land use and city infrastructure: 'highway-line', 'landuse-polygon', 'building-polygon', 'water-polygon', 'water-line', 'railway-line'. The relief features were analysed through morphometric indicators (slopes, Topographic Wetness Index (TWI)) calculated from the digital elevation model ALOS DEM.

To delineate arboreous/grass vegetation in green urban areas and to assess anthropogenic impact on greenery, as well as to estimate the degree of sealing in urban mapping units, two radiometric indices, the normalized difference vegetation index NDVI (Rouse et al. 1973), and the normalized built-up index NDBI (Chen et al. 2020; Zha et al. 2003), have been calculated for the Sentinel-2A scene (August 2021). The formulas for calculating indices are NDVI = (NIR-R)/(NIR+R), NDBI = (SWIR1-R)/(SWIR1+R), where R, NIR, and SWIR refer to Sentinel bands 4, 8, and 11, respectively. The resulting images had a spatial resolution of 10 m.

The history of land use, mainly on wastelands (unused sites with patches of grasses), was reconstructed using the 1979 Hexagon image and old maps, as well as available satellite data for previous decades.

Terrain research comprised special studies of soils for mapping, both conventionally natural ones and urban soils, in 2019-2022 – morphological descriptions of 46 soil profiles; analytical parameters: soil texture, pH, and organic carbon content of the upper soil horizons were measured at 105 sampling points. Auxiliary materials, that is, field descriptions of 38 soil pits made within the framework of student soil-geochemical training in the Faculty of Geography of Moscow State University in 2020-2021 were used, as well as published data on soils of the area (Prokof'eva and Gerasimova 2018; Prokof'eva et. al. 2020).

[1] https://www.openstreetmap.org

RESULTS AND DISCUSSION

Compilation of the soil map. Since the study has been oriented on methodological issues, its main result comprised the consecutive procedures applied and the map as an example of their application (Figs. 2 and 3). The compilation included two major processing stages: the subdivision of the drainage basin into spatial mapping units (SMUs) using geoprocessing and operations of spatial analysis in GIS, and defining soil units (SUs). Outlines of spatial mapping units are relevant for 2022; their dimensions correspond to a cartographic scale of 1:60,000. To characterize the predominant land use in city blocks, units of multi-storey, middle-storey and low-rise residential areas, as well as administrative, commercial, and business blocks, industrial zones, construction sites, etc., were identified.

The interpretation of open surface areas in the Setun River drainage basin in terms of soils occurring there was based on the knowledge gained in recent years on urban soils (Fig. 1), on the descriptions of soil pits available and supplied with some analytical data, and on the data from the auxiliary GIS layers (georeferenced published maps, remote sensing data, morphometric indicators derived from the ALOS DEM).

Spatial mapping units, except ekranozems and TSFs of construction sites and Salar'yevo landfill (non-soils), were grouped into homogeneous and heterogeneous units (Fig. 2). Almost all homogeneous SMUs, which are sites where the only land use type predominates, correspond to green urban spaces. Limited and diverse field data were the reasons for separating non-disturbed and weakly disturbed soils. Naming urban soils was performed mainly

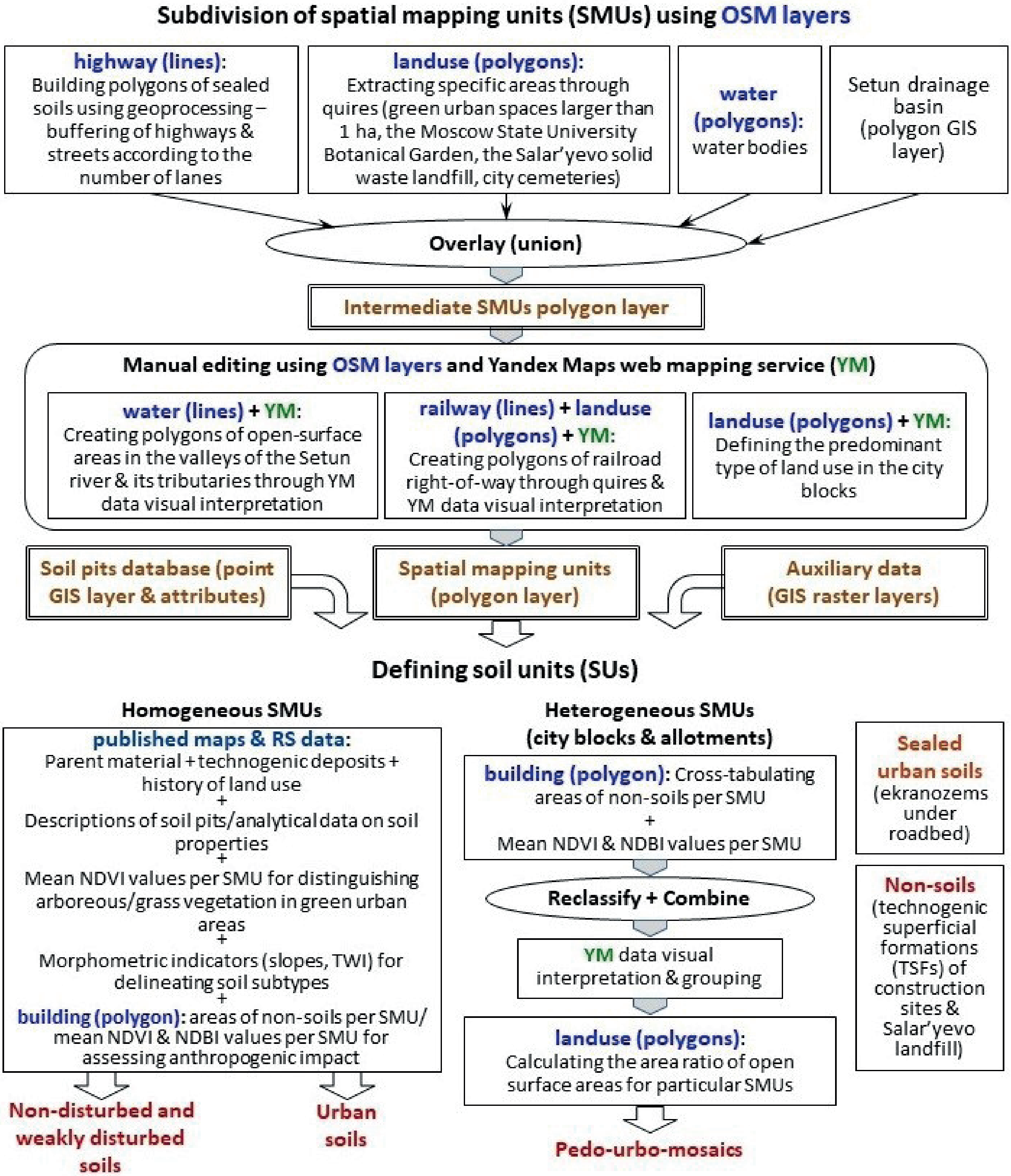

Fig. 2. Sequence of compilation procedures. Auxiliary data: georeferenced published maps[2], Sentinel-2A scene, ALOS DEM. OSM layers are highlighted in blue, Yandex Maps data - in green. Geoprocessing operations are shown as ovals

[2] http://www.etomesto.ru

through interpreting the history of land use and the map of technogenic deposits (Grand comprehensive atlas of Moscow 2012). Grassy areas/wastelands were compared with the corresponding sites on the 1979 Hexagon image and other historic images to distinguish between non-disturbed gray-humus (soddy) soils, and postagrogenic and postindustrial (gray-humus (soddy) soils on technogenic material). Slopes and the Topographic Wetness Index (TWI, calculated in SAGA GIS) were used for delineating different subtypes of conventionally natural soils. Therefore, areas with gradients greater than five degrees were interpreted as gray-humus (soddy) soils. Spaces with large TWI values were considered as sites with moisture accumulation and were qualified for soddy-podzolic gleyic and gleyed soils.

City blocks and allotments were considered as heterogeneous units with various combinations of urban soils and non-soils (areas under buildings). The proportion of areas under buildings was calculated using cross-tabulating areas in GIS. Commercial and administrative districts, as well as industrial zones, are built up to the greatest extent – on average, about 17-18%; up to a maximum of 55% of the territory is under buildings and facilities. In residential blocks, the share of land under buildings averages about 16%, with a maximum of 35-40%. In suburban areas with low-rise buildings, approximately 5% of the territory is built up.

Soil cover. The soil map (Fig. 3) demonstrates a prominent mosaic pattern of the soil cover in the Setun River drainage basin. The majority of mapping units are of similar size, about 10-20 ha, and almost all of them have a strict geometric shape with curved boundaries, sharp angles, and direct lines. The imprint of urbanization on the soil cover is manifested by the broad ratio of urban mosaics to conventionally homogeneous soils, whose largest areas are composed of zonal soddy-podzolic soils. They occur under green urban areas all over the basin, although they are more common in its western part, and they have some human-produced features. These are artefacts on the soil surface, such as single pieces of urban garbage, fragments of construction materials, either wood, or concrete, fireplaces; the soil surface is sometimes distorted, forest litter may be destroyed, and layers or piles of alien urban material may be spread over the soil surface. Such mapping units are named "soddy-podzolic urbostratified and surficially turbated". The intensity of anthropogenic impact on forests and forest parks was additionally assessed by the differences in the average NDBI values for the relevant mapping units. Interpretation of differences reflects the V-I-S (vegetation-impervious surface-soil) conceptual model for mixed pixels of urban areas (Ridd 1995). Higher average NDBI values, indicating a certain proportion of impervious surfaces, may be considered as a sign of recreational activities: the presence of buildings, walking paths, playgrounds, and sports grounds with an artificial cover. The only Podushkinskyi forest (northwest of the basin) has the least changed soddy-podzolic soils.

Conventionally, natural and semi-natural soils occur in very small mapping units in some sections of the Setun River and its tributary valleys, except for areas under arboreal vegetation.They are confined to better drained sites, – humus-alluvial soils, and to weakly drained ones, depressions, and/or places with high ground water table, – mucky alluvial gleyic and gleyed soils. One more group of soils forming homogeneous units are gray-humus (soddy) soils on steep slopes, rather old sediments overgrown with grasses, or on any technogenic materials, as well as on old artificial lawns.

Non-disturbed and weakly disturbed soils of green urban spaces occupy 27.8% of the drainage basin, urban soils in homogeneous spatial units (except ekranozems under roadbed with 6.5%) – 5.2% of the mapping area.

The rest of the area, composed of diverse city blocks where unbuilt areas alternate with buildings, is pedo-urbo-mosaics. Eleven types of such mosaics were specified in accordance with the participation of semi-natural and urban soils, as well as technogenic superficial formations. In low-rise residential areas, semi-natural soils (soddy-podzolic urbostratified and surficially turbated and

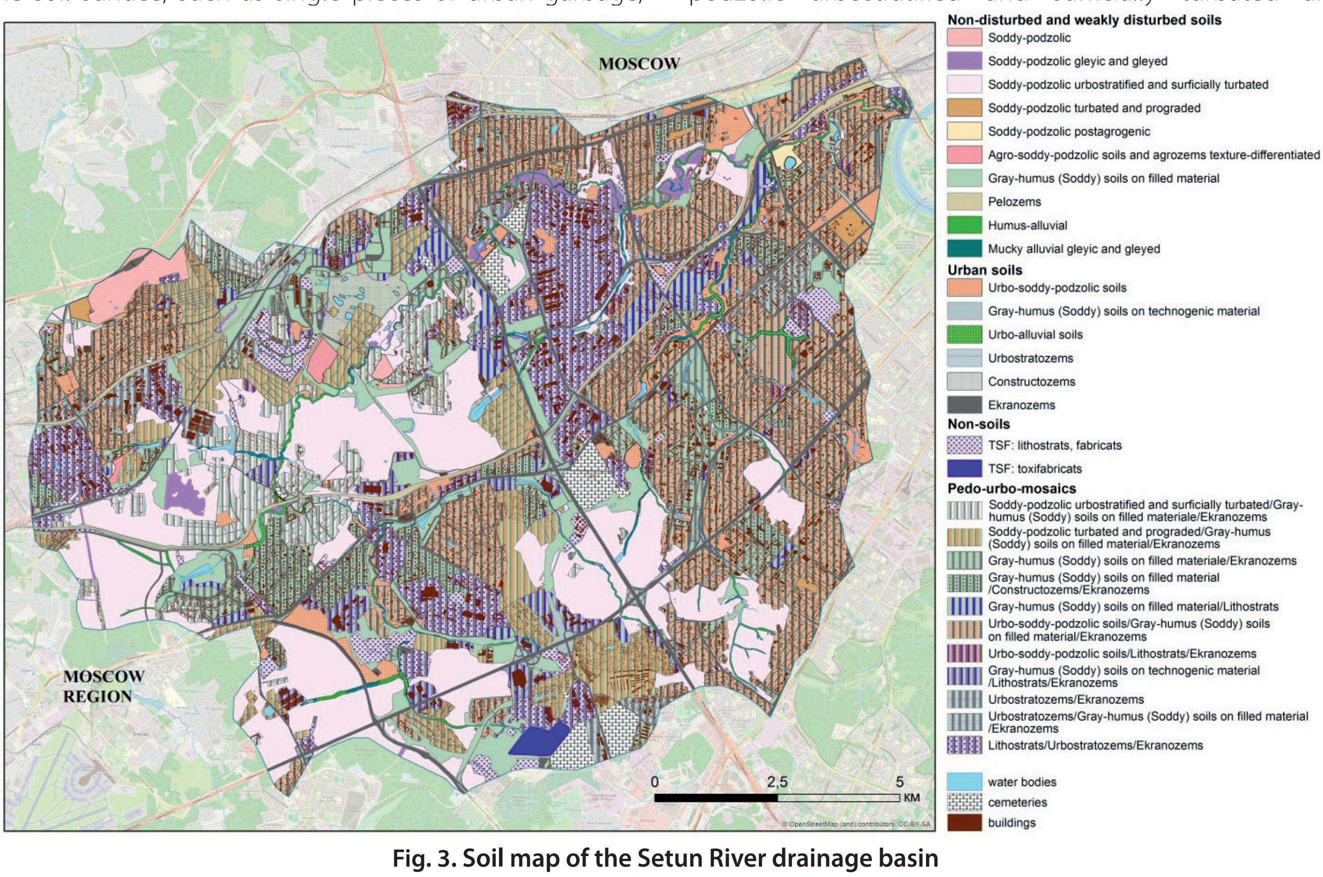

Fig. 3. Soil map of the Setun River drainage basin

soddy-podzolic turbated and prograded) alternate with ekranozems. Mosaics for multi-storey, middle-storey, and administrative spatial units include mainly urbo-soddy-podzolic, gray-humus (soddy) soils, and ekranozems, with a significant ratio of constructozems in newly built quarters. Pedo-urbo-mosaics of industrial and commercial areas comprise urbostratozems, lithostrats, gray-humus (soddy) soils on technogenic material, and ekranozems (Fig. 3).

Using the 'landuse-polygon' OSM layer allowed for estimating spatial ratios of open surface soils and non-soils in different pedo-urbo-mosaics. For example, in pedo-urbo-mosaic of multi-storey and middle-storey units, urbo-soddy-podzolic, gray-humus (soddy) soils, and ekranozems occupy 50-65, 5-10, and 10-15%, respectively. In administrative spatial units, this ratio is 30-35, 5-10, and 25-30%, respectively. The rest are non-soils under buildings.

The share of pedo-urbo mosaics in the drainage basin is 55.8%. This ratio agrees well with the area occupied by city blocks and allotments with residential, administrative, and industrial land use type, defined when analyzing heterogeneous SMUs – 34, 9, and 11% of the territory, respectively. The rest of the drainage basin is under TSFs and other objects (water bodies, cemeteries) – 2.4 and 2.3% of the area, respectively.

Comparison with the soil maps of other cities. The proposed methodology for compiling soil maps of urbanized areas using open spatial data and GIS-technologies is in good agreement with the approaches proposed in the works of Aparin and Sukhacheva (2014); Charzyński and Hulisz (2017a); Kulik et al. (2015); Shestakov et al. (2013); Sobocká et al. (2020). Similar to these studies, the determining factors in soil units' identification were land use types and transformations of the soil cover in the course of city development. We mapped the heterogeneous soil cover of built-up areas as soil combinations rather than as individual soil units. In addition to detailed remote sensing data, open-source spatial database OSM data were used, which made it possible to specify the structure of land use in urban areas and quantify the ratio of areas under different soils and non-soils in combinations, named pedo-urbo-mosaics. The proposed concept of pedo-urbo-mosaics, derived from Fridland's theory of soil cover pattern, develops the concept of urbopedocombinations used by Aparin and Sukhacheva (2014).

Remote sensing data of medium spatial resolution, similar to those used in our study, was mostly applied for assessing the degree of urbanized territory sealing (Chen et al. 2020; Gordienko et al. 2019). The methodology we propose involves the use of radiometric indices calculated from RS data of medium spatial resolution to assess the degree of anthropogenic impact on soils, primarily in green urban areas. Similar to the above-mentioned studies (Aparin and Sukhacheva 2014; Kulik et al. 2015); Shestakov et al. 2013; Sobocká et al. 2020), we included data on relief. However, we used digital elevation model (DEM), not a topography map, which simplified the use of these data in GIS. The use of auxiliary GIS data (RS and DEM) made it possible, despite the limited field data, to increase reliability when dividing soils into conventionally natural and urban ones as well as to identify variants of conventionally natural and semi-urban soils.

CONCLUSIONS

Soil mapping of urban areas, which has important applied significance, faces certain difficulties. The low efficiency of detailed soil surveys in urban areas, owing to their significant spatial heterogeneity in terms of soil profile composition and soil properties, the high costs of terrain and laboratory research, as well as the particularities of land use in cities, requires using non-traditional approaches to compiling maps of the soil cover in cities and towns. For mapping, we propose to integrate open spatial data and various predictors (published maps, processed remote sensing data, and digital elevation models) in GIS, similar to approaches used in digital soil mapping (DSM) of natural soils. However, the direct use of DSM procedures to predict soil units in urban areas is not possible since the heterogeneity of the soil cover in city blocks, in combination with the rather homogeneous soil cover of green urban spaces, limits the application of a single mathematical model describing relationships among predictors for the mapping area.

The soil map of the Setun drainage basin at a scale of 1:60,000 has been compiled that allows to use it to solve many applied problems in integrated environmental research. The proposed methodological approaches to mapping the soil cover of an urbanized area based on GIS technologies, open spatial data, and current concepts on urban soils allowed for mapping an area with a moderate level of urbanization at a large scale, obtaining a more adequate and detailed its spatial representation than in the case of applying the traditional approach.

The concept of pedo-urbo-mosaics, implemented in accordance with the soil cover pattern theory, promotes the development of the methodology for mapping urban soils. One more new trend implemented in this work was the differentiation of urban and semi-urban soils in accordance with recent ideas on their classification and land use variants.

REFERENCES

Aparin B.F. and Sukhacheva E.Yu. (2014) Principles of soil mapping of a megalopolis with St. Petersburg as an example. Eurasian Soil Science, 47, 650–661, DOI: 10.1134/S1064229314070035.

Aparin B.F. and Sukhacheva Ye. Yu. (2015). Classification of urban soils in Russian soil classification system and international classification of soils. Dokuchaev Soil Bulletin, 79, 53-72, DOI: 10.19047/0136-1694-2015-79-53-72.

Bityukova V.R. and Akynzhanov T.B. (2023) Sources of anthropogenic impact in the Setun river valley (territory of Moscow and the Moscow region): identification and assessment of the territorial structure. In: Mkrtchyan F.A., ed, Proceedings of the international symposium Engineering ecology. Moscow, 164-169 (in Russian with English summary).

Bobáľová H., Falťan V., Benová A., Kožuch M., Kotianová M., Petrovič F. (2024). Measuring the quality and accessibility of urban greenery using free data sources: A case study in Bratislava, Slovakia. Urban Forestry & Urban Greening, 93, 128217, DOI: 10.1016/j.ufug.2024.128217.

Borkowska S. and Pokonieczny K. (2022). Analysis of OpenStreetMap Data Quality for Selected Counties in Poland in Terms of Sustainable Development. Sustainability, 14(7), 3728, DOI: 10.3390/su14073728.

Burghardt W., Kneib W.D., Höke S., Lehmann A., Makowsky L., Kocher B., Steinweg B. (2022). Soil science within German cities. Journal of Plant Nutrition and Soil Science, 185(4), 462-474, DOI: 10.1002/jpln.202200211.

Charzyński P., Hulisz P., Bednarek R. (eds.). (2013). Technogenic Soils of Poland. Torun: Polish Society of Soil Science.

Charzyński P. and Hulisz P. (2017a). The case of Toruń, Poland. In: M. L. Levin et al., eds, Soils within Cities. Global approaches to their sustainable management – composition, properties and functions of soils of the urban environment. Stuttgart: Schweizerbart Science Publisher, 123-128.

Charzyński P., Kabala C., Galbraith J., Kuehn D., Prokof'eva T.V., Vasenev V.I. (2017b). Classification of urban soils. In: M. L. Levin et al., eds, Soils within Cities. Global approaches to their sustainable management – composition, properties and functions of soils of the urban environment. Stuttgart: Schweizerbart Science Publisher, 93–106.

Chen J., Chen S., Yang C., Hea L., Hou M., Shi T. (2020). A comparative study of impervious surface extraction using Sentinel-2 imagery. European Journal of Remote Sensing, 53 (1), 274–292, DOI: 10.1080/22797254.2020.1820383.

Chen B., Tu Y., Song Y., Theobald D.M., Zhang T., Ren Z., Li X., Yang J., Wang J., Wang X., Gong P., Bai Y., Xu B. (2021). Mapping essential urban land use categories with open big data: Results for five metropolitan areas in the United States of America. ISPRS Journal of Photogrammetry and Remote Sensing, 178, 203-218, DOI: 10.1016/j.isprsjprs.2021.06.010.

Fonte C.C., Lopes P., See L., Bechtel B. (2019). Using OpenStreetMap (OSM) to enhance the classification of local climate zones in the framework of WUDAPT. Urban Climate, 28, 100456, DOI: 10.1016/j.uclim.2019.100456.

Ecological atlas of Moscow. (2002). Moscow: Moscow Master Plan Institute (in Russian).

Fridland V.M. (1972). Soil cover pattern. Moscow: Mysl (in Russian).

Gerasimova M.I., Stroganova M.N., Mozharova N.V., Prokof'eva T.V. (2003). Anthropogenic soils: genesis, geography, reclamation. 1st ed. Smolensk: Ecumene (in Russian).

Grand comprehensive atlas of Moscow. (2012). Moscow: Feoriya (in Russian).

Gordienko O.A., Manaenkov I.V., Kholodenko A.V., Ivantsova E.A. (2019). Mapping and Assessment of Sealing Rate of Soils in the City of Volgograd. Eurasian Soil Science, 52(11), 1439-1446, DOI: 10.1134/S106422931911005X.

Hernandez L., Levin M., Calus J., Galbraith J., Muñiz E., Ryan K., Riddle R., Shaw R.K, Dobos R., Peaslee S., Southard S., Surabian D., Lindbo D. (2017). Urban Soil Mapping through the United States National Cooperative Soil Survey. In: R. Lal and B. A. Stewart, eds, Urban Soils. Boca Raton: CRC Press. DOI: 10.1201/9781315154251.

IUSS Working Group WRB (2022). World Reference Base for Soil Resources. International soil classification system for naming soils and creating legends for soil maps. 4th ed. Vienna: IUSS.

Kawahigashi M. (2017) Specific properties of soils underneath pavement construction. In: M. L. Levin et al., eds, Soils within Cities. Global approaches to their sustainable management – composition, properties and functions of soils of the urban environment. Stuttgart: Schweizerbart Science Publisher, 177-180. 78-84.

Klimanova O.A. and Illarionova O.A. (2020). Green infrastructure indicators for urban planning: applying the integrated approach for Russian largest cities. Geography, Environment, Sustainability. 13(1), 24-34, DOI: 10.24057/2071-9388-2019-123.

Klimanova O.A., Kolbovsky E.Yu., Illarionova O.A. (2020). Urban greenery: status assessment and designing development. Moscow: KMK Publishing House (in Russian).

Kulik K.N., Kretinin V.M., Kosheleva O.Yu. (2015). Experience in mapping the soil cover of the city of Volgograd. Bulletin of Voronezh State University. Series: Geography. Geoecology, 1, 40-45 (in Russian).

Kuznetsov V.A., Ryzhova I.M., Stoma, G.V. (2017). Changes in the properties of soils of Moscow forest parks under the impact of high recreation loads. Eurasian Soil Science, 50, 1225-1235, DOI: 10.1134/S1064229317100052.

Lal R. (2017) Urban agriculture and food security. In: M. L. Levin et al., eds, Soils within Cities. Global approaches to their sustainable management – composition, properties and functions of soils of the urban environment. Stuttgart: Schweizerbart Science Publisher, 177-180.

Lehmann A. and Stahr K. (2007): Nature and Significance of Anthropogenic Urban Soils. Journal of Soils and Sediments, 7 (4) 247–260, DOI: 10.1065/jss2007.06.235

Maantay J. and Ziegler J. (2006). GIS for the urban environment. Redlands: ESRI Press.

Makarov V.Z., Novakovsky B.A., Chumachenko A.N. (2002). Ecological-geographical mapping of cities. Moscow: Scientific World (in Russian).

Mankiewicz P., Morin T., Cheng Z. (2017). Soils in Green Infrastructure. In: M. L. Levin et al., eds, Soils within Cities. Global approaches to their sustainable management – composition, properties and functions of soils of the urban environment. Stuttgart: Schweizerbart Science Publisher, 139–147.

Mapping guide for a European Urban Atlas. (2011). European Union.

Patriarca J., Fonte C.C., Estima J., de Almeida J.-P., Cardoso A. (2019). Automatic conversion of OSM data into LULC maps: comparing FOSS4G based approaches towards an enhanced performance. Open Geospatial Data, Software and Standards 4, 11, DOI: 10.1186/s40965-019-0070-2.

Paramonova T.A., Tishkina E.V., Krasnov S.F., Tolstihun D.O. (2010). Soil cover structure and main soil properties of national park Vorobievy Gory. Moscow University Bulletin. Series 17. Soil science, 1, 24-34 (in Russian with English summary).

Pindral S., Kot R., Hulisz P., Charzyński P. (2020). Landscape metrics as a tool for analysis of urban pedodiversity. Land Degradation and Development, 31(16), 2281–2294, DOI: 10.1002/ldr.3601.

Prokof'eva T.V. (1998). Urban soils sealed by road covers: example of Moscow. Candidate thesis. Moscow.

Prokof'eva T.V., Gerasimova M.I., Bezuglova O.S., Bakhmatova K.A., Gol'eva A.A., Gorbov S.N., Zharikova E.A., Matinyan N.N., Nakvasina E.N., Sivtseva N.E. (2014) Inclusion of soils and soil-like bodies of urban territories into the Russian soil classification system. Eurasian Soil Science, 10(47), 959-967, DOI: 10.1134/S1064229314100093.

Prokof'eva T.V. and Gerasimova M.I. (2018). Urban Soils: Diagnostics and Taxonomic Position according to Materials of Scientific Excursion in Moscow at the Suitma-9 Workshop. Eurasian Soil Science, 51, 995-1007, DOI: 10.1134/S1064229318090090.

Prokof'eva T., Umarova A., Bykova G., Suslenkova M., Ezhelev Z., Kokoreva A., Gasina A., Martynenko I. (2020). Morphological and physical properties in diagnostics of urban soils: case study from Moscow, Russia. Soil Science Annual, 71(4), 309–320. DOI: 10.37501/soilsa/131598.

Ridd M.K. (1995) Exploring a V-I-S (vegetation-Impervious surface-soil) model for urban ecosystem analysis through remote sensing: comparative anatomy for cities. International Journal of Remote Sensing, 16(12), 2165-2185, DOI: 10.1080/01431169508954549.

Rouse J. W., Haas R. H., Schell J. A., Deering D. W. (1973). Monitoring vegetation systems in the great plains with ERTS. Third ERTS Symposium, NASA SP-351, 1, 309–317.

Shestakov I.E., Eremchenko O.Z., Fil'kin T.G. (2013). Approaches toward soil mapping of urban territories with the city of Perm as an example. Eurasian Soil Science, 46(12), 1130-1138, DOI: 10.1134/S1064229314010104.

Shishov L.L., Tonkonogov V.D., Lebedeva I.I., Gerasimova M.I. (2004). Classification and diagnostics of soils of Russia. Smolensk: Eucumene (in Russian).

Sobocká J., Saksa M., Szatmári D., Ferane J., Kopecká M. (2020). A complexity related to mapping and classification of urban soils (a case study of Bratislava city). Soil Science Annual, 71(4), 321–333, DOI: 10.37501/soilsa/127525.

Sobocká J., Saksa M., Feranec J., Szatmári D., Holec J., Bobáľová H., Rášová A. (2021). Mapping of urban environmentally sensitive areas in Bratislava city. Journal of Soils and Sediments, 21, 2059–2070, DOI: 10.1007/s11368-020-02682-4.

State Geological Map of the Russian Federation. (1997). Map of Quaternary deposits. Sheet N-37-II (Moscow) (in Russian).

Stroganova M., Myagkova A., Prokof'ieva T., Skvortsova I. (1998) Soils of Moscow and Urban Environment. Moscow: PAIMS.

Stroganova M.N., Gerasimova M.I., Prokof'ieva T.V. (2005). Approaches to grouping the technogenic soils. Eurasian Soil Science, 38(1), 66-71.

Tonkonogov V.D. (2001). Evolutionary-Genetic Classification of Soils and Nonsoil Surface Formations. Eurasian Soil Science, 34(6), 577-583.

Van De Vijvera E., Delbecquea N., Verdoodta A., Seuntjens P. (2020). Estimating the urban soil information gap using exhaustive land cover data: The example of Flanders, Belgium. Geoderma, 372, 114371, DOI: 10.1016/j.geoderma.2020.114371.

Vlasov D.V., Kasimov N.S., Kosheleva N.E. (2017). Mapping of landscape and geochemical structure of urban territory (Moscow case study). In: InterCarto InterGIS, 1(23), 242-255. DOI:10.24057/2414-9179-2017-1-23-242-255 (in Russian with English summary).

Zamotaev I.V. and Shevelev D.L. (2012) Concepts of technopedogenesis of football fields of Moscow Region. Scientific bulletin of Belgorod State University. Series Natural Sciences, 20, 141-150 (in Russian with English summary).

Zha Y., Gao J., Ni S. (2003). Use of normalized difference built-up index in automatically mapping urban areas from TM imagery. International Journal of Remote Sensing, 24, 583–594, DOI: 10.1080/01431160304987.

Zheng S. and Zheng J. (2014). Assessing the Completeness and Positional Accuracy of OpenStreetMap in China. In: T. Bandrova et al., eds. Thematic Cartography for the Society. Lecture Notes in Geoinformation and Cartography. Cham: Springer, DOI: 10.1007/978-3-319-08180-9_14.

RESEARCH PAPER

POST-FIRE SUCCESSION OF PSEUDO-TAIGA LARCH FOREST IN THE TARVAGATAI MOUNTAIN RANGE, MONGOLIA

M. Undraa[1,3], Sergey N. Bazha[2*], B. Oyunsanaa[3], Ch. Dorjsuren[1]
[1] Botanic Garden and Research Institute, Mongolian Academy of Sciences, Ulaanbaatar, 13330, Mongolia
[2] A.N.Severtsov Institute of Ecology and Evolution of the Russian Academy of Sciences, Moscow, 119071, Russia
[3] Department of Environment and Forest Engineering, School of Engineering and Applied Sciences, National University of Mongolia, Ulaanbaatar, 14201, Mongolia
*Corresponding author: monexp@mail.ru
Received: November 15th, 2023 / Accepted: June 11th, 2024 / Published: July 1st 2024
https://DOI-10.24057/2071-9388-2024-3121

ABSTRACT. Understanding post-fire recovery and succession is crucial for determining the forest's further reestablishment rate and development tendency, facilitating the restoration and protection of degraded forests, and planning post-fire forest management. The main aim of this study was to evaluate forest regeneration and reveal the tendency of plant succession after large-scale fire in the Tarvagatai Mountain range, Central Khangai, Mongolia. The monitoring study on post-fire plant succession and regeneration in the forbs-*Rhytidium* mosses pseudotaiga larch forests was conducted on permanent sample plots from 2007 to 2021 in the forest sites, which were damaged by severe fires in 1996 and 2002. Our results indicated that burned forest was regenerated sufficiently through the several serial stages of post-fire successions as fireweed (*Chamaenerion angustifolium*) community (up to 5 years after fire), fireweed-bonfire moss (*Funaria hygrometrica*) community (from 6 to 10 years), forbs community (11-16 years), grass-forbs young larch forest (17-25 years). Species numbers gradually increased with time in the forest affected by fires, whereas they rose drastically in the forest damaged by fire and livestock browsing due to the increase of ruderal species. In spite of the long recovery period, the post-fire similarity indexes of species composition and coenotic percentage compared with the control forest were relatively low, indicating a slow pre-fire vegetation recovery.

KEYWORDS: forest fire, *Larix sibirica*, forest regeneration, succession, pseudo-taiga forest

CITATION: Undraa M., Bazha S. N., Oyunsanaa B., Dorjsure Ch. (2024). Post-fire succession of pseudo-taiga larch forest in the Tarvagatai Mountain range, Mongolia. Geography, Environment, Sustainability, 2(17), 139-149
https://DOI-10.24057/2071-9388-2024-3121

ACKNOWLEDGEMENTS: We appreciate researchers from the Laboratory of Forest Phytocenology, Botanic garden and Research Institute, Mongolian Academy of Sciences, and the Joint Russian-Mongolian complex biological expedition for their assistance in the fieldwork.

Conflict of interests: The authors reported no potential conflict of interest.

INTRODUCTION

The forest ecosystems of the world, which cover nearly a third of the total land area, provide important forest goods and a wide range of services such as carbon sink and storage, soil and water protection, biodiversity maintenance and conservation (Jenkins and Brian 2018; FAO 2020; FAO and UNEP 2020). Boreal forests cover 27% of the global forest area (FAO 2020). The boreal forests of Mongolia cover 12.6 million hectares or 8.07% of the country's territory (Forest Research and Development Center 2021).

Fire is one of the natural and human-induced forces that have influenced the development of boreal and hemiboreal forests over time. However, it is also a significant source of emitted carbon, contributing to global warming and leading to biodiversity changes (Nasi et al. 2002), altering soil and light conditions, affecting seedbanks, and removing seed trees (Kristi Parro et al. 2015), decreasing the biomass of forest trees (Altrell 2019), transforming the environment of forest existence, and changing the composition and structure of the plant cover (Matveev et al. 2012).

Annual mean air temperature in Mongolia has increased by 2.24°C, whereas annual precipitation has decreased by 7% from 1940 to 2015 (MET 2018). Climate change is expected to increase fire severity and frequency (Hille and Ouden 2004; Jacquelyn et al. 2017; Boucher et al. 2020), as well as increase the burned area in the boreal forest (Ponomarev et al. 2016). Across the country from 1995 to 2020, 179 fires occured annually, covering an average of 357 thousand hectares of forest. Fire in Mongolia damaged 2367 thousand hectares, 2710 thousand hectares, and 583 thousand hectares of forest in 1996, 1997, and 2002, respectively (National Emergency Management Agency 2020). As a result of fires in 1996 and 1997, almost 500 thousand hectares of forests were completely burned and lost their ecological function (Tsogtbaatar 2004).

Monitoring studies on post fire succession are needed, specifically in the Tarvagatai mountain range after the large-scale fires that occurred in 1996 and 2002. Large-scale fires are classified as more than 200 hectares of burnt areas (Valendik et al. 1979). In the Tarvagatai Mountain Range, 114.3 thousand hectares or 52% of forest areas were damaged by fire in 1996, 2002 and 2003 (Jagdag and Gerelbaatar 2016).

Various studies on post-fire succession in the boreal forest exist (Bergeron and Dubue 1988; Bergeron and Dansereau 1993; Johnstone et al. 2004; Greene et al. 2004; Johnstone et al. 2010; Ivanova et al. 2014; Gamova 2014; Tautenhahn et al. 2016). However, only few studies on post-fire regeneration and succession in boreal larch forests are so far available (Uemura et al. 1990; Abaimov et al. 2002; Tsvetkov 2006; Takahashi 2006; Danilin 2009; Lytkina and Mironova 2009; Zyryanova et al. 2010; Matveev et al. 2012; Prokushkin and Zyryanova 2013; Cai et al. 2013, Cai et al. 2018). In particular, few studies on larch forest regeneration after fires have been conducted in Mongolia (Tsogt 1993; Zoyo 2000; Park 2005; Dugarjav 2006; Dorjsuren et al. 2007; Dorjsuren 2009; Park et al. 2009; Undraa et al. 2015; Chu et al. 2017; Undraa et al. 2020).

The monitoring of post-fire forest natural regeneration and succession is crucial to both ecological research on the forest further reestablishment rate and the development tendency and development of scientifically justified policies of forest management and protection (Abaimov and Sofronov 1996; Hille and Ouden 2004; Chen et al. 2014; Chen et al. 2018).

The overall aim of this study was to study natural regeneration and succession after large-scale fires in the Tarvagatai Mountain Range. The objectives of this study were: 1) to investigate the natural regeneration of burnt larch forest; 2) to reveal serial stages of post-fire successions; and 3) to determine the species composition and diversity after fire.

MATERIALS AND METHODS

Study area

The study on post-fire regeneration and succession of pseudo-taiga larch forests (*Larix sibirica Ledeb.*) was carried out in the Tarvagatai Mountain Range of Central Khangai, Tosontsengel Soum, Zavkhan Province, located 890 km northwest of Ulaanbaatar, Mongolia (Fig.1). The Tarvagatai Mountain Range within the Khangai Mountain main range of Mongolia is located in the Central Khangai forest vegetation province, which occupies 1.74 million hectares, or 13.6% of the forest area of Mongolia (Tungalag 2020). The forests of Central Khangai are represented by two altitude-zonal complexes of forest types: pseudo-taiga (83%) and sub-alpine (17%). The most widespread forest type is forbs-Rhytidium mosses pseudo-taiga larch forests (35%) (Dorjsuren 2009). Pseudo-taiga larch forests were first described by Dugarjav et al. (1975) under the name "dry mossy larch forests" in the Tarvagatai Mountain Range. As physiognomy, dry mossy larch forests are similar to green mossy larch taiga; medium-high-density uneven-aged stands, and a well-developed moss layer; however, they are sharply distinguished by many attributes: it has an extreme continental cold and arid climate; the forest soil is mountain forest coarse-humus permafrost soil; the herbaceous layer consists of tundra-alpine, meadow-forest, and forest steppe species; and the moss layer is dominated by the dry mosses *Rhytidium rugosum* and *Abietinella abietina*. Their common feature is that they are very susceptible to anthropogenic influences (Krasnoshekov 1983; Krasnoshekov 1996). Therefore, dry mossy larch forests are named pseudo-taiga (Korotkov 1976).

According to data from 1996-2021, the annual average air temperature is -4.9°C, the annual average precipitation is 223.7 mm (Institute of Meteorology and Hydrology 2021), and the plant growth-intensive period is 141 days (Dorjsuren 2009).

Field data collection

Fieldwork was conducted at the middle of growing seasons (late July and early August), 2007, 2010, 2012, 2015, 2016, 2019, and 2021. Permanent sample plots (PSP) were established to conduct periodic long-term monitoring survey on post-fire regeneration and vegetation. We selected two study areas, Baitsiin Ar and Bayan-Uul in the Tarvagatai Mountain range. The two study areas were nearly 35 km apart from each other. At each study area,

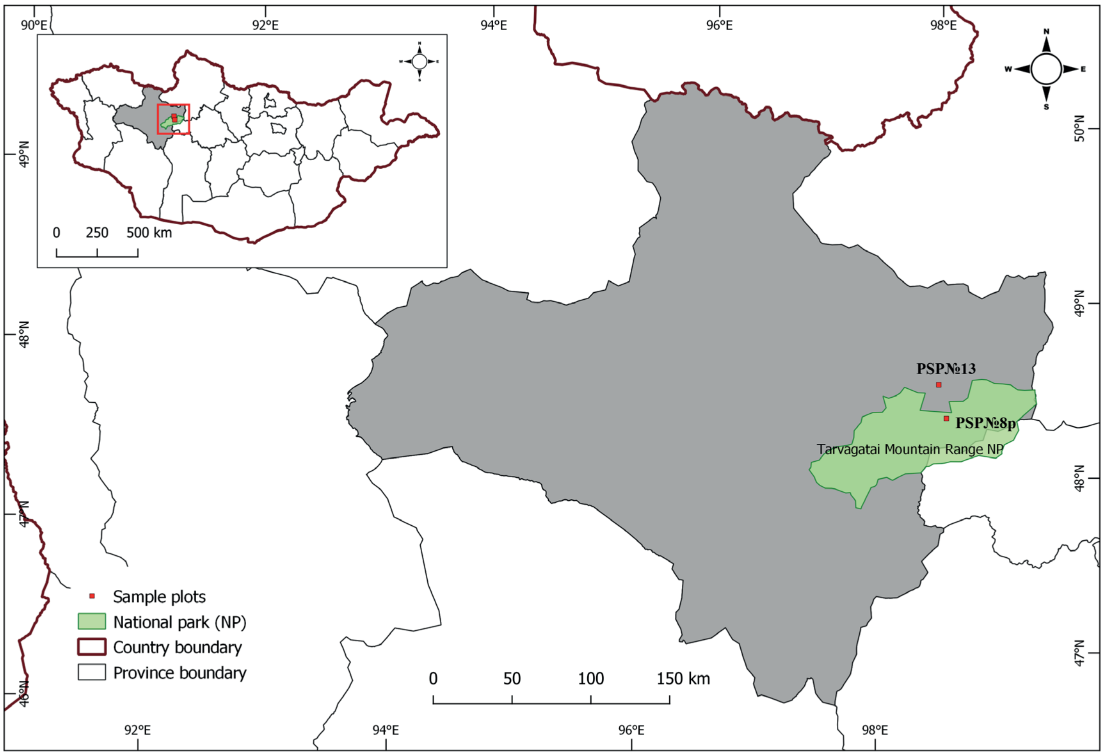

Fig. 1. Location of the study sites

we defined two sites, control forest and burned forest. Site size was provided in Table 1. Two permanent sample plots (PSP №8p and №13) were established in 2007 at 48°16´N, 98°21´E (burned in 2002) and 48°27´N, 98°15´E (burned in 1996) (Table 1). The measurements of number of seedlings and saplings, plant cover, diversity indexes were labelled with year after the fire (AF), which showed the time since the fire. For example, in plot №8p, which burned in 2002, data from 2007 were labelled as AF5 (5 years since the last fire) etc.

The size of permanent sample plot №8p was 20×20 m, which was divided into 16 subplots of 5×5 m. Inventory of seedlings and saplings was conducted each subplots. The size of permanent sample plot №13 was 40×50 m, that was divided into 20 subplots of 10×10 m. The inventory of seedlings and saplings was conducted in 2×2 m quadrates in each subplots. Seedlings and saplings were divided into five height classes: 0-10 cm, 11-50 cm, 51-150 cm, 151-300 cm, and ≥ 300 cm. Plants under 1 year old were considered seedlings, whereas plants ≥ 2 years old were considered saplings. The upper limit of a sapling is a woody plant with up to 8 cm diameter at breast height. We measured the diameter at breast height (DBH; breast height=1.3 m) and height of all standing trees in each subplot of PSP №13.

Shrub, herbaceous, and lichen-moss projective covers were evaluated visually in each quadrate. We conducted a vegetation survey in all quadrates, wherein species composition and cover were recorded in the shrub, herbaceous, and moss-lichen layers. To identify vascular plants and mosses, we used the Key to the Vascular Plants of Mongolia (Grubov 1982) and the Key to the Mosses of Mongolia (Tsegmid 2001).

Data analysis

The post-fire changes in the plant community can be identified by two parameters: 1) a change in the plant species composition, and 2) a change in the plant species projective cover. Based on these two parameters, we calculated the post-fire similarity index in species composition and in coenotic percentage (plant community species projective cover, %) for sample plots.

The species composition similarity index (S_s) was calculated for all pairs of sites, including control and burned stands, using the Sørenson (1948) Eq. 1:

$$S_s = \frac{2c}{a+b} \times 100\% \quad (1)$$

where *a* is the number of species in sample A, *b* is the number of species in sample B, and *c* is the number of common species in both samples.

The coenotic percentage similarity index (CPS) was calculated using Renkonen's (1938) Eq. 2, which was interpreted as follows:

$$CPS = \sum_{i=1} min\left(p_{1i}, p_{2i}\right) \quad (2)$$

where p_{1i} the proportion of projective cover (pc_{1i}) multiplied by frequency (*k1i*) of the *i*-th species in sample A $\left(p_{1i} = \frac{pc_{1i} * k_{1i}}{\Sigma\left(pc_{1i} * k_{1i}\right)}\right)$; p_{2i} the proportion of projective cover (pc_{2i}) multiplied by frequency (k_{2i}) of the *i*-th species in sample B. $k_{1i} = \frac{n_{1i}}{N_1}$, n_{1i} number of subsamples with *i*-th species, N_1 total number of subsamples in given sample A

Yearly differences in mean projective covers in shrub and herbaceous, lichen, and moss layers at the study sites were analyzed by the Tukey-Kramer test using the statistic software JMP 4.0.

The Steel Dwass test was performed to detect yearly difference in species richness and species diversity.

In total, 16 quadrates in plot №8p and 20 quadrates in plot №13 were used for species analysis over time post-fire. Shannon-Weaver (Shannon and Weaver 1949), Simpson diversity (Simpson 1949), and Pielou's evenness (Pielou 1975) indices were calculated to identify changes in species diversity after forest fire.

Shannon –Weaver's index (*H´*)

$$H' = -\sum_{i=1}^{S} p_i * In\left(p_1\right) \quad (3)$$

where *s* is the number of species, p_i is the proportion of individuals or the abundance of the species expressed as a proportion of total cover

$$D = 1 - \sum_{i=1}^{S} \left(p_1\right)^2 \quad (4)$$

Simpson's diversity index (*D*)

$$J = H'/In\,(S) \quad (5)$$

Pielou's evenness (*J*)

where *H'* is Shannon-Weaver's diversity index, *S* is the total number of species within a plot and *In(S)* is denotes the maximum value of *H'*.

Detrended correspondence analysis (DCA) was performed to identify differences in species composition among sub-quadrats in the sample plots. All statistical analyses were performed using R version 4.1.1[1].

Table 1. Description of the permanent sample plots (PSP) and degradation factors

№	Location	Size of plot, m^2	Elevation a.s.l, m	Coordinate, slope, exposure	Degradation factor
1	Baitsiin Ar (PSP № 8p)	20 × 20 m	2072	N 48^{0}16'366 E 98^{0}21'219 15-180, N	Fire (2002)
2	Bayan-Uul (PSP № 13)	40× 50 m	1963	N 48^{0}27'691 E 98^{0}15'776 5-70, N	Fire (1996)
3	Mukhar valley	40 × 40 m	1876	N 48^{0}37'588 E 98^{0}15'411 5-70, NW	Control forest

[1] R Development Core Team. R: a language and environment for statistical computing, reference index version 4.1.1. Vienna:R Foundation for Statistical Computing, Available at: http://www.R-project.org/ 2021

RESULTS

Tree and regeneration dynamics

No living standing trees remained in PSP №8p. All standing dead trees had already been logged by 5 years post-fire. In plot №13, we compared forest structures of AF20 and AF23 time categories (Table 2). Living tree density per hectare didn't change, and dead tree density decreased 35.0 to 25.0 trees per hectare.

Fig. 2a and Fig. 2b illustrate the numbers of larch saplings in each height class in the permanent sample plots burned in 2002 and 1996. Sapling ages ranged from 2 to 6 years for 1-10 cm saplings, from 8 to 11 years for 51-150 cm saplings, and from 14 to 15 years for 151-300 cm saplings, and from 16 to 22 years for > 300 cm saplings. Larch seedlings have appeared intensively on fresh burnt area. Eight years after the fire, larch seedlings with a height class of 11-50 cm and 51-150 cm were predominated. Ten years after the fire, seedlings with a height class of 51-150 cm have prevailed and saplings with a height class of 151-300 cm have begun to establish. Moreover, on the 14-year-old burnt area, saplings with a height class of 151-300 cm were dominated and saplings with a height class more than 300 cm were formed; and saplings with a height class of 151-300 cm and more than 300 cm have predominated on the 17-year-old burnt area (Fig. 2a). On the PSP №8p, 5 years after the fire, 41.9 thousand two-four-year-old larch seedlings were counted per 1 hectare. Salvage cuttings were carried out on this sample plot in 2007, as a result of which some seedling and saplings were damaged and destroyed. Therefore, in 2010, 8 years after the fire, the number of seedling and saplings was decreased to 26.9 thousand per hectare. In 2012, the number of seedling and saplings was increased to 39.3 thousand per 1 hectare due to sprouting of a seedling from a seed in 2010 and 2011. The number of seedling and saplings from 2015 to 2021, 13-19 years after the fire, was decreased to 25.7 thousand per hectare due to natural thinning of seedlings and saplings (Fig. 2a).

Table 2. Change in forest structure in plot №13 from AF20 to AF23

Fire history	AF20	AF23
Living tree density (individuals ha^{-1})	90.0	90.0
Dead tree density (individuals ha^{-1})	35.0	25.0
Average diameter of living trees (cm)	22.3	23.6
Maximum DBH size (cm)	45.7	47.3
Basal area (m^2 ha^{-1})	3.52	4.16

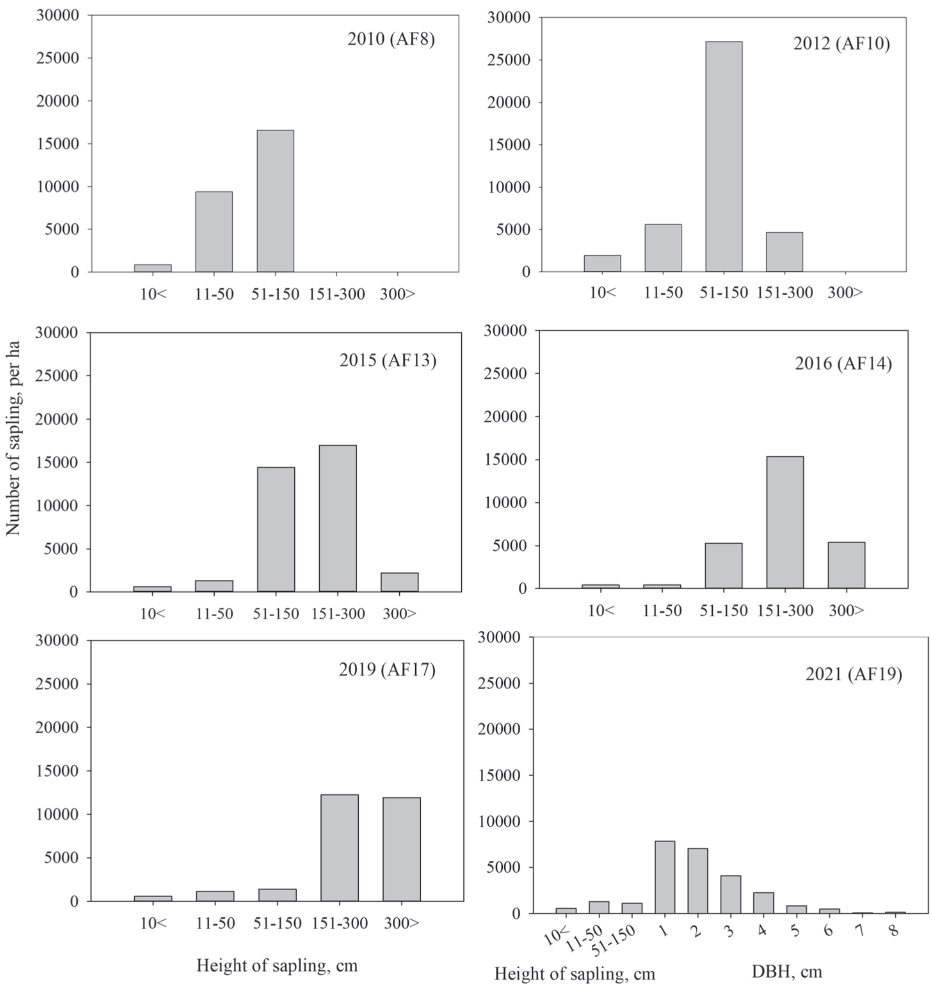

Fig. 2a. Change in the number of larch saplings in PSP №8p height class. DBH - woody plant with up to 8 cm diameter at breast height

PSP №13 is located 4 km south of the Rashaant brigade, and it was observed that livestock of herders' households who reside along the Khojuul river, such as cattle, horses, sheep, and goats graze daily. According to a local herder, 6000 heads of livestock from 30 households graze along the Khojuul river near the Rashaant brigade. The top part of all seedlings and saplings counted were browsed by livestock such as goats and sheep, and their height increment was decreased. Eleven and fourteen years after the fire, larch seedlings with a height class of <10 cm and 11-50 cm, 11-50 cm and 51-150 cm were predominated, respectively. On the 16, 19 and 20-year-old burnt areas, seedlings with a height class of <10 cm were dominated due to sprouting of a seedling from a seed in previous years (Fig. 2b). Eleven years after the fire, 26.9 thousand two-eleven years old larch seedlings were counted per 1 hectare on the PSP №13. In 2012, 16 years after the fire, the number of seedling and saplings was increased to 96.0 thousand per hectare due to sprouting of a seedling from a seed in 2011. The number of seedling and saplings from 2015 to 2021 or in 19-23 years since the fire, was decreased to 46.2 thousand per hectare. Most of the saplings were grazed and damaged by livestock (Fig. 2b).

Understory plant community succession

The shrub layer is not well developed on the burned area. Individual shrubs such as *Lonicera altaica* and *Ribes nigrum*, *Salix spp.*, *Dasiphora fruticosa*, have been occurred in all years since fire in PSP №8p. The projective cover of shrub layer ranged from 1.5 to 4.6% in PSP №8p. The projective cover of shrub layer was not significantly different between 8, 10, 13, 14, 17, and 19 years after the fire (Tukey-Kramer test, $P > 0.05$). However, significant difference was found only between 8 and 14 years after the fire (Tukey-Kramer test, $P < 0.05$) due to increase of *Lonicera altaica* (Table 3).

In PSP №8p, herbaceous cover was 55.5% in AF5 data, where *Chamaenerion angustifolium* dominated. Herbaceous cover was 17.4±1.61 in AF13, where *Poa pratensis* (4.4±1.14) and *C. angustifolium* (3.5±0.54), *Poa attenuate* (3.5±1.3) dominated. In AF19 data, herbaceous cover was 11.8±1.6%, where *P. attenuate* (3.38±1.02), *P. botryoides* (3.13±0.9), *C. angustifolium* (1.8±0.3) dominated (Fig. 3a). The Tukey-Kramer test revealed no significant difference in herbaceous cover between the 6 years after the fire ($P > 0.05$). By fifth year after the fire, ground vegetation develops into **fireweed community** dominated

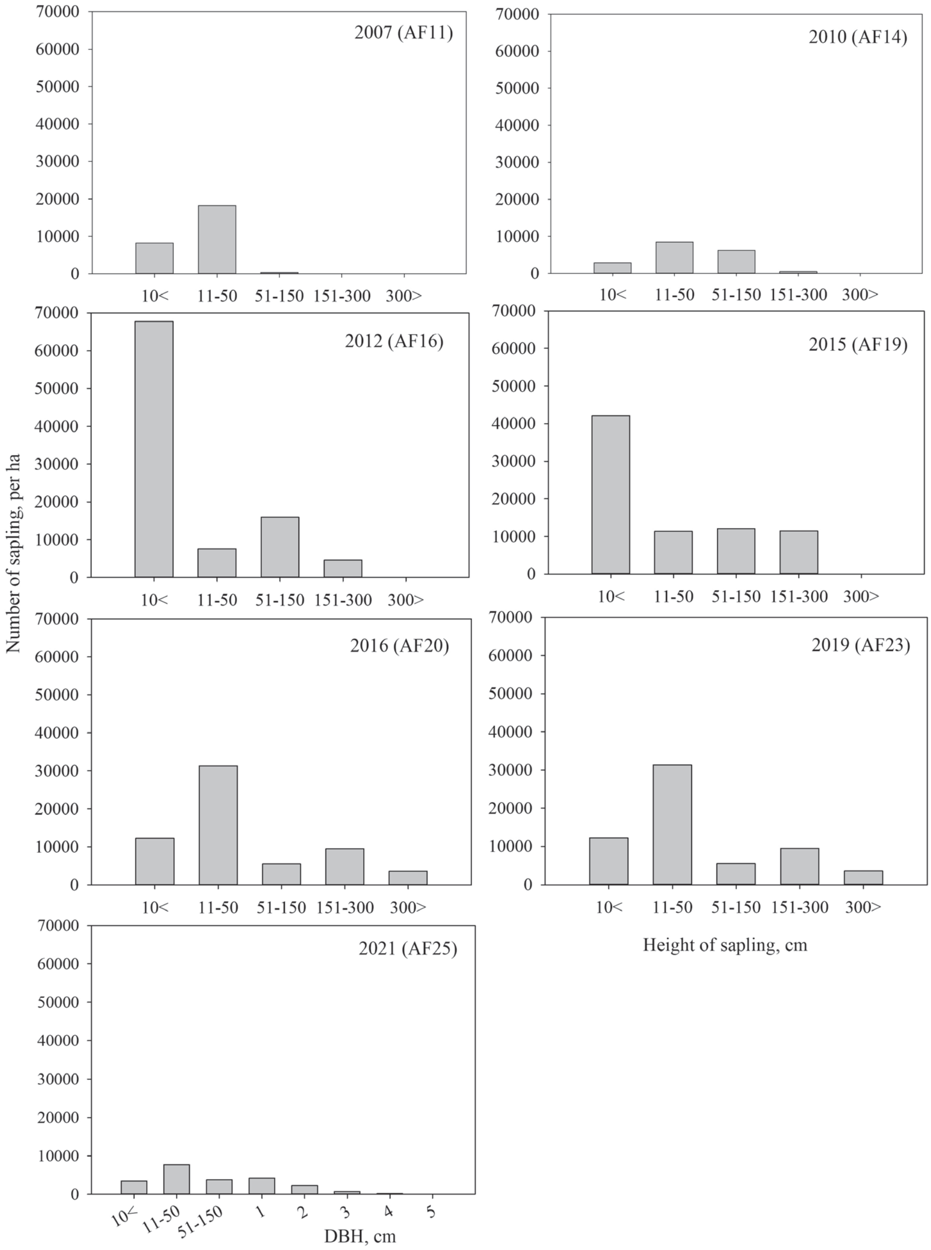

Fig. 2b. Change in the number of larch saplings in PSP №13 height class. DBH - woody plant with up to 5 cm diameter at breast height

Table 3. Change of plant coverage, and species diversity indices for years after the fire of 2002 (PSP №8p)

Variables	Sample plots					
Years after the fire	AF8	AF10	AF13	AF14	AF17	AF19
Coverage of shrub	1.5[b]	3.75[ab]	4.6[ab]	5.25[a]	3.6[ab]	3.8[ab]
Coverage of herb	12.4[a]	15.8[a]	17.5[a]	17.3[a]	12.75[a]	11.8[a]
Coverage of moss and lichen	17.8[a]	16.6[a]	6.3[b]	4.9[b]	3[b]	1.5[b]
Shannon index (H')	1.3[a]	1.6[ab]	1.84[b]	1.83[b]	1.84[b]	1.6a[b]
Simpson index (D)	0.62[a]	0.71[a]	0.79[b]	0.78[b]	0.79[b]	0.76[b]
Species richness (number of species)	7[a] (22)	9.9[b] (31)	9.6[b] (30)	9.31[b] (28)	8.81[ab] (31)	6.63[a] (24)
Evenness (J)	0.7[a]	0.7[a]	0.8[b]	0.8[b]	0.8[b]	0.86[b]

[a, b] Different alphabet denote significantly different among the years after the fire (Steel Dwass test in BZ, $p < 0.05$).

by *Chamaenerion angustifolium*. Species such as *Achillea millefolium, Cerastium pauciflorum, Saussurea stubendorfii, Taraxacum officinale, Koeleria macrantha, Poa attenuate, Poa pratensis, Sedum aizoon, Veronica longifolia*, annuals and biennials such as *Androsace septentrionalis, Corydalis sibirica, Erigeron acer*, fire mosses such as *Funaria hygrometrica, Marchantia polymorpa* newly appeared during years after the fire. In 10 years after the fire, **fireweed-forbs community** dominated by forbs such as *C.angustifolium, Taraxacum officinale* was formed. At the same time, new species such as *Artemisia sericea, Draba nemorosa, Rumex acetosa, Agropyron cristatum* emerged. Within 13-19 years after the fire, a **grasses-forbs** community was formed with the dominance of grasses, including *Poa pratensis, Poa botryoides, Poa attenuata*, and forbs as *C. angustifolium, Taraxacum officinale* (Fig. 3a).

At the early stage of the post-fire succession, the first colonizers as fireweed, *Funaria hygrometrica, and Marchantia polymorpa*, appeared from seeds dispersed over the burned area, and a fireweed community dominated by *Chamaenerion angustifolium* was established by the fifth year after the fire.

The projective cover of lichen and moss layer in control forest was 45.3%, where *Rhytidium rugosum* (27.13%) and *Abietinella abietina* (17.78%) dominated. There was a sharp decline in moss cover due to decrease of *Rhytidium rugosum* immediately after the fire. The cover rose significantly 8 years after the fire due to growth of *Funaria hygrometrica* as fire moss. It decreased significantly 10 years after the fire (Tukey-Kramer test, $P < 0.05$) (Fig. 3a).

The species composition and coenotic percentage similarity indexes of ground vegetation between the control stand and the burned forest (PSP №8p) show a significant difference, indicating a noticeable change in the plant community of the burned area (Fig. 4). Sorenson species composition similarity index ranged from 16.13 to 36.36, with the value from 17 years after the fire being the highest. Coenotic percentage similarity index ranged from 0.42 to 6.23, with the value from 17 years after the fire being the highest and 5 years after the fire as the lowest (Fig. 4a).

In PSP №13, very few shrubs were present in burned forest, and we found only two species (*L.altaica and Cotoneaster melanocarpa*). The projective cover of the shrub layer varied between 0.07 and 0.25% but did not significantly differ among the 7 years (Tukey-Kramer test, $P>0.05$) (Table 4).

(a)

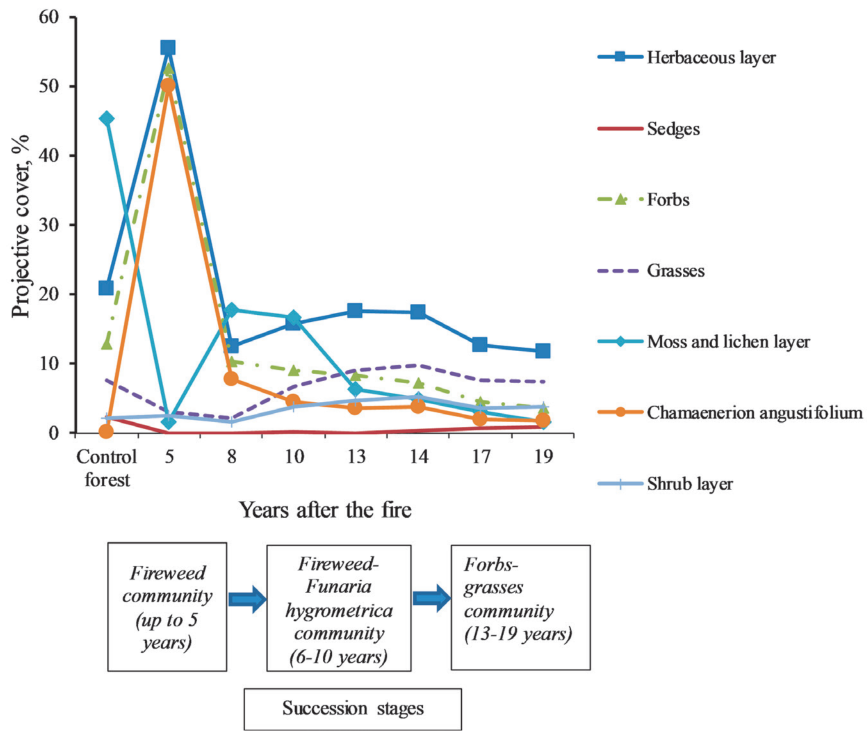

(b)

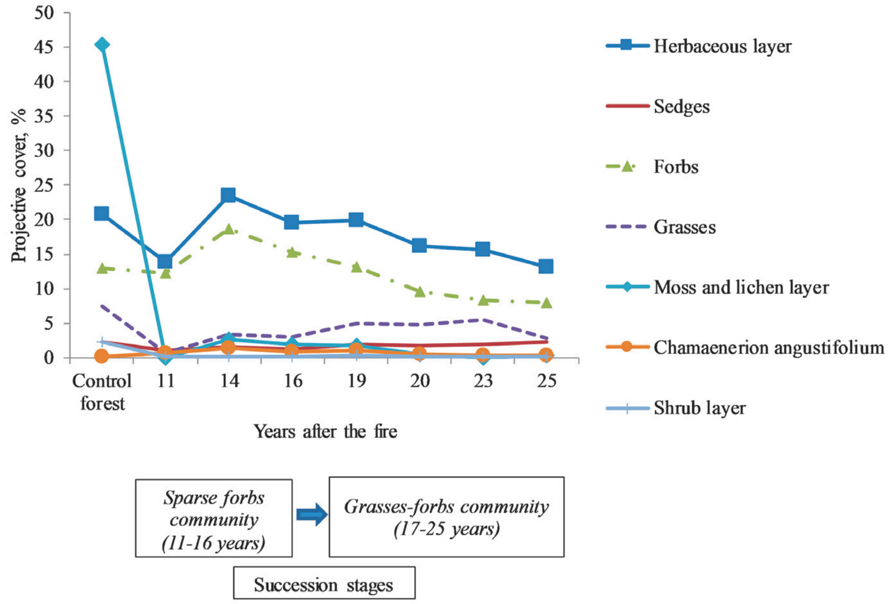

Fig. 3. Dynamic in projective cover of burned forbs-Rhytidium mosses pseudotaiga larch forest (a-in PSP №8p, b-in PSP №13)

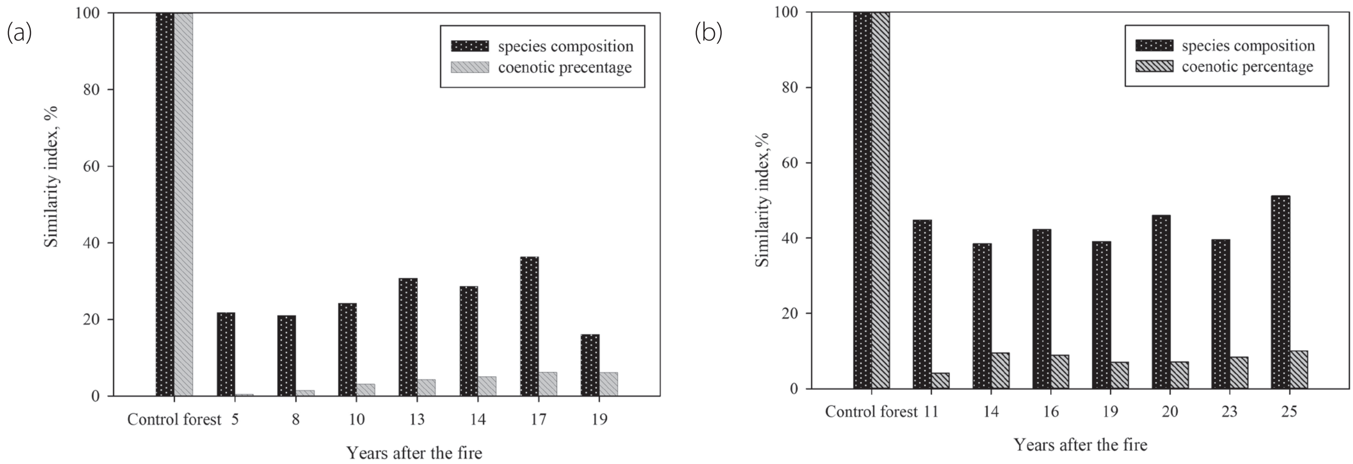

Fig. 4. Similarity indexes of plant communities in burned and unburned stands of forbs-Rhytidium mosses larch forest (a-in PSP №8p, b-in PSP №13)

Table 4. Change of plant coverage, and species diversity indices for years after the fire of 1996 (PSP13)

Variables	Sample plots						
Years after the fire	AF11	AF14	AF16	AF19	AF20	AF23	AF25
Coverage of shrub	0.07^{a}	0.16^{a}	0.15^{a}	0.25^{a}	0.2^{a}	0.08^{a}	0.18^{a}
Coverage of herb	13.9^{a}	23.5^{a}	19.6^{a}	19.9^{a}	16.1^{a}	15.7^{a}	13.1^{a}
Coverage of moss and lichen	0	2.68^{a}	2.03^{a}	1.75^{a}	0.43^{a}	0	0.3^{a}
Shannon index (H')	1.26^{a}	1.85^{b}	2.2^{c}	2.17^{c}	2^{bc}	2^{bc}	1.9^{bc}
Simpson index (D)	0.7^{a}	0.8^{b}	0.9^{b}	0.8^{b}	0.8^{b}	0.8^{b}	0.78^{b}
Species richness (number of species)	6.3^{a} (32)	10.3^{b} (43)	14.5^{c}(55)	13.4^{bc}(52)	12.15^{bc}(52)	12.6^{bc}(51)	10.2^{ab}(47)
Evenness (J)	0.8^{a}	0.8^{a}	0.85^{a}	0.8^{a}	0.8^{a}	0.8^{a}	0.8^{a}

^{a,b} Different alphabet denote significantly different among the years after the fire (Steel Dwass test in BZ, $p < 0.05$).

The projective cover of herbaceous layer was not significantly different between the 7 years (Tukey-Kramer test, P > 0.05). The plant community succession trend in the burned area (plot13) was found to be similar to that of PSP №8p (Fig. 4b).

From 11 to16 years after the fire, sparse forbs community was developed by the dominance of forbs, including *Artemisia gmelinii, Potentilla bifurca, Taraxacum officinale, Artemisia macrocephala*. In 19-25 years after the fire, grasses-forbs community was found by dominant species such as *Poa attenuate, Poa botryoides, Artemisia gmelinii* (Fig. 4b).

On the burned sample plot (PSP №13), the ground vegetation of which was grazed severely by the livestock, newly appeared ruderal species such as *Chenopodium album, Urtica cannabina, Potentilla conferta, Veronica incana, Plantago major, Schizonepeta multifida, Leontopodium ochroleucum, Artemisia Adamsii, A.dracunculus, A.frigida, A.scoparia, Heteropapus hispidus, Elymus dahuricus, E. sibiricus, and K. macrantha, annuals and biennials as well as C. sibirica, A. septentrionalis, D. nemorosa, Lappula myosotis, Artemisia macrocephala, E. acer,* and fire mosses such as *Ceratodon purpureus, F. hygrometrica*.

The projective cover of lichen and moss layers in the control forest was 45.3%, where *Rhytidium rugosum* (27.13%) and *Abietinella abietina* (17.78%) dominated. It dropped dramatically post-fire (Fig. 3b). The projective cover of lichen and moss layers was not significantly different between the 7 years after the fire (Tukey-Kramer test, P > 0.05) (Table 4).

Species composition and coenotic percentage similarity indexes of plan communities between the burned forest and unburned larch stand was shown in Fig. 4. Sorenson species composition similarity indexes of plan communities between the burned forest and unburned larch stand were 38.46-51.22 during 11-25 years after the fire. There was the highest similarity (51.22) for 25 years after the fire and the lowest similarity for (38.46) for 14 years after the fire. Coenotic percentage similarity indexes were 4.12-10.04. There was the highest similarity in 25 years after the fire. However, the lowest similarity was found in 11 years after the fire (Fig. 4b).

Species richness and species diversity change in burned forest

For PSP №8p, the Shannon index was 1.3 by 8 years after the fire (AF8). Then it increased significantly from 1.83 to 1.84 (Steel Dwass test, p < 0.05), which indicates a slight increase in species diversity in old-burned areas (AF13, AF14, AF17) and the diversity index value can be considered very low (Fernando 1998). In the burned area, which was overgrazed (PSP 13), the species diversity increased gradually (Steel Dwass test, p < 0.05), ranged from 1.2 to 2.2 and the values of the Shannon index belong to the class from very low to low (Tables 3, 4).

Species composition

DCA for PSP №8p indicated that the eigen values of axis 1 and 2 were negligible (0.23). However, isolated subquadrates post fire years may be grouped along the second floristic axis into three groups with same species composition: 1) AF8 and AF10; 2) AF13 and AF14; 3) AF17 and AF19 (Fig.6a).

The differences of species composition between groups can be explained by change of the shrub, moss, and

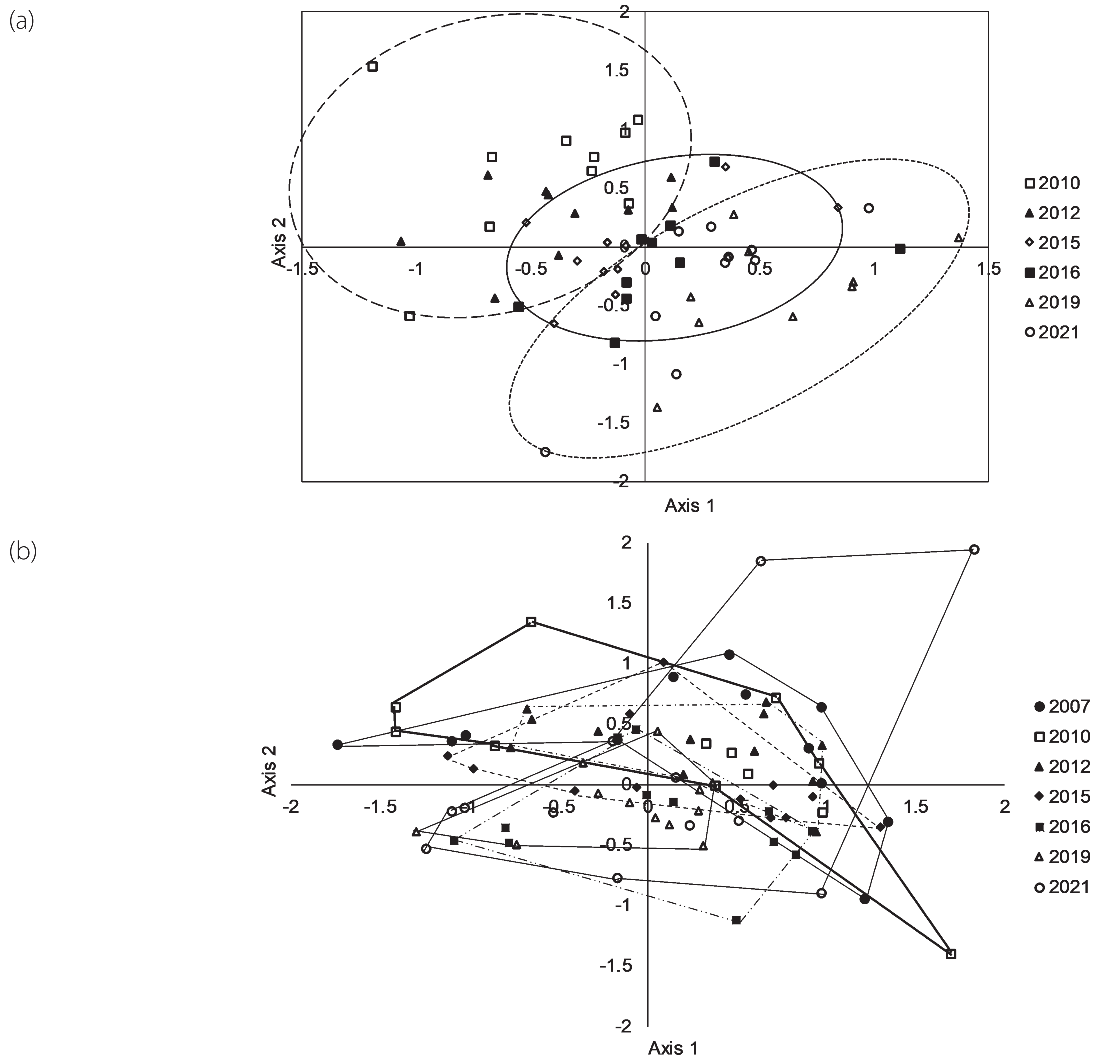

Fig. 5. Yearly change of DCA scores in each sub-quadrate (a-in PSP №8p, b-in PSP №3)

lichen layers. Moss and lichen layers in AF8 and AF10 were significantly higher than AF14, AF17, and AF19. The shrub layer in AF14 was significantly higher than AF8 (Table 3). In PSP №13, the eigen value of axis 1 and 2 were 0.40 and 0.21, respectively. The variance of species composition decreased annually. On the overgrazed burnt area (PSP 13), subquadrates were not grouped by species composition during post-fire years due to grazing of livestock on the ground vegetation and undergrowth (Fig. 5b).

DISCUSSION

Our findings suggested that the pseudo-taiga larch forests damaged by large-scale high-intensity fires in our study area were successfully regenerated by Siberian larch through the following serial succession stages: fireweed (*Chamaenerion angustifolium*) community (up to 5 years after fire), fireweed-bonfire moss (*Funaria hygrometrica*) community (from 6 to 10 years), forbs community (11-16 years), and grass-forbs young larch forest (17-25 years). The expansion of *Funaria hygrometrica, Chamaenerion angustifolium*, and *Corydalis sibirica* on the burnt areas is common in the early stage of the pyrogenic succession of larch forests in the permafrost zone of Central Siberia and Central Yakutia, Mongolia (Takahashi 2006; Dorjsuren 2009; Lytkina and Mironova 2009; Zyryanova et al. 2010).

The primary characteristic of post-fire succession in the larch forest of the Central Khangai region, including the Tarbagatai ridge, is regeneration without tree species replacement. It is generally associated with the cold and dry climate of the Central Khangai region, where Siberian larch trees are distributed and deciduous tree species such as birch and aspen are absent. In contrast, in the Khentey region and North-Eastern Khangai province in Mongolia, as well as in Siberia, Russia, the burned larch forest areas can be regenerated by birch, and aspen tree species or mixed with larch trees (Abaimov and Sofronov 1996; Abaimov et al. 2002; Lytkina and Mironova 2009; Dorjsuren 2009; Zyryanova et al. 2010; Otoda et al. 2013; Undraa and Dorjsuren 2017).

Fires burn thick moss layers in *forbs-Rhytidium* mosses-larch forest and by this create favorable conditions for the regeneration of larch seedlings. In forest stands with a dense moss cover, the emergence and peak of young larch regeneration mostly occur after high-severity fires due to reducing stand competition for moisture and nutrients. Additionally, they destroy shrub and herbaceous layers, moss cushion, slash and litter, which hinder the emergence and development of larch seedlings. Fires enhance soil mineralization, enrich nutrients through ash deposition, and raise temperatures, all of which contribute to favorable conditions for seed germination, seedling rooting, and the development of a self-sown crop (Matveev and Usoltsev 1996; Babintseva and Titova 1996; Sofronov and Volokitina 2010). Moreover, post-fire successful larch tree regrowth depends on soil hydrology such as high plant-available field capacity and hydraulic conductivity in the uppermost soil horizons, which reduces the evaporation loss and the competition of larch saplings with grasses and herbs for water in pseudo-taiga larch forests under semi-arid conditions of the Tarvagatai Mountain range (Schneider et al. 2021).

In the Tarvagatai Mountain Range, 114,3 thousand hectares or 52% of forest areas were damaged by fire in 1996, 2002 and 2003 (Jagdag and Gerelbaatar 2016). In Central Khangai, 70 % of burned forests are regenerating successfully by larch trees (Tungalag and Dorjsuren 2017). According to a long-term study, 70-75 % of the forest area burned by high-intensity fires regenerates naturally (Dugarjav 2006). Our study reveals that the number of seedling and saplings 19-23 years after the fire ranged from 25.7 thousand to 46.2 thousand per hectare. In some areas affected by the 2002 fire, 71,100 young trees were counted per hectare in 2021. Therefore, we suggest the recommendation to conduct thinning in dense young stands originated post-fire. Thinning reduces tree density, crown closure, and fire intensity and increase forest productivity (Agee et al. 2006; Khongor and Tsogt 2019, Banerjee 2020).

CONCLUSION

In the Tarvagatai Mountain range, Siberian larch trees are predominated; however, deciduous tree species such as birch and aspen are absent due to the cold and dry climate of the Central Khangai region. *Forbs-Rhytidium* mosses pseudo-taiga larch forests disturbed by the large-scale forest fires in the Tarvagatai Mountain range were sufficiently recovered by Siberian larch without tree species replacement. Post-fire regenerative succession proceeds through several serial stages and establishes grass-forbs young larch forest in 17-25 years after fire. Species numbers gradually increased with time in the forest affected by fires, whereas they rose drastically in the forest damaged by fire and livestock browsing due to the increase of ruderal species. Despite the long recovery period, the post-fire similarity indexes of species composition and coenotic percentage compared with the control forest were relatively low, indicating a slow pre-fire vegetation recovery.

REFERENCES

Abaimov A.P., Sofronov M.A. (1996). The main trends of post-fire succession in near tundra forests of Central Siberia. In: Goldammer J.G., Furyaev V.V. eds., Fire in Ecosystems of Boreal Eurasia. Forestry Sciences, vol 48. Springer: Dordrecht, pp. 372-386.

Abaimov A.P., Zyryanova O.A., Prokushkin S.G. (2002). Long-term investigations of larch forests in Cryolithic zone of Siberia: brief story, recent results and possible changes under global warming. Eurasian Journal of Forest Research., N.5-2, pp. 95-106.

Altrell D. (2019). Multipurpose National Forest Inventory in Mongolia, 2014-2017 - A tool to support sustainable forest management. Geography, environ. sustainability. 12(3), pp. 167-183.

Babintseva R.M., Titova Y.V. (1996). Effects of Fire on the Regeneration of Larch Forests in the Lake Baikal Basin. In: Goldammer JG., Furyaev VV. eds., Fire in Ecosystems of Boreal Eurasia. Forestry Sciences, , vol 48. Springer, Dordrecht, pp. 358-365.

Bergeron Y, Dansereau P.R. (1993). Predicting the Composition of Canadian Southern Boreal Forest in Different Fire Cycles. Journal of Vegetation Science, 4(6), pp. 827–832.

Bergeron Y, Dubue M. (1988). Succession in the southern part of the Canadian boreal forest. Vegetatio, 79, pp. 51–63.

Boucher D, Gauthier S, Thiffault N, Marchand W, Girardin M, Urli M. (2020). How climate change might affect tree regeneration following fire at northern latitudes: a review. New Forests, 51, pp. 543–571.

Cai W, J Yang, Z Liu, Y Hu, PJ Weisberg. (2013). Post-fire tree recruitment of a boreal larch forest in Northeast China, Forest ecology and Management. (307), pp. 20-29.

Cai Wen H, Liu Zhihua, Yang Yuan Z, Yang Jian. (2018). Does Environment Filtering or Seed Limitation Determine Post-Fire Forest Recovery Patterns in Boreal Larch Forests? Frontiers in Plant Science, vol. 9, 1318, pp. 1-12.

Chen Wei, Kazuyuki Moriya, Tetsuro Sakai, Lina Koyama, Chunxiang Cao. (2014). Monitoring of post-fire forest recovery under different restoration modes based on time series Landsat data, European Journal of Remote Sensing, 47:1, pp. 153-168.

Chen Wei, Jiang Houzhi, Moriya Kazuyuki, Sakai Tetsuro, Cao Chunxiang. (2018). Monitoring of post-fire forest regeneration under different restoration treatments based on ALOS/PALSAR data. New Forests, 49, pp. 1-17.

Chu T, X Guo, K Takeda. (2017). Effects of Burn Severity and Environmental Conditions on Post-Fire regeneration in Siberian Larch Forest. Forests, 8, (76), pp. 1-27.

Danilin I.M. (2009). Structural and functional organization of a larch phytocenosis in a postfire progressive succession in the North of Central Siberia. Contemporary Problems Ecology, vol. 2, No. 1, Pleiades Publ., pp. 55–65.

Dorjsuren Ch., D Zoyo, Z Tsogt, M Undraa. (2007). Long-term monitoring for post-fire succession in herbs-rhytidium rugosum larch forest in Tarbagatai mountain range of Mongolia. In: Proceeding of scientific conference titled Geoecology of Mongolia - UB, pp. 234-241.(in Mongolian).

Dorjsuren Ch. (2009). Anthropogenic succession of the larch forests in Mongolia. Russian Agricultural Academic Press: Moscow. p. 209 (Biological resources and natural environment of Mongolia: Proceeding of the Joint Russian-Mongolian Complex Biological Expedition; vol. 50) (in Russian, summary in English).

Dugarjav Ch. (2006). Larch forests of Mongolia, Ulaanbaatar: Bembi san printing, 318 p. (in Mongolian).

Dugarjav Ch., Korotkov I. A., Savin E. N., Semechkin I. V., Tetenkin A. E., Yanovskii V. M. (1975). Forests of Tarvagatai Mountain Range in Mongolia, Forestry. V. 2. pp. 38–46 (in Russian).

FAO. (2020). lobal Forest Resources Assessment 2020 – Key findings. Rome.

FAO and UNEP. (2020). The State of the World's Forests 2020. Forests, biodiversity and people. Rome.

Fernando E.S. (1998). Forest formations and flora of Philippines: Handout in FBS 21.UPLB, Philippines.

Forest Research and development center (2021). Forest resources of Mongolia - 2021.

Gamova N.S. (2014). Post-fire vegetation changes of Central Khamar-daban (Southern Baikal region), Problems of botany of South Siberia and Mongolia. in: Proceeding of the 13th International scientific practical conference (Barnaul, 20-23 October, 2014), pp. 55–59. (in Russian).

Greene D. F, J Noël, Y Bergeron, M Rousseau, S Gauthier. (2004). Recruitment of Picea mariana, Pinus banksiana, and Populus tremuloides across a burn severity gradient following wildfire in the southern boreal forest of Quebec, Canadian Journal of Forest Research. 34, pp. 1845–1857.

Grubov V.I. (1982). Key to the vascular plants of Mongolia (with an atlas). Leningrad: Nauka. Leningrad. Branch, 817p.

Hille M., den Ouden J. (2004). Improved recruitment and early growth of Scots pine (Pinus sylvestris L.) seedlings after fire and soil scarification. Eurasian Journal of Forest Research, 123, pp. 213–218.

Institute of meteorology and hydrology. (2021). Meteorological data in Tosontsengel station, Tosontsengel meteorological station, Institute of meteorology and hydrology, Mongolia,

Ivanova A.A, E.O. Kopylova-Guskova, A.B. S h i p u n o v, P.A. Volkova. (2014). Post-fire succession in the northern pine forest in Russia: a case study. Wulfenia, vol 21, pp. 119-128.

Jacquelyn K Shuman, Adrianna C Foster, Herman H Shugart, Amanda Hoffman-Hall, Alexander Krylov, Tatiana Loboda, Dmitry Ershov, Elena Sochilova. (2017). Fire disturbance and climate change: implications for Russian forests. Environmental Research Letter, 12 035003, pp. 1-13.

Jagdag D., Gerelbaatar S. (2016). Current situation and changes of forest resources in Tarvagatai Nuruu National Park, Mongolia, Proceeding of International conference on Central Asian Environmental and Agricultural Problems, Potential solutions, pp. 204-208.

Jenkins M., & Schaap B. (2018). Forest ecosystem services. In: United Nations Forum on Forests,

Johnstone Jill F, Teresa N Hollingsworth, F Stuart Chapin III; Michelle C Mack. (2010). Changes in fire regime break the legacy lock on successional trajectories in Alaskan boreal forest. Global Change Biology, 16(4), pp. 1281–1295.

Johnstone Jill, Chapin III, F Stuart, Foote J, Kemmett S, Price K, Viereck LA. (2004). Decadal observations of tree regeneration following fire in boreal forests. Canadian Journal of Forest Research. 34, pp. 267-273.

Korotkov I. A. (1976). Geographic patterns of distribution of forests in the People's Republic of Mongolia, Journal of Botany, T. 61, № 2, pp. 145-153 (in Russian).

Krasnoshekov Yu.N. (1983). Some features of the Soil-Protective Role of Pseudotaiga Larch Forests. In: The Forests of Mongolian People's Republic (Larch forests of the Central Khangai). Novosibirsk: Science, pp. 73– 81 (in Russian).

Krasnoshekov Yu.N. (1996). Structure of vertical soil zonality and soils of forest landscapes in Northern Mongolia, Soil science, № 4, pp. 401-410 (in Russian).

Kristi Parro, Marek Metslaid, Getter Renel, Allan Sims, John A Stanturf, Kalev Jõgiste, Kajar Köster. (2015). Impact of postfire management on forest regeneration in a managed hemiboreal forest, Estonia, Canadian Journal of Forest Research, 45, pp. 1192-1197.

Lytkina L.P., Mironova S.I. (2009). Postfire succession in a forest of the Cryolithozone: the example of Central Yakutia. Russian Journal of Ecology N.40(3), pp. 154-159.

Matveev A., Matveeva T.A., Baksheeva E.O. (2012). Influence of fires in the resumption of larch in different orographic conditions. Sovremenny problem naukil obrazovaniya. N.5. Available at: http://www.science-education.ru/105--7217 [Accessed 2 March. 2015] (in Russian).

Matveev P.M., Usoltsev V.A. (1996). Post-fire mortality and regeneration of Larix sibirica and Larix dahurica in conditions of long-term permafrost. In: J.G.Goldammer and V.V.Furyaev, eds., Fire in Ecosystems of Boreal Eurasia, Kluwer Academic Publishers, pp. 366-371.

Ministry of Environment and Tourism. (2018). Third National Communication of Mongolia (TNC). 416p.

National Emergency Management Agency of Mongolia, 2020.

Nasi R., Dennis R., Meijaard E., Applegate G., & Moore P. (2002). Forest fire and biological diversity. UNASYLVA-FAO, pp. 36-40.

Otoda T., Doi T., Sakamoto K., Hirobe M., Nachin B., & Yoshikawa K. 92013). Frequent fires may alter the future composition of the boreal forest in northern Mongolia. Journal of forest research, 18(3), pp. 246-255.

Park Y.D. (2005). Ecological studies on rehabilitation of forests degraded by fire or logging in Southern Khentii, Mongolia.Ph.D thesis. Seoul., South Korea, 110p.

Park, Y.D; Lee D.K., Stanturf J.A., Woo S.Y., Zoyo D. (2009). Ecological indicators of forest degradation after forest fire and clear-cutting in the Siberian larch (Larix sibirica) stand of Mongolia. Journal of Korean Forest Society, 98(5), pp. 609-617.

Pielou E.C. (1975). Ecological Diversity. Wiley, New York, 165p.

Ponomarev E.I., Kharuk V.I., Ranson K.J. (2016). Wildfires Dynamics in Siberian Larch Forests. Forests. 7.125, pp. 1-9.

Prokushkin S.G., Zyryanova O.A. (2013). Influence of Gmelin larch trees on postfire restoration of forest communities in the permafrost zone of Central Siberia. Contemporary Problems of Ecology, 6, pp. 486–492.

Renkonen O. (1938). Statistisch-ökologische Untersuchungen über die terrestische Käferwelt der finnischen Bruchmoore. An Zool Soc Zool-Bot Fenn Vanamo 6:1–231.

Schneider F, Klinge M, Brodthuhn J, Peplau, T, Sauer D. (2021). Hydrological soil properties control tree regrowth after forest disturbance in the forest steppe of central Mongolia, SOIL(7) pp. 563–584.

Shannon C.E, W Weaver. (1949). The mathematical theory of communication. Univ. of Illinois press. Urbana 117p.

Simpson E.H. (1949). Measurement of diversity. Nature 163, 688p.

Sofronov M. A., Volokitina A. V. (2010). Wildfire ecology in continuous permafrost zone. In: Permafrost ecosystems, Siberian Larch Forests, Ecological Studies. V. 209. pp. 59–82.

Sorenson, T. A. (1948). Method of Establishing Groups of Equal Amplitude in Plant Sociology Based on Similarity of Species Content and Its Application to Analyses of the Vegetation on Danish Commons. In: Kongelige Danske Videnskabernes Selskab, Biologiske Skrifter, 5, pp. 1-34.

Takahashi K. (2006). Future perspective of forest management in a Siberian permafrost area. Symptoms of environmental change in Siberian permafrost/Ed.R.Hatano, G.Guggenberger. Sapporo: Hokkaido University Press, pp. 163-170.

Tautenhahn S, Lichstein JW, Jung M, Kattge J, Bohlman SA, Heilmeier H, Prokushkin A, Kahl A, Wirth C. (2016). Dispersal limitation drives successional pathways in Central Siberian forests under current and intensified fire regimes. Global Change Biology. Jun; 22(6), pp. 2178-2197.

Tsegmid Ts. (2001). Key to the moss of Mongolia. Ulaanbaatar: Soyombo Printing, 473 p. (in Mongolian).

Tsogt Z. (1993). Formation, structure and productivity of young larch forests of the Central Khangai and Eastern Khentey and their thinning. Abstract of PhD in agricultural sciences, UB, 24p.

Tsogtbaatar J. (2004). Forest Policy Development in Mongolia. In: Institute for Global Environmental Strategies (IGES). Policy Trend Report. Yokohama: Sato Print. pp. 60–69.

Tsvetkov P.A. (2006). The results of the investigations of forest fires in northern taiga of Central Siberia. Conifers of the boreal area, N.1, pp. 186-195. (in Russian)

Tungalag M. (2020). Forest resource and management of the forest vegetation provinces of Mongolia, Ph.D thesis. Ulaanbaatar, School of Engineering and Applied Sciences, National University of Mongolia, 151p.

Uemura S., Tsuda S., Hasegawa S. (1990). Effects of fire on the vegetation of Siberian taiga predominated by Larix dahurica. Canadian Journal of Forest Research, 20, pp. 547-553.

Undraa M., Dorjsuren Ch. (2017). Regeneration and plant community change after fire in mesophyte herbs subtaiga larch forest in Eastern Khentey. Proceedings of General and Experimental Biology, MAS №33, pp. 185-189. (in Mongolian).

Undraa M., Dorjsuren Ch., Zoyo D. (2020). Post-fire plant community change and regeneration in pseudotaiga larch forest in Tarbagatai mountain range, Mongolian Journal of Botany, 02, pp. 102-110. (in Mongolian).

Undraa M., Kawada K., Dorjsuren Ch., Kamijo T. (2015), After fire regenerative successions in larch (Larix sibirica Ledeb.) forests of the Central Khangai in Mongolia. In: Sibirskij Lesnoj Zurnal (Siberian Journal of Forest Science). N. 4, pp. 40–50. (in English with Russian abstract).

Valendik E.N., Matveev P.M., Sofronov M.A. (1979). Large scale forest fire, Nauka: Moscow, 197 p. (in Russian).

Zoyo D. (2000). The changes of herbaceous and bush cover in larch and pine forests after cutting and forest fire (by example of Khantai and Selenge forest-vegetation region) 03.00.05. Ph. D in Biological Sciences. Dissertation. Mongolian National University, Ulaanbaatar, Mongolia. (in Mongolian).

Zyryanova O.A., Abaimov A.P., Bugaenko T.N., Bugaenko N.N. (2010). Recovery of forest vegetation after fire disturbance. In: Permafrost ecosystems, Siberian Larch Forests, Ecological Studies. V(209), pp. 83-96.

ges.rgo.ru/jour/

ISSN 2542-1565 (Online)